Report No. 2236

400 MHz Scatterometer

Final Report

Prepared For

NATIONAL AERONAUTICS AND SPACE AGENCY

MANNED SPACECRAFT CENTER

HOUSTON, TEXAS

NASA CR 101976

Report No. 2236

400 MHz Scatterometer

Final Report

Prepared For

NATIONAL AERONAUTICS AND SPACE AGENCY

MANNED SPACECRAFT CENTER

HOUSTON, TEXAS

13 DECEMBER 1968

Document No. 2236

13 December 1968
Rev. A 13 October 1969

400 MHz SCATTEROMETER

FINAL REPORT

CONTRACT NO. NAS 9-6742

Prepared By

EMERSON ELECTRIC COMPANY

ELECTRONICS AND SPACE DIVISION

For

NATIONAL AERONAUTICS AND SPACE AGENCY

MANNED SPACECRAFT CENTER

HOUSTON, TEXAS

TABLE OF CONTENTS

LIST OF ILLUSTRATIONS

LIST OF ILLUSTRATIONS

(CONTINUED)

LIST OF TABLES

SECTION I

INTRODUCTION AND PROGRAM SUMMARY

1.1 INTRODUCTION

Early work by Dr. R. K. Moore and others indicated that the back scattering characteristics, as a function of the angle of incidence of transmitted energy, could possibly serve as an unique signature of various terrains particularly when obtained for different polarizations, cross polarizations, and frequencies.

An airborne Scatterometer could serve many purposes in the study of the earth's surface. By comparing the data through computer correlation techniques with stored signatures of known terrains, large areas could be mapped and categorized particularly with respect to agricultural products and forest areas. Many other usages have been proposed such as measurement of the height of waves, moisture content and surface mineral contents.

A Scatterometer System around 400 MHz was particularly attractive due to its ability to penetrate clouds and to a certain degree penetrate snow, ice and water. Emerson Electric personnel began working with NASA technical personnel and their scientific advisers as early as November, 1965. These efforts resulted in the technical specifications for a 400 MHz Scatterometer using state-of-the-art techniques. NASA's RFP BG721-11-6-747P, incorporating these specifications, was issued on 24 May 1966. Emerson's Proposal NB66-1069 was submitted to NASA on 3 June 1966. A contract was awarded to Emerson on 24 February 1967 to deliver a feasibility demonstration model within eight months.

1.2 MAJOR MILESTONES

The relatively short delivery schedule was recognized and provisions were made for advance approval of long lead items prior to the Design Review. The Transmitter and Receiver Procurement Specifications were submitted on 6 April. Three others, Antenna Switch, 5 MHz and 55 MHz Oscillators were submitted on 21 April 1967. Approval was received on 18 May 1967.

The Receiver-Transmitter Unit Design Review was held nine weeks after contract receipt on 2-3 May 1967. Emerson was requested to add telemetry tones to the Calibrate Receiver indicating the Mode of Operation and the position of the two Receiver Gain Switches. Design approval was received on 22 June 1967.

NASA had been investigating various locations for mounting the antenna to the wing. Patterns were taken on the 1/5 scale model for the various configurations. These were reviewed on 9 June along with the basic NASA antenna mount design. The antenna mount places the antenna ground plane 2 3/4 inches from the wing. Long fairing were required (greater than 5:1) to avoid excessive pattern degradation.

The fifth scale antenna model design activity was completed during June, 1967. The H plane dipole was of conventional design. The E plane dipole has the arms bent toward the ground plane by 35^{o}.

Both were mounted with the arms not quite a half wavelength from the ground plane to help reduce the gain at Nadir. Each array has a front and rear set of 12 dipoles fed with difference energy. A small amount of sum energy, in phase quadrature, was injected for better control of the Nadir null. Parasitic elements were placed between each front and rear pair to help control the Nadir null and effectively reduce Nadir sidelobes.

Dipoles design was critical considering the pylon length (15 inches), weight and drag. To meet the 15g vibration requirements, an "A" design was selected in July, 1967. The Antenna Design Review was held on 6-7 September 1967 but late prototype tests indicated that the use of the "A" frame design for both E and H dipole was coupling energy reducing the array isolation below acceptable values.

The antenna mount and antenna interface design which was agreed to on 17 August 1967 was reconsidered on 19-20 October 1967 based on NASA's new antenna mount design to allow quick removal of the antenna mount and antenna from the P3A aircraft. On 18 December 1967 the Antenna Dummy Panels to the new design were shipped to NASA.

Functional testing of the R/T Unit was completed during December, 1967 except for the inclusion of the antenna switch which had been damaged during inadvertent no load operation. EMC tests were completed on 29 January 1968. Temperature-Altitude tests were concluded on 5 February and vibration tests completed on 17 February 1968. Acceptance tests of the R/T Unit were run on 21 February and 24 February 1968. The R/T Unit was shipped to NASA on 24 February and received on 26 February 1968.

Extreme difficulty was encountered during the developmental vibration tests of the antenna dipoles and simulated mount, in attempting to meet the 15g, nine hours requirements of MIL-STD-810A. The final design required 4130 steel and adequate gusseting at the arms and mounting feet. At the second Antenna Design Review on 25 January 1968 the E and H plane active dipoles and the E parasitic dipole successful vibration test results were presented and subsequent approval received. On 9 February 1968, a properly fabricated H parasitic dipole passed vibration tests.

All antenna elements were shipped to NASA by 29 February 1968. Panels were mounted to the P3A wing mock up by 4 March 1968. Boresight range testing of the antenna and mock up started on 14 March 1968. Side lobe levels, particularly around Nadir, were high and the beamwidths wider than expected. Testing stopped on 18 April 1968 until a resolution could be made as to the best approach required to improve the patterns.

Adequate laboratory test equipment to conduct R/T Unit checkout and calibration arrived at NASA on loan from Emerson on 14 March 1968.

Subsequent bench check out revealed marginal isolation between H & V channels when one was set with 30 db or more higher gain than the other. This was resolved by the addition of a 340 MHz Bandpass filter in the first mixer of the Vertical Receiver. No other changes or failures occurred in the R/T Unit.

Patterns taken with and without simulated fairings were sent to NASA on 26 April 1968. NASA's antenna consultant from the U of Kansas, Dr. Lewis Bailin, reviewed these patterns at NASA on 3 May 1968. His opinion was that fuselage fairings would help the patterns around Nadir. Full sets of E & H patterns, with simulated fairings were sent to NASA and to the users on 8 May 1968. The boresight range and aircraft schedule was such that NASA requested the field engineer be recalled on 9 May 1968, until October 1968. The field office was closed on 10 May 1968.

On 20 May 1968, Dr. Moore of the U of Kansas, reported on his analysis of the patterns with fairings. The data obtained would be useable except for the region 5^{o} to 20^{o} forward for the E dipole array. Computer simulation programs showed that the vertical separation of the dipoles due to fuselage curvature and the 6^{o} dihedral of the wing and the consequent attempt to remove the effects of this vertical separation by phasing produced a large end fire beam which after reflection off the engine nacelles contributed heavily to the high side lobes at Nadir. The results of the computer study were discussed with NASA at the U of Kansas on 26 June 1968, where it was decided that rephasing of the array to focus at an angle of 53^{o} provides the best compromise between defocusing with beam broadening at Nadir and magnitude of end fire beam.

The panels were shipped back from NASA on 24 June 1968 to accomplish this rephasing. In addition, components were selected to obtain a better balance between front and rear dipoles of a set in both phase and amplitude. The panels were returned to NASA on 23 August 1968.

The P3A wing mock-up had approximately a 1.5^{o} error in alignment of the wings to the fuselage. Correction of this was completed by 20 September 1968. Emerson engineers arrived at NASA on 23 September 1968. The antenna panels were mounted and phase and amplitude at each dipole were checked. Dipoles were mounted and radiation from each was measured. The mock-up was installed on the positioner and pattern taking began on 2 October 1968. Phasing and sum channel amplitude adjustment of the Horizontal Array produced acceptable patterns. The Vertical or E-Array could not be made acceptable in the Nadir region out to roughly $\pm 20^{o}$. The best arrangement was determined and the Acceptance Tests started on 20 October 1968.

Dr. Lewis Bailin of U of Kansas, reviewed the ATP patterns on 23-24 October 1968, and together with Dr. Richard Moore concluded that the E-Array patterns could not be improved and that the reflectivity data around Nadir for the E-Array could not be used. However, in this region vertical and horizontal polarized reflectivity data are essentially identical, and can be substituted for the other.

During the Acceptance Testing the mock-up was rotated 90^{o} so that cross track patterns could be taken beyond the $\pm 20^{o}$ limitation on the elevation axis.

Patterns taken showed that range effects were present in the Nadir where control of patterns 40db down from the peak gain are required. In this region, the high gain portions of the antenna are looking at structures being illuminated by the transmitting source. Airborne measurement of the patterns will be required. If this proves too difficult or cannot be accomplished because of priority or other ulitization, empirical corrections can be determined and applied to the antenna characteristics used in the Data Reduction Program.

1.3 Major Achievements and Equipment Features

1.3.1 Pre-Contract

As discussed in the Introduction, the technical requirements were translated into detailed technical specifications prior to the issuance of the RFP. The proposal effort further resulted in the definition of hardware concepts to satisfy the requirements. The major features defined during this phase that allowed the equipment to meet specifications were the use of interrupted CW, offset audio carrier (500Hz) thereby removing doppler foldover, antenna pattern shaping approaching the reciprocal of the square root of σ_o, four simultaneous reflectivity measurements each helping to better identify the terrain, continuous accurate calibration for more precise measurement of Pr/Pt (or σ_o) and, the use of time gated signals to more accurately measure small values of σ_o at large angles.

1.3.2 During Contract

All of these concepts were applied and reduced to hardware during the ensuing contract. Two other major achievements were the use of all solid state circuitry and the ability to easily adjust the antenna pattern especially in the region around the Nadir. The solid state circuitry particularly in the transmitter, modulator and antenna switch materially increases the Scatterometer reliability.

By feeding the front and rear rows of an array separately, the position of the null in the along track direction can be varied by phase adjustment between the front and rear rows. By changing the amount of sum energy fed into the array, the Nadir null can be easily shaped and controlled without affecting the pattern outside of $\pm 20^{\circ}$ around the null.

SECTION II

THE 400 MHz SCATTEROMETER SYSTEM

2.1 FUNCTIONAL DESCRIPTION

The 400 MHz Scatterometer System is made up of two aircraft assemblies; The Antenna System and the Receiver/Transmitter Unit (R/T). The R/T unit is designed for rack mounting at the operator's station. The antenna system is designed to be attached under the wing of a P3A aircraft between the two inboard engines. All operating controls of the Scatterometer system are on the front panel of the R/T Unit.

The primary mode of operation of the system is automatic where the pulse width and duty ratio of transmission are controlled by an altimeter. This tie-in is accomplished by a voltage picked off a potentiometer that is driven by the aircraft radar altimeter. Ideally, in the automatic mode, the transmitted pulse width would be equal to the two way radar transit time at the nadir and the receiver on-time would be twice the transmitted pulse width. This would allow for complete reception of signals from target returns at all angles between ± 60 degrees from the nadir.

The antenna system is made up of two independent antennas - one for horizontal polarization and one for vertical polarization. The H vector is parallel to the line of flight in the horizontally polarized antenna and perpendicular to the line of flight in the vertically polarized antenna.

An RF pulse is radiated alternately from the horizontally and vertically polarized antennas. Following an RF transmission, each of the antennas is coupled to a receiver. Thus reflectivity measurements are made for transmitted signals having horizontal and vertical polarizations. In addition, cross polarized reflectivity measurements for each transmitted polarization are also made.

The consecutive pulses are alternately switched between the two antennas by a solid state switch. In addition, the switch serves as a duplexer - disconnecting the input to the receivers during the transmission interval and connecting the receivers to their respective antennas during the receive interval.

A calibrate signal located 500 hertz above the transmitter frequency is fed into each receiver channel. Both receivers process the backscatter and calibrate signals simultaneously. The end result is a translated replica of the doppler spectrum about the center line of the transmitter spectrum plus the calibrate signal 500 hertz above the zero doppler point. By knowing aircraft velocity and the transmitter frequency, it is possible to make a transformation between doppler frequency and angle. A measurement of the power within a subinterval of the doppler spectrum will give the power returned from a target cell between the corresponding angles.

The radar backscatter per unit area, σ_o , is obtained by data processing which takes into account antenna gains, antenna beamwidth, transmitter power, target size, and altitude. The final data is a plot of σ_o 's versus incidence angle. These will include the following:

σ_o - versus incidence angle for horizontally polarized transmission and a horizontally polarized reception.

σ_o - versus incidence angle for a horizontally polarized transmission and a vertically polarized reception.

σ_o - versus incidence angle for a vertically polarized transmission and a vertically polarized reception.

σ_o - versus incidence angle for a vertically polarized transmission and a horizontally polarized reception.

2.2 PHYSICAL DESIGN

2.2.1 R/T UNIT

The R/T unit contains the receiver-transmitter elements plus the operator controls. The R/T unit is shown in Figure 2.1. The unit contains all the circuitry necessary for the processing of the signal returns and for generating the transmitted signal. The power supplies are a part of the R/T unit. The package weight is 105 pounds and the size is 15.72 x 19.00 x 21.84 inches. Power requirements are 117 VAC, 400 hertz, 3 phase with a maximum input of 160 volt-amperes.

The internal packaging is shown in Figures 2.2, 2.3, and 2.4. The unit has been carefully designed to prevent susceptibility to radiated and conducted interference.

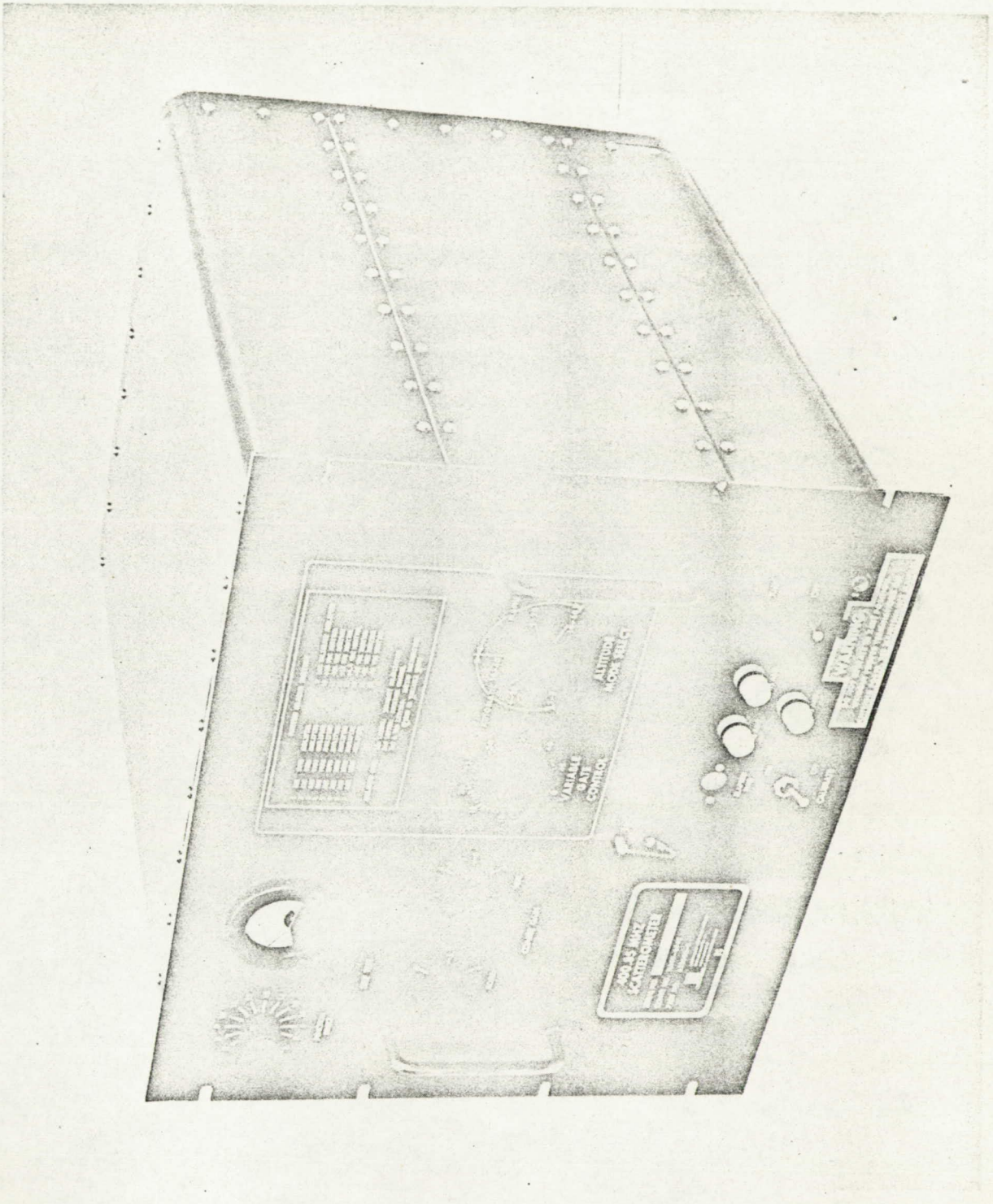

FIGURE 2.1 RECEIVER/TRANSMITTER UNIT

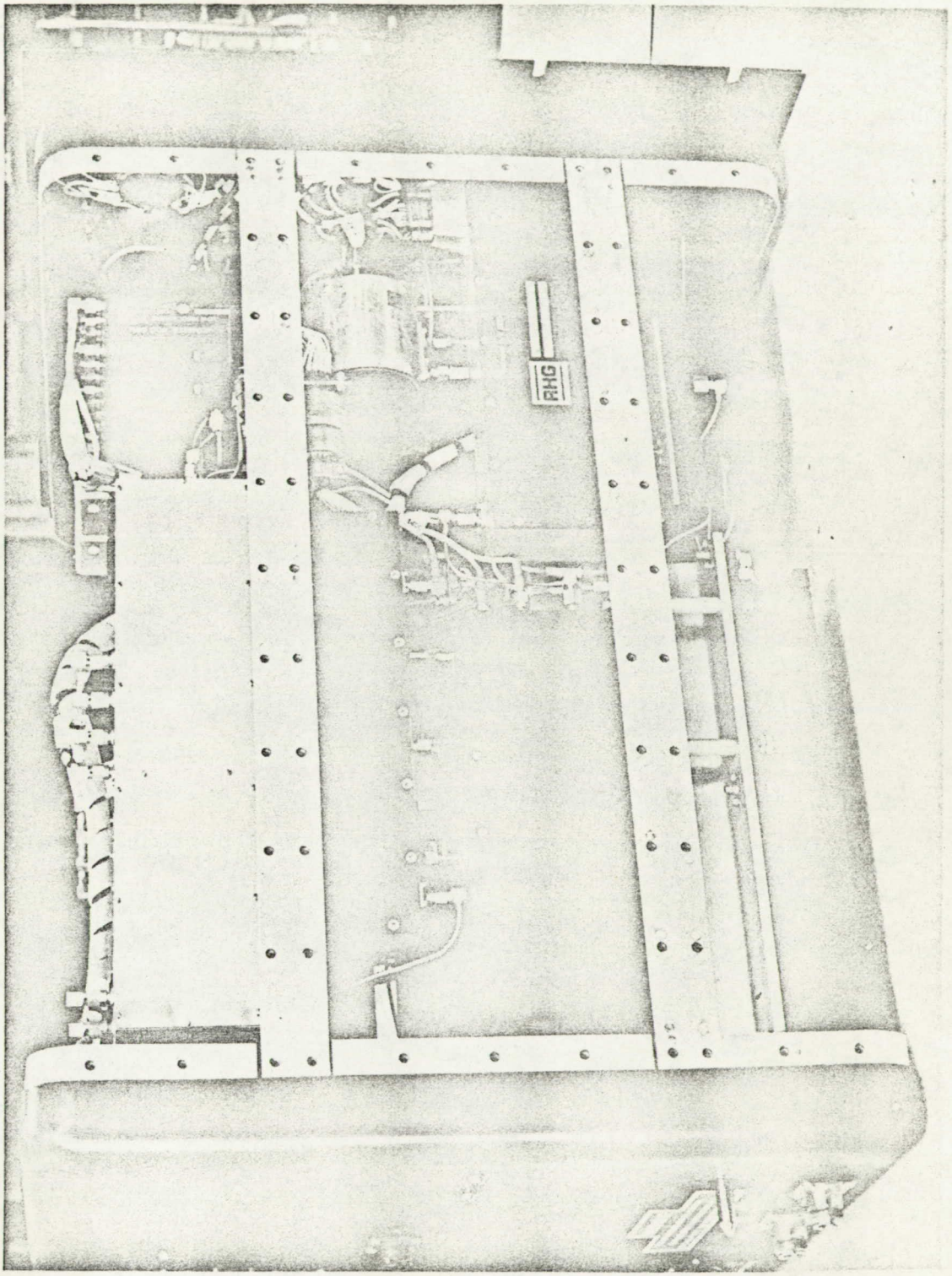

FIGURE 2.2 R/T UNIT, RIGHT SIDE

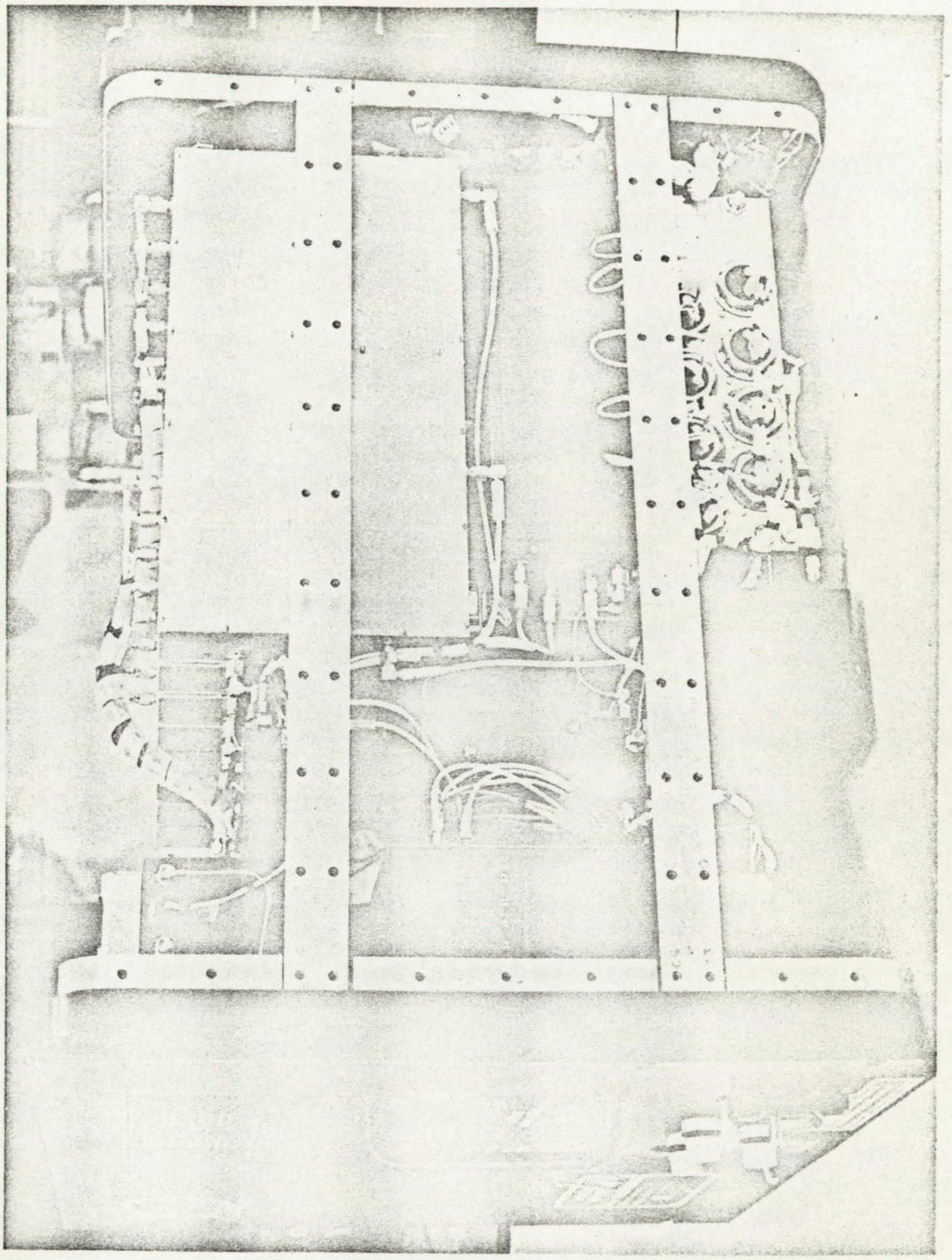

FIGURE 2.3 R/T UNIT, LEFT SIDE

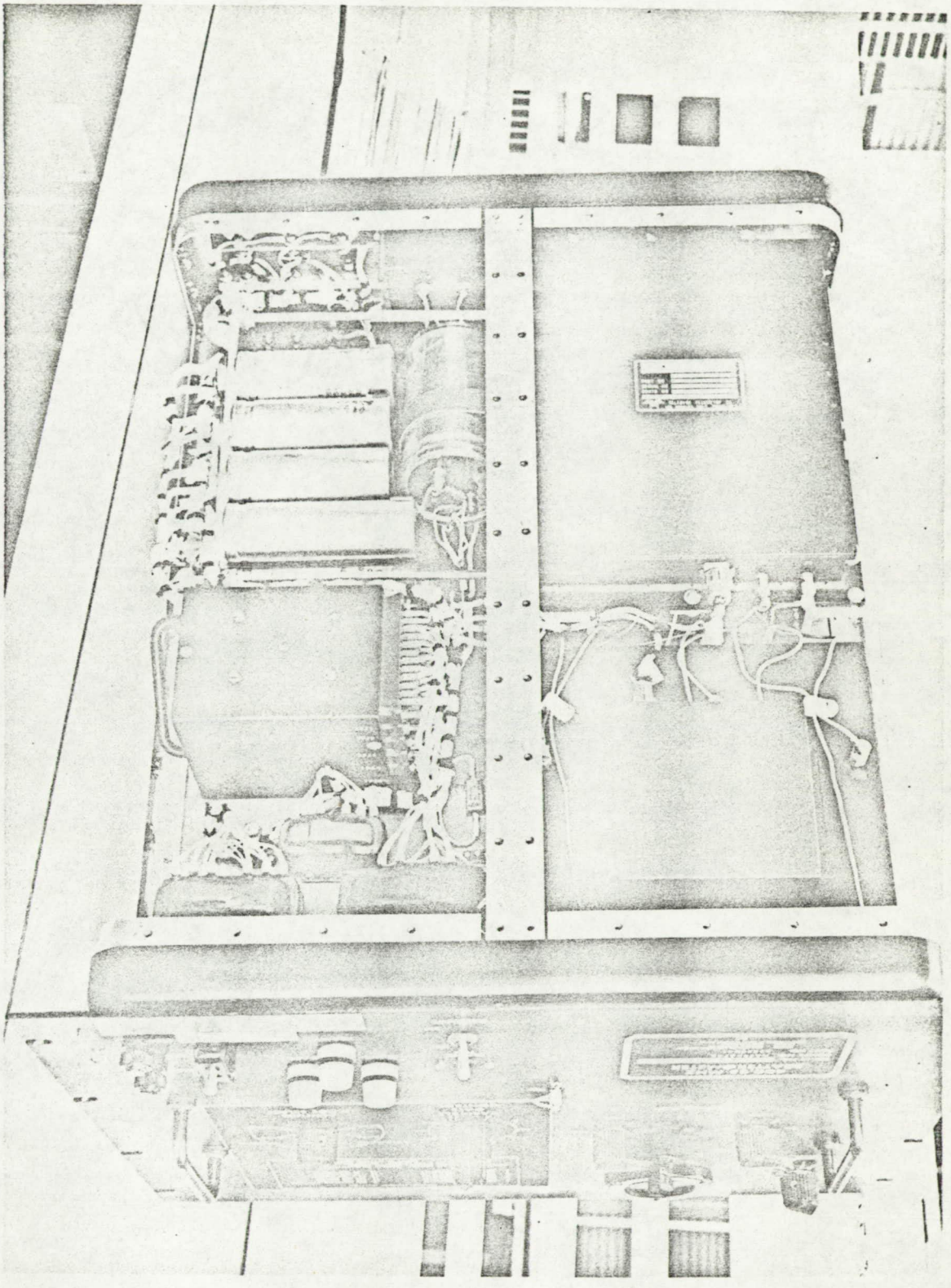

FIGURE 2.4 R/T UNIT, BOTTOM VIEW

The R/T unit has five connectors; the primary power, the signal output, the altimeter, and two RF connectors.

Figure 2.5 shows the R/T unit installed in the P3A aircraft.

2.2.2 ANTENNA

The 400 MHz Scatterometer antenna consists of two separate arrays orthogonal to each other and interspersed on a 35-inch wide ground plane located 2-3/4 inches below the wing over approximately 24.5 feet of the wing and fuselage between the two in-board engine nacelles. There are 12 electrical dipoles for each array in each of two rows with 12 parasitic dipoles of each type between the rows. The radiating arms of the electrical dipoles are approximately 1/2 wave length or 15 inches below the ground plane to help obtain the null at the nadir.

The ground plane consists of six panels, two each of three types. Each panel contains the dipole couplers, dipole receptacles and feed lines for the arrays. The out-board panels have five sets of three dipoles (2 active, one parasitic) and extend from the antenna mount support beam to within about one-foot of the nacelle fairing. The middle panels have four sets of dipoles and are located between the antenna mount beams to within nine inches of the fuselage curvature. The center fuselage panels have three sets of dipoles and are mounted on either side of Butt Line 0.0.

A control box for each array is located in the fuselage and contains the components to form the sum and difference energy feeding the front and rear rows. Coaxial cables connect the control boxes with the R/T unit.

The following is the weight breakdown for the antenna:

48 Active Dipoles	141.0 lbs.
24 Parasitic Dipoles	38.6 lbs.
2 Outboard Panels	106.0 lbs.
2 Middle Panels	90.0 lbs.
2 Fuselage Panels	56.0 lbs.
Total	431.6 lbs.

The control boxes weigh 10.95 lbs. each for a total antenna weight of 453.5 lbs. The antenna, as mounted on the P3A, is shown in Figure 2.6. Figure 2.7 shows the internal components of the control box.

TO BE SUPPLIED AFTER INSTALLATION IN P3A

FIGURE 2.5 R/T UNIT INSTALLED IN P3A AIRCRAFT

TO BE SUPPLIED AFTER ANTENNA INSTALLATION

FIGURE 2.6 400 MHz SCATTEROMETER ANTENNA ON P3A

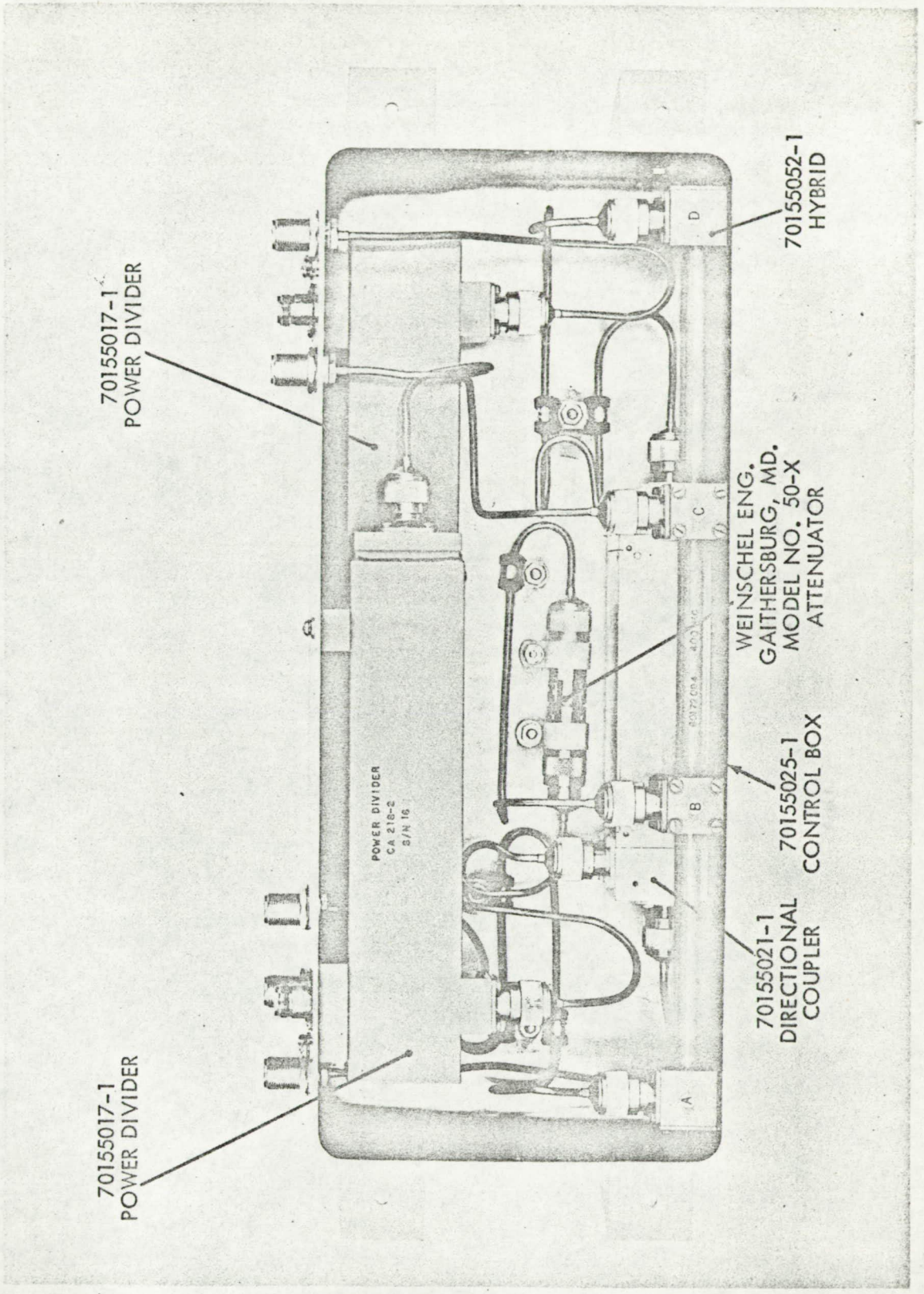

FIGURE 2.7 ARRAY CONTROL BOX

2.3 SCATTEROMETER REQUIREMENTS

2.3.1 DESIGN REQUIREMENTS

The design requirements specified for the system include the following:

Transmitter Frequency - 400.85 $\pm$ 1 MHz

Antenna Coverage -

Along Track - $\pm$ 60 degrees

Cross Track - 6 degrees or less

(one-way 3 db points)

Minimum σ_o - -40 db

2.3.2 OPERATIONAL REQUIREMENTS

The Scatterometer System design must be compatible with the P3A Lockheed "Electra". This requires that the equipment be capable of operating over the altitude range of 1,000 feet to 40,000 feet. The require velocity range is 200 knots nominal and 350 knots maximum. The output data from the Scatterometer is recorded on magnetic tape and the final results obtained by ground processing. The recording equipment is not a part of the Scatterometer System.

2.3.3 DATA REQUIREMENTS

The 400 MHz Scatterometer is required to supply backscatter data suitable for storage on magnetic tape. The data must retain doppler information to provide a means of separating the received power as a function of angle of incidence. The backscatter information includes the signals received from horizontally and vertically polarized antennas. The receivers must provide four outputs which include the following:

Transmit horizontal polarization - receive nontranslated signals in horizontally polarized antenna.

Transmit vertical polarization - receive nontranslated signals in vertically polarized antenna.

Transmit horizontal polarization - receive 90° translated backscatter signals in vertically polarized antenna.

Transmit vertical polarization - receive 90° translated backscatter signals in horizontally polarized antenna.

The output data must be conditioned to be compatible with a Sonex multiplexing unit.

2.3.4 DATA REDUCTION

The data reduction will be done with ground based equipment. The method of determining the backscatter coefficients is covered in detail in Section III of this report.

2.4 SYSTEM DESIGN

2.4.1 MODES OF OPERATION

The 400 MHz Scatterometer System has two modes of operation designated AUTO and MANUAL. Each mode has three overlapping altitude intervals, one of which is selected by the operator. The AUTO mode is the preferred mode of operation since the duty cycle is high and provides maximum signal return, thereby providing the better signal-to-noise ratio. The range intervals provided include the following:

(1-5) K feet
(4-20) K feet
(16-40) K feet

The three altitude intervals were selected to improve the timing accuracy of the system and to improve the signal-to-noise ratio of the backscatter returns.

In the AUTO mode of operation, the pulse recurrence frequency and pulse width are controlled by the altimeter. The pulse width is determined by the radar transit time for nadir signal returns. The pulse width is narrower than the ideal case to allow for altimeter error and for antenna switch switching delays. The antenna switching delays become less significant for the higher altitude ranges, therefore, it is possible to operate the system at a higher duty cycle in these ranges than for the low altitude interval. The interpulse interval is set to provide sufficient time to receive the complete pulse return from targets at θ equal to $\pm 60^{\circ}$ plus additional time for altimeter error.

In the MANUAL mode, the transmission pulse width is established by the lower altitude limit and the interpulse period is determined by the upper altitude limit.

The pulse width - pulse recurrence relationships can be expressed by the following:

AUTO Mode

$$\text{Pulse Width} = \frac{2h}{c}(1-k) - D$$

where h = altitude in feet

c = velocity of propagation

k = error allowance factor

D = delay for antenna switching

$$\text{Time between pulses} = \frac{4h}{c}(1 + k) + D$$

MANUAL Mode

$$\text{Pulse Width} = \frac{2h_1}{c}(1 - k) - D$$

where h_1 = lower altitude limit

$$\text{Time between pulses} = \frac{4h_2}{c}(1 + k) + D$$

where h_2 = higher altitude limit

2.4.2 DYNAMIC RANGE

2.4.2.1 DYNAMIC RANGE REQUIREMENTS

The system dynamic range requirements have been establish to be 121db. This is based on the following contributing factors:

σ_o	65 db
Altitude	32 db
Fading	18 db
Slant Range	6 db
TOTAL	121 db

In addition, it is desirable to obtain data on cross polarized signals and these are expected to be down 7 to 20 db below the nontranslated returns.

The σ_o variation of 65 db was obtained from a report by Dr. R. K. Moore.[1]

2.4.2.2 DYNAMIC RANGE REDUCTION

The dynamic range requirements may be reduced in a variety of ways, however, the following methods are most practical:

---

[1] Radar Cross Section of Terrain Near Vertical Incidence at 415 Mc. 3,800 Mc and Extension of Analysis to X-Band by F. J. Janza, R. K. Moore, B. D. Warner

Antenna Beam Shaping

Separate H and V Receiver

Manual Gain Control

Multiple Channels

Automatic Gain Control

Variable Time Gating

All the above methods are incorporated in the Scatterometer design. Antenna Beam Shaping is used to reduce the signals returned at the nadir and raise the level of the returns at large incidence angles. The ideal pattern would give nearly equal return at all angles. Since the return is a function of terrain, it is not possible to have an ideal antenna pattern for all terrain with a single antenna pattern. Because of the difficulty in obtaining a narrow beam antenna at 400 MHz, the 400 MHz Scatterometer is limited to a single pattern. The shape of the antenna pattern is discussed later in this section.

Separate H and V receivers are used to compensate for differences in reflectivity due to transmitter polarization.

Manual Gain Control is used to compensate for altitude and total reflectivity changes. Each backscatter receiver has 50 db of manual gain control available for operator adjustment.

Multiple Channels on each receiver are used to separate the nontranslated from the 90^{o} translated signals.

Automatic Gain Control is incorporated within each receiver to place the output of each receiver at the proper level for recording and to increase the dynamic range of the receiver. In addition, the gain of each receiver channel has a 40 db laboratory adjustment gain control. This gain is preset to compensate for the expected difference in received signal level. For example, the receivers for the cross polarized signals will be set for higher gains than those receiving the nontranslated signals.

Variable Time Gating has also been incorporated in four channels for selective examination of a range of angles. Time gating attenuation is a function of the position of the variable gates. Since the returns vary in time as a function of incidence angle, it is possible to do selective gating. For example, delaying the leading edge of the receiver gate will result in greater attenuation of nadir returns than those that occur at a later time.

The antenna pattern requirements are obtained by examining the radar range equation:

$$P_R = \frac{P_T \lambda^2 G^2(\theta) \sigma_o(\theta) A(\theta)}{(4\pi)^3 R^4(\theta)} \qquad (1)$$

Where P_R = Received Power

P_T = Effective Transmitter Power

λ = Wavelength

$G(\theta)$ = Antenna Gain

θ = Angle of Incidence

$A(\theta)$ = Area of Resolution Cell

$\sigma_o(\theta)$ = Radar Cross Section of Cell

$R(\theta)$ = Range to Resolution Cell

The above expression can be modified to express the received power in terms of bandwidth, aircraft velocity, and altitude.[1]

$$P_R = \frac{P_T \lambda^3}{2(4\pi)^3} \frac{\Delta f}{Vh^2} \sigma_o(\theta) \int_{-\phi_1}^{+\phi_1} G_T^2 (\psi)_\theta \, d\psi \qquad (2)$$

Where

Δf = Frequency Interval

V = Aircraft Velocity

h = Altitude

The desired condition is to have P_R constant over the total angular coverage. This occurs if the following holds:

$$\sigma_o(\theta) \int_{-\phi_1}^{+\phi_1} G_T^2 (\psi)_\theta \, d\psi = \text{constant}$$

---

[1] Emerson Report No. 2200, 400 MHz Scatterometer Maintenance Manual, Vol. I, Appendix A.

It is apparent that the antenna cannot be optimized for all terrain conditions.

The value of σ_o versus angle may be estimated from the graphs shown in Figure 2.8. These curves were obtained from a report by Dr. R. K. Moore for a transmitter frequency of 415 MHz. The dashed lines are an extrapolation of these curves and the limit line is set by the -40 db limit set for the equipment. The two curves illustrated represent limiting cases for unknown terrain. It is anticipated that curves for all terrain types will be between these limits. These curves are average curves obtained from averaging the results of many data points at the same angle.

Data points from the curves are tabulated in Table 2.1 together with the normalized antenna gains required to produce the desired results.

The initial antenna specifications represent an engineering compromise. The design goal pattern limits are given in Table 2.2.

The actual along track patterns obtained are shown in Figure 2.9 and Figure 2.10.

2.4.3 SIGNAL POWER LEVELS

The expected signal power levels have been calculated and the results are shown in Figure 2.11. The curves are for an altitude of 1,000 feet. The maximum signal level expected is -44.2 dbm and occurs over water. The method of calculating return power is discussed in Appendix B. The points on the curves are for discrete areas. The cell size was taken to be 3^o along track and 5^o cross track. The peak power is obtained by summing the energy received from all the cells

2.4.4 TRANSMITTER REQUIREMENTS

2.4.4.1 POWER LEVEL

The transmitter used in the 400 MHz Scatterometer is a solid state device with a nominal peak power output of 20 watts. The transmitter power level selection was based on a received power calculation for which the following restraints were placed:

a. σ_o - -40db
b. Square Resolution Cell
c. Altitude - 40,000 feet
d. Incidence Angle θ - 60 degrees
e. Signal-to-noise ratio - 30db (design goal)

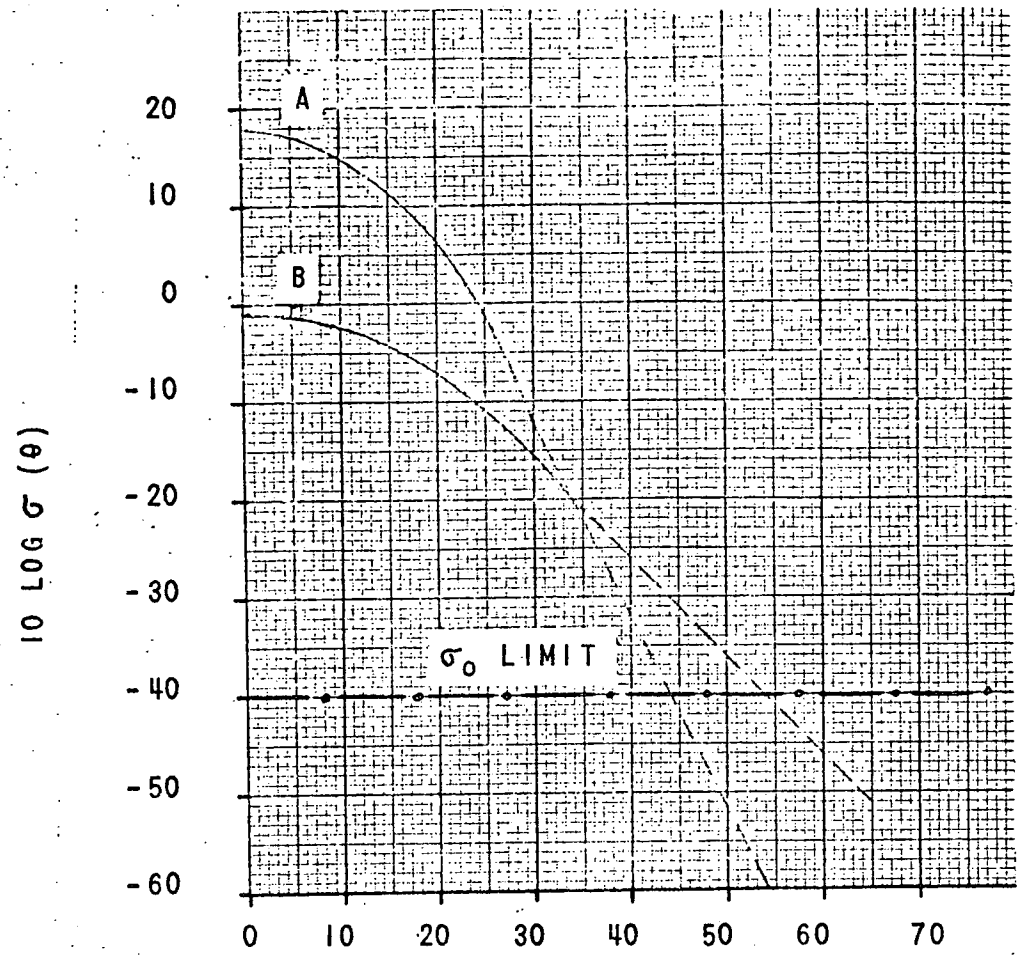

RELATIVE PLOTS OF σ_o VS θ
FOR WATER (A) AND WOODS (B)
FROM REPORT BY DR. R.K. MOORE.
A. WATER LAKE BEMIDJI, MINN.
B. WOODS PINE ISLAND, MINN.
----- EXTRAPOLATION

FIGURE 28

SIZE	CODE IDENT NO.	
A	20418	2236
SCALE	REV	SHEET 2-17

TABLE 2.1

REFLECTIVITY AND ANTENNA GAIN VS ANGLE

	σ_o		$G(\psi)_\theta$ NORMALIZED	
θ	WATER	WOODS	WATER	WOODS
0^o	+18.0db	-1.2db	0.0db	0.0db
5	+17.5	-1.5	.2	.2
10	+15.0	-2.5	1.5	.6
15	+11.5	-4.2	3.2	1.5
20	+6.5	-6.8	5.8	2.8
25	-2.5	-11.0	10.2	4.9
30	-12.5	-16.0	15.2	7.4
35	-22.0	-21.0	20.0	9.9
40	-32.0	-26.0	25.0	12.4
45	-42.0	-31.0	30.0	14.9
50	-52.0	-36.0	35.0	17.4
55	-62.0	-41.0	40.0	19.9
60	-72.0	-46.0	45.0	22.4

TABLE 2.2

ANTENNA SPECIFICATIONS

(DESIGN GOAL)

VSWR Less than 1.2 at R.F. Terminals

GAIN (One Way)
17 db minimum at plus and minus 60° from nadir in fore and aft directions.

SIDE LOBES One way side lobe level should be at least 10 db less than main beam at all along track angles.

PATTERN SHAPE Both horizontal and vertical polarization

ANGLE	MINIMUM	MAXIMUM
0	-28.6 db	-22.6
±5	-27.8	-21.8
±10	-27.1	-21.1
±15	-25.4	-19.4
±20	-22.7	-16.7
±25	-18.7	-12.7
±30	-16.1	-10.1
±35	-13.1	- 7.1
±40	-10.0	- 4.0
±45	- 7.6	- 1.6
±50	- 5.1	+ 0.9
±55	- 2.6	+ 3.4
±60	0	+ 6.0

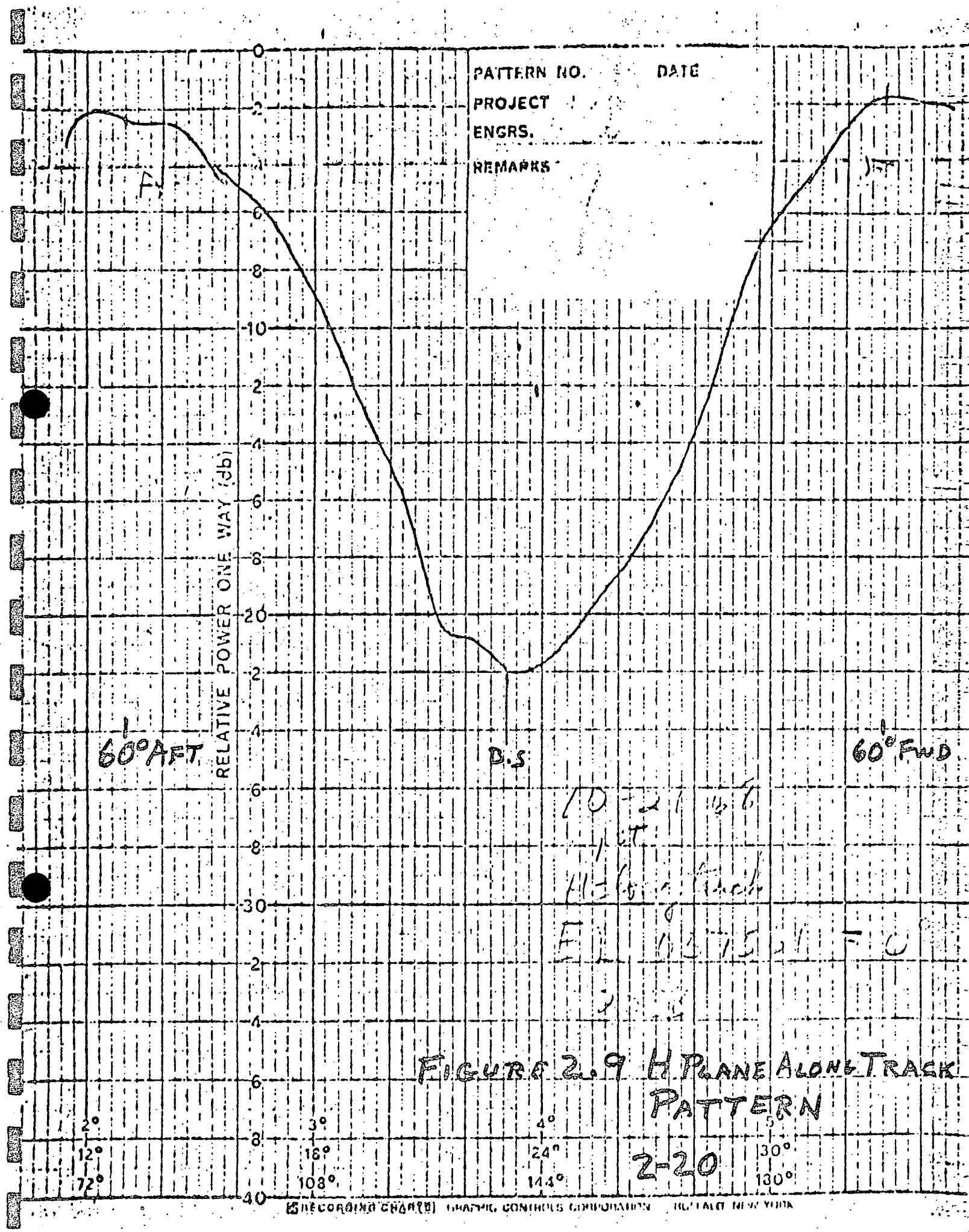

FIGURE 2.9 H PLANE ALONG TRACK PATTERN

2-20

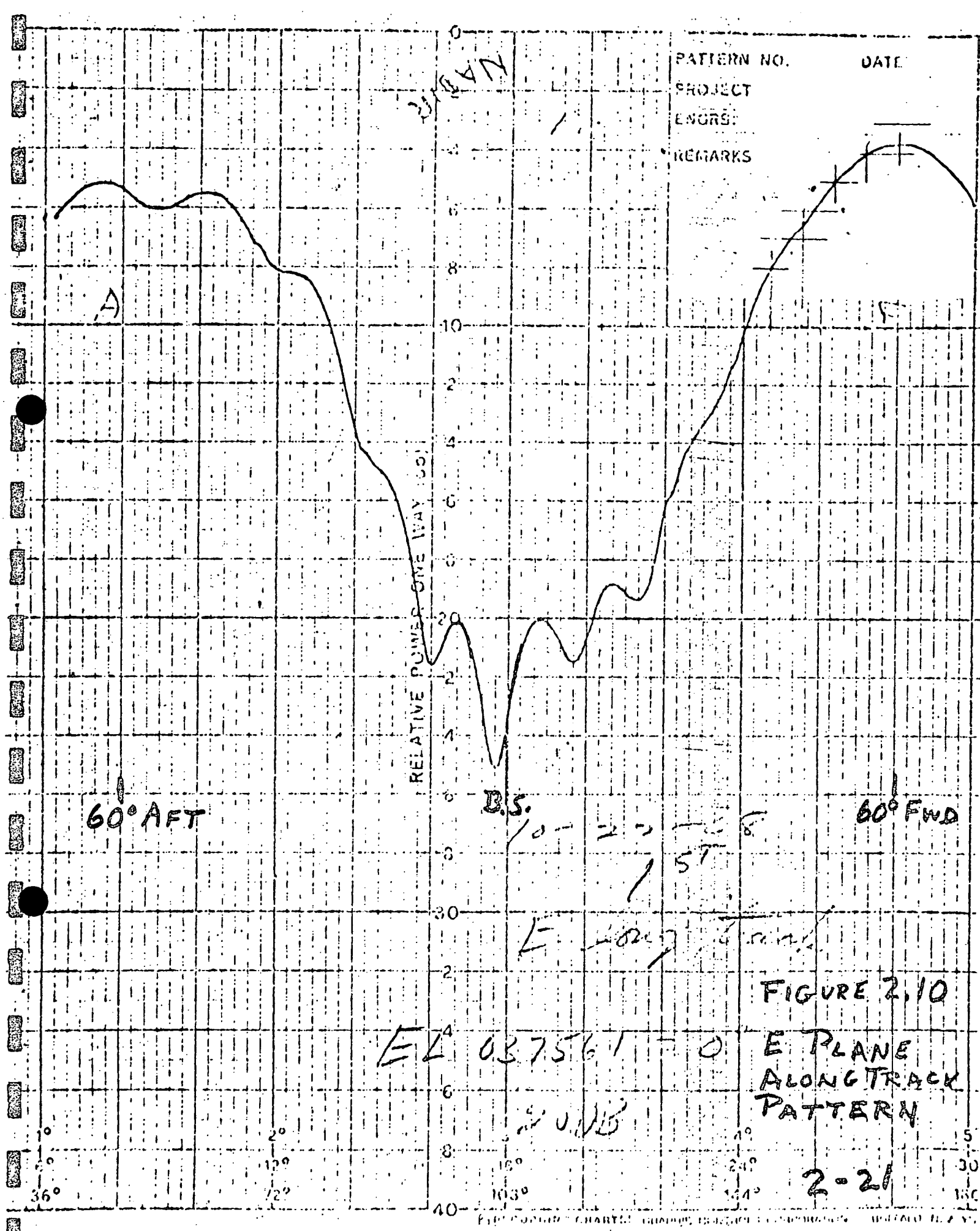

FIGURE 2.10
E PLANE ALONG TRACK PATTERN

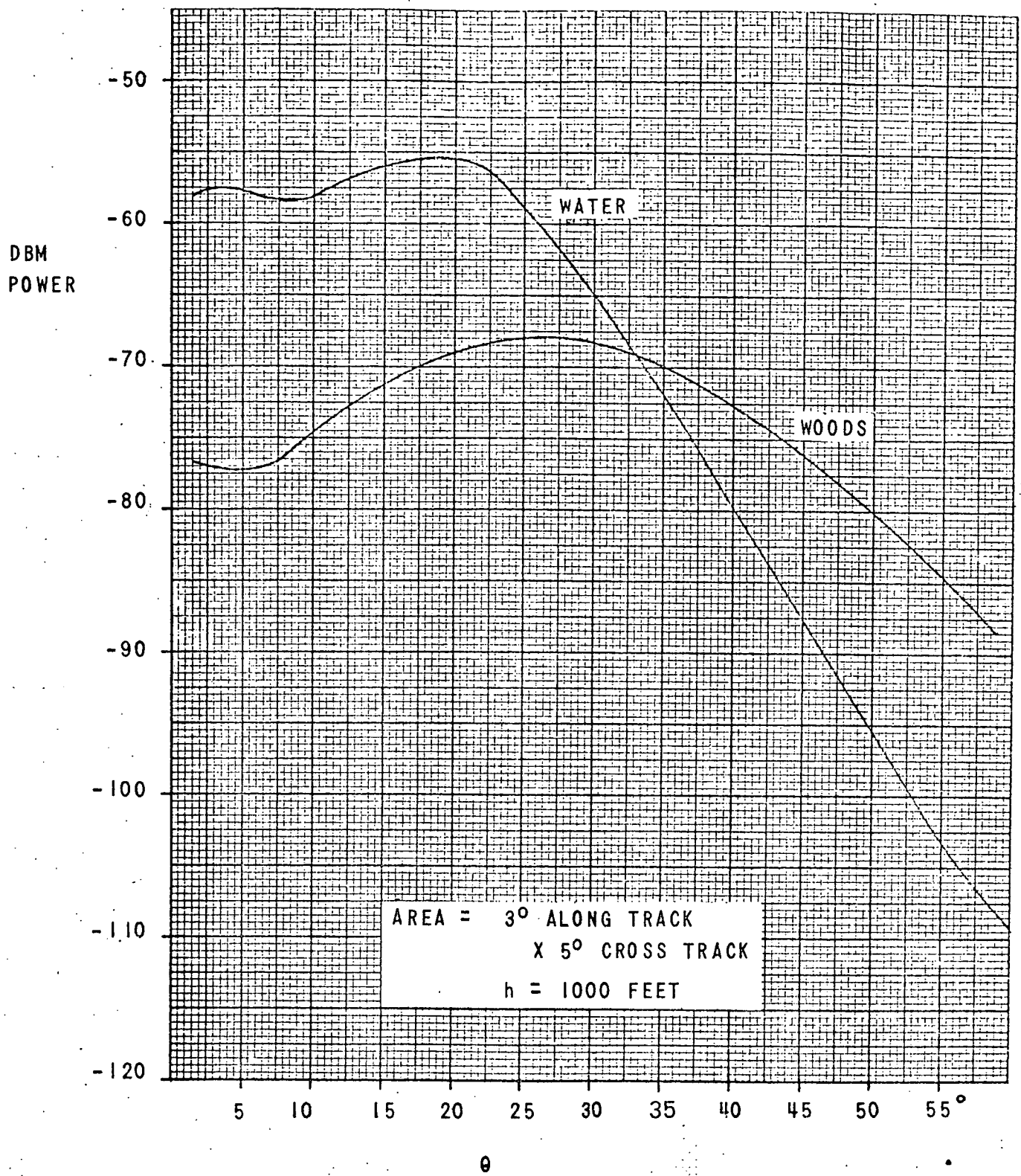

FIGURE 2.11 RECEIVED POWER VS θ

SIZE	CODE IDENT NO.	
A	20418	2236
SCALE	REV	SHEET 2 - 22

SD FORM 481-2 AUG 64 (2C)

The received power can be expressed as:

$$P_R = \frac{P_T \lambda^2}{(4\pi)^3} \quad \frac{G^2(\theta) \; A(\theta) \; \sigma_o(\theta)}{R^4(\theta)}$$

The above can be expressed in terms of altitude by the following expression for a square cell:

$$P_R = \frac{P_T \lambda^2}{(4\pi)^3} \quad \frac{G^2(\theta) \; \sigma_o(\theta) \; (\psi)^2 \cos^2(\theta)}{h^2}$$

Where

h = Altitude in feet

ψ = Cross Track Angle

An RF power summary is given in Table 2.3 for the conditions listed above. The data listed are measured values and the expected signal-to-noise ratio under the conditions specified is less than 3 db short of the design goal of 30 db.

2.4.4.2 OUTPUT PULSE RISE TIME

A finite rise time on the output pulse will give negligible error on the backscatter measurement because the rise time will affect both the transmitted and received signals in the same manner. However, a finite rise time does represent a loss in power. This loss will be most pronounced at the lowest altitudes where the pulse width is shortest. The loss due to finite rise time is given by:

$$L_{t_r} = \frac{tr}{2PW}$$

Assuming symmetrical and equal rise and fall times, the total loss would double.

$$\text{Total} = L_{t_r} = \frac{tr}{PW}$$

Solving for the rise time which gives a one db loss using the shortest pulse width gives a value of 270 nanoseconds. This loss occurs at the lowest altitude where the altitude loss is a minimum. The transmitter has a rise and fall time of less than 200 nanoseconds.

TABLE 2.3

SCATTEROMETER SYSTEM RF POWER SUMMARY

RADIATED POWER	Output of Power Amplifier	+43 dbm
	Antenna Switch Loss	-.7 db
	Antenna Feed Line Loss (30 ft)	-1.3 db
	Antenna VSWR (<1.5)	-.2 db
	Filter Loss	-1.0 db
	Radiated Peak Power	39.8 dbm
PROPAGATION CONSTANT	λ^2 (2.5 ft.)	+8.0 db
	G^2 (60°)	29.0 db
	$(1/4\pi)^3$	-33.0 db
	$(1/h)^2$ (40,000 ft.)	-92.0 db
	σ_o (θ) (minimum requirement)	-40.0 db
	$\cos^2(\theta)$ (at 60°)	- 6.0 db
	$(\psi)^2 - (3^{o2}) - (52 \times 10^{-3})^2$	-25.6 db
		-159.6 db
RECEIVED POWER	Received Power at Antenna Terminals	-119.8 dbm
	Antenna Feed Line Loss	-1.3 db
	Received Power at R/T Unit Terminals	-121.1 dbm
	Power in Central Spectral Line (.15 Duty)	-137.6 dbm
RECEIVER NOISE	Receiver Noise Figure	5.4 db
	KT	-174.0 dbm/cycle
	B.W. (Resolution Cell for 350 knots) 6.17 cycles	7.9 db
	Receiver Noise Reduction Due to Gating	-4.5 db
	Receiver Noise Power	-165.2 dbm
	Signal to Noise Ratio	27.6 db

2.4.4.3 OUTPUT PULSE JITTER

This calculation provides estimates for the effect of pulse position and pulse width modulation on the scatterometer measurements. Two kinds of modulation are assumed: deterministic, due to sinusoidal modulation at specific frequencies; and random, due to modulation by a spectrum of frequencies. The following results are obtained:

a) Single-edge pulse width modulation - if the rms jitter due to noise is less than 20 nanoseconds on a 2 microsecond pulse, the power measurement will be less than 1% in error for any 10 cps band in the spectrum.

b) Pulse position jitter - Jitter of the order of 20 nanoseconds (either peak due to deterministic signals or rms due to random signals) will cause negligible measurement error.

The above estimates are "worst case" under the assumption that all interfering signals are 30 db higher than the true signal. A more extensive analysis would be required to get more precise estimates. However, a worst case estimate suffices for establishing specifications.

Random Modulation - The equations used for determining the effects of random jitter are: (1)

a) for pulse width jitter

$$P_r = \frac{\sigma_\tau^2}{\tau^2} \quad \frac{\Delta f}{fr} \qquad (1)$$

b) for pulse position jitter

$$P_r = \sigma_\tau^2 \ \omega^2 \quad \frac{\Delta f}{fr} \qquad (2)$$

Equation (1) is the ratio of the noise power in a bandwidth Δf to the power in the central spectral line, where f_r is the pulse recurrence frequency, σ_τ is the single-edge, rms width jitter, and τ is the pulse width. Equation (2) is the ratio of the noise power in a bandwidth Δf to the power in the central spectral line, where ω is the center of the band being considered, σ_τ is the rms position jitter, and all other quantities are defined as in equation (1).

---

1 Stable Transmitter Study, HDL Report No. 2146, Harry Diamond Laboratories, Washington, D.C.

As an example, let:

$$\sigma_\tau = 20 \text{ nanoseconds}$$
$$\tau = 2 \text{ usec}$$
$$\Delta f = 10 \text{ cps}$$
$$fr = 83.3 \times 10^3 \text{ pps}$$

By the use of these values and Equation (1), the power ratio due to random width jitter is -79.2 db. If the bandwidth of the signal spectrum is 100 cps, then all frequencies within a 1,000 cps band will interfere in a given filter. Thus, the total noise power will be -49.2 db relative to the signal power. If all the interfering signals are 30 db higher than the true signal component in a given filter, (this is our worst case assumption, and is obviously not realistic) the total interfering noise power would be -19.2 db relative to the signal. This causes approximately a 1.2% error in the power measurement. It is safe to say that 20 nanoseconds rms width jitter would cause less than 1% error in the actual case.

The total interfering power due to pulse position jitter can be obtained by integrating equation (2) over the total signal spectrum. Assuming the same numbers used above for width jitter, (and the same worse case situation) the total interfering power due to 20 nanoseconds width jitter is approximately -60 db relative to the signal.

Deterministic Modulation - In this case the two pertinent equations are:[2]

a) for pulse width jitter

$$P_r = \frac{\varepsilon^2}{\tau 2} \qquad (3)$$

b) for pulse position jitter

$$P_r = \omega^2 \varepsilon^2 \qquad (4)$$

Equations 3 and 4 are the power in an interfering sideband relative to the signal power, where ε is the peak jitter, τ is the pulse width and ω is the modulation frequency. It can be seen that Equations 3 and 4 are very similar to 1 and 2 except that random modulations distributes the interfering power among a band of frequencies.

---

[2] N. Wallace, "Spectra of Sinusoidal Pulse Position and Pulse Width Modulation", Emerson Memo MR-120-37, November 28, 1961.

Assume $\mathcal{E}$ = 2 nanoseconds, τ = 2 usec. Then Equation (3) yields an interfering power -60 db relative to the signal. Interfering signals, which differ from the signal being measured by the interference frequency pulse or minus 5 cycles, will be present in a 10 cycle filter bandwidth. If, in addition, we again assume that the interfering signals are 30 db higher than the true signal, the total interfering power will be -20 db relative to the signal power. This will cause a 1% measurement error.

Deterministic pulse position jitter is a small problem compared to width jitter. For example, the total worst case interfering power due to 400 cycle, 20 nanosecond peak position modulation is -60 db relative to the signal power.

2.4.4.4 FREQUENCY STABILITY

In data processing, a return at a given angle is identified by the doppler frequency. The power reflected from a ground cell subtended by a given angle increment is measured for a narrow band of frequencies determined by the angle limits of the increment. In order to maintain the accuracy of the data for very large changes in reflectivity between adjacent angle increments, it is necessary to use a transmitter with a very low spectral density adjacent to the carrier frequency or cancellation techniques.

The system uses a cancellation technique to relax the spectral density requirements of the transmitter. As an illustration of the technique, consider a frequency modulation carrier which is modulated by a single sine wave. The transmitter output is given by:

$$e(t) = E \sin \left(2 \pi f_o t + \frac{\Delta f}{f_m} \sin w_m t\right) \qquad (1)$$

The wave reflected from a ground cell at the nadir (0 doppler) is given by:

$$e_d = A \sin \left[2 \pi f_o (t-d) + \frac{\Delta f}{f_m} \sin w_m (t-d) \right] \qquad (2)$$

where d is the time delay.

If this signal is mixed with an LO signal which has the same modulation as the transmitted signal, the difference signal is given by:

$$e_{if} = B \sin \left[2 \pi f_{if} t - 2 \pi f_o d + \frac{\Delta f}{f_m} (\sin w_m (t-d) - \sin w_m t) \right] \qquad (3)$$

Using trig identities, it is possible to expand the term

$$\frac{\Delta f}{f_m} \left[\sin w_m (t-d) - \sin w_m t \right] \qquad (4)$$

into

$$\frac{\Delta f}{f_m} \left[-2 \sin \frac{w_m d}{2} \cos w_m \frac{(t-d)}{2} \right] \qquad (5)$$

This term represents frequency modulation at the same frequency as in the transmitted signal with an added phase shift and a new modulation index.

$$2 \frac{\Delta f}{f_m} \sin w_m \frac{d}{2} \qquad (6)$$

And is a function of time delay in transmit.

For small phase deviations, the ratio of the power in the sideband to the power in the carrier is given by:

$$\frac{P_{sb}}{P_c} = 1/4 \; M^2 \qquad (7)$$

where M is the modulation index.

The transmitted signal has a modulation index of $\Delta f/f_m$ and the IF signal has a modulation index

$$\frac{\Delta f}{f_m} \left(2 \sin \frac{w_m d}{2}\right) \qquad (8)$$

The ratio of the power in the sideband at IF to the power in the sideband of the transmitted signal is given by:

$$\frac{P_{if}}{P_{sb}} = \left(2 \sin \frac{w_m d}{2}\right)^2 \qquad (9)$$

This ratio has a maximum value of 4 when $W_m d = N \pi$ and a value of $(W_m d)^2$ for small values of $W_m d$.

The maximum time delay (40 K ft. altitude, $\pm 60^{\circ}$) for the scatterometer is equal to 160 microseconds. At all modulating frequencies below 1 KC, this technique introduces an improvement in the IF spectrum. Above 2 KC the improvement varies between a degradation of 6 db and infinite improvement. Since the close-in spectral density is of prime concern in the scatterometer and the spectral density far removed from the oscillator frequency is generally very low in a stable oscillator, this method of obtaining improvement is well suited for the scatterometer.

2.4.4.5 TRANSMITTER PERFORMANCE SPECIFICATIONS

The following requirements are specified for the 400 MHz transmitter.

Power Requirement - 20 watts peak (minimum)

Frequency Stability -

Long Term drift - 1.2 KHz per year maximum.

Short Term drift - 8 Hz maximum

Temperature (Steady State) $\pm$ .8 KHz over the temperature range of 0° C to $+60^{\circ}$ C

Transient Temperature - $\pm$.2 KHz over a temperature range of 0° to $+60^{\circ}$ C at a rate of change of 2°C per minute.

Spectral Purity: The power spectral density shall be down at least 55 db with respect to the carrier frequency for all frequencies displaced from the center frequency by more than 40 Hz and down by more than 90 db at frequencies displaced from the center frequency greater than 1 KHz as measured in a one Hz bandwidth. The specified db levels are single sideband signal to phase noise.

Pulse Rise Time - The rise time measured from the 10 to 90% points shall be less than 100 nanoseconds.

Pulse Fall Time - The fall time measured from 10 to 90% points shall be less than 100 nanoseconds.

Modulation Time Delay Variation - The modulation time delay shall not vary more than $\pm$ 20 nanoseconds from a fixed value.

The method of measuring spectral purity and test results of the transmitter are included in Appendix A of this report.

2.4.5 SIGNAL CHANNEL RECEIVER DESIGN

2.4.5.1 RECEIVER REQUIREMENTS

The receivers used in the 400 MHz Scatterometer must process the received backscatter signals and convert them to levels suitable for magnetic tape recording. Particular attention has been given to the following:

Transmitter-to-receiver Isolation
Dynamic Range
Channel Crosstalk
Signal-to-noise Ratios

2.4.5.2 FUNCTIONAL DESCRIPTION

The horizontal and vertical receivers are identical and interchangeable; hence, the following discussion applies to both receivers. In each receiver, triple conversion translates the received spectrum to a center frequency of 500 hertz for recording by a Sonex Multiplexer and AR 1600 recorder. The three intermediate frequencies selected for the receiver are:

1st IF	60 MHz
2nd IF	5 MHz
3rd IF	500 Hz

The final output from each receiver retains the central spectral line of the received signal. The filtering which selects the central spectral line occurs before the final frequency conversion. This is done to prevent spectrum foldover.

The receiver is functionally divided into three sections; Receiver-Amplifier, IF Switch and Post IF Receivers. A block diagram of the receivers is shown in Figure 2.12.

The Receiver-Amplifier section amplifies and translates the received pulse signal to a center frequency of 60 MHz. Each of the four channels of the horizontal (or vertical) receiver obtain a signal from this amplifier by way of the IF switch.

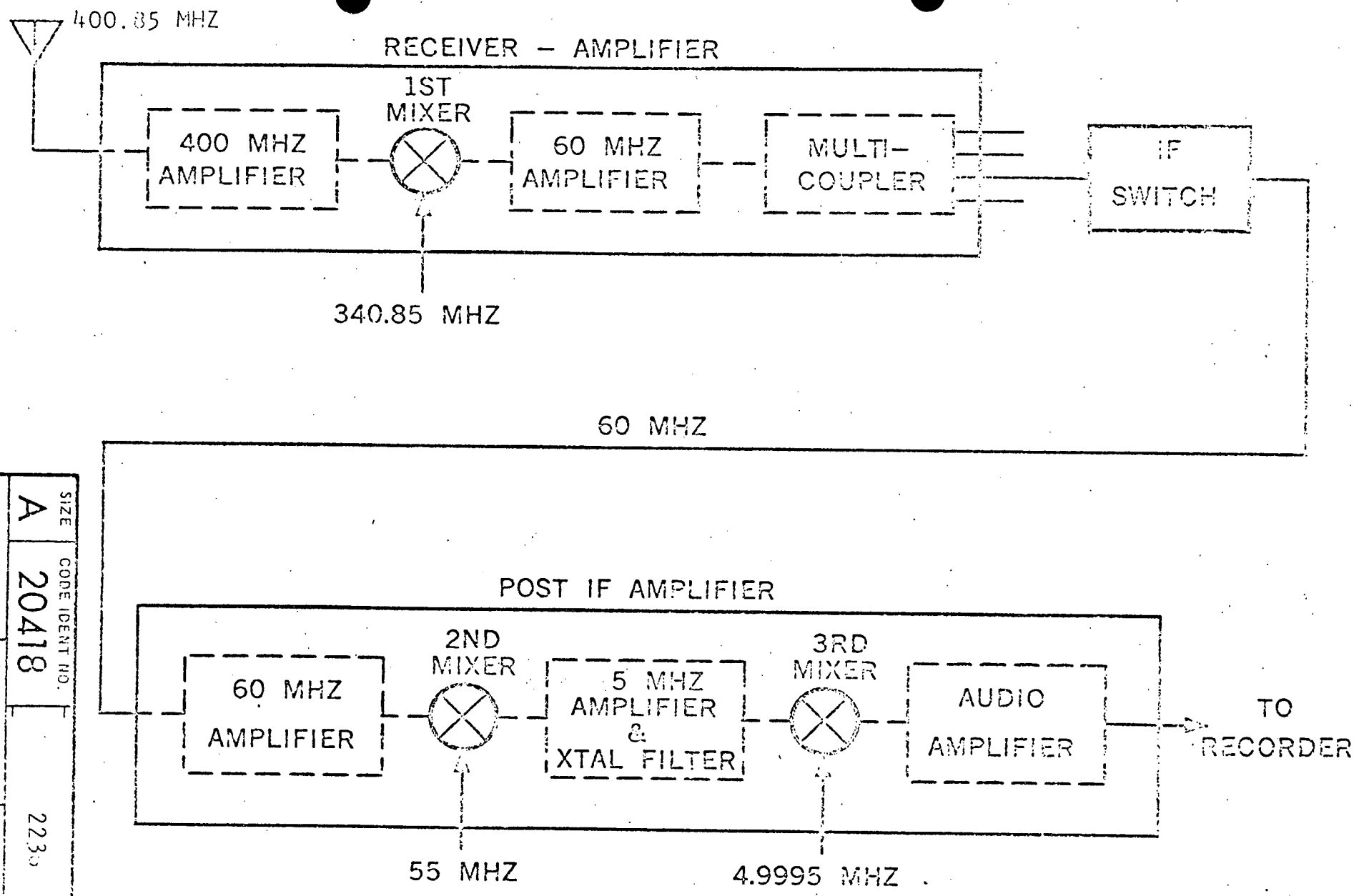

FIGURE 2.12 BLOCK DIAGRAM – 400 MHZ SCATTEROMETER RECEIVER

The IF switch section consists of four solid-state switches (8 total) which are opened and closed by signals from the synchronizer. These switches route the horizontal (vertical) backscatter returns to the proper channel.

The outputs of the IF switch section are coupled to four identical Post IF receivers. The signal at the input to a Post IF Amplifier is at the 1st intermediate frequency of 60 MHz. The signal is amplified and translated to 5 MHz before filtering by a narrow band crystal filter. The filter removes that portion of the spectrum due to the pulse modulation of the transmitter, leaving the carrier component (a continuous signal) which is proportional to the peak pulse power of the backscatter signal. The 5 MHz signal is translated to 500 hertz by the third mixer. The output from the mixer is amplified and combined with a DC offset voltage for recording.

2.4.5.3 DOPPLER SIGNAL AT 400.85 MHz

The doppler shift in the signal return is given by the following expression:

$$f_D = \frac{103V}{\lambda} \sin \theta \text{ hertz}$$

where V is in knots

λ is wavelength in centimeters

θ is the angle of incidence

The doppler range as a function of velocity is given in Table 2.4

TABLE 2.4
DOPPLER VS VELOCITY

AIRCRAFT VELOCITY		HERTZ MAXIMUM
KNOTS	FT/SEC	DOPPLER AT 60°
100	169	119
125	211	149
150	253	179
175	295	208
200	338	238
225	380	268
250	422	298
275	464	327
300	506	357
325	549	387
350	591	417
375	633	446

The maximum doppler returns that must be processed by the 400 MHz Scatterometer are ±417 hertz which occur at an aircraft velocity of 350 knots.

2.4.5.4 SIGNAL SPECTRA IN THE SCATTEROMETER SYSTEM

The Fourier development of an infinite pulse train is given by:[1]

$$F(t) = \sum_{n=0}^{\infty} \frac{2-\delta_{n,0}}{2} \frac{\sin \pi n \tau fr}{\pi m} [\sin 2\pi(f_o + nf_r)t + \sin 2\pi(f_o - nf_r)t]$$

where f_o = carrier frequency

fr = pulse recurrence frequency

$\delta_{n,0}$ = 1 when n = o, otherwise it equals zero

τ = pulse length

A typical spectra is illustrated in Figure 2.13.

The special components of the transmitted pulse, of a typical signal, and of the calibrate tone are illustrated in Figure 2.14. Illustrated are the spectral components at various stages in the receiver system. Each receiver sees two waveforms; that returned from every other pulse when the transmit polarization is the same as the receiver (and its associated antenna) and another waveform when the transmit polarization is orthogonal. Since the returns from the two transmit polarizations are each at a prf of 2000 (and do not cancel because their amplitudes are different) the spectral bands would be spaced by 2000 Hz.

The shape of the narrow band filter is given in Fig. 2.15. Illustrated is the attenuation of possible interfering signals. The lowest PRF used in the Scatterometer is 3.9 KHz. This is the PRF for an altitude of 40,000 ft. in the AUTO mode of operation. A possible signal energy distribution is shown in Fig. 2.15. The signal PRF lines are separated by a frequency of 1.95 KHz since any one receiver is only turned on following alternate transmitter pulses. From the filter characteristics and spectral data, it is evident that the PRF line components will be attenuated in excess of 30db. The foldover signals will not degrade system performance. In addition, the foldover signals will be greater than one kilohertz with the exception of the lower PRF line of the calibrate tone. This will foldover to 950 hertz but its amplitude will be 30 db below the calibrate tone. At lower altitudes, the PRF lines are further apart, i.e. higher pulse recurrence frequency, resulting in even greater attenuation of the PRF line components.

2.4.5.5 RECEIVER NOISE FIGURE

The receiver noise figure is established with reference to Figure 2.16. The overall noise figure of a cascaded system is given by the following:

---

[1] Threshold Signals, Lawson-Uhlenbeck, Vol. 24 MIT, Radiation Laboratory Series, McGraw-Hill, Page 18.

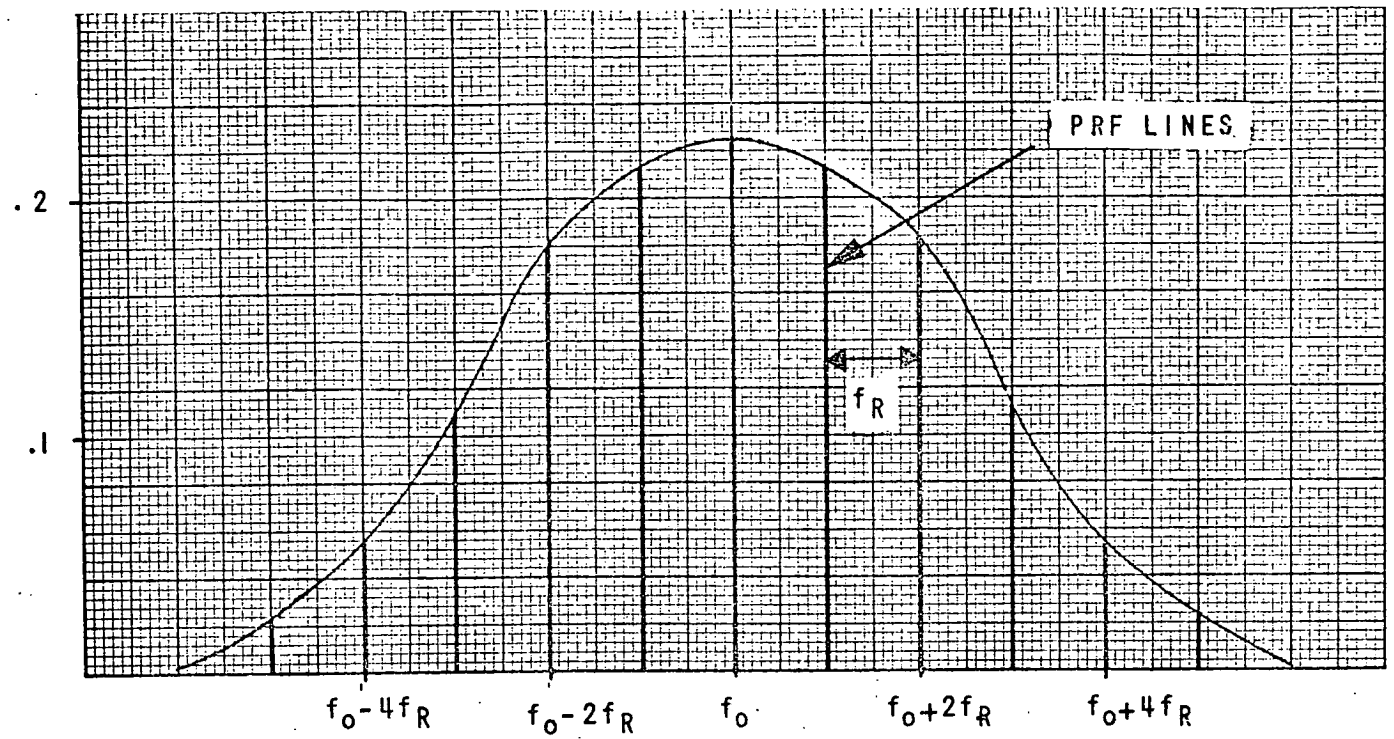

f_o - CARRIER FREQUENCY
f_R - PULSE RECURRENCE FREQUENCY
DUTY RATIO - .15

FIGURE 2.13 TYPICAL PULSE SPECTRA

SIZE	CODE IDENT NO.	
A	20418	2236
SCALE	REV	SHEET 2-34

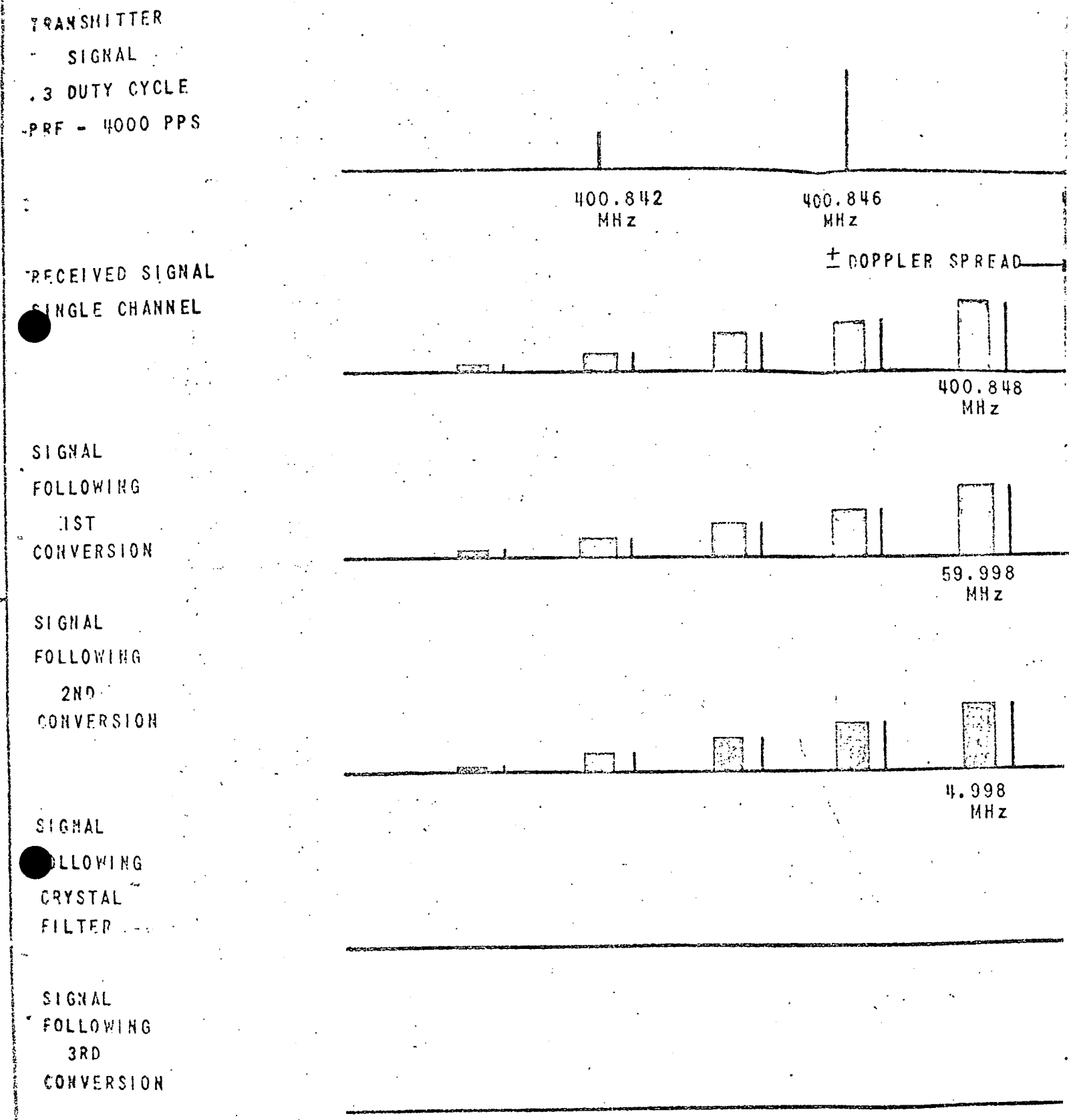

FIGURE 2.14 SCATTEROMETER SIGNAL SPECTRA

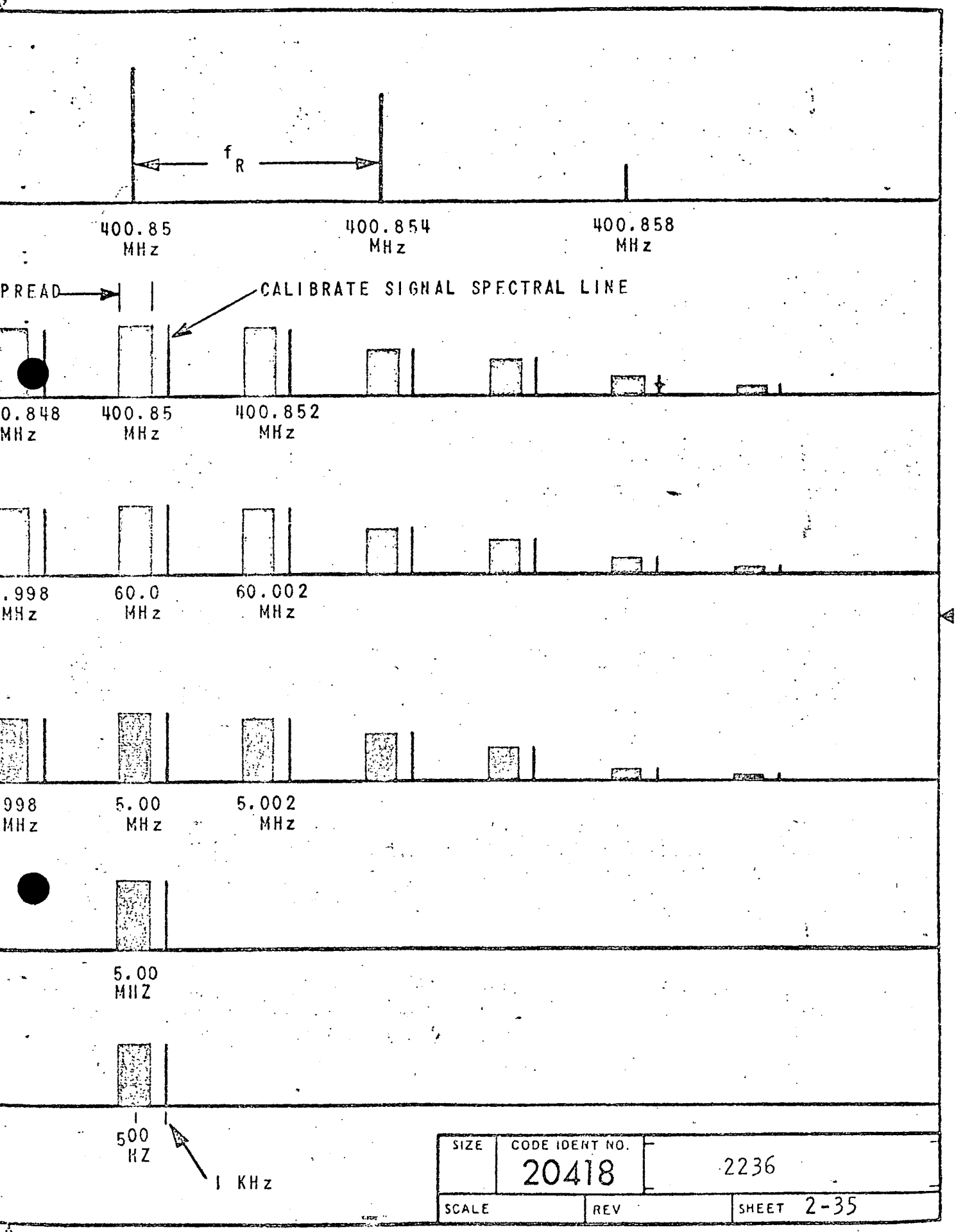

SIZE	CODE IDENT NO.	2236
	20418	
SCALE	REV	SHEET 2-35

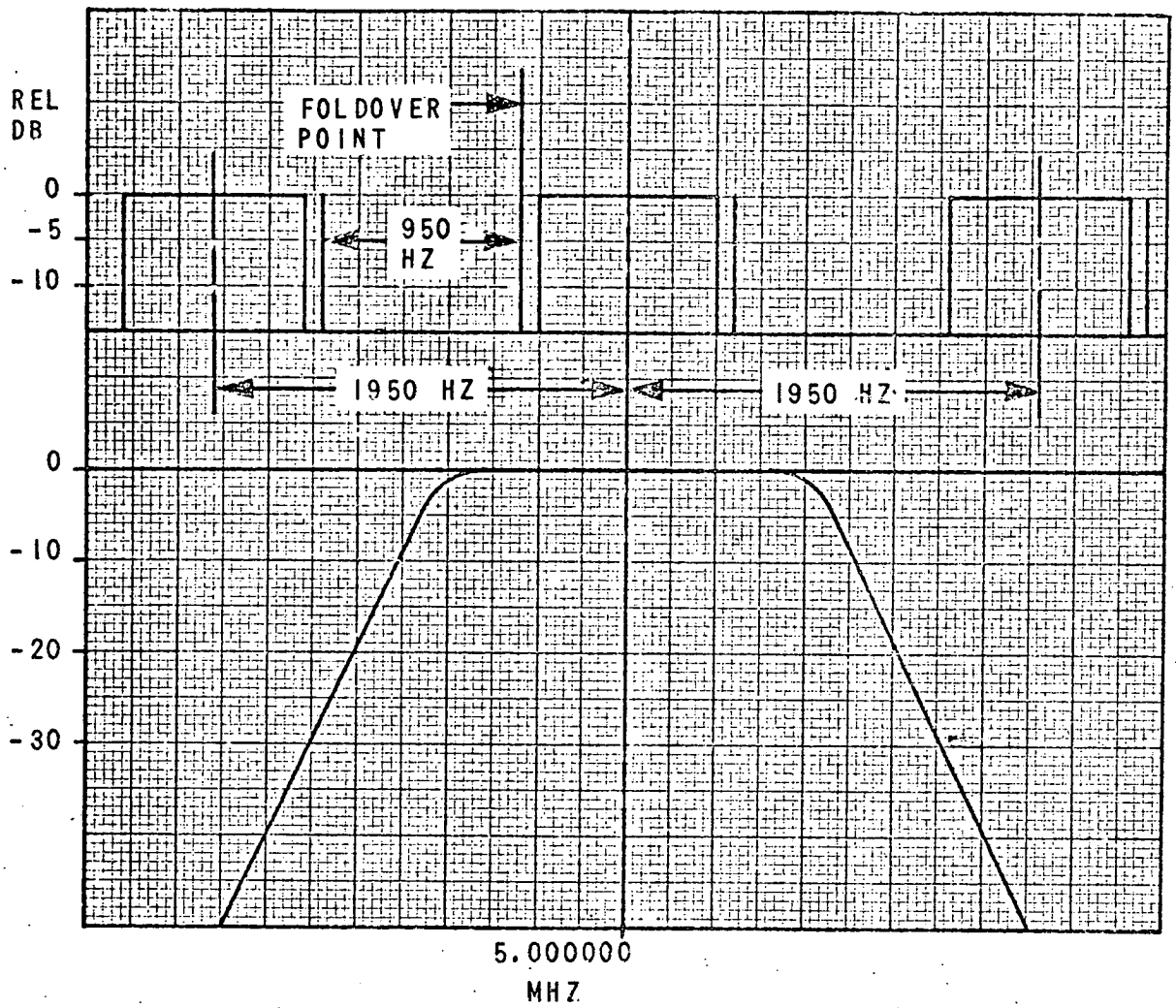

FIGURE 2.15 IF PASSBAND FILTER CHARACTERISTICS

SIZE	CODE IDENT NO.	
A	20418	2236
SCALE	REV	SHEET 2-36

SD FORM 481-2 AUG 64 (2C)

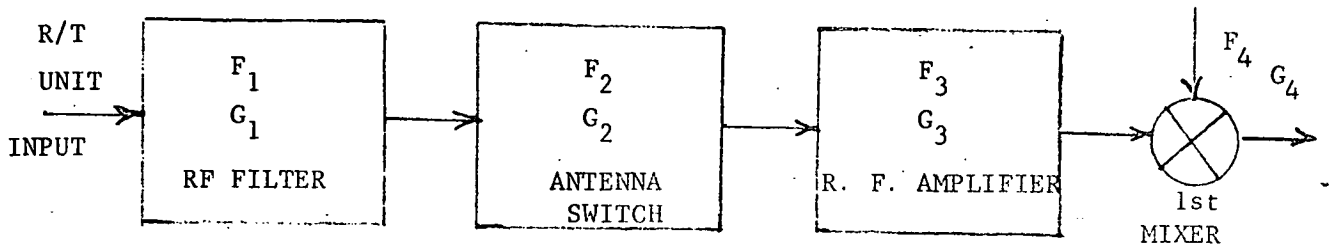

FIGURE 2.16 RECEIVER NOISE FIGURE

$$F_{overall} = F_1 + \frac{F_2-1}{G_1} + \frac{F_3-1}{G_2} + \frac{F_4-1}{G_3}$$

The measured values for the quantities involved are the following:

$$F_1 = 1.0 \text{ db}, \quad F_2 = .7 \text{ db}, \quad F_3 = 3.7 \text{ db}, \quad F_4 = 10 \text{ db}$$

$$G_1 = -1.0 \text{ db}, \quad G_2 = .7 \text{ db}, \quad G_3 = 27 \text{ db}$$

Using these values, the overall noise figure is 5.14 db.

2.4.5.6 TRANSMITTER-TO-RECEIVER ISOLATION DURING TRANSMISSION

During the transmission of energy, it is essential that precautions be taken to prevent excessive leakage of the transmitted signal into the receiving channels. Any leakage that does occur appears as a signal at 500 hertz which is equivalent to energy having zero doppler or from the nadir returns.

In the 400 MHz Scatterometer system isolation is obtained by using the antenna switch, by gating the first local oscillator signal and by gating the IF signal. A block diagram of these circuits is given in Figure 2.17.

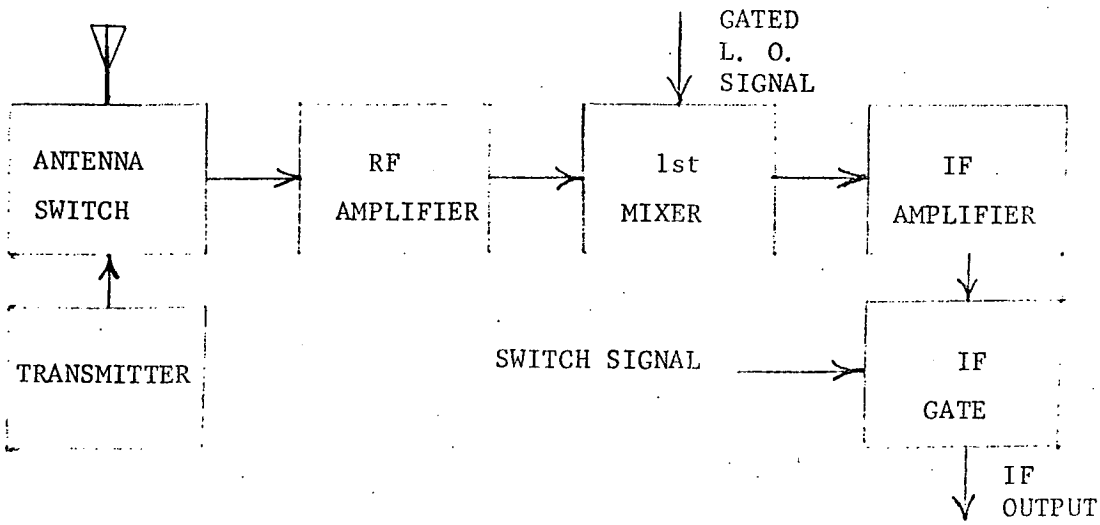

FIGURE 2.17 BLOCK DIAGRAM - TRANSMITTER-RECEIVER ISOLATION

Typical measured values of isolations are given below:

Antenna Switch	-80 db
IF Switch	-70 db
Mixer Rejection	-50 db
	-200 db

The transmitter power level is +43 dbm so the equivalent input to the receiver is -157 dbm.

The expected received power for the minimum σ_o is -121.1 dbm. There is duty cycle difference of 6 db, thus the transmitter leakage signal is expected to be 29.9 db below the minimum signal. This will introduce negligible error in the data.

2.4.5.7 TRANSMITTER-TO-RECEIVER ISOLATION DURING RECEPTION

During the reception interval, it is again necessary to prevent leakage of transmitter signal into the receiving channels. The required isolation is obtained by reducing the power output of the transmitter and introducing isolation between transmitter and receiver by use of the antenna switch.

The power reduction of the transmitter has been measured to be 122 db. The antenna switch isolation from transmitter port to receiver port has been measured to be in excess of 80 db. Thus the transmitter leakage signal into the receiver channels is +43 dbm reduced by 202 db, or -159 dbm. As indicated in Section 2.4.5.6, this level of signal will introduce negligible error in the data.

2.4.5.8 RECEIVER CHANNEL CROSSTALK

Possible sources of signal crosstalk have been considered in the design of the receiver channels. The design goal has been to keep the total crosstalk between channels to less than -30 db. Possible sources of crosstalk are the following:

a. Antenna cross coupling
b. Antenna switch coupling
c. Coupling through 1st Mixers
d. Coupling through IF Switches
e. Coupling through 2nd Mixers
f. Coupling through 3rd Mixers

Antenna Cross Coupling

Measurements made at the boresight range at NASA indicated the minimum isolation was 16 db at Nadir. Range effects as indicated by aperture probing at angles of 0^{o}, 30^{o} and 60^{o} would indicate that most of this is due to cross polarized range reflections entering through the high gain portions of the antenna. Prototype measurements wherein the first two sets of E dipoles (one on each side of aircraft centerline) radiated and the first two sets of H dipoles received, energy typically 45 db down was measured. Degradation due to fuselage and nacelle curvature and contributions from the remaining dipoles would reduce this isolation to about 35 db. The design goal was 34 db.

Antenna Switch Isolation

The antenna switch isolation between receive channels was specified to be at least 40 db minimum. The measured values are typically in excess of 120 db.

Coupling Through 1st Mixers

There is a common signal path between the two receiver channels through the 1st L.O. injection arms. This is indicated in Figure 2.18. The 3 db hybrid has a typical isolation value of 27 db or greater. The isolation in the balanced mixer is approximately 20 db in all conditions. The isolation between channels should be on the order of 67 db or greater. If the coarse gain controls are set at opposite extremes; i.e. Horizontal Gain - Pos 1 and Vertical Gain - Pos 6, the calibrate signals differ by 60 db. Under these conditions, some interaction was experienced in the Scatterometer system in that the calibrate tone from the horizontal channel reacted with the calibrate tone in the vertical channel. This effect was eliminated by the addition of the 340 MHz filter in the 1st L.O. line supplying the vertical receiver. The filter adds an additional 30 db of isolation.

IF Switch Isolation

The IF switches are two pole double throw units. The two poles of each switch are actuated by a common trigger and the units are incased in a single housing. The typical measured isolation between channels of an IF Switch is 70 db or more.

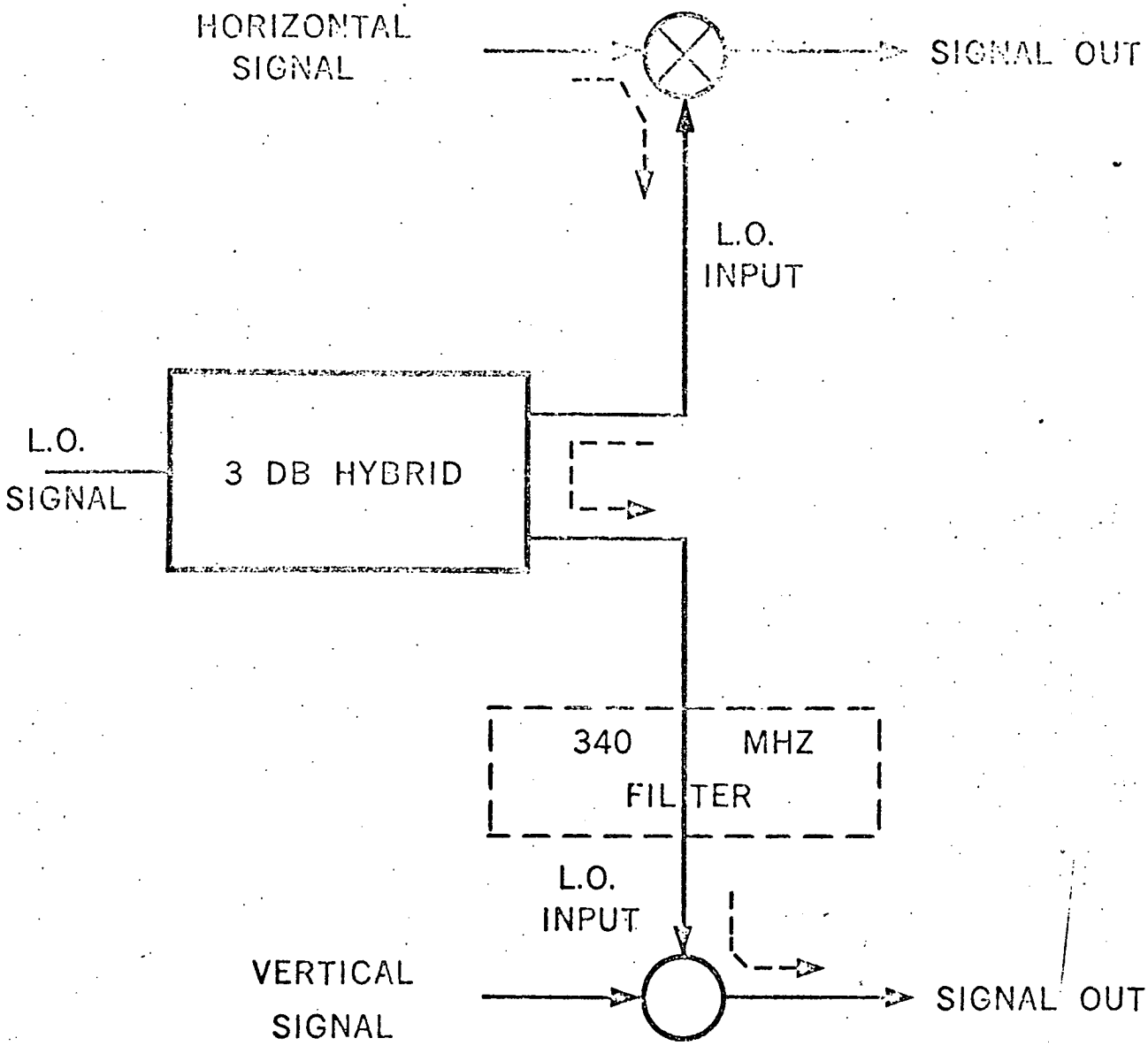

FIGURE 2.18 SIGNAL COUPLING THROUGH 1ST MIXERS

SIZE	CODE IDENT NO.	
A	20418	2236
SCALE	REV	SHEET 2-40

SD FORM 481-2 AUG 64 (2C)

Isolation Between 2nd Receiver Mixers

The 2nd mixer of each receiver obtains its local oscillator signal from the LOW FREQUENCY SOURCE. A functional diagram of the circuits being discussed is given in Figure 2.19. It is apparent that there must be sufficient isolation to prevent the composite signals that enter the 2nd mixers from intermixing.

The feed through path is as follows:

1. Coupling of the input port of the 2nd mixer to the local oscillator port.
2. Reverse gain of the local oscillator amplifier.
3. Coupling of the matching pad.
4. Coupling between output ports of the power divider.
5. Coupling of the input matching pad.
6. Forward gain of the local oscillator amplifier.
7. Coupling of the local oscillator port to the output port of the 2nd mixer.

The overall isolation between mixers is obtained as follows:

ITEM	COUPLING
2nd Mixer Coupling	-20 db
Reverse Gain of 55 MHz Amplifier	-27 db
Coupling of Matching Pad	- 4 db
Power Divider	-25.4 db
Coupling of Matching Pad	- 4 db
Forward Gain of Amplifier	+13 db
2nd Mixer Coupling	-20 db
	-87.4 db

The power divider selected for power division consists of a single resistive network, as shown in Figure 2.20. The isolation obtainable with this circuit is given by the ratio of the power out of J_{N2} (due to an input signal on J_{N1}) to the power in on J_{N1}.

With the transformer matched to the impedance at the junction of the output resistances, the input impedance measured at the junction of the resistors would be 10.9 ohms. The ratio of Eout/Ein is given by the following:

$$\frac{Eout}{Ein} = \frac{51}{98} \cdot \frac{5.45}{52.45} = .0542$$

The attenuation expressed in db is 25.4 db.

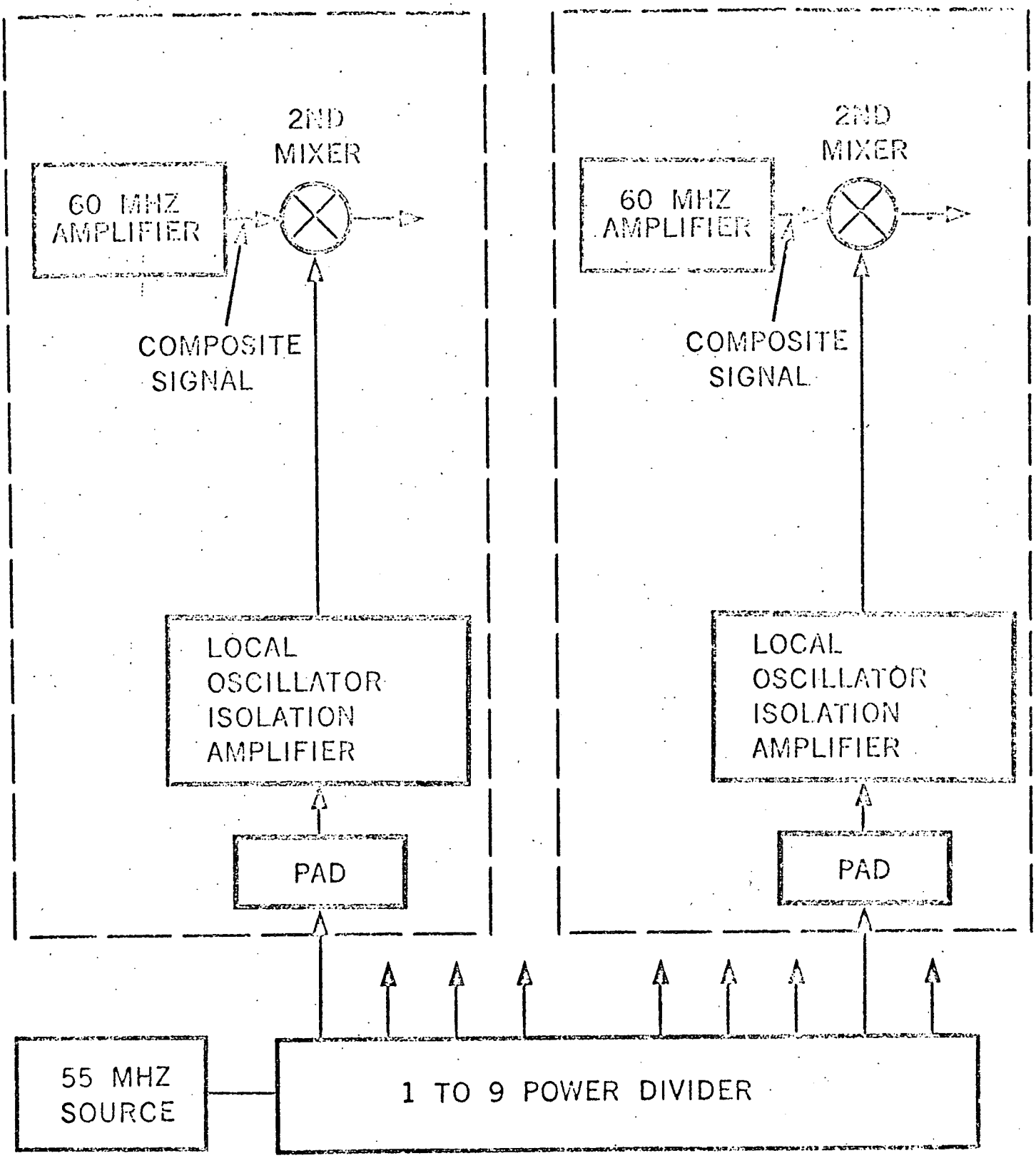

FIGURE 2.19 2ND MIXER ISOLATION DIAGRAM

SIZE	CODE IDENT NO.	
A	20418	2236
SCALE	REV	SHEET 2-42

SD FORM (31-2 AUG 64 (2C)

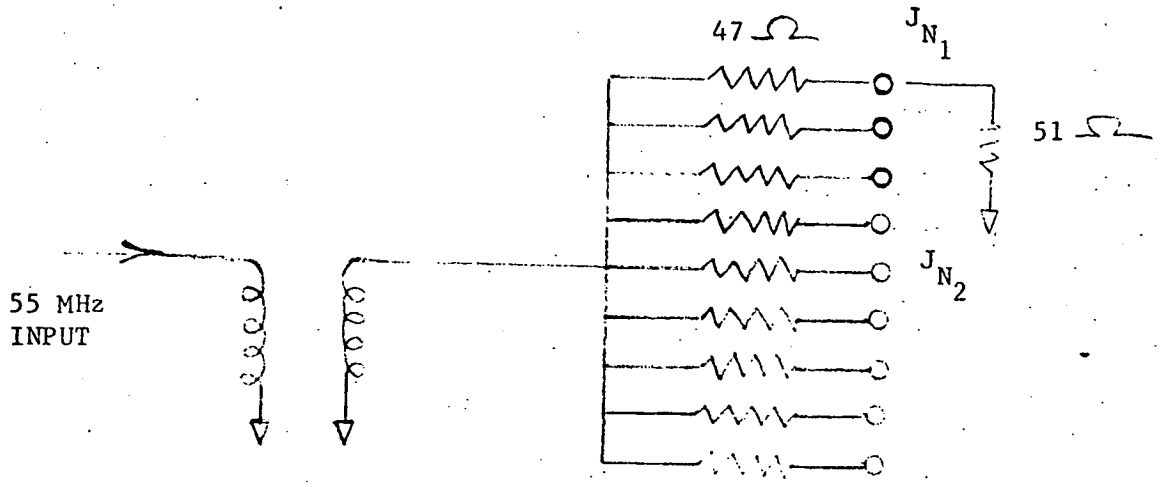

FIGURE 2.20 POWER DIVIDER - SECOND L.O.

Isolation Between 3rd Receiver Mixers

The isolation diagram for the 3rd receiver mixers would be similar to the 2nd mixer and the isolation values are essentially the same. The isolation value is such that system performance will not be degraded because of signal feed-through between the 3rd receiver mixers.

2.4.5.9 SIGNAL LEVELS IN 1ST L.O. EXCITATION GENERATION

The block diagram showing the generation of the 1st L.O. signal is given in Figure 2.21. The method of generating the 1st L.O. signal is to mix the 55 MHz and 5 MHz signal to produce 60 MHz and then mix the 60 MHz signal with a CW signal generated in the transmitter and at the transmitter frequency of 400.85 MHz to produce the 1st L.O. signal at 340.85 MHz.

When this method of producing anL.O. signal is used, it is important that the transmitter frequency be well suppressed. The transmitter signal level at various points in the 1st L.O. source are indicated in the block diagram. The two 340 MHz passband filters were added for the express purpose of attenuating the 400.85 MHz signal. In addition, the 340 MHz amplifier is selective and adds to the suppression of the 400.85 MHz signal. The leakage value of the 400.85 MHz signal is well below the noise level at the output of the first mixer of a receiver channel.

2.4.5.10 ISOLATION CALIBRATE SOURCE TO 1ST MIXER

An isolation diagram showing the feed-through path of the calibrate signal into the 1st mixers of the receivers is given in Figure 2.22. The maximum calibrate input to the signal receivers is approximately -70 dbm. The receiver RF amplifier provides 27 db gain and the 1st mixer gives an 8 db loss for a net gain of 19 db.

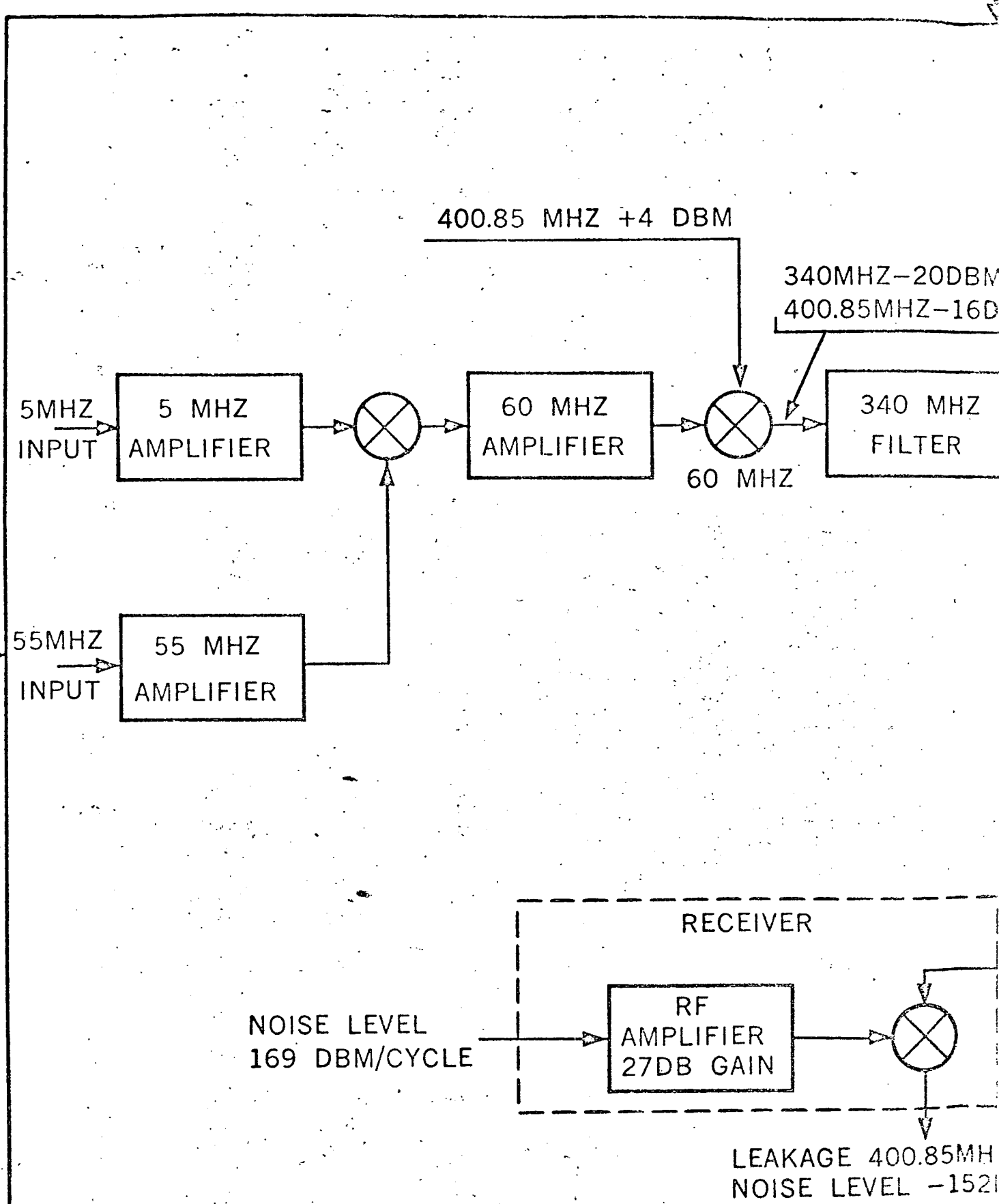

FIGURE 2.21 1ST L.O. SI

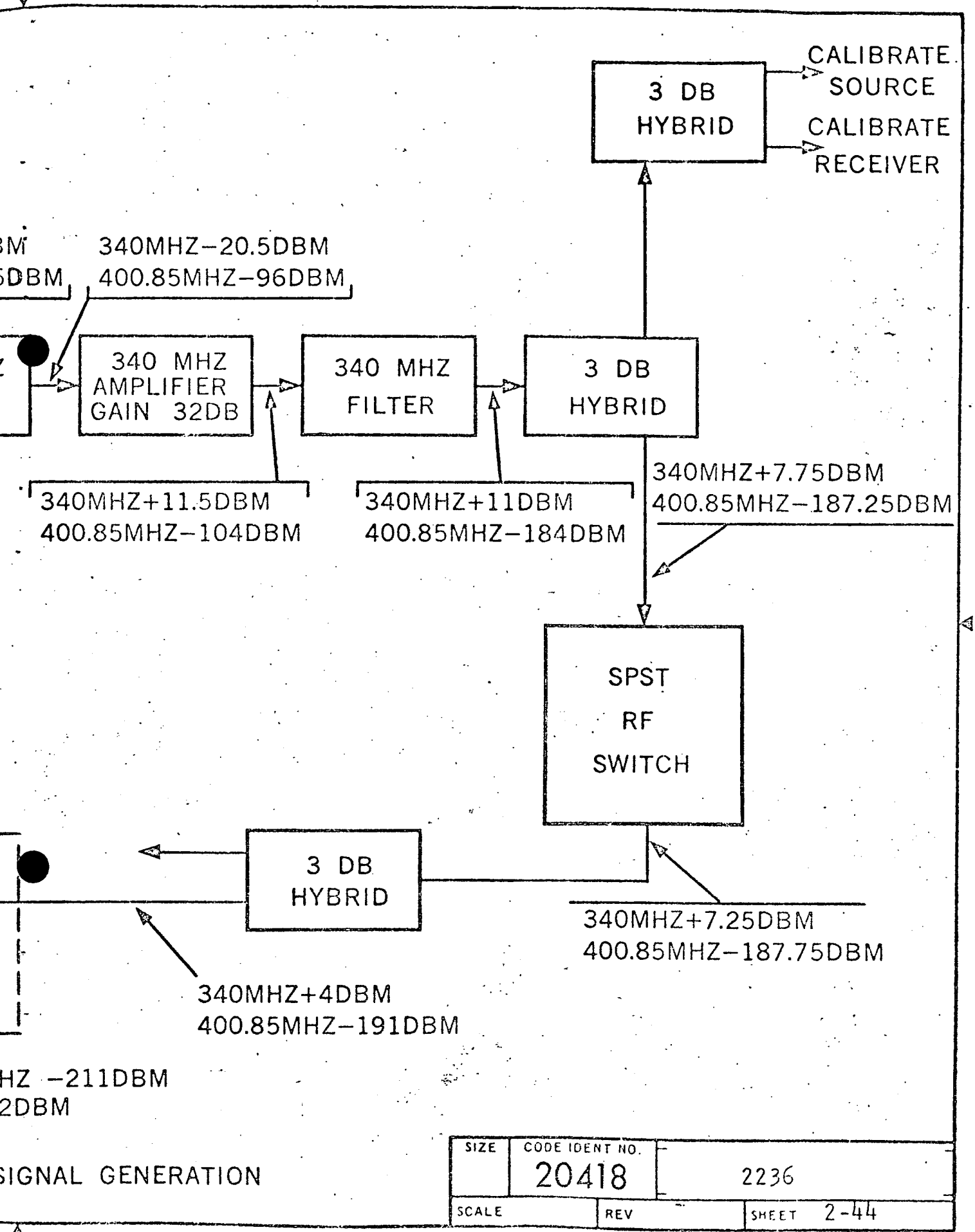

SIGNAL GENERATION

SIZE	CODE IDENT NO.	2236
	20418	
SCALE	REV	SHEET 2-44

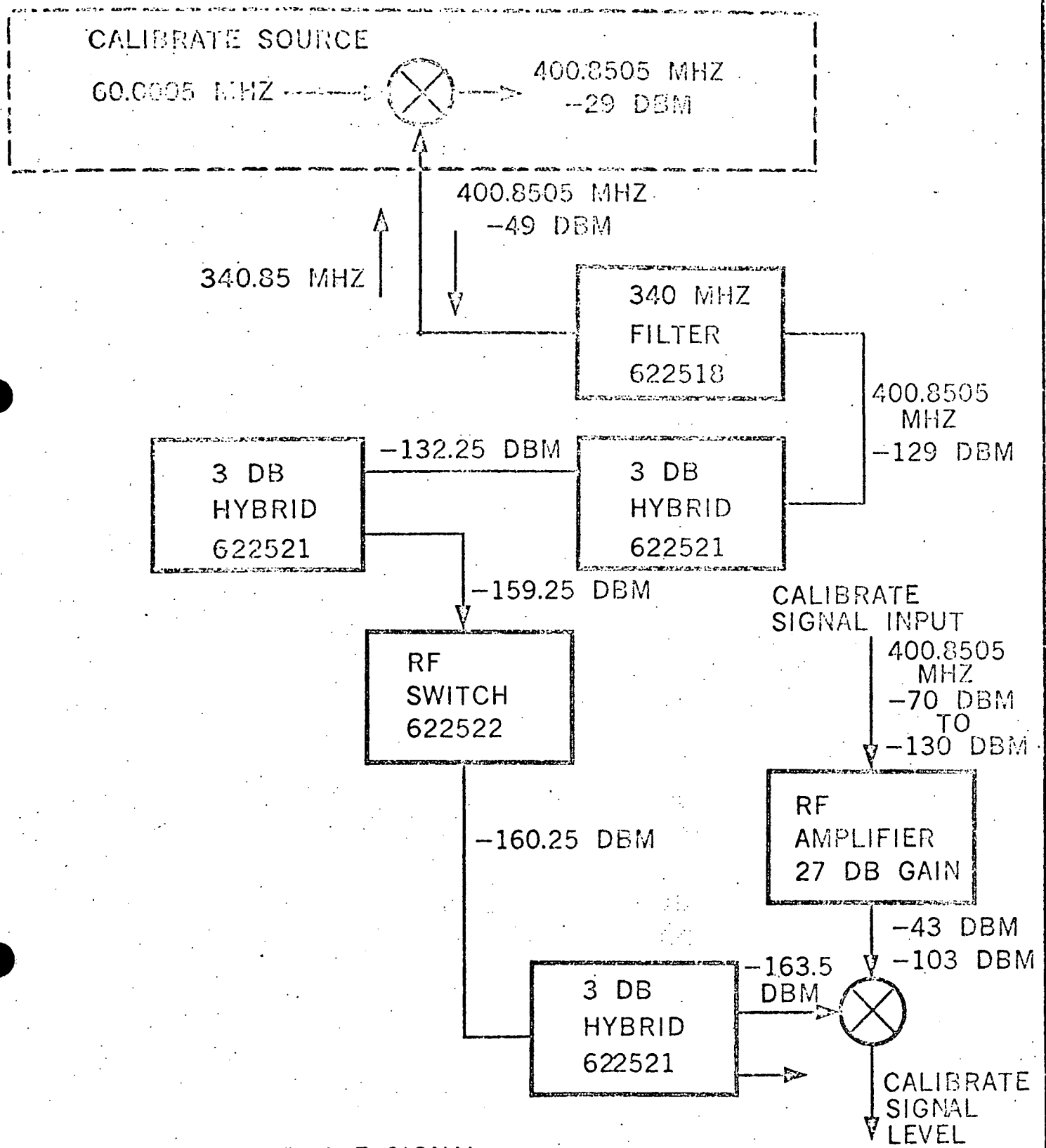

FIGURE 2.22 CALIBRATE SIGNAL ISOLATION

SIZE	CODE IDENT NO.	
A	20418	2236
SCALE	REV	SHEET 2-45

The calibrate level at the output of the mixer is -51 dbm. Increasing the coarse gain of the receiver by 50 db decreases the calibrate signal out of the receiver mixer to -101 dbm. For the low level calibrate signal, the signal becomes -111 dbm. The leakage value should be held to -131 dbm or lower. The design value is -183.5 dbm which results in a 52.5 db margin in this design.

2.4.5.11 RF AMPLIFIER CHARACTERISTICS

The RF amplifier, 622509, has the following normal characteristics:

GAIN	27 db
BANDWIDTH	30 MHz (3db)
CENTER FREQUENCY	400.85 MHz
NOISE FIGURE	3.7 db

The input-output characteristics are shown in Figure 2.23. The one db compression point occurs at a signal input level of -23.6 dbm.

2.4.5.12 IF AMPLIFIER CHARACTERISTICS

The IF amplifier, 622511, has the following nominal characteristics:

GAIN	75 db
BANDWIDTH	10 MHz
CENTER FREQUENCY	60 MHz
NOISE FIGURE	4.5 db
GAIN CONTROL RANGE	50 db

The input-output characteristics are shown in Figure 2.24. The one db compression point occurs at a signal input level of -64 dbm at maximum gain setting. At a gain reduction of 50 db, the input level for one db compression occurs at -14 dbm.

The gain control characteristics of the IF amplifier are shown in Figure 2.25. The temperature effects were compensated for in the design of the gain control network.

2.4.5.13 POST IF AMPLIFIER CHARACTERISTICS

The Post IF amplifiers have the following characteristics:

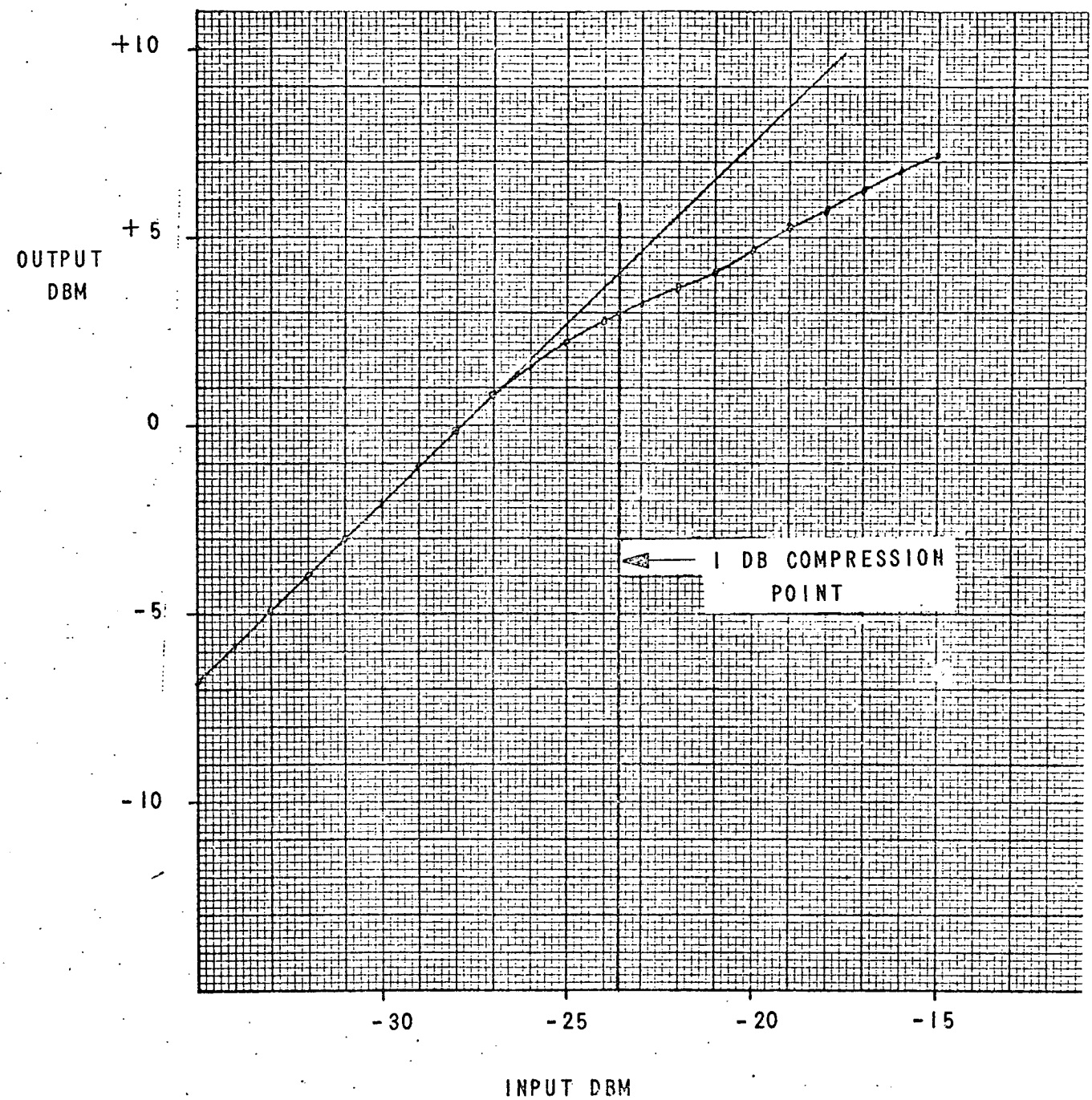

FIGURE 2.23 RF AMPLIFIER GAIN CHARACTERISTIC

SIZE	CODE IDENT NO.	
A	20418	2236
SCALE	REV	SHEET 2-47

SD FORM 481-2 AUG 64 (2C)

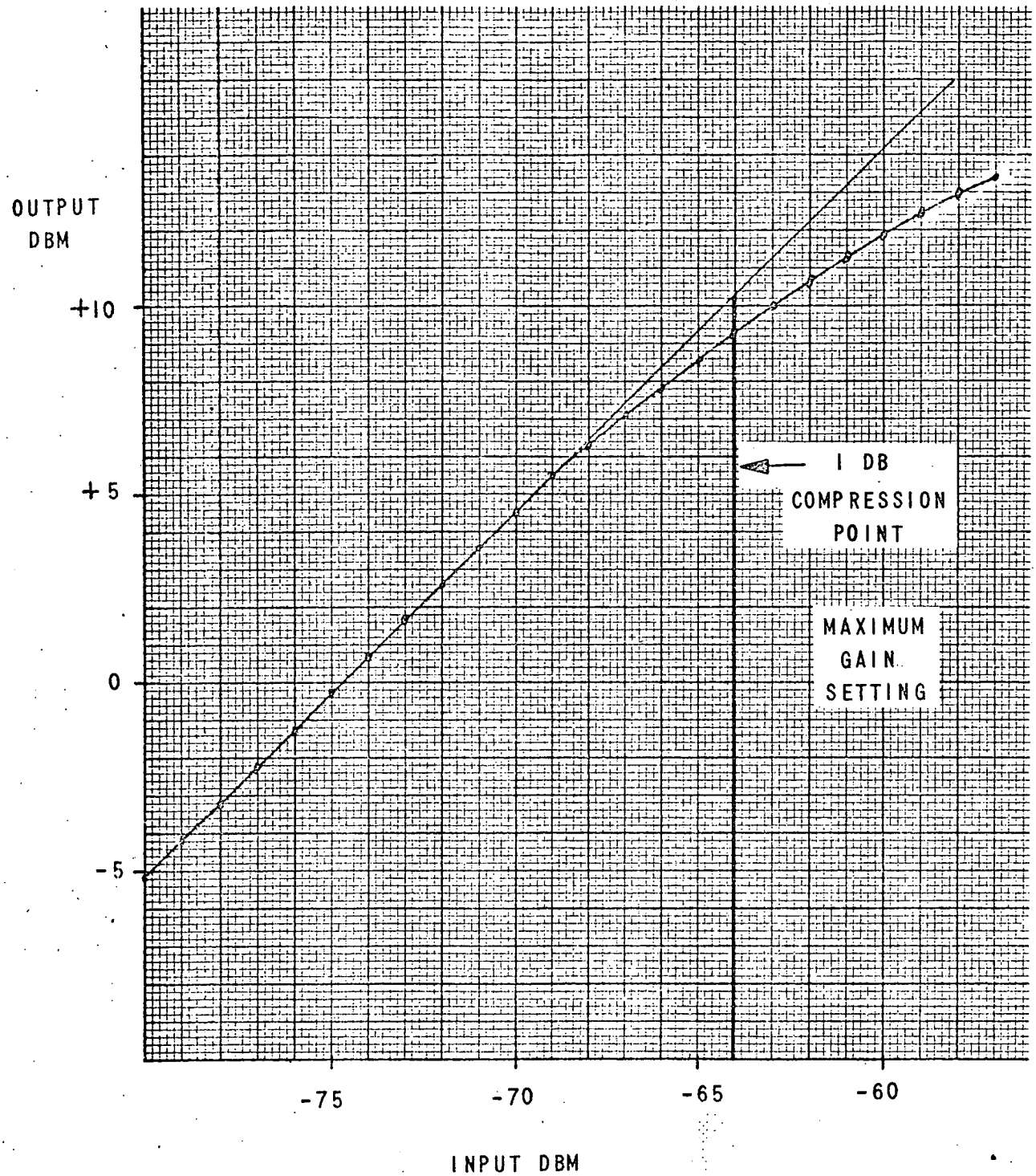

FIGURE 2.24 IF AMPLIFIER GAIN CHARACTERISTIC

SIZE	CODE IDENT NO.	
A	20418	2236
SCALE	REV	SHEET 2-48

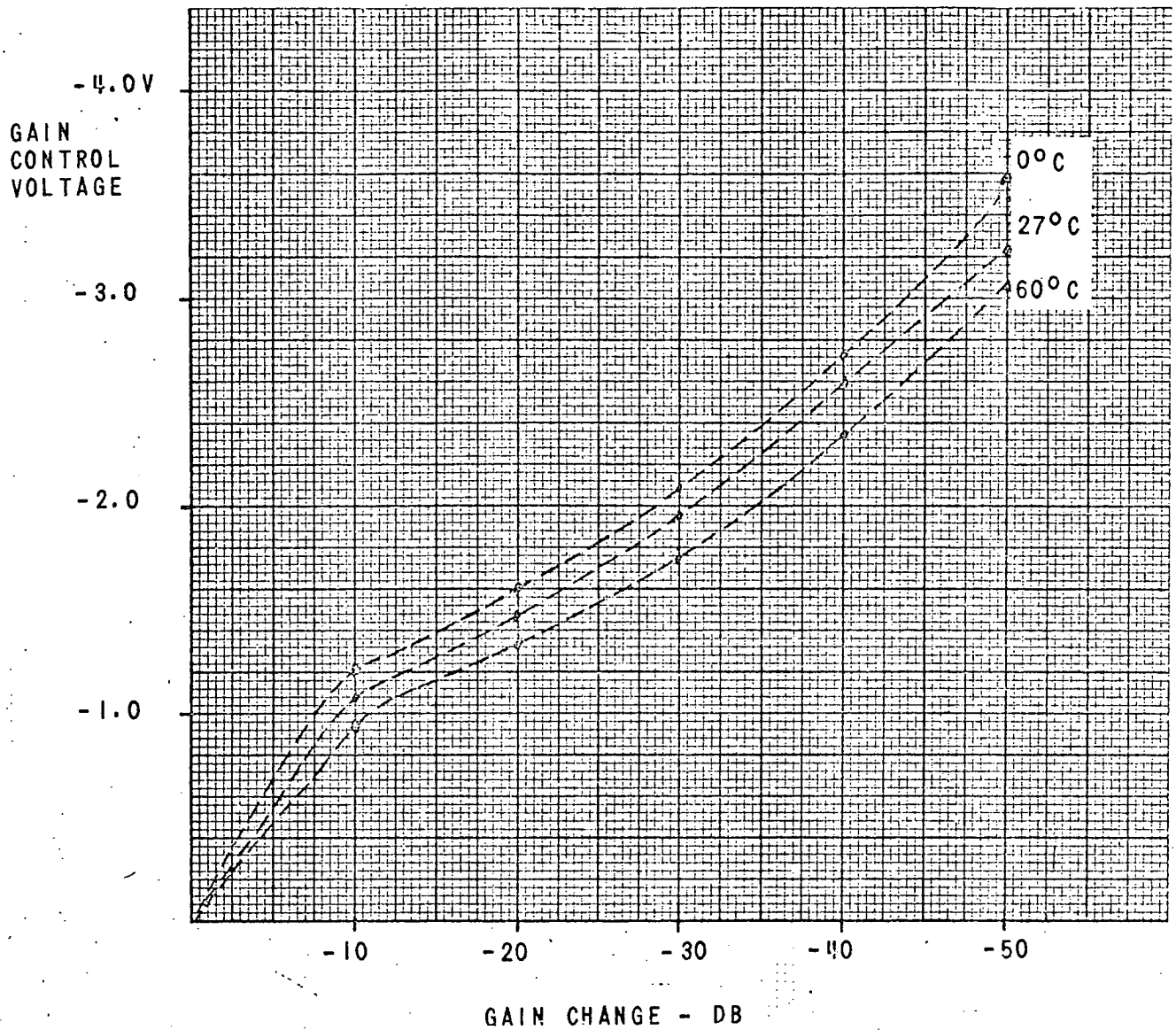

FIGURE 2.25 IF AMPLIFIER GAIN CONTROL CHARACTERISTICS

SIZE	CODE IDENT NO.	
A	20418	2236
SCALE	REV	SHEET 2-49

GAIN	75 db Maximum
MANUAL GAIN CONTROL	40 db
AGC RANGE	40 db
AGC THRESHOLD	Adjustable-nominal setting .9 volts rms output
BANDWIDTH	Determined by crystal filter (see Figure 2.15)

2.4.5.14 RECEIVER OUTPUT

The output of each receiver is maintained at a nominal value of .9 volts rms. This AC signal is superimposed on a dc level of +2.5 volts to make it compatible with the Sonex multiplexer which accepts signals from zero to +5 volts. Thus, the .9-volt rms level allows for a peak to rms ratio of 9 db. If the output signals are noise like; that is, the power spectra density is constant over the frequency band of interest, the output signal will exceed the input range of the multiplexer less than one percent of the time.

2.4.6 CALIBRATE RECEIVER DESIGN

The channel designated the calibrate receiver has five output frequencies. These include three telemetry signals, the 500 hertz transmitter sample, and a 1,000 hertz calibrate signal. The three telemetry signals are generated by three oscillators which comply to IRIG standards. Channels 1, 2, and 3 units are used. These units are incorporated in the Scatterometer system to provide information on mode of system operation and signal receiver gain positions. This information is necessary for data reduction.

The calibrate receiver consists of a mixer and a Post IF amplifier unit. The signal levels into the receiver and the output levels are shown in Figure 2.26. The resistive divider is used to combine the oscillator tones with the transmitter sample signal and the 1,000 hertz signal.

Channels 1, 2, and 3 subcarrier oscillators were chosen since their output frequencies fall in the desired frequency band and do not interfere with the 500 hertz and 1,000 hertz signals.

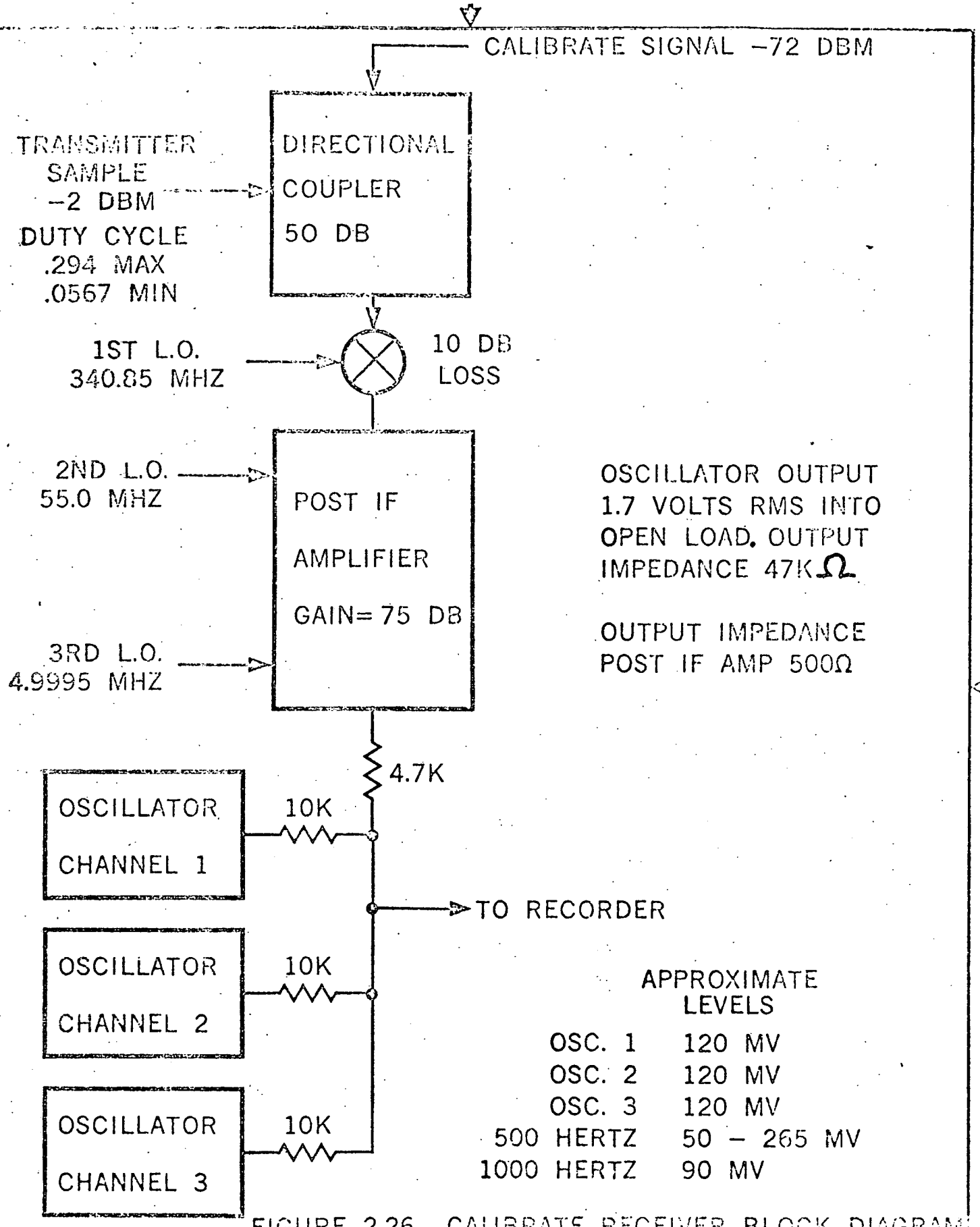

FIGURE 2.26 CALIBRATE RECEIVER BLOCK DIAGRAM

SIZE	CODE IDENT NO.	
A	20418	2236
SCALE	REV	SHEET 2-51

SD FORM 481-2 AUG 64 (2C)

2.5 ANTENNA

2.5.1 ANTENNA REQUIREMENTS

The original proposal and contract contained the general antenna specifications. Additional system analysis and design requirements imposed detail antenna specifications which were used as design guidelines as presented in Table 2.2. Not all of these were subsequently met, as discussed in this report.

2.5.1.1 VSWR

The Voltage Standing Wave Ratio of the antenna at the input terminals of the horizontal and vertical arrays shall be less than 1.2.

2.5.1.2 GAIN

The two arrays shall have a peak one-way minimum gain of 17 db occurring between $+55^{o}$ and $+65^{o}$ and -55^{o} and -65^{o}. The theoretical gain of the E-Array, based on the element gain, is only 13 db. This is the value now applicable to the E-Array.

2.5.1.3 PATTERN

Both arrays shall have an along track pattern lying between the two limits as indicated in Table 2.2. The G_{max} to G_{min} (at Nadir) will be between 22.6 and 34.6 db. The cross track two-way beam width shall be less than 3^{o} at the half power points. The two-way beam width shall be less than 20^{o} at the -20 db point.

2.5.1.4 SIDELOBES

The one-way side lobe level shall be at least 20 db lower than the main beam at the corresponding along track angle.

2.5.1.5 ISOLATION

The coupling between arrays will be less than -30 db.

2.5.2 ANTENNA DESIGN

The design of the 400 MHz Scatterometer Antenna was arrived at through the use of fifth scale models. These models verified the approach taken and gave early indication of the expected performance.

This fifth scale model activity is summarized in Appendix C, Scatterometer Antenna Element Pattern Investigation. A summary of the Antenna design is presented here.

2.5.2.1 ANTENNA THEORY

The operation of the 400 MHz Scatterometer Antenna can best be described in terms of array theory which is based on the principle of superposition. This principle states that the net radiation in any given direction is the vector sum of contributions from all the radiating elements. An auxiliary principle is the separation of aperture distribution along two independent orthogonal coordinates. This separation is possible when all the elements along a coordinate direction are identical. Based on these two principles, it is possible to explain the operation of the antenna as consisting of two orthogonal linear arrays. One is a 12-element array lying along the wing in the cross track plane and the other is a two-element array in the track plane. Each array controls the radiation pattern shape in its own coordinate plane independently of the other array.

2.5.2.2 CROSS TRACK PATTERN

First of all, consider a cross track array consisting of twelve identical radiating dipoles. The number of elements and their spacing ($.83\lambda$) is chosen to produce a cross track pencil beam radiation pattern having a beam width of 6^{o} at the 3 db points. The amplitude of each dipole radiation is adjusted so that all side lobes of the radiation patterns are theoretically -24 db below the main beam peak. The phase of each dipole radiation is adjusted so that the main beam direction is perpendicular to the average axis of the array. A linear array normally lies in a straight line and all elements are excited with equal phase. This is only approximately true for the Scatterometer Antenna because some elements are mounted on the fuselage which is not flat and because there is a dihedral angle of the wing. The dipole phases were adjusted so that the energy from all the dipoles arrives in phase at any horizontal plane below the airplane, that is, the radiated beam is collimated by proper adjustment of the phase of the radiated energy from each of the twelve dipoles. The amplitude and phases of the dipoles are adjusted in the feed system which divides the total input among the 12 elements.

The circuit of the array feed is shown in Figure 2.27. The dipoles are fed in series from the center outward by a coaxial transmission line and five stripline directional couplers.

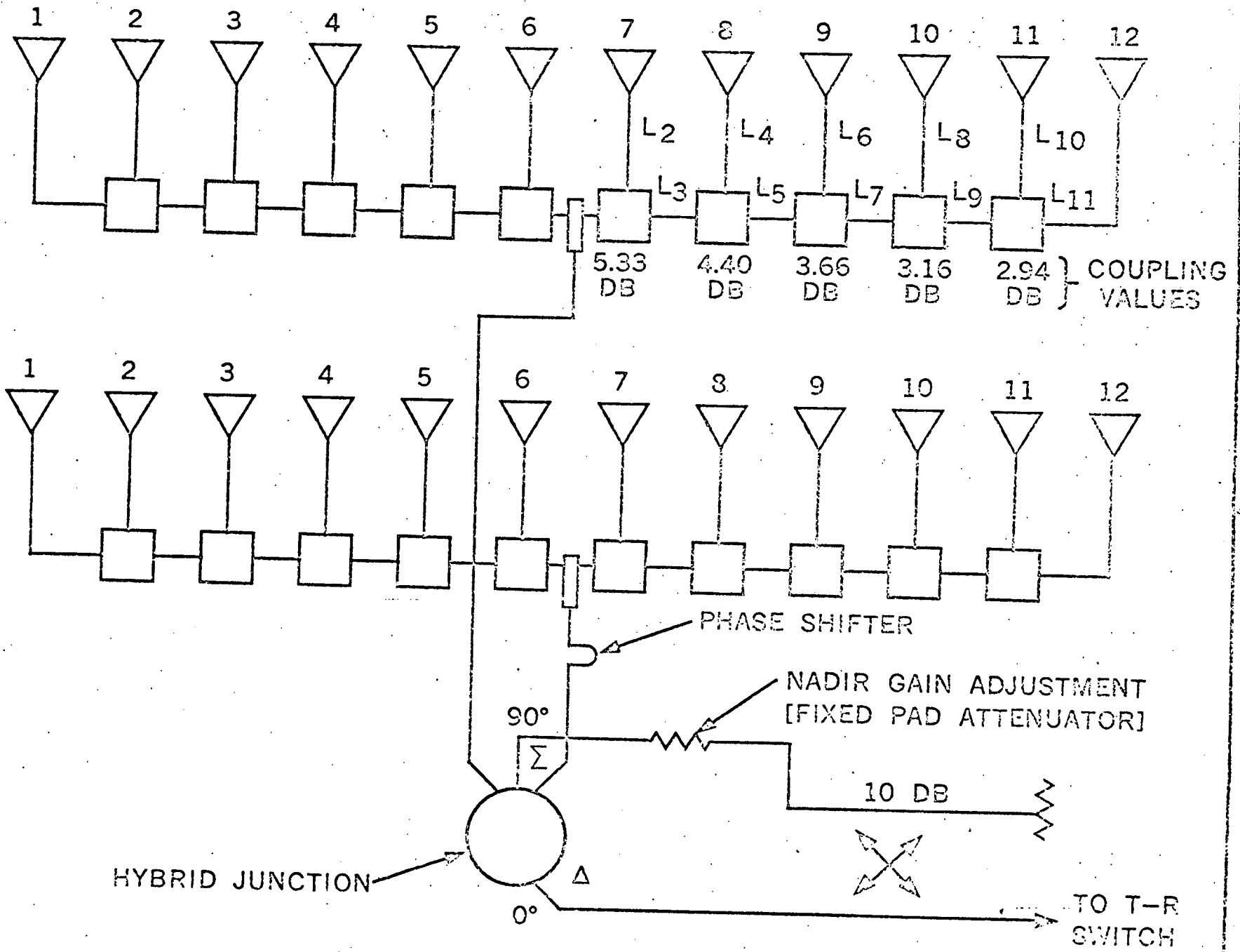

FIGURE 2.27 ARRAY FEED SYSTEM FOR ONE POLARIZATION

SD FORM 481-2 AUG 64 (2C)

SIZE	CODE IDENT NO.	
A	20418	
SCALE	REV	2236
	SHEET	2-54

The coupling ratios are chosen to produce the correct amplitude of radiation from each dipole while the phases of the dipole are adjusted by the lengths of transmission line connecting them to the directional couplers. The left and right halves of the array are identical and they are fed at the center by a strip line power divider. Of course, there are two 12-element arrays as shown in the circuit diagram and each of these is one complex element of a two-element array in the track plane.

2.5.2.3 ALONG TRACK PATTERN

The design of the two-element track plane array gives the Scatterometer Antenna its unique radiation pattern shape. The radiation pattern in the track plane has minimum radiation in the direction of the Nadir and maximum radiation between 55 and 65 degrees in the fore and aft directions. This is achieved by the selection of spacing between the forward and aft elements (each element now consisting of 12 dipoles) and by feeding the elements out of phase by 180^{o}. The power split and phasing is accomplished in a "rat-race" type hybrid junction with the input signal connected primarily to the difference terminal. This feed arrangement produces a null in the nadir direction and to fill this null to the correct level, some of the input signal is removed from the input line through a 10 db directional coupler and fed into the sum terminal of the rat-race hybrid junction. Only when there is 90^{o} phase difference will the sum and the difference radiation patterns add together symmetrically in the fore and aft directions. The phase shifter shown in the circuit diagram adjusts the phase between the fore and aft elements to set the null of the radiation pattern exactly at the Nadir. Primary purpose of this adjustment was to correct for the 3^{o} angle of incidence of the antenna panels when mounted to the P3A.

The track plane radiation pattern shape is obtained primarily by the method of feeding described above but in addition to this, the individual dipoles are designed to assist in shaping the track plane pattern. The dipoles are mounted a half wavelength below the wing panels so that a dipole and its image combine to produce minimum radiation in the Nadir direction and maximum at about 55^{o} to 65^{o} from the Nadir. This helps to produce a wider and more linear null pattern shape. If the dipole image was complete, then the dipole would produce nulls in the direction of the Nadir regardless of whether the track plane array were fed from the sum terminal or not.

This situation is eliminated and a more positive control of the radiation pattern near the Nadir is maintained by adding parasitic dipoles midway between the fore and aft dipoles. The parasitic dipoles are excited only when the fore and aft dipoles are fed in phase from the sum terminal. Therefore, their amplitudes are small and they do not affect the track plane pattern shape outside a few degrees from the Nadir. However, in this range of angles, the parasitic elements improve the control of the cross track pattern shape since without the parasitic elements the dipole radiation patterns would have nulls that are conical shaped about the Nadir direction and would reduce the cross track beam peak relative to cross track side lobe levels.

2.5.2.4 ORTHOGONAL ANTENNA

The foregoing description applies to one complete antenna for a single linear polarization. Two orthogonal polarizations are required for the Scatterometer system so two complete antennas are assembled in the same location on the wing with the two sets of dipoles mounted alternately and at right angles to each other. By virtue of the symmetry, the total cross coupling between the two sets of dipoles was expected to be less than the specified value of -30 db. The complete Scatterometer antenna system consists therefore of 48 active dipole radiators and 24 parasitic dipoles plus the essential feed system and control circuitry. The E-dipoles are bent up toward the wing in an effort to achieve greater radiation at wide angles in the fore and aft direction.

2.5.2.5 DIPOLE DESIGN

The physical design of the E & H plane dipoles was most critical primarily because the effective radiation center of the arms are one-half wavelength or about 15 inches from the base. This length aggravated the vibrational problem.

Drag and weight, although not specified, were to be kept to a minimum. Early mechanical design considerations were given to cast aluminum pylons and arms. This approach gave way, because of weight and lead time for any casting design variations, to the use of welded streamline steel tubing. Tubing of 1020 steel was first used. Stress and vibration analysis indicated adequate margins of safety. However, initial vibration tests to MIL-STD-810A, as reported in Appendix D, Summary Discussion of Vibration Test Results,

revealed strength deterioration in the areas neighboring the welds. Final design not only used 4130 steel tubing but required gussets at the foot/leg and leg/arm weld joints. Photographs of the four dipoles are shown in Figure 2.28 H-Plane Dipole; Figure 2.29 E-Plane Dipole; Figure 2.30 H-Plane Parasitic Dipole, and Figure 2.31 E-Plane Parasitic Dipole.

2.5.2.6 DEVELOPMENT TESTS

The dipole design was established as a result of the fifth scale model activity and early vibration tests of prototype models. Isolation measurements indicated that the E dipole could not have the same "A" frame design as the H dipole. The design that evolved for the E dipole was an inverted "Y" with a conventional balun between the arms. The electrical characteristics are discussed below:

Impedance Match

The H dipole was matched initially by locating the cross brace approximately one quarter wavelength from the apex. This then formed a triangular balun. Length of the arm was also adjusted to give a better match. The center conductor pigtail also affected the dipole impedance.

Temperature

The active dipoles were temperature soaked at -54°C and +85°C. No physical or electrical failures occurred when later tested at room temperatures.

Isolation

As previously reported, energy radiated from two sets of one type of dipole was measured in two sets of the other type dipole, connected as the center two dipole sets of the array. The isolation measured 45 db.

Pattern and Gain

Limited prototype measurements were made on a simulated wing and mount section capable of mounting four sets of dipoles. Figure 2.32, Antenna Development Test Fixture, shows the set up used. Measurements confirmed the fifth scale model results.

Vibration

The development vibration tests to MIL-STD-810A are covered in Appendix C. As part of the vibration and stress an air load analysis was conducted. The

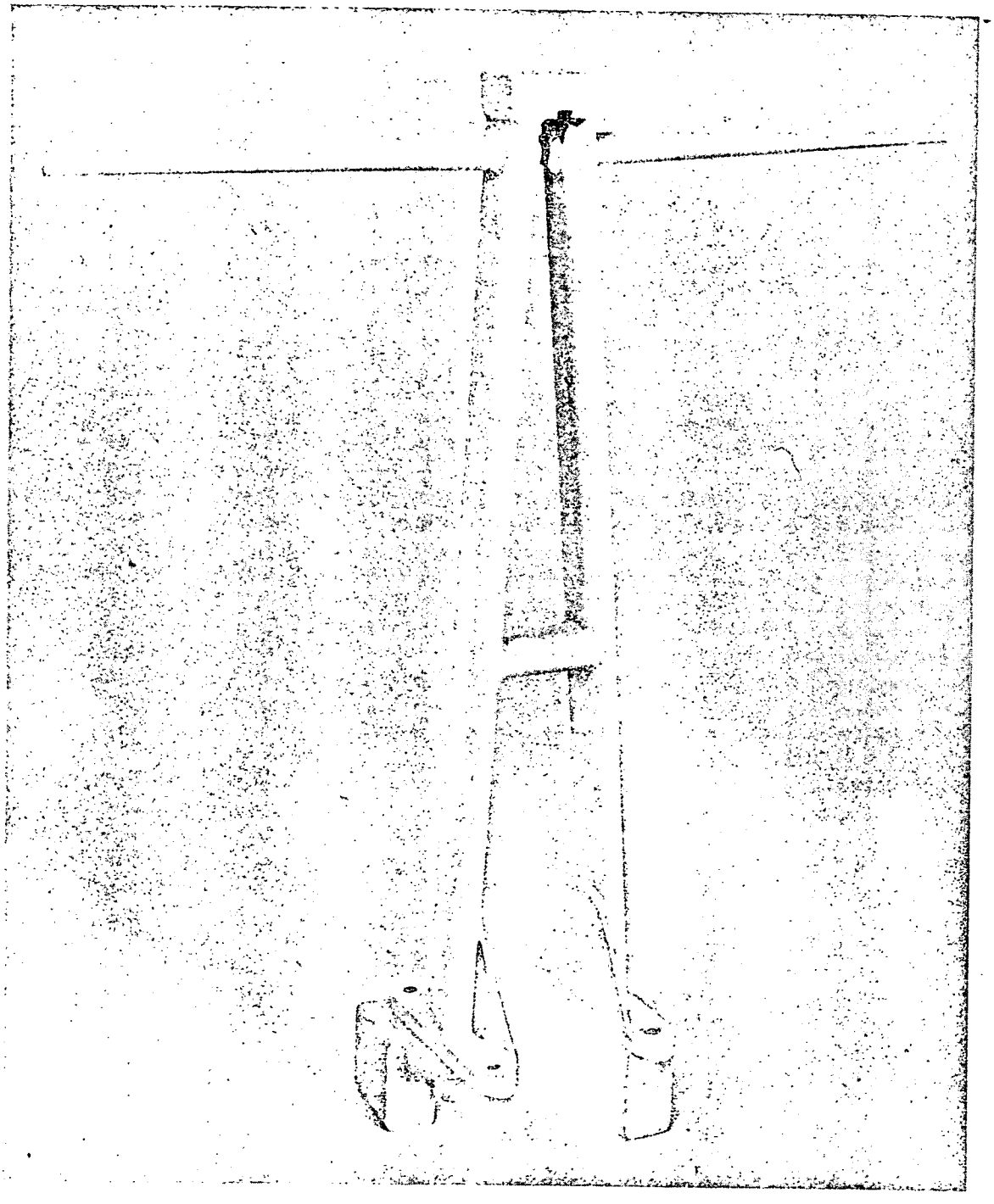

FIGURE 2.28 H PLANE DIPOLE

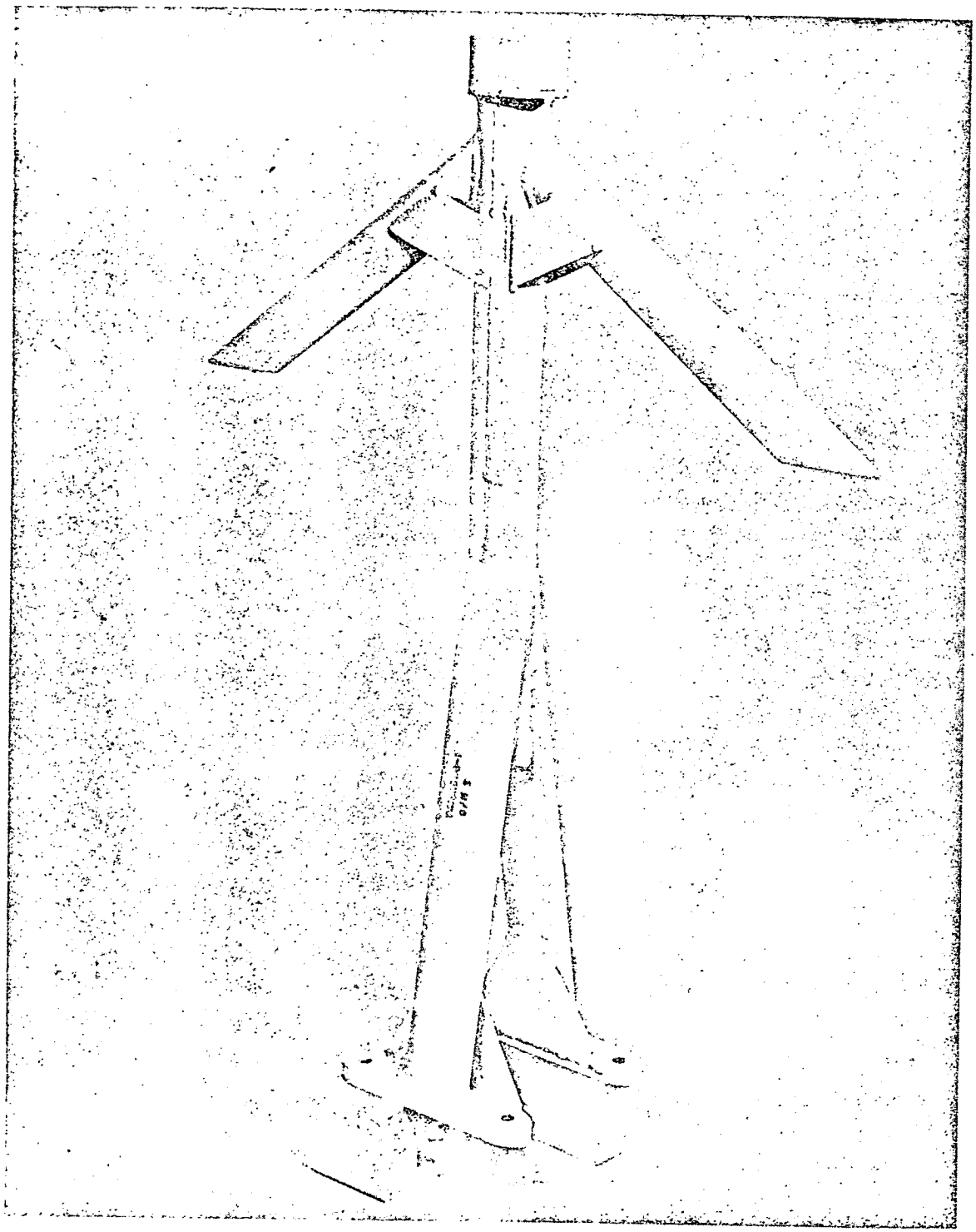

FIGURE 2.29 E PLANE DIPOLE

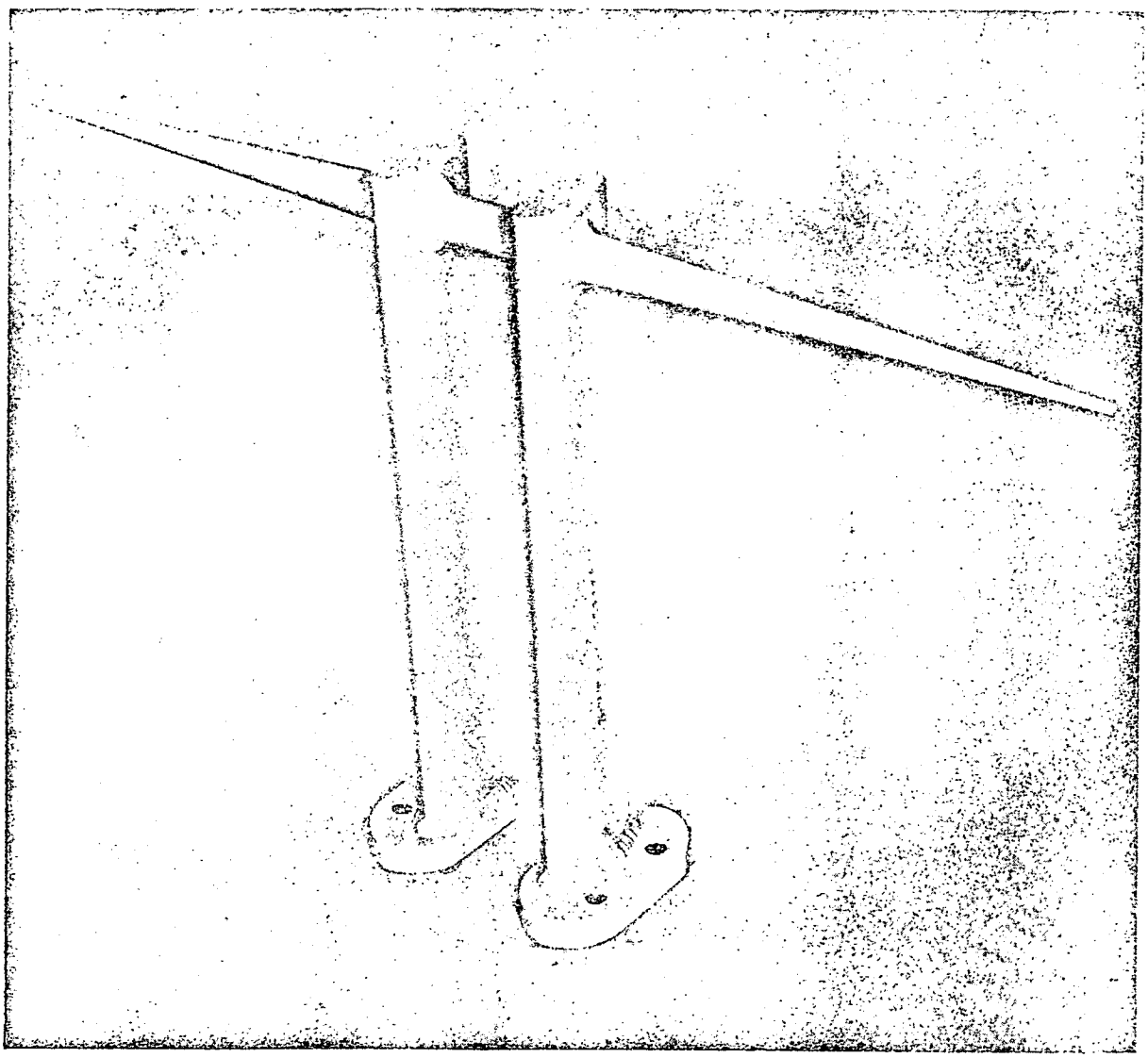

FIGURE 2.30 H PLANE PARASITIC DIPOLE

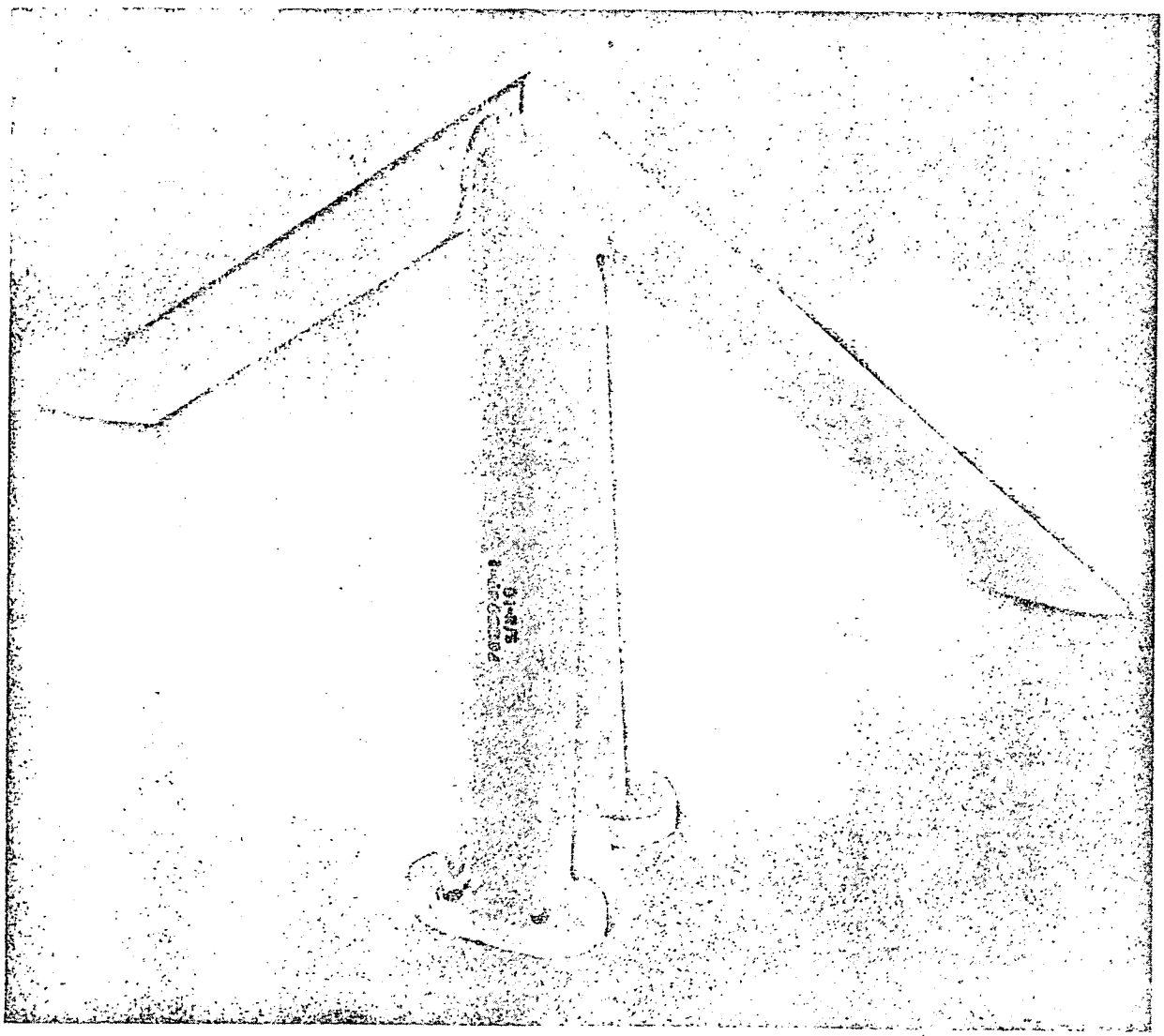

FIGURE 2.31 E PLANE PARASITIC DIPOLE

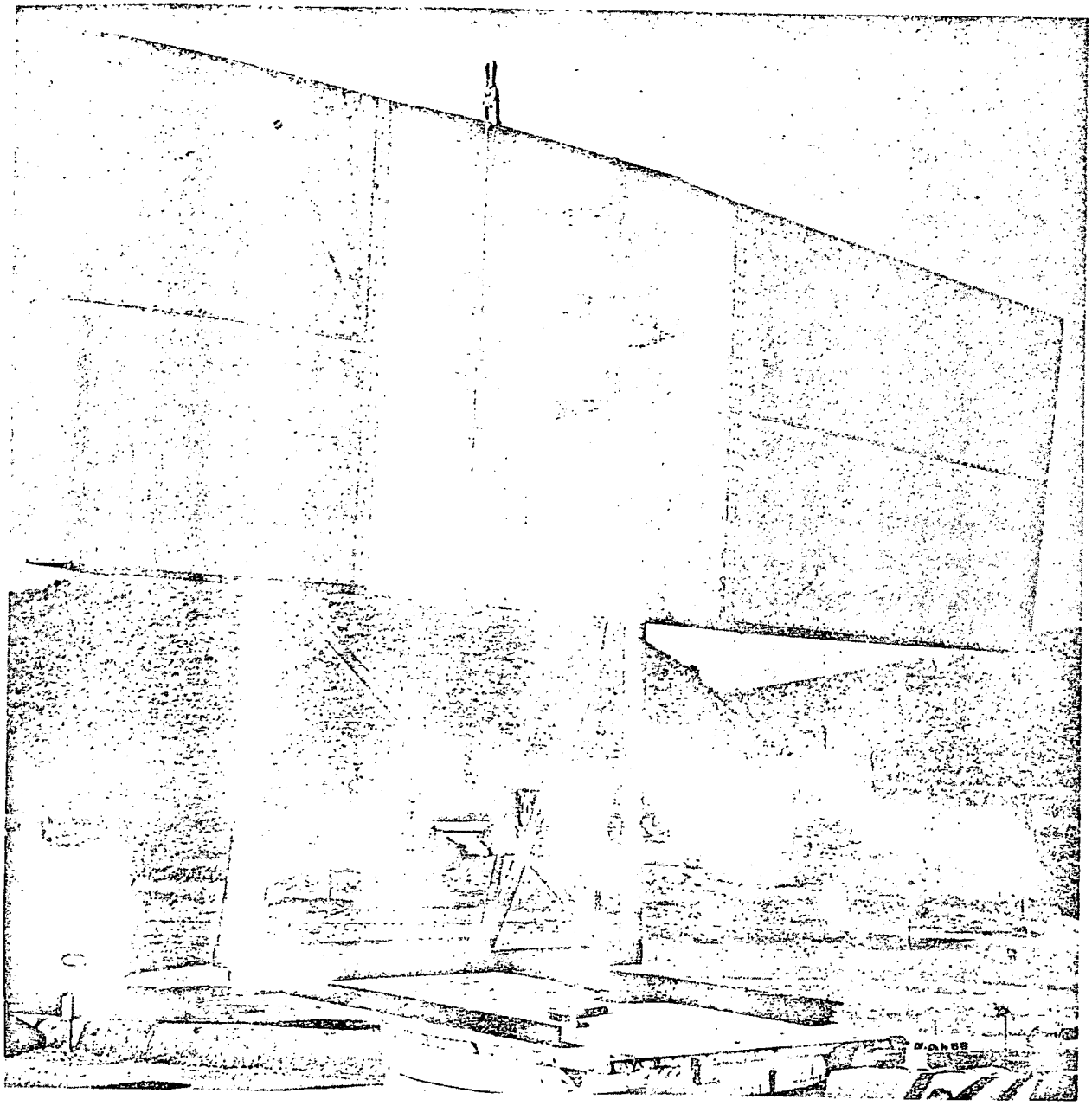

FIGURE 2.32 ANTENNA DEVELOPMENT TEST FIXTURE

results of this analysis are shown in Figure 2.33, Air Loads Analysis. The equivalent drag area taking into account the location of the dipoles was calculated to be 4.2 square feet. The tabulation of Equivalent Drag Area is given in Figure 2.34.

2.5.3 ANTENNA TESTS

2.5.3.1 COMPONENT TESTS

The 400 MHz frequency precluded conducting any full scale antenna tests prior to delivery of the antenna to NASA, Houston. However, all components were tested to appropriate specifications at Rantec, Division of Emerson Electric, Calabasas, California. The control boxes were tested fully assembled and the three types of panels were interconnected and phase and amplitude measurements made.

2.5.3.1.1 DIPOLES

Neither the E or H production dipoles required trimming or adjustment of the center conductor pigtail to consistently obtain an impedance match of between 1.10 and 1.15 VSWR

2.5.3.1.2 DIPOLE COUPLERS

The 40 dipole couplers all had a VSWR of less than 1.5.

2.5.3.1.3 CONTROL BOX

The two control boxes feeding the six panels with dipole ports loaded had VSWR less than 1.3. Phase of all front to rear output ports was $180^{\circ} \pm 5^{\circ}$. Power split was within $\pm$ .15 db between the four output ports.

2.5.3.1.4 ARRAY

The six panels and the two control boxes were interconnected as in Figure 2.27 and the coax cables between dipole couplers were adjusted to give less than 10° phase difference between front and rear ports and $\pm 10^{\circ}$ from the desired phase at each port. Amplitude difference between all front and rear ports was less than $\pm$.5 db.

2.5.3.2 BORESIGHT RANGE TEST

NASA MSC, Houston, Texas, had prepared a full scale mock-up of the P3A wing, inboard nacelle to inboard nacelle.

MAXIMUM AIR LOADS ON ANTENNA ELEMENTS

- Straight and Level Flight
- Aircraft Velocity - 350 Knots
- Altitude - Sea Level
- Angle of Attack and Side Slip - 0 Degrees
- Atmosphere - 1959 ARDC Standard
- Location - Propeller Wake

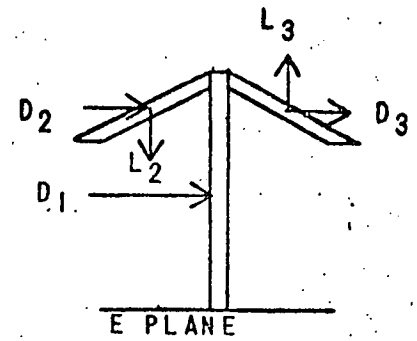

FORCE (LBS.)	E-PLANE		H-PLANE	
	ACTIVE	PARASITE	ACTIVE	PARASITE
D_1	21	7.2	23	8.2
D_2	0.6	0.6	22	26
D_3	0.6	0.6		
L_2	0.9	0.9		
L_3	0.9	0.9		

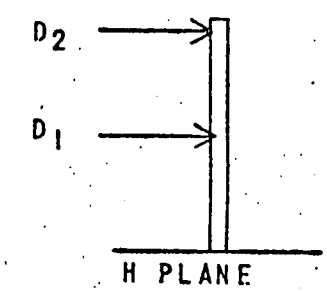

AIR LOADS ANALYSIS
FIGURE 2.33

SIZE A | CODE IDENT NO. 20418 | SCALE | REV | SHEET 2-64 | 2236

Element Type	No. Of Element Sets	Location	C_DA (in^2)
H	3	Propeller Wake	130.4
E	3	Propeller Wake	56.4
H	4	Wing	152.2
E	4	Wing	65.8
H	5	Fuselage	135.9
E	5	Fuselage	58.8
	24		599.5 in^2
			4.2 ft^2

FIGURE 2.34 EQUIVALENT DRAG AREA - C_DA

The antenna mount and antenna was fastened to the mock-up and mounted on a three-axis positioner as shown in Figure 2.35, Boresight Test Facility. Initial patterns indicated that too much difference energy was present in the cross track direction for along track angles $\pm 20^{\circ}$ of Nadir. Two typical patterns are presented in Figure 2.36, Cross Track Pattern, Az. = 0°; and Figure 2.37, Cross Track Pattern, Az. = 10° Fwd. These are for the E-Plane array which consistently appeared worse than the H-Plane. The peak gain at these angles is designed to be 20 - 24 db down from the peak array gain at $\pm 60^{\circ}$. The requirement to have side lobe energy down 10 db from this reduced peak gain requires very exact control of energy. Small phase and amplitude errors, dissymmetry of front and rear ground planes, and particularly the rapid transition from the antenna panel to the fuselage skin and the falloff of the leading edge of the wing accounted for the wide beamwidth and large sidelobes obtained. Of the many things tried, the one having the best improvement was the continuation of the wing 10:1 fairing across the fuselage. The resulting patterns are shown as Figure 2.38, Cross Track Pattern, Az. = 0° with Fairings; and Figure 2.39, Cross Track Pattern, Az. = 10° Fwd. with Fairings. The pattern improvement is considerable although beamwidths are wider than 6° and the sidelobes are above the -10 db value.

2.5.3.3 COMPUTER SIMULATION

A digital simulation of the array was undertaken to investigate possible causes of the poor E array patterns around Nadir. Initially a simplified mathematical model, where all dipoles were on a 6° dihedral, perfect ground plane, revealed that the phasing of the dipoles to provide a plane wave at Nadir caused an end fire beam only 9 db down from the peak gain at Nadir. The model was then expanded so that all dipoles had the proper vertical separation. A perfect ground plane and isotropic radiators were used in order to keep the problem from becoming too cumbersome. The phase tapers to the dipoles were varied such that focusing of a plane wave occurred at angles other than straight down (Nadir). A linear scaling of the phasing required to focus at Nadir was applied using the values of 1.0, 0.8, 0.75, 0.7, 0.65, 0.55, and 0.5. These correspond to focusing at 0°, 37°, 41°, 46°, 50°, 57°, and 60° respectively.

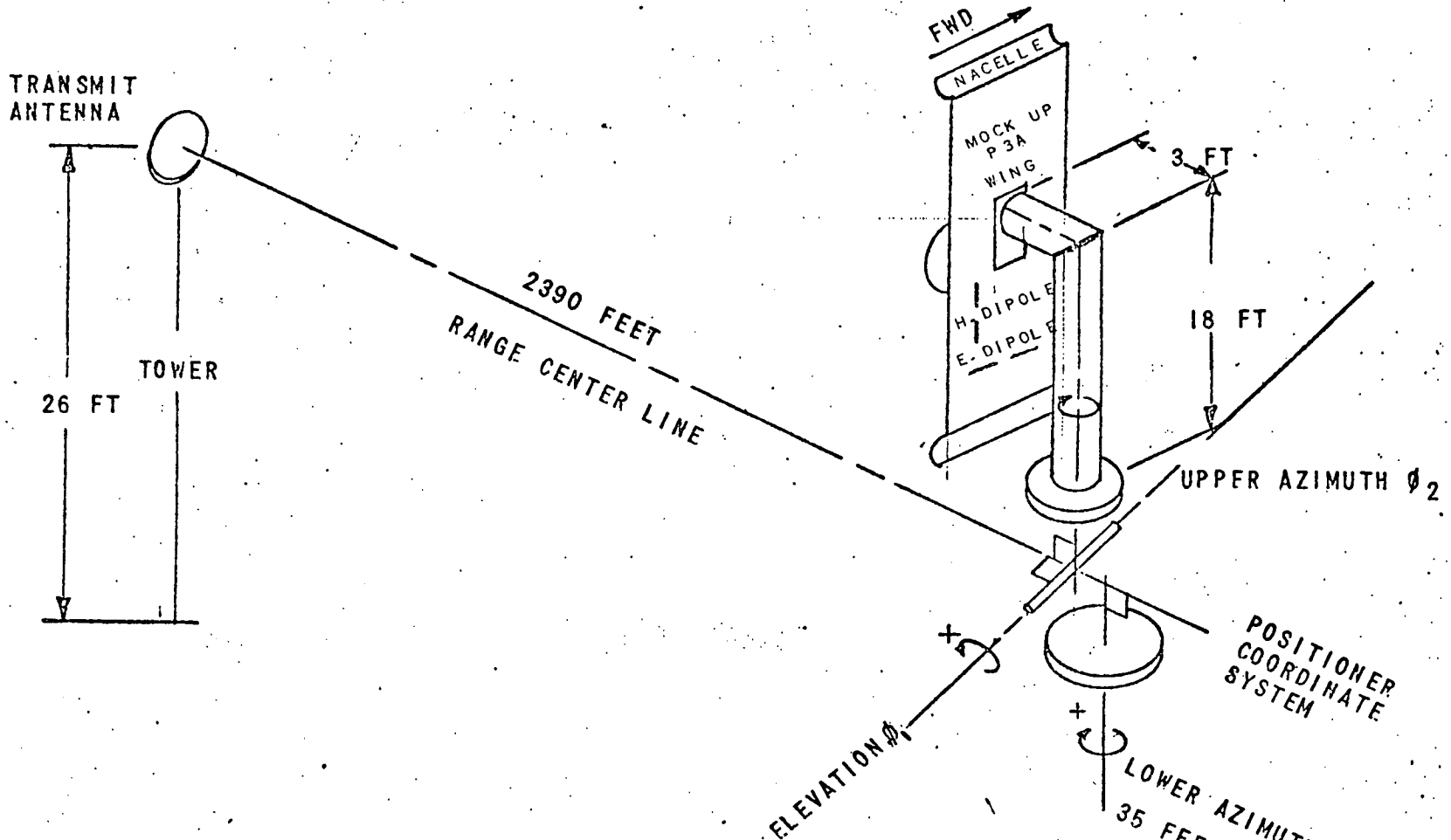

FIGURE 2.35 BORESIGHT TEST FACILITY

PATTERN NO. DATE

PROJECT

ENGRS.

REMARKS

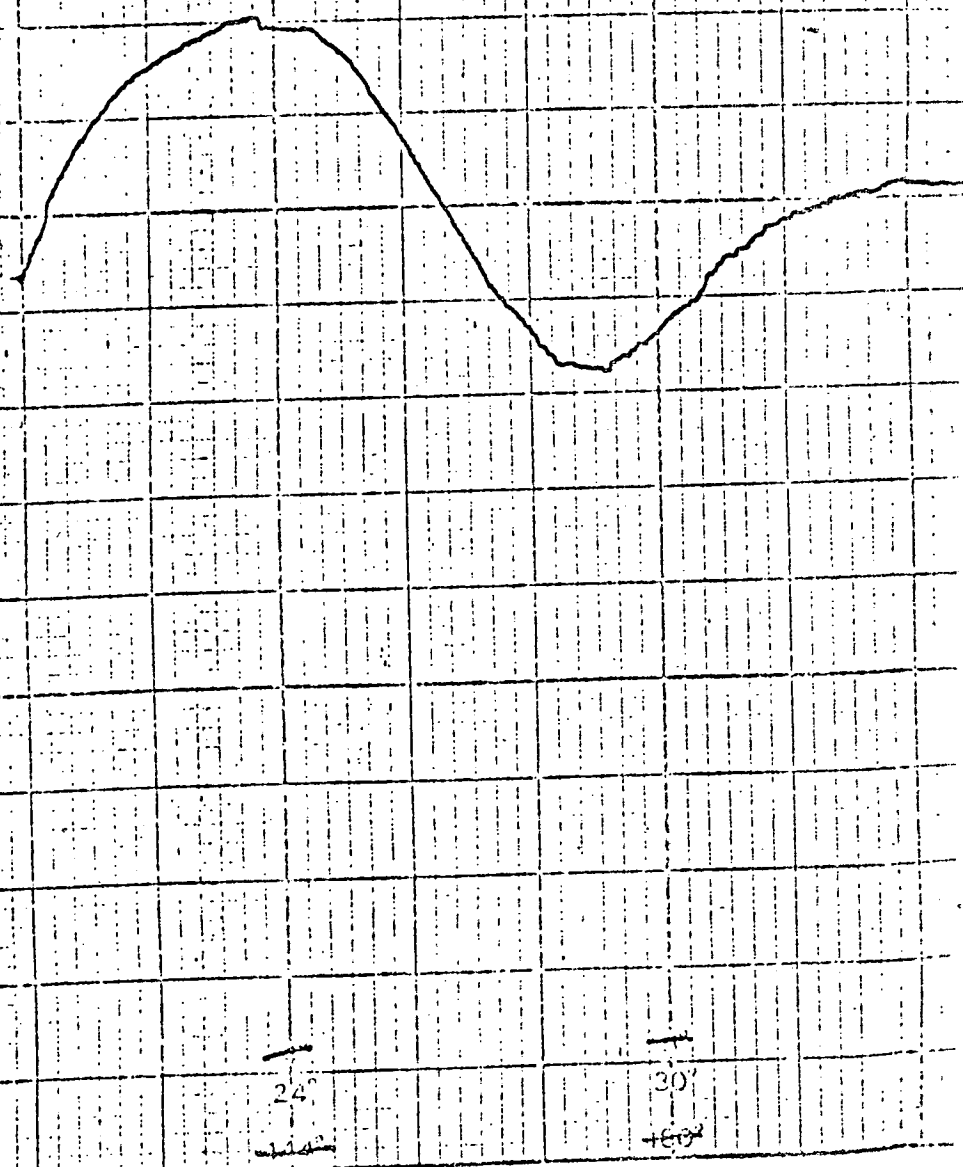

24°

30°

+60°

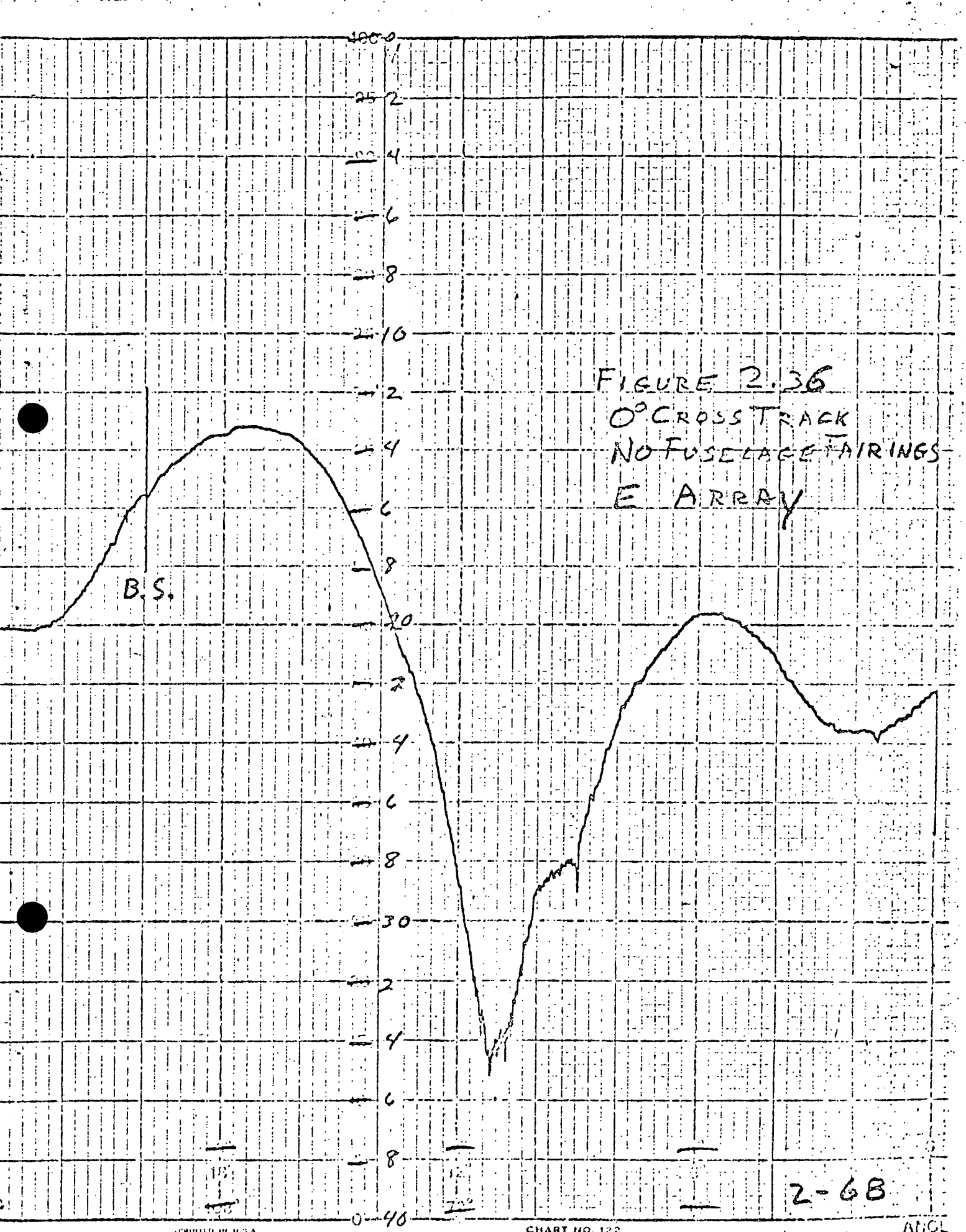

FIGURE 2.36
0° CROSS TRACK
NO FUSELAGE FAIRINGS
E ARRAY

2-68

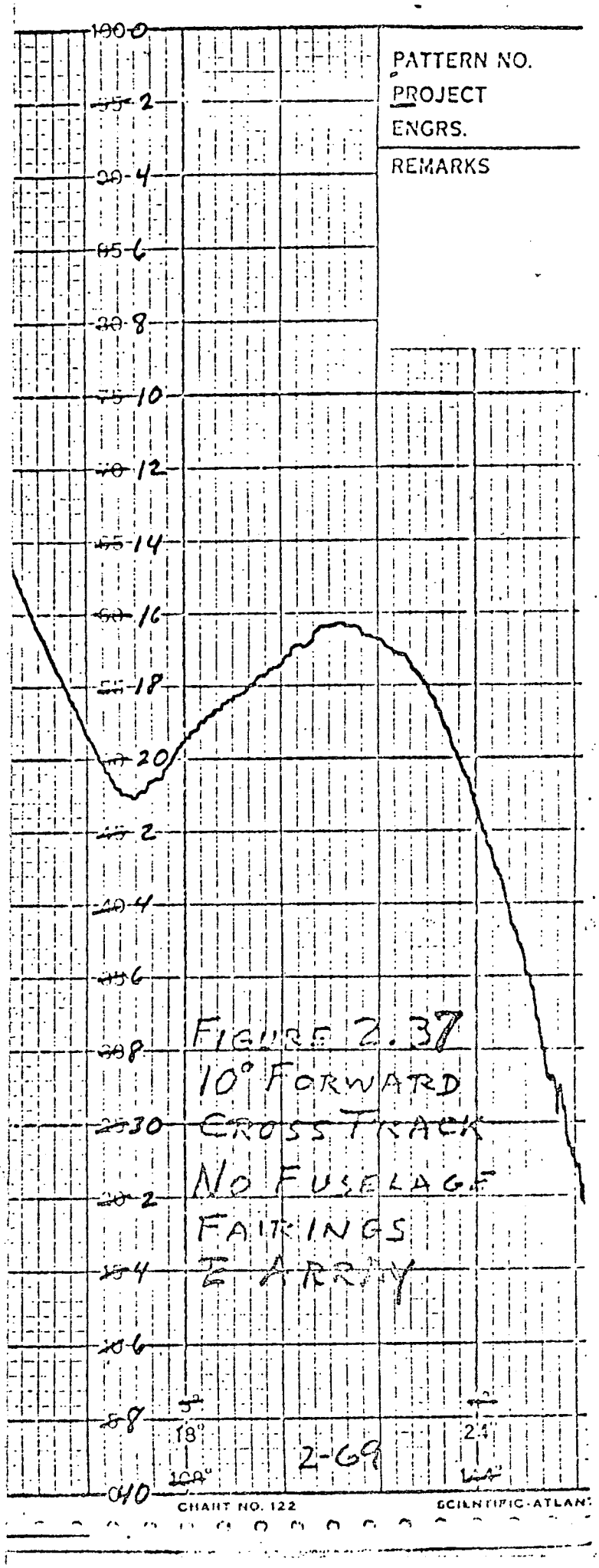
PATTERN NO.
PROJECT
ENGRS.
REMARKS
FIGURE 2.37
10° FORWARD
CROSS TRACK
NO FUSELAGE
FAIRINGS
T-ARRAY
2-69
CHART NO. 122
SCIENTIFIC-ATLANTA

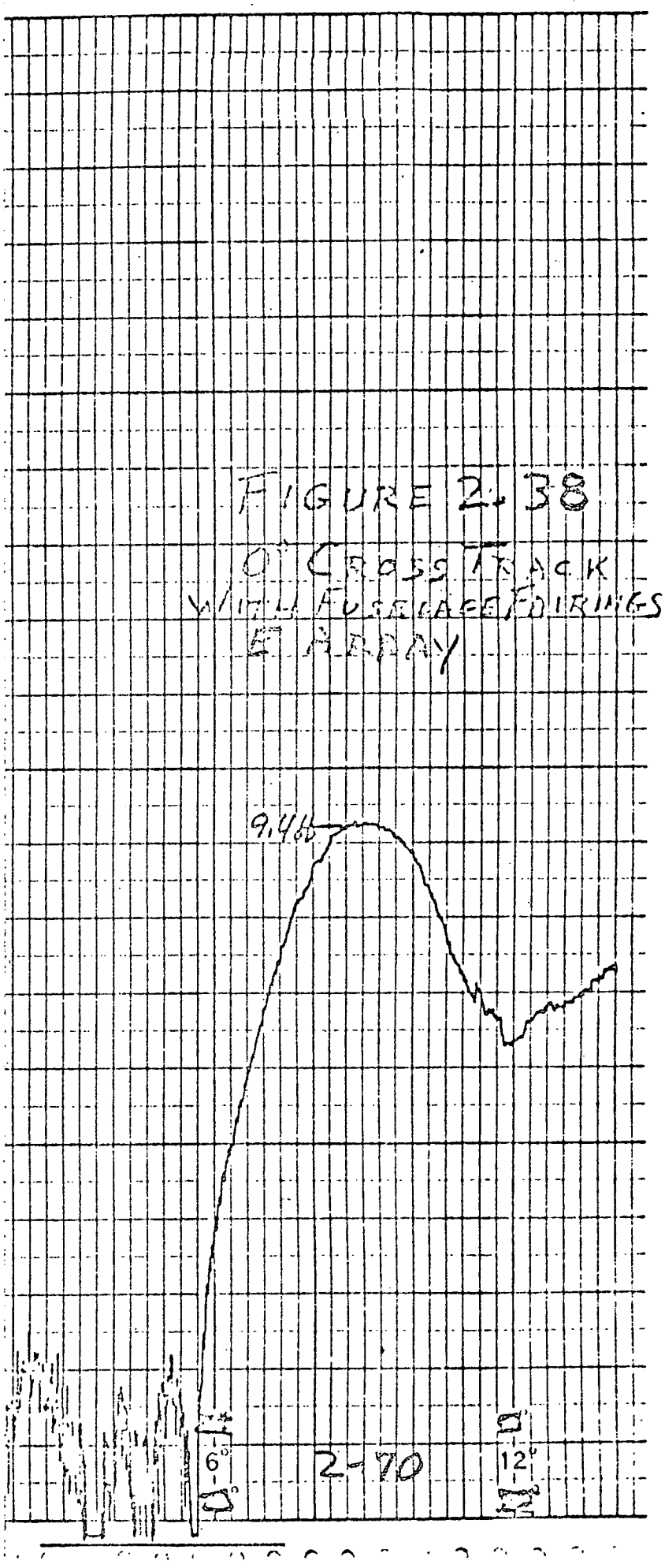

FIGURE 2-38
O° CROSS TRACK
WITH AUXILIARY RINGS
E ARRAY

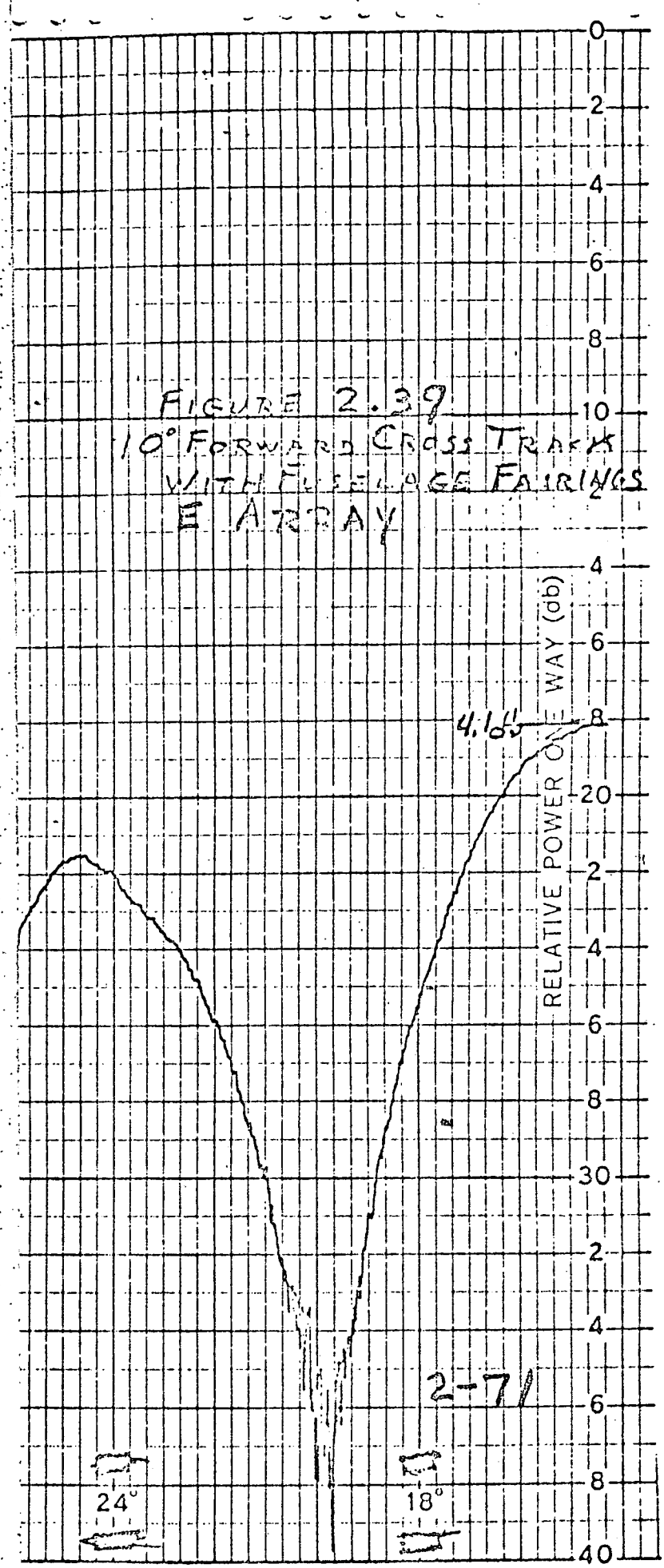

FIGURE 2.39
10° FORWARD CROSS TRACK
WITH FUSELAGE FAIRINGS
E ARRAY

A brief summary of the results are given in Table 2.5, Antenna Simulation Results, for the phase reduction factors of 1.0, 0.8, 0.7, and 0.5.

Angle of Focus	0^{o}	37^{o}	46^{o}	60^{o}
Nadir HPBW	6.33^{o}	6.40^{o}	6.46^{o}	6.72^{o}
60^{o} HPBW	6.65^{o}	6.43^{o}	6.37^{o}	6.34^{o}
Nadir Sidelobe Level	-23.7db	-25.3db	-23.2db	-19.2
60^{o} Sidelobe Level	-15.9	-19.3	-24.2	-24.0
Nadir End Fire Level	-13.2	-15.9	-17.5	-20.9
60^{o} End Fire Level	-22.7	-23.7	-29.3	-32.0

TABLE 2.5 ANTENNA SIMULATION RESULTS

As the angle at which the energy is focused is increased (farther from Nadir) the Nadir beamwidth and sidelobe levels worsen. However, the total energy in the end fire beam is materially reduced. The effect of the end fire beam as it reflects off the nacelles on the sidelobes at Nadir could not be determined without a very large extension of the simulation program. NASA, U of Kansas and Emerson agreed that a phasing factor of 0.6 corresponding to 53^{o} should be the best compromise.

2.5.3.4 FINAL BORESIGHT RANGE TESTS

Various phases of preparation for and conduction of the final antenna tests took place as indicated in this section. Activities at the Antenna Facility MSC, Houston, Texas, began on 23 September and were completed on 24 October 1968.

2.5.3.4.1 CHANGES INCORPORATED

The major change to the antenna was the rephasing of the energy at each dipole port to focus a plane wave at 53^{o} rather than in a plane perpendicular to the Nadir. In addition dipole couplers were selected to give the closest pairing between front and rear ports at each location.

Cable lengths were adjusted to give closer phase tolerances between front and rear dipole pairs.

Two days before the antenna was returned to NASA, an alignment error between the fuselage and the wing amounting to a 1.5^{o} pitch up of the wing was detected. Five weeks later the error had been corrected and the mock up returned to NASA.

Starting on 23 September the antenna mount and antenna were installed on the mock up. The fuselage fairings were simulated without the benefit of profile support plates. Nacelle fairings were also simulated for the first time. Correction of the fuselage to wing angular error removed the one inch gaps previously experienced between the front fairing and the wing.

2.5.3.4.2 RANGE VALIDATION

A sixteen foot arm and probe carriage, sequentially mounted in eight radial positions, was used to measure field amplitude in a plane perpendicular to the transmitting source. Amplitude variations were of the order of $\pm$ 0.5 db. This is indicative of reflected energy no more than 23 db down from the direct energy. This reflected energy coming in through the high gain regions of the antenna could be almost equal to the direct energy at Nadir. Reflected energy should be 40 db or more below the direct energy.

Amplitude probes were also made in vertical planes $\pm 30^{o}$ and $\pm 60^{o}$ from boresight. Cross polarization reception was also measured in each vertical plane. The results obtained at these angles would be more indicative of what the Scatterometer antenna would experience since the high gain of the antenna is at $\pm 60^{o}$. The Range Validation report has not been available for study or comparison to the measured antenna data.

2.5.3.4.3 ADJUSTMENT PROCEDURE

Each array was designed with two adjustments. The phase of the rear array was to be adjusted so as to position the difference null at the mock up boresight position. The sum attenuator was then to be used to adjust the null depth. A third minor adjustment was the phasing of the sum and difference energy to give symmetrical addition at the front and rear cross-over in the along track patterns. These adjustments were not independent insofar as the phasing of front and rear array gave a deep difference null only when perpendicular to the panels. Depth of the difference pattern

affected the array null depth even though the difference was 10 db or more lower than the sum. The reason for this is that at boresight (or null) the difference energy is 180^{o} from the sum and subtracts. Amplitude and phase proved more critical than expected. It was found that the sum and difference phasing normally set for 90^{o} in order to obtain fore and aft symmetry also affected null position and had a large effect on near Nadir cross track pattern sidelobes. The effects of phasing the sum and difference energies were especially pronounced between $\pm 20^{o}$ along track where the difference energy is low compared to the peak energy. Difficulty in controlling energy comes from ground plane variance and reflections off nacelles and fuselage.

Final configurations were a compromise between along track and cross track patterns using all three adjustments to give the best overall performance regardless of the initial function of the parameter.

2.5.3.4.4 ELEMENT PATTERNS

The H Array adjustments easily brought the patterns into acceptable shape. However, the E Array was much more difficult and the best had two to four nulls near Nadir with higher sidelobes. Fundamental patterns were taken of the front and rear arrays by themselves, their sum, difference and combination, to determine why the two arrays reacted so differently. Figure 2.40 is the H Array, Along Track, Front and Rear Arrays. These patterns were taken with the parasitics installed and the other row of dipoles loaded through the power divider. This pattern shows the pronounced coupling of the parasitic in the almost mirror imaging for the front and rear arrays of the deep null occuring not at Nadir as it does for a single dipole only but at 40^{o} toward the parasitic.

Figure 2.41 is the H Array Along Track, Sum, Difference and Full Array Patterns. For these particular patterns the phasing of the sum to the difference was not the best as evident in the pattern dissymmetry. The sum is 11.7 db higher than the difference at Nadir showing almost exactly 180^{o} phase difference to produce a full array gain 3.9 db down from the sum.

Figure 2.42 is the H Array Nadir Cross Track, Sum, Difference and Full Array Patterns. In this minimum energy plane the sum and difference patterns are formed from the front and rear arrays with peak gain 20 db or higher than the resulting patterns. Imperfections in the ground plane, nacelle

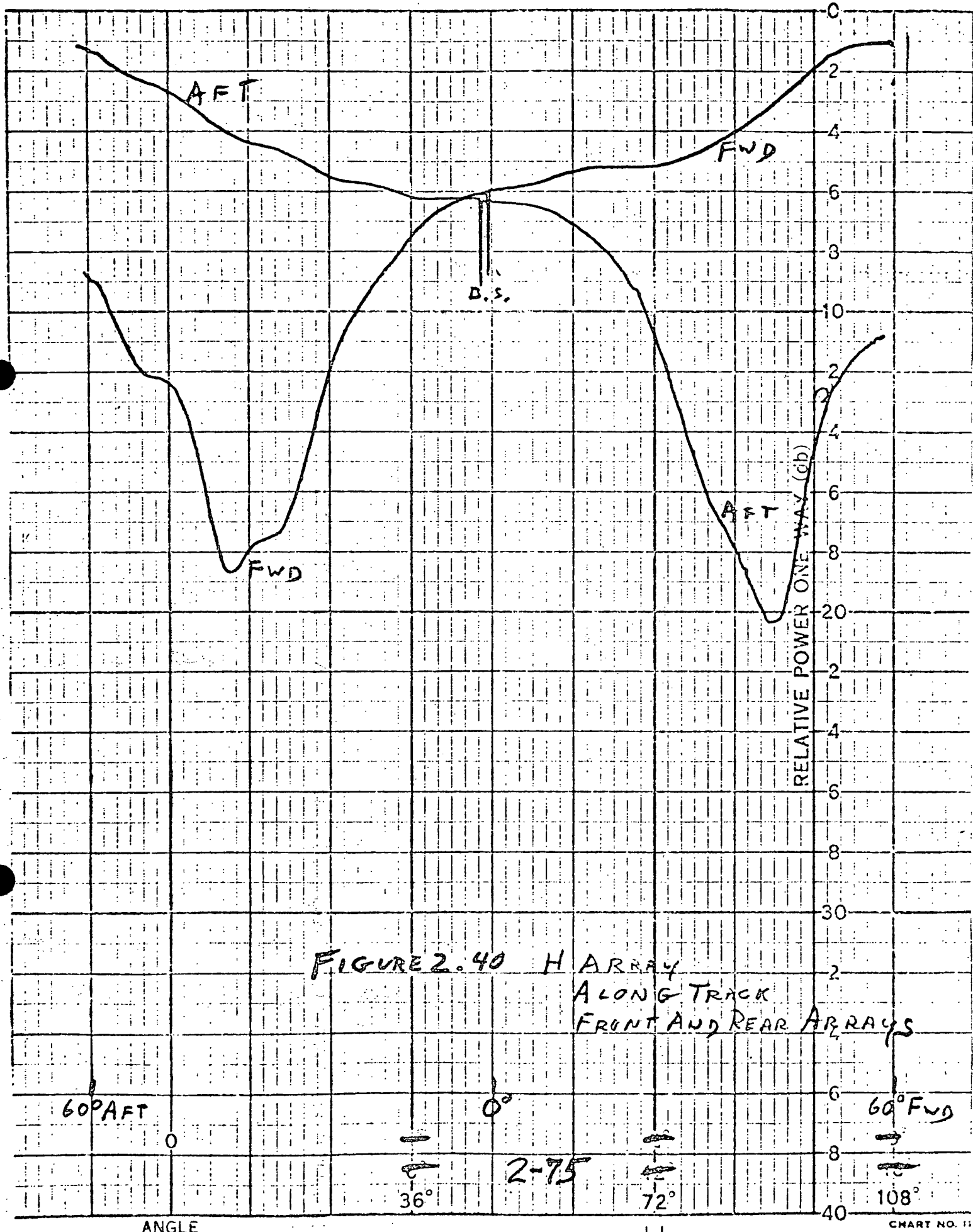

FIGURE 2.40 H ARRAY
ALONG TRACK
FRONT AND REAR ARRAYS

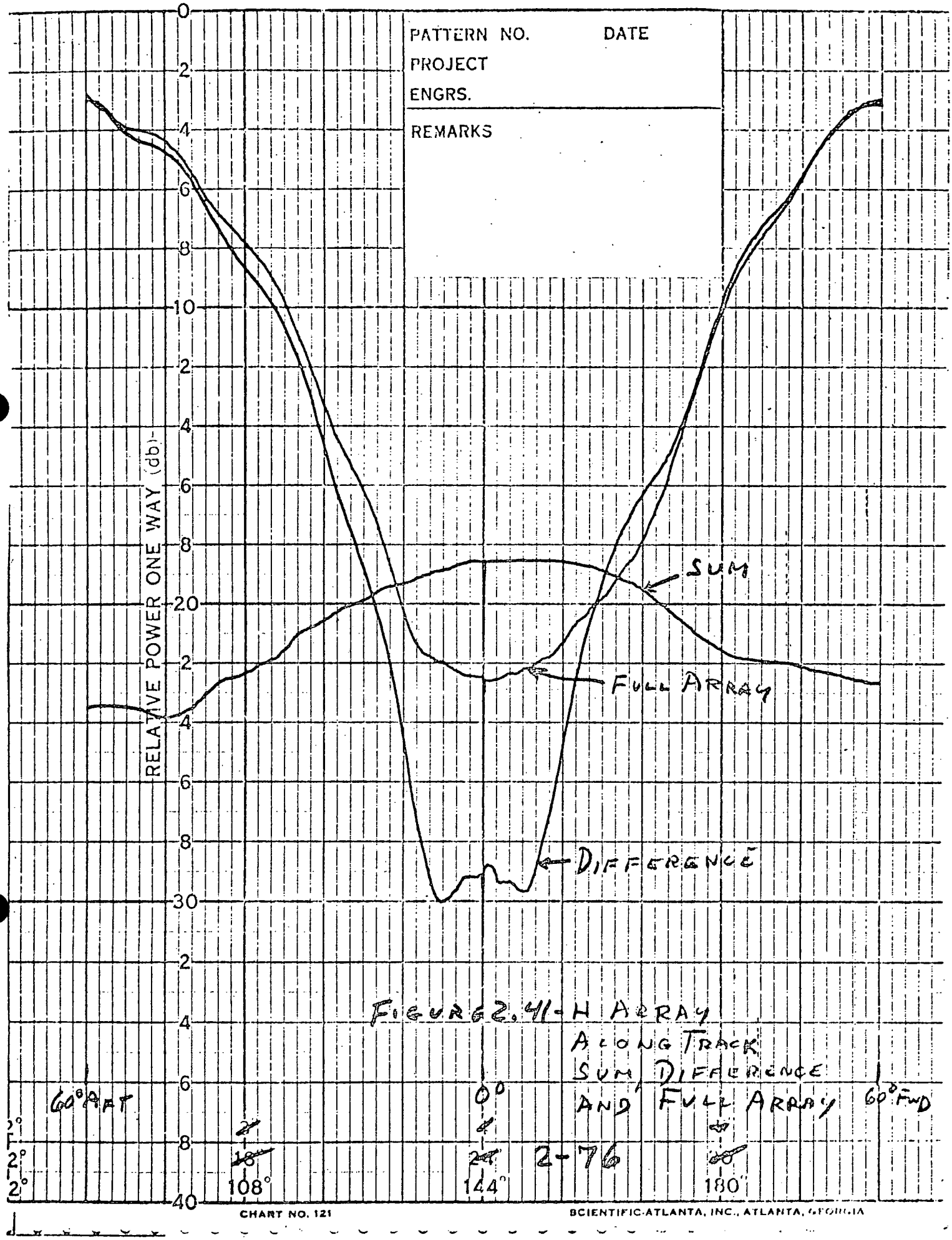

FIGURE 2.41-H ARRAY ALONG TRACK SUM, DIFFERENCE AND FULL ARRAY


20° LEFT
30°
0°
20° RIGHT
2-77

reflections and phase and amplitude unbalance would be expected to produce wide deviation in phase and amplitude with cross track angle. The Full Array pattern is surprisingly good.

The element patterns for the E-Array are shown in Figure 2.43, E Array Along Track, Front and Rear Arrays. The comparison with the H Array pattern points out the difficulty with the E Array. The along track patterns have ripples caused by the interruptions to the ground currents running longitudinally around the wing by the discontinuities in the ground plane at the fairings and the drop off of the leading edge of the wing. The H Array currents run laterally and do not see these physical interruptions. Another factor is that near Nadir there are several crossovers of the front and rear array patterns indicating areas where the amplitude of front and rear arrays are equal and the phase is near 180^{o}.

Figure 2.44 is The E Array Along Track, Sum, Difference and Full Array Patterns. The difference pattern near Nadir has several nulls and peaks resulting from the multiple cross over of the element patterns. The phasing of the sum and difference is essentially correct as shown by the good symmetry of the full array patterns. However near Nadir the sum and difference are near 180^{o} and subtract so that the peaks of the difference cause the multiple nulls of the full array. Much time and effort were expended on the E Array in the attempt to improve the Nadir region. The dip at Nadir in the Sum pattern was felt to be indicative of insufficient parasitic action. The parasitics were blocked off the ground with little beneficial effect. At all times cross track patterns had to be investigated at various along track angles, particularly in the along track nulls to see the total effect of the phase and amplitude adjustments.

Figure 2.45 is the E Array Nadir Cross Track, Sum, Difference and Full Array Patterns. The fact that the sum and difference phasing varies such that the two patterns add at certain cross track angles and subtract at others contribute to the relative height of the side lobes on both the right and left sides for certain along track angles.

This discussion was presented since it is the best explanation known for the difference between the E and H Array patterns.

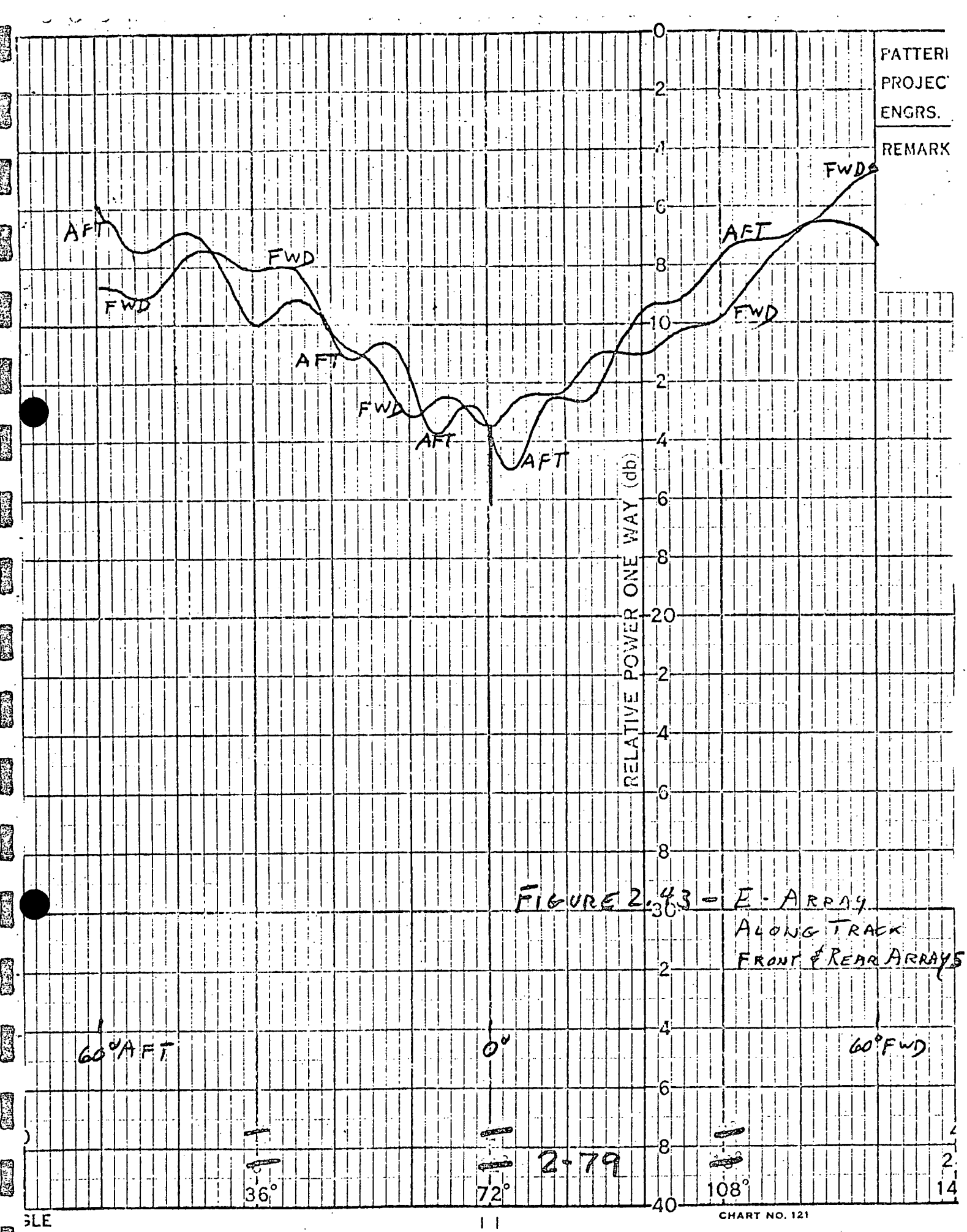

FIGURE 2.43 - E-ARRAY ALONG TRACK FRONT & REAR ARRAYS

2-79

CHART NO. 121

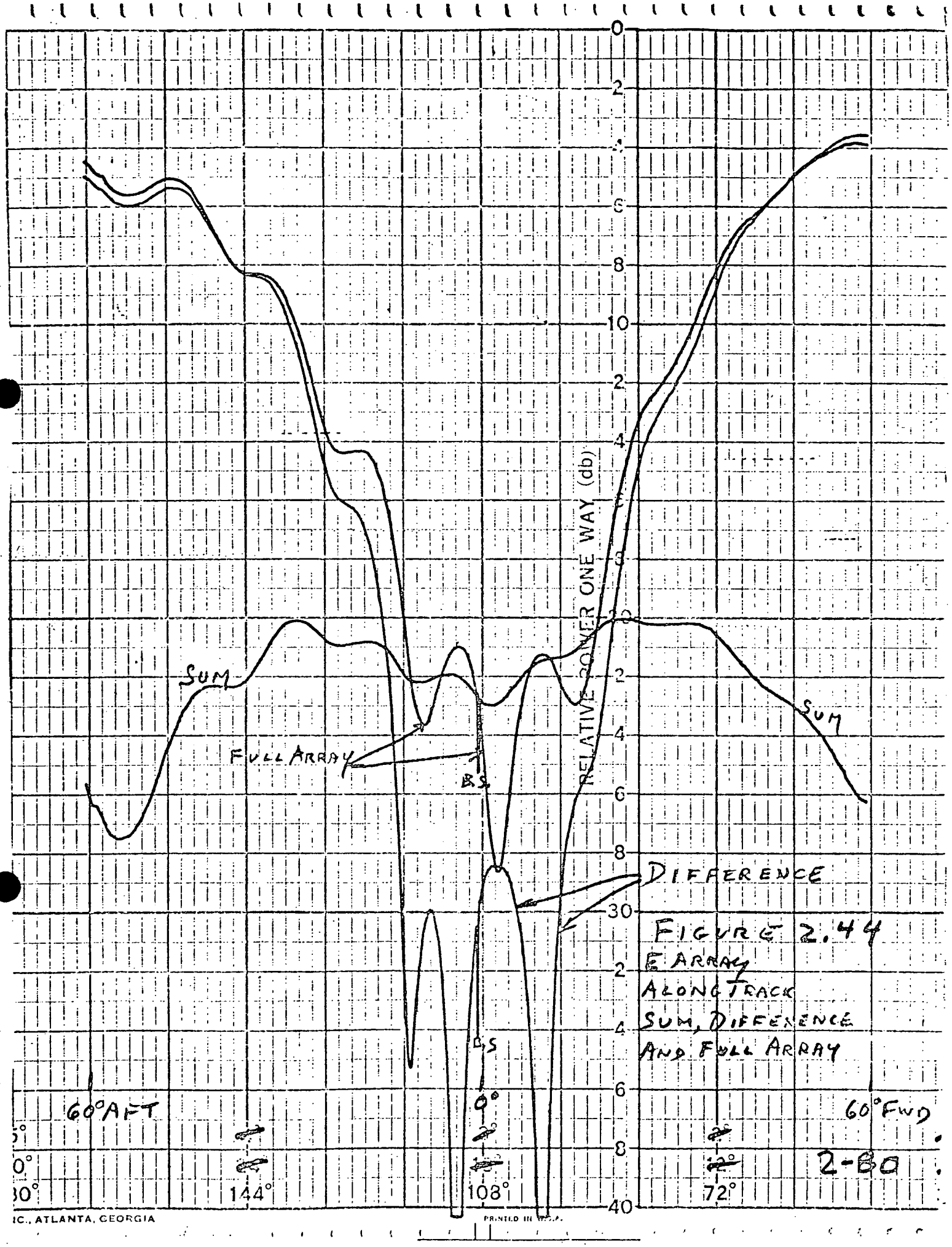

FIGURE 2.44
E ARRAY
ALONG TRACK
SUM, DIFFERENCE
AND FULL ARRAY

2-80

PATTERN NO. DATE

PROJECT

ENGRS.

REMARKS

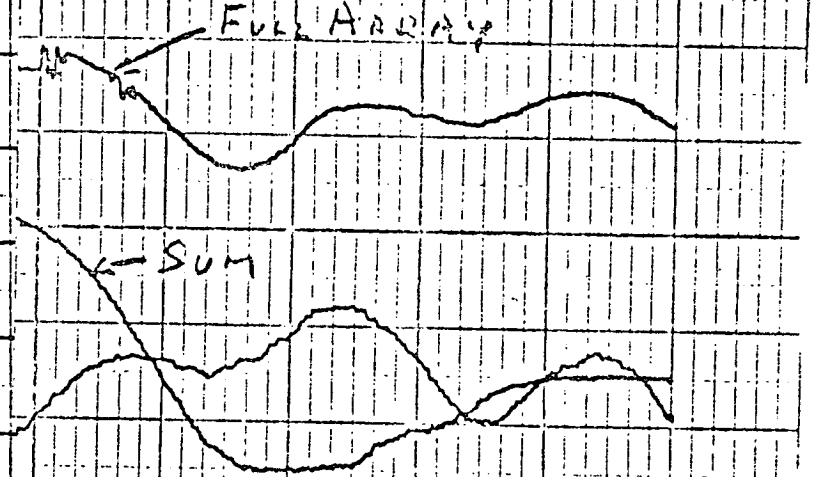

2.45 — E ARRAY
NADIR CROSS TRACK
SUM, DIFFERENCE AND FULL ARRAY

20° LEFT 20° RIGHT

18° 24°

72°

CHART NO. 121

SCIENTIFIC-ATLANTA, IN

2.5.3.4.5 ANTENNA MEASUREMENTS

The results of the antenna acceptance tests and a summary of the antenna patterns are given in this section.

Null Location - The H Array null was located by the midpoint between 5 db above minimum and 3 db down from minimum peak gain. The H Array null location was

	Along Track	Cross Track
Mid Pattern Point	4.03^{o} FWD	0.45^{o} Left
Minimum Peak	1.43^{o} FWD	0.62^{o} Left

The multiple nulls and the shape of the E-plane along track pattern around Nadir did not allow meaningful data taken at pattern midpoints. The minimum peak gain location was found to be the following for the E Array.

Along Track	Cross Track
2.65^{o} aft	2.58^{o} left

Peak Location - The location of the peak gain was found by taking a 0^{o} along track pattern. At the indicated peak gain a cross track pattern determined the skew of the peak. An along track cut was then made at this skew angle to determine the true peak gain.

	FWD	AFT
H Array	61.48^{o}; 1^{o} Left	60.35^{o}; 1.55^{o} Left
E Array	59.56^{o}; 1.28^{o} Left	62.59^{o}; 1.13^{o} Left

Notch Depth - The relative gains were measured at the indicated peak and null locations. The notch depth referred to each peak is as follows:

	FWD	AFT
H Array	19.8 db	19.6 db
E Array	19.7 db	18.3 db

VSWR - The Voltage Standing Wave Ratio was measured at the input to the two Control Boxes. The cable losses to the Control Boxes which were as high as 2.2 db, were used to compute the worse VSWR. The results were the following:

	398.35 MHz	400.85 MHz	403.35 MHz
H Array	1.08	1.15	1.27
E Array	1.74	1.16	1.78

Gain - The absolute gain of the arrays were measured referenced to a standard dipole and a Yagi antenna. The results are given below.

	FWD	AFT
H Array	17.85 db	17.65 db
E Array	16.4 db	15.1 db

Port-Starboard Patterns - These cross track pattern were taken every 1^{o} along track from 70^{o} forward to 70^{o} aft. The torque of the mock up on the Elevation axis limited motion to 20^{o} right to 20^{o} left. These patterns were recorded on magnetic tape and will be computer processed to give gain, equivalent square beamwidth and skew for the three cases of E^2, H^2 and EH for later use in the data reduction of reflectivity measurements. Patterns every 5^{o} were analyzed and a summary for the H Array is given in Table 2.6. A summary of the E Array patterns is given in Table 2.7.

Cross Polarization Patterns - The principle along track and the Nadir cross track patterns were taken using the correct transmitter polarization and also the cross polarization. After the mockup was rotated 90^{o} the same patterns were taken. The effects of range refections for both polarizations were evident. The 0^{o} Azimuth 0^{o} Elevation (Nadir) cross polarization attenuation is given below.

H Array

	Wings Vertical	Wings Horizontal
Along Track	18.6 db	19.5 db
Cross Track	26.0 db	18.0 db
	Average 20.5 db	

E Array

	Wings Vertical	Wings Horizontal
Along Track	18.3 db	24.4 db
Cross Track	21.2 db	19.3 db
	Average 20.8 db	

2.5.3.4.6 ANTENNA TEST DATA REDUCTION

It is extremely difficult to appraise the probable accuracy of reflectivity measurements by looking at an antenna pattern. Side lobe level is not the only factor affecting performance. The Scatterometer system measures total

TABLE 2.6

H ARRAY PATTERN SUMMARY

	HPBW	SKEW	10 db BW	Left Sidelobe	10° Left Skirt	10° Right Skirt	Right Sidelobe
70° FWD	6.2°	0.7°L	12.2°	20.9 @ 10.2			18.9 @ 13.0
65°	6.2°	.9°L	10.7°	22.6 @ 10°			18.7 @ 14.0
60°	6.1°	.7°L	11.0°	20.6 @ 15°			17.1 @ 12.0
55°	6.3°	.7°L	11.2°	19.7 @ 14.3			15.9 @ 12.7
50°	6.6°	.4°L	11.3°	19.5 @ 10			15.6 @ 13.3
45°	7.1°	.8°L	11.3°	21.0 @ 16.3		18.9	18.4 @ 14.0
40°	6.0°	.9°L	12.0°	22.4 @ 15.3			20.8 @ 11.2
35°	5.3°	.5°L	10.5°	15.9 @ 10.7		18.0	
30°	5.8°	.1°R	10.8°	10.9 @ 10.0		11.3	18.0 @ 17.7
25°	8.2°	.4°R	12.9°	15.7 @ 16.0	8.6	10.0	13.9 @ 18.0
20°	8.1°	2.1°L	13.4°	15.7 @ 20.3	10.3	15.1	14.3 @ 19.0
15°	6.5°	1.2°L	15.6°	13.3 @ 19.9	14.7		19.3 @ 15.7
10°	5.5°	.8°L	14.0°	14.4 @ 19.3	17.6	17.0	17.6 @ 17.0
5° FWD	6.7°	.8°L	14.1°	15.1 @ 17.8	11.6		18.1 @ 16.8
0°	7.2°	.3°R	16.1°	13.8 @ 17.0	10	15.3	13.2 @ 18.0
5° AFT	5.9°	.5°L	17.8°	13.2 @ 20.3	11.3	14.5	18.1 @ 16.8
10°	7.4°	1.9°L	19.0°	16.1 @ 15.0	9.7	11.7	18.0 @ 14.6
15°	7.2°	.2°L	17.4°	16.0 @ 19.5	10.6	10.5	24.8 @ 17.3
20°	5.9°	1.0°L	14.2°	15.0 @ 20.0	13.8	12.4	18.6 @ 20.0
25°	6.5°	.9°L	14.0°	17.8 @ 20.0	12.6	15.7	17.5 @ 18.9
30°	6.6°	.6°L	11.7°	19.1 @ 19.3	12.8	14.1	19.1 @ 18.0
35°	6.1°	.3°L	11.2°	18.0 @ 20.0°	15.5	20.0	
40°	5.9°	.8°L	11.1°		17.5	20.7	
45°	6.8°	1.3°L	10.8°		17.5	21.6	
50°	6.0°	.6°L	10.6°	20.6 @ 10.1			23.2 @ 11.5
55°	5.5°	.9°L	10.7°		23.8		21.0 @ 13.3
60°	6.7°	1.5°L	10.4°	23.8 @ 15.0			19.9 @ 12.5
65°	6.2°	0°	10.6°	23.2 @ 15.0			21.3 @ 12.2
70°	4.9°	.8°L	10.5°		22.2		23.1 @ 13.0

TABLE 2.7

E ARRAY PATTERN SUMMARY

	HPBW	SKEW	10 db BW	Left Sidelobe	10° Left Skirt	10° Right Skirt	Right Sidelobe
70° FWD	6.4°	1.1°L	11°	16.3 @ 14			17.2 @ 12.0
65°	6.7°	1.0°L	11.7°	15.2 @ 14			16.4 @ 13.0
60°	7.0°	1.1°L	12.3°	14.4 @ 13.5		15.5	
55°	7.1°	1.1°L	12.8°		14.8		14.8 @ 12.0
50°	7.0°	1.0°L	12.8°	15.0 @ 14.8			14.2 @ 18.0
45°	7.0°	1.2°L	12.7°	16.6 @ 15.0			14.4 @ 15.0
40°	6.9°	1.2°L	12.7°		14.2		14.8 @ 16.5
35°	7.0°	1.7°L	19.0°		8.9	11.0	
30°	7.2°	1.8°L	32.4°		6.1	8.2	
25°	7.5°	2.6°L	OPEN R	10 @ 15.2	5.2	7.5	8.2 @ 18.5
20°	6.3°	2.4°L	OPEN R	10 @ 17.3	6.1	7.2	6.3 @ 18.0
15°	6.2°	2.5°L	14.1°	8 @ 15.0	10.0		6.8 @ 20.0
10°	5.7°	2.2°L	10.5°	7.8 @ 15.2		9.8	7.6 @ 20.0
5° FWD	6.0°	2.1°L	14.5°		9.1	7.6	
0°	6.6°	2.5°L	15.6°		4.4	6.0	6.6 @ 20.0
5° AFT	7.1°	1.9°L	15.5°	9.4 @ 15.0	7.7	9.5	7.9 @ 20.0
10°	6.4°	1.7°L	14.8°		7.9	7.3	10.0 @ 20.0
15°	5.6°	2.1°L	10.6°	11.9 @ 17.0		9.5	
20°	6.6°	2.1°L	14.4°		8.3	7.8	
25°	6.6°	1.4°L	13.5°		10.1	8.8	
30°	6.3°	1.5°L	13.4°		11.1	11.0	
35°	6.9°	1.8°L	12.9°		11.7	13.0	
40°	6.8°	1.2°L	11.8°		14.3		16.9 @ 20.0
45°	6.8°	1.3°L	11.7°		16.6	18.3	
50°	6.5°	1.1°L	11.3°		19.2		17.9 @ 17.0
55°	6.8°	1.2°L	11.3°	21.7 @ 16.0			19.6 @ 15.5
60°	6.9°	0.9°L	11.9°	21.1 @ 16.0			20.7 @ 14.0
65°	6.8°	1.2°L	11.9°	19.7 @ 14.0			20.1 @ 14.0
70° AFT	7.0°	1.2°L	11.9°	18.9 @ 14.0			20.3 @ 13.0

signal power within a Doppler cell corresponding to a specific along track angle. This power is proportional to $\sigma_o(\phi) \int_{-\phi_1}^{+\phi_1} G_T \, G_R \, d\phi$ for that angle. The beamwidth is small enough so the σ_o can be considered constant except for the E Array between 5° aft and 30° forward. A more accurate computation of effective square beamwidth in this region should include a weighting factor of a normalized average σ_o versus cross track angle.

Two of the worse 90° to 90° cross track patterns, at Nadir and 20° forward, were analyzed in a fashion similar to that required to compute the antenna characteristics to be used as inputs for the σ_o Data Reduction Program The process involves a normalization to peak gain, squaring to represent two way transmission and reception through an array, in this case the E Array, and conversion of the gain squared to the equivalent of relative signal level. Integration then provides the effective square beamwidth. In this case however, weighting by σ_o was not used so that the values obtained will be slightly worse than if it had been used. If the integration is performed from the largest angle of interest, right and left, toward the 0° point, the percent of energy in the tail (from that angle to the largest angle of interest) can be obtained. The true energy centroid or beam skewness can also be obtained as the intersection of the right and left cumulative energy curves. The effects of energy in the sidelobes can be analyzed by determining the angle at which 10% of the total energy is contained from that point to the limit of angle measurement. The spread of angles containing 50% of the energy is also of interest. A tabulation of this pattern analysis is given below for the two cases studied.

	Effective Square Beamwidth	Energy Centroid Skew	10% Left	10% Right	25% Left	25% Right
Nadir	8.65°	1.3° Left	12°	22°	5°	3.6°
20° Forward	7.93°	1.6° Left	10°	20°	5°	2.0°

The 90° to 90° cross track patterns could only be taken from 20° forward to 20° aft. An examination of the same two cases was made to see how much energy was contained beyond 20°.

	20° Left	20° Right
Nadir	10.1%	9.6%
20° Forward	3.0%	8.1%

Since these patterns represent high sidelobe conditions, the errors associated with integrating the patterns only from 20° to 20° for those angles where 90° to 90° data is not available should be small. As an example, the E Array 20° aft 90° to 90° cross track, was analyzed. Less than 9% of the total energy was contained beyond 4° on either side. Only 0.11% existed beyond 20° left and 1.2% beyond 20° right.

The antenna patterns were further analyzed along with the variations of reflectivity coeficients to determine the probable range of received signal strength as a function of along track angle or Doppler frequency. The relative gain values from the along track patterns of Figures 2.9 and 2.10 were used in the equation.

$$P = K \sigma_{o(\theta)} \quad G^2_{p(\theta)} \quad \left(\frac{HPBW_{(\theta)}}{6} \right)$$

where K = constant

σ_o = reflectivity coefficient

G_p = gain at the along track angle

HPBW = Half power beam width

The effective square beam width should have been used but since they had not been computed at all angles the HPBW was used. This has been shown to be sufficiently close. The division by six rationalizes the beamwidth to an expected average. The reflectivity coefficents from Dr. R. Moore's report for the case of water and woods were used to generate Figure 2.46, Received Signal Distribution.

Several comments should be made about this graph. The amplitude is relative only but does give the dynamic range for any particular altitude and mode. The maximum contribution from the variation in beam width was only 2 db. The mock up boresight was aft of the minimum gain for both the E and H Array producing the slight fore-aft dissymmetry causing higher signal levels from the aft returns.

The dynamic range of signals over woods will be a maximum of 22.5 db over the 60° to 60° along track angles. The dynamic range over water, to the limits of -40 db σ_o, is 32 db. The variable gate channels will have to be used to measure the small signal returns beyond 44°. Increasing the

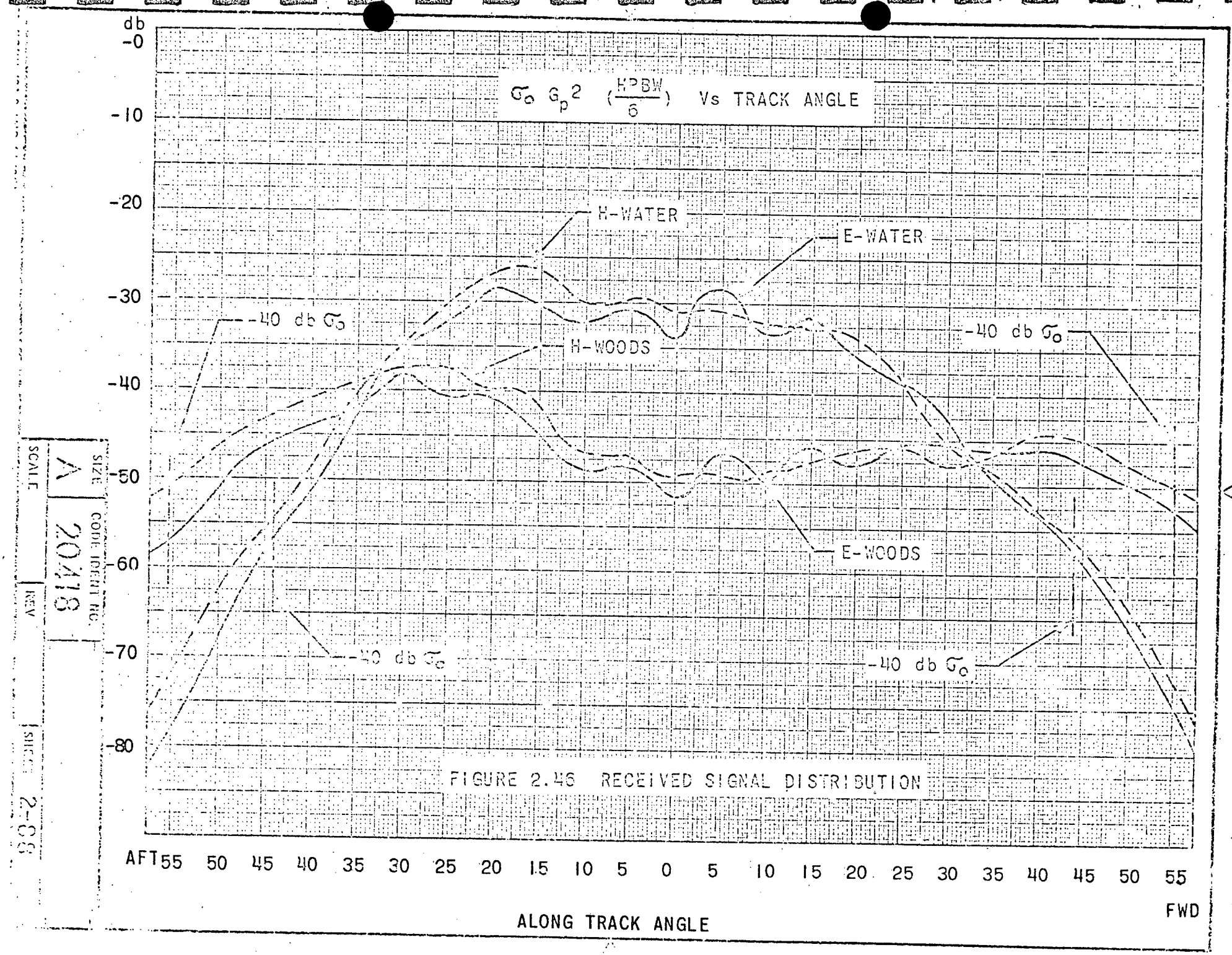

FIGURE 2.46 RECEIVED SIGNAL DISTRIBUTION

SIZE A | CODE IDENT NO. 80418 | REV

SCALE

SHEET 2-83

SECTION III

DATA ANALYSIS

3.1 DETERMINATION OF σ_o

The value of σ_c (θ) is obtained by using the following expression derived in Section 2.4.2.2, page 2-15 of this report.

$$\sigma_c(\theta) = \frac{P_R}{P_T} \quad \frac{2(4\pi)^3}{\lambda^3} \quad \frac{Vh^2}{\Delta f} \quad \frac{1}{\int_{-\phi_1}^{+\phi_1} G_T(\psi)_\theta \, G_R(\psi)_\theta \, d\psi}$$

where θ = Angle of incidence, angle from nadir in the along-track direction.

P_R = peak received power in the doppler window defined by Δf

P_T = peak effective transmitter power

λ = wavelength

V = aircraft velocity

h = altitude

$G_T(\psi)\,\theta$ = transmit antenna gain at fixed θ and variable cross track angle, ψ.

$G_R(\psi)\,\theta$ = receiver antenna gain at fixed θ and variable cross track angle, ψ.

Δf = doppler window. $= \dfrac{2\,V\,d_2\cos^3\theta}{h\,\lambda}$

d_2 = length of along track ground patch, over which an average σ_o (θ) is computed.

The recorded output data from the Scatterometer system contains the relationship between the transmitted power, P_T, to the received power, P_R. This relationship is established at a common point in the system, and combined with antenna pattern, aircraft velocity, altitude, and attitude data, it is possible to ascertain the desired reflection coefficient.

Calibration signals are generated in the Scatterometer system which serve as references in the recorded data. In any one signal channel, the recorded data includes backscatter signal and a calibrate signal. The ratio of backscatter signal to calibrate signal is established in the data reduction. In a similar manner, the calibrate receiver output is used to establish the ratio of transmitted signal level to calibrate signal level. These ratios have been given the following designations:

$$\frac{\text{Transmitter Sample}}{\text{Calibrate Signal}} = A$$

$$\frac{\text{Received Signal}}{\text{Calibrate Signal}} = B$$

The calibrate signals are related by a constant which varies as a function of receiver gain positions and mode of operation. The desired relationship is given by the following:

$$P_R/P_T = K\ B/A$$

3.2 SUMMARY OF DATA REDUCTION PROCESS

Data reduction of the Scatterometer data is best illustrated by following through the computations in the detailed flow diagram as given in Figure 3.1. Across the diagram, the data flow begins with the analog data input from the FM demultiplexer that has been used to read out the aircraft analog tape. Next, the demultiplexed data is converted by analog to digital converters into a form that is suitable for input to the computer. This input mode can be either digital tape as indicated on the drawing or it can be a direct access entry into the computer disk. Across the central portion of the diagram a number of data selection operations and computations for programmed values of θ are accomplished. Finally, the computer outputs are written on data output tapes which can be either duplicated or read into peripheral equipment. The output data can be automatic plots from the peripheral equipment, punched cards, computer listings, or the copied tape which could be used directly by the user.

For a given flight, the data output consists of σ_0 data in one of two forms as determined by the interests of the user: 1) σ_0 vs θ plots 2) σ_0 vs distance at various incidence angles. For each of the two forms of data the user has the further option of using specific patches or resolution

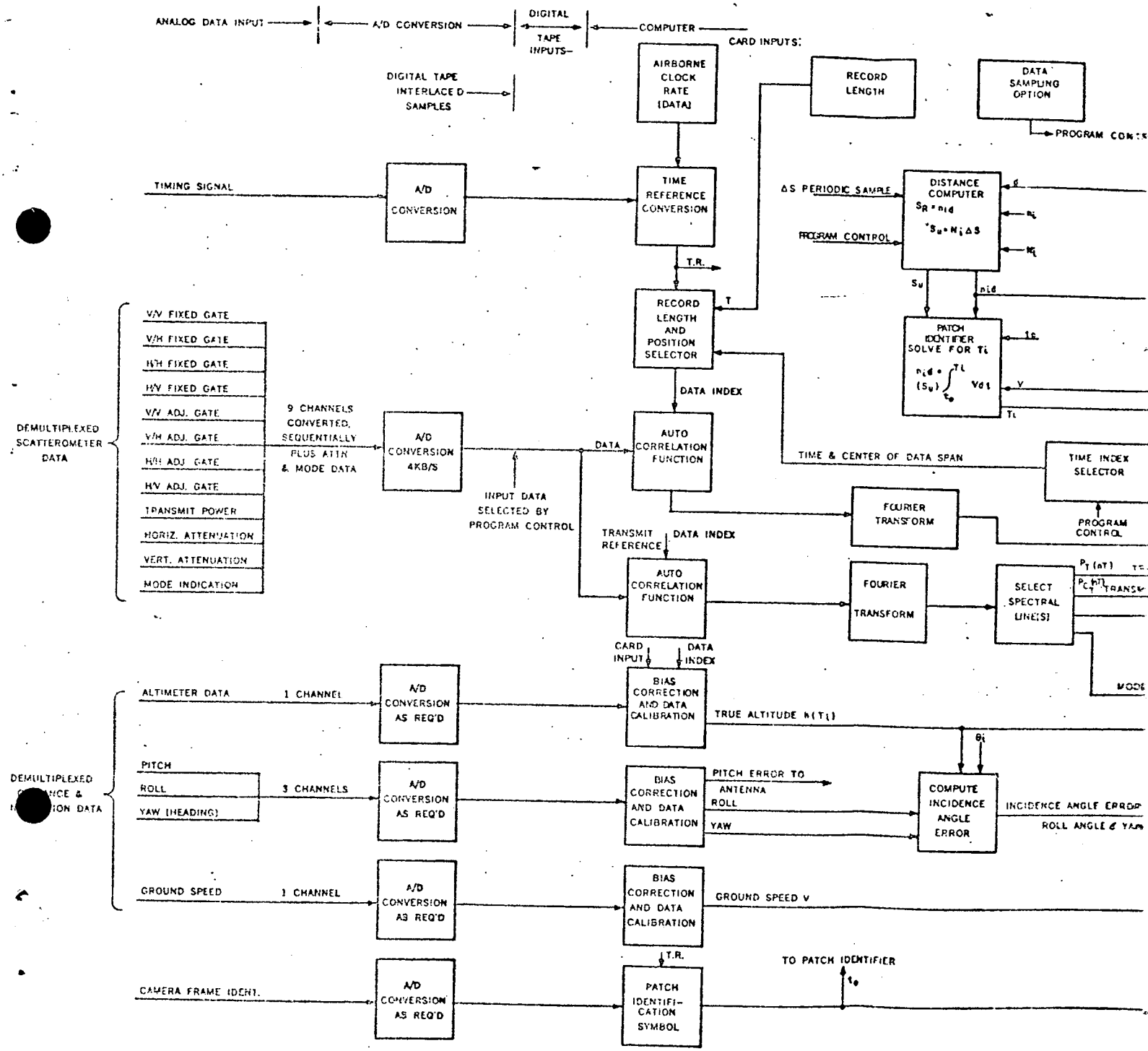
ANALOG DATA INPUT
A/D CONVERSION
DIGITAL TAPE INPUTS
COMPUTER
CARD INPUTS:
DIGITAL TAPE INTERLACED SAMPLES
AIRBORNE CLOCK RATE (DATA)
RECORD LENGTH
DATA SAMPLING OPTION
PROGRAM CONTROL
TIMING SIGNAL
A/D CONVERSION
TIME REFERENCE CONVERSION
ΔS PERIODIC SAMPLE
PROGRAM CONTROL
DISTANCE COMPUTER
T.R.
RECORD LENGTH AND POSITION SELECTOR
PATCH IDENTIFIER SOLVE FOR Tᵢ
DATA INDEX
V/V FIXED GATE
V/H FIXED GATE
H/H FIXED GATE
H/V FIXED GATE
V/V ADJ. GATE
V/H ADJ. GATE
H/H ADJ. GATE
H/V ADJ. GATE
TRANSMIT POWER
HORIZ. ATTENUATION
VERT. ATTENUATION
MODE INDICATION
DEMULTIPLEXED SCATTEROMETER DATA
9 CHANNELS CONVERTED, SEQUENTIALLY PLUS ATTN & MODE DATA
A/D CONVERSION 4KB/S
INPUT DATA SELECTED BY PROGRAM CONTROL
DATA
AUTO CORRELATION FUNCTION
TIME & CENTER OF DATA SPAN
TIME INDEX SELECTOR
FOURIER TRANSFORM
PROGRAM CONTROL
TRANSMIT REFERENCE
DATA INDEX
AUTO CORRELATION FUNCTION
FOURIER TRANSFORM
SELECT SPECTRAL LINE(S)
CARD INPUT
DATA INDEX
ALTIMETER DATA
1 CHANNEL
A/D CONVERSION AS REQ'D
BIAS CORRECTION AND DATA CALIBRATION
TRUE ALTITUDE h(Tᵢ)
PITCH
ROLL
YAW (HEADING)
3 CHANNELS
A/D CONVERSION AS REQ'D
BIAS CORRECTION AND DATA CALIBRATION
PITCH ERROR TO ANTENNA
ROLL
YAW
COMPUTE INCIDENCE ANGLE ERROR
INCIDENCE ANGLE ERROR
ROLL ANGLE & YAW
GROUND SPEED
1 CHANNEL
A/D CONVERSION AS REQ'D
BIAS CORRECTION AND DATA CALIBRATION
GROUND SPEED v
T.R.
TO PATCH IDENTIFIER
CAMERA FRAME IDENT.
A/D CONVERSION AS REQ'D
PATCH IDENTIFICATION SYMBOL

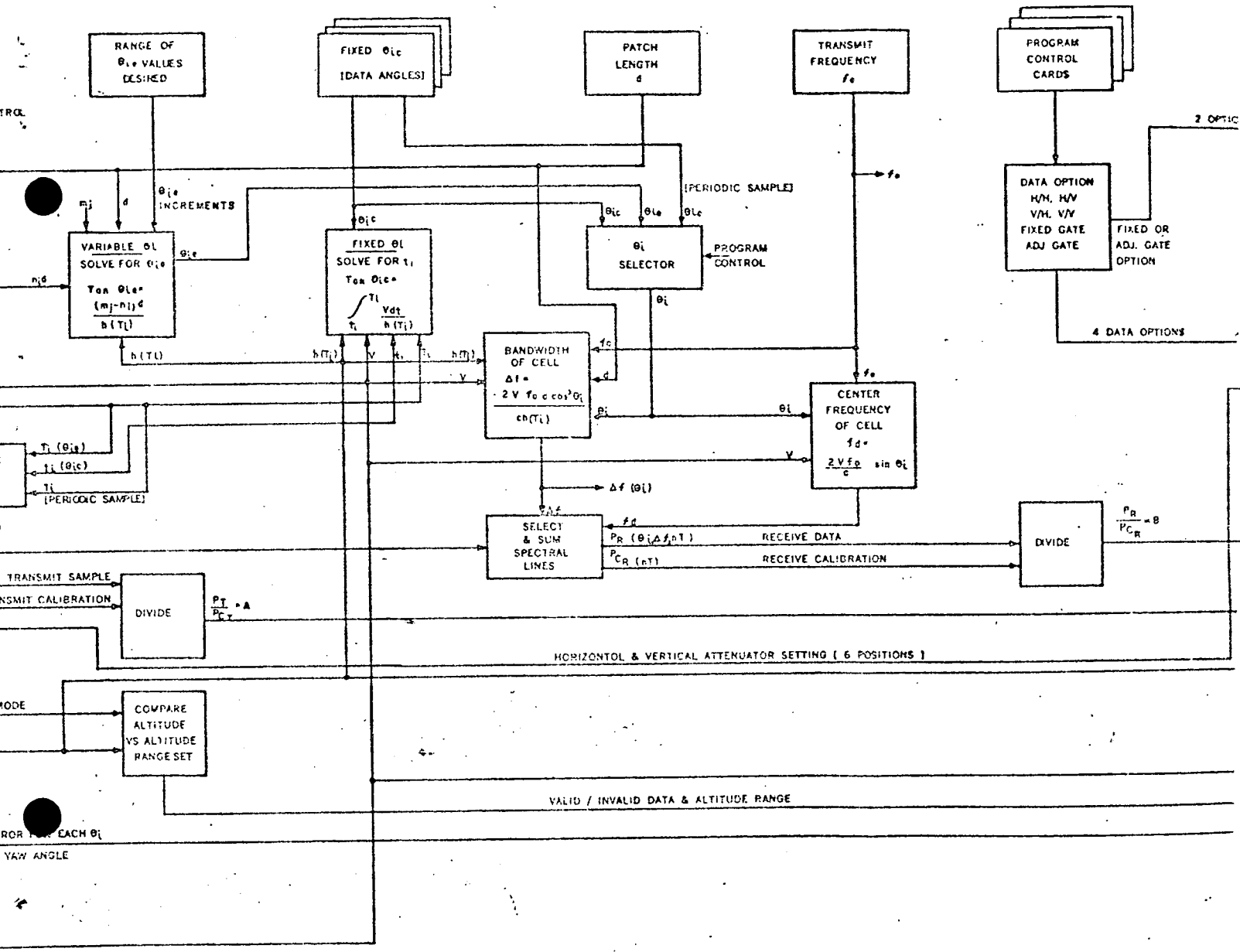
RANGE OF θi,e VALUES DESIRED
FIXED θi,c [DATA ANGLES]
PATCH LENGTH d
TRANSMIT FREQUENCY fo
PROGRAM CONTROL CARDS
2 OPTIC
[PERIODIC SAMPLE]
θi,e INCREMENTS
VARIABLE θL SOLVE FOR θi,e
Tan θi,e = (mj-nj)d / h(Tl)
FIXED θL SOLVE FOR ti
Tan θi,c = ∫ Vdt / h(Ti)
θi SELECTOR
PROGRAM CONTROL
DATA OPTION H/H, H/V V/H, V/V FIXED GATE ADJ GATE
FIXED OR ADJ. GATE OPTION
4 DATA OPTIONS
BANDWIDTH OF CELL Δf = 2 V fo c cos²θi / cb(Tl)
CENTER FREQUENCY OF CELL fd = 2Vfo/c sin θi
Ti (θi,e)
Ti (θi,c)
Ti [PERIODIC SAMPLE]
Δf (θi)
SELECT & SUM SPECTRAL LINES
PR (θi, Δf, nT) RECEIVE DATA
PCR (nT) RECEIVE CALIBRATION
DIVIDE
PR / PCR = B
TRANSMIT SAMPLE
NSMIT CALIBRATION
DIVIDE
PT / PCT = A
HORIZONTOL & VERTICAL ATTENUATOR SETTING [6 POSITIONS]
ODE
COMPARE ALTITUDE VS ALTITUDE RANGE SET
VALID / INVALID DATA & ALTITUDE RANGE
ROR FOR EACH θi
YAW ANGLE

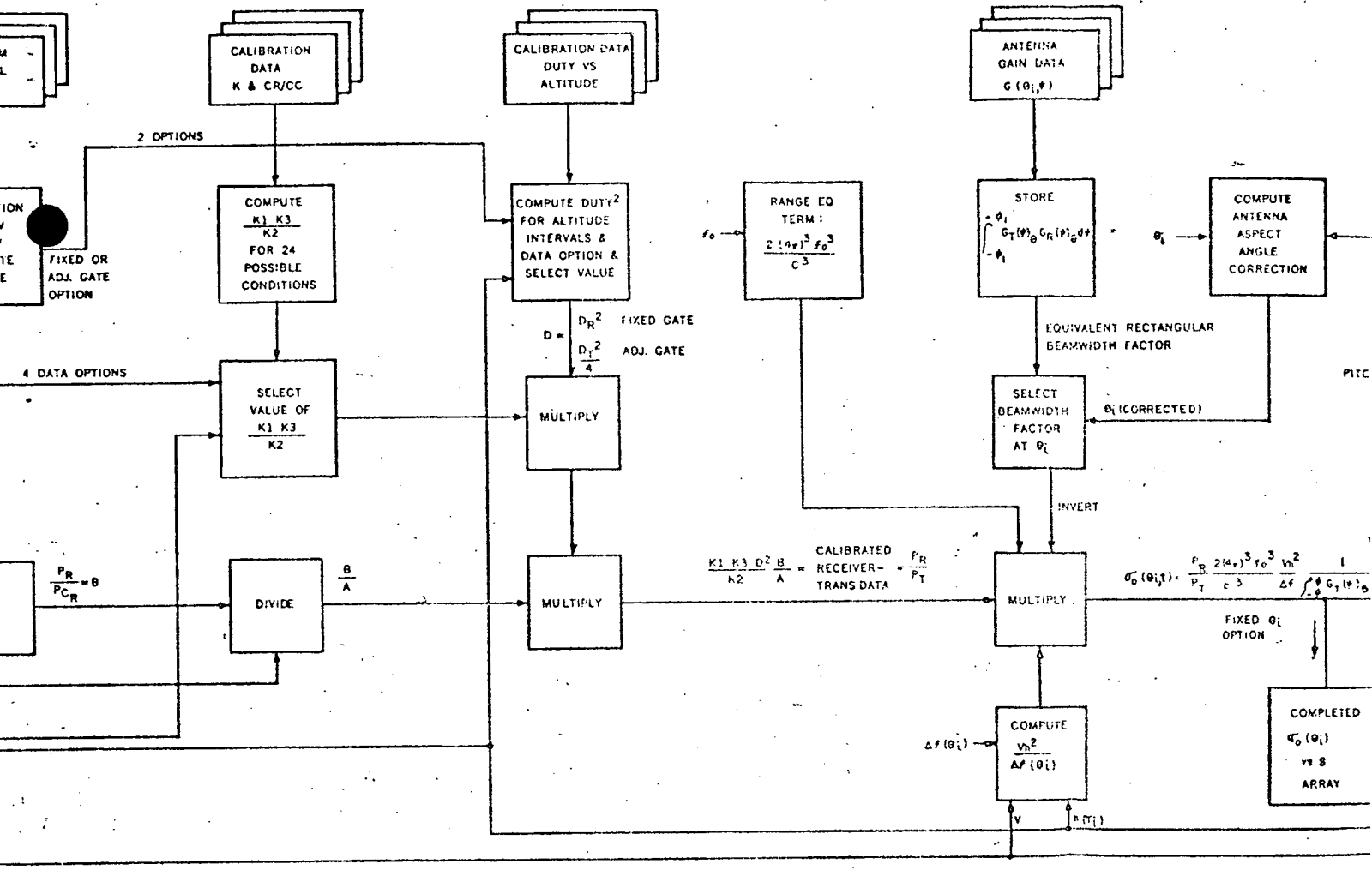
CALIBRATION DATA K & CR/CC
CALIBRATION DATA DUTY VS ALTITUDE
ANTENNA GAIN DATA G(θi,φ)
2 OPTIONS
COMPUTE K1 K3 / K2 FOR 24 POSSIBLE CONDITIONS
COMPUTE DUTY² FOR ALTITUDE INTERVALS & DATA OPTION & SELECT VALUE
RANGE EQ TERM : 2(4π)³ fo³ / c³
STORE ∫ GT(φ)θ GR(φ)θ dφ
COMPUTE ANTENNA ASPECT ANGLE CORRECTION
FIXED OR ADJ. GATE OPTION
D = DR² FIXED GATE
DT²/4 ADJ. GATE
EQUIVALENT RECTANGULAR BEAMWIDTH FACTOR
4 DATA OPTIONS
SELECT VALUE OF K1 K3 / K2
MULTIPLY
SELECT BEAMWIDTH FACTOR AT θi
θi (CORRECTED)
INVERT
PR/PCR = θ
DIVIDE
B/A
MULTIPLY
K1 K3 D² B / K2 A = CALIBRATED RECEIVER-TRANS DATA = PR/PT
MULTIPLY
σo(θi,t) = PR/PT 2(4π)³ fo³/c³ Vh²/Δf ∫ GT(φ)θ
FIXED θi OPTION
COMPUTE Vh²/Δf(θi)
Δf(θi)
COMPLETED σo(θi) vs θ ARRAY
V
R(Ti)

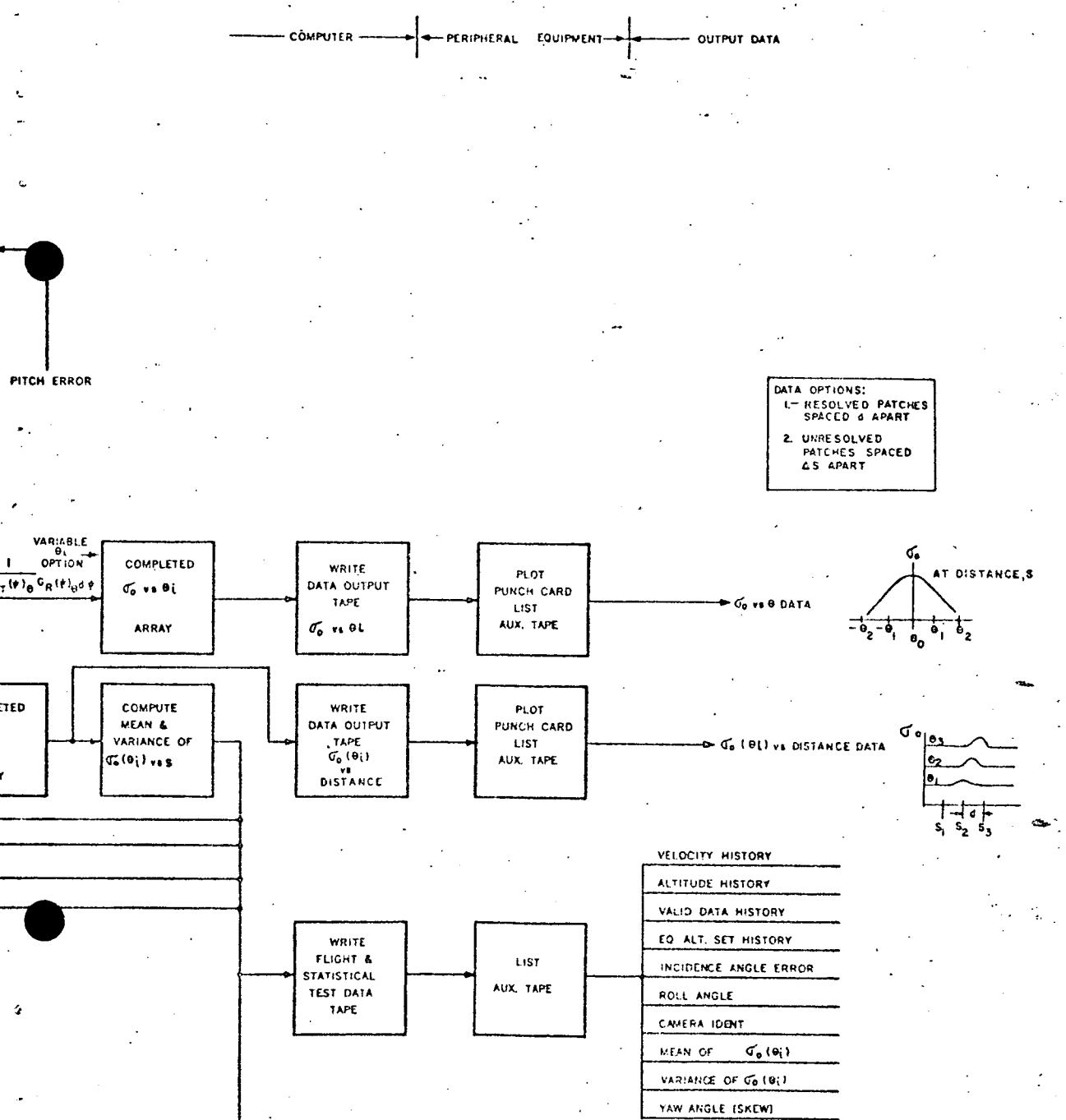

COMPUTATIONAL FLOW DIAGRAM
FIGURE 3.1

SIZE	CODE IDENT NO.	2236
	20418	
SCALE	REV	SHEET 3 – 3

cells along the flight path or using a simplified computation which does not retain resolved cells. The later is more adaptable to homogeneous terrain such as water in the measurement of sea states.

Another output of the program is a listing of the flight data that influences the data quality but cannot be readily used to compute corrections in the results or to apply statistical tests on the data such as to obtain average value of σ_o and variance of σ_o versus distance. Included in this output is the velocity and altitude history, a recording of the Scatterometer altitude mode, a history of incidence angle error as computed from roll pitch and yaw angles and yaw angle alone which is a measure of the skew of the beam relative to the flight path.

3.3 DETAILED DATA REDUCTION DISCUSSION

Continuing the discussion of the computations required to process the Scatterometer data, the program is fed with fixed data inputs as shown across the top of the diagram in the form of control cards and data card inputs. It should be pointed out that all data can be correlated with ground position by the timing, camera and navigation (e.g. Loran), signals recorded along with Scatterometer data. Data is initially referenced to some benchmark such as a camera frame or position fix, and then related back to this benchmark by using the recorded ground speed and altitude data in timing formulas. Two timing methods are discussed for resolving specific patches and one method is shown for faster plotting of σ_o vs distance for patches that vary slightly in location with incidence angle but are entirely adequate for homogeneous surfaces such as water.

As indicated in the upper left of Figure 3.1, the record length T is used to control the timing signal counter which selects the data input length to be used in the autocorrelation function computation. For each record length which might typically be 2 seconds duration, a complete set of computations is performed to arrive at the σ_o (θ) quantity that is fully corrected for all hardware and propagation effects. The autocorrelation function previously generated serves as a matched filter to optimize signal to noise in the data record. Then a Fourier transform is taken of the autocorrelation function to generate the power within a bandwidth cell corresponding to a given patch along the flight path, the spectral lines would be summed over the bandwidth Δ f determined by the equation shown in the Bandwidth of Cell block of Figure 3.1.

The doppler bandwidth Δf used to select the spectral lines and the center frequency has been calculated from the quantities of aircraft ground speed and aircraft altitude for each record length as indicated by the control lines from the bottom of the diagram. Other fixed inputs are the transmitter frequency, the patch length, and the velocity of light.

For each angle of incidence, θ_i, the output of the "Select, Sum Spectral Lines" block is the total received power in the bandwidth for the θ_i corresponding to the patch desired.

The computations that follow are derived from the overall system equation for back-scattering cross section σ_o given in Section 3.1. The quantity B which is the ratio of power received to the calibrate tone power is derived as follows. The previously computed power received is divided by the calibrate tone power which is also a narrow band signal appearing in the power spectrum and sorted out by the Select and Sum Spectral Lines block. In a similar fashion, the transmit reference signal, which is a sample of the transmitted power, is digitally filtered and compared to a sample of the calibration signal in order that the ratio identified as A may be obtained. The quantity B/A is formed and multiplied by the equipment calibration constants K_1, K_2, K_3, and D^2 that are applicable to the data. The system calibration constants are formed by selecting values which depend on the data option being exercised, that is, the channel being processed, the aircraft altitude, and a minor correction in the duty cycle term of the computation. (It is anticipated that as the altitude changes and hence the time duration of the transmit pulse and receive interval, there will be a slight change in received or transmitted duty cycle. This function will be tabulated as part of the test data and also used in the computation as shown.)

Completion of the σ_o computation requires multiplication by the range equation term,

$$\frac{2\,(4\pi)^3\,fo^3}{c^3}$$

and the value of the integral shown for the antenna gain factor at θi.

An additional scattering coefficient term,

$$\frac{Vh^2}{\Delta f\,(\theta_i)}$$

reflecting the doppler bandwidth is also computed for each θ_i and enters the overall computation. The computations just described are repeated for each value of incidence angle θ_i. The input data is then advanced and the process repeated until all record lengths in the data run have been completed.

3.4 DATA SAMPLING FOR FIXED θ_i (θ_{ic})

As aircraft speed and altitude vary, the times at which data should be sampled also vary, if data at specific incidence angles and for specific ground patches is desired. The computation for this problem is particularly complex since a detailed time history of speed and altitude is used by the computer to track and maintain a specific ground patch under observation from 60^o forward to 60^o aft.

The data sampling procedure for this fixed θ_i case is as follows:

A. Pick a specific patch of interest as in Figure 3.2 centered at $S = \int_{t_o}^{T_i} V dt$ from some bench mark, i.e. camera frame or time mark. Solve for T_i.

B. Select (input) the desired angle θ_{ic}.

C. Solve $\tan \theta_{ic} = \dfrac{\int_{t_i}^{T_i} V dt}{h_{t_i}}$ for t_i, where h_{t_i} is a flight variable associated with t_i.

E. Process data - Fourier Transform - and select doppler cell corresponding to data centered on θ_{ic} from

$$\Delta f = \frac{2 V_{t_i} f_o d \cos^3 \theta_{ic}}{c h_{t_i}}$$

where d is the along track length of the patch and c is the velocity of light

$$f_d = \frac{2 V_{t_i} f_o \sin \theta_{ic}}{c} + 500 \text{ Hz}$$

Measure amplitude compared to calibrate tone.

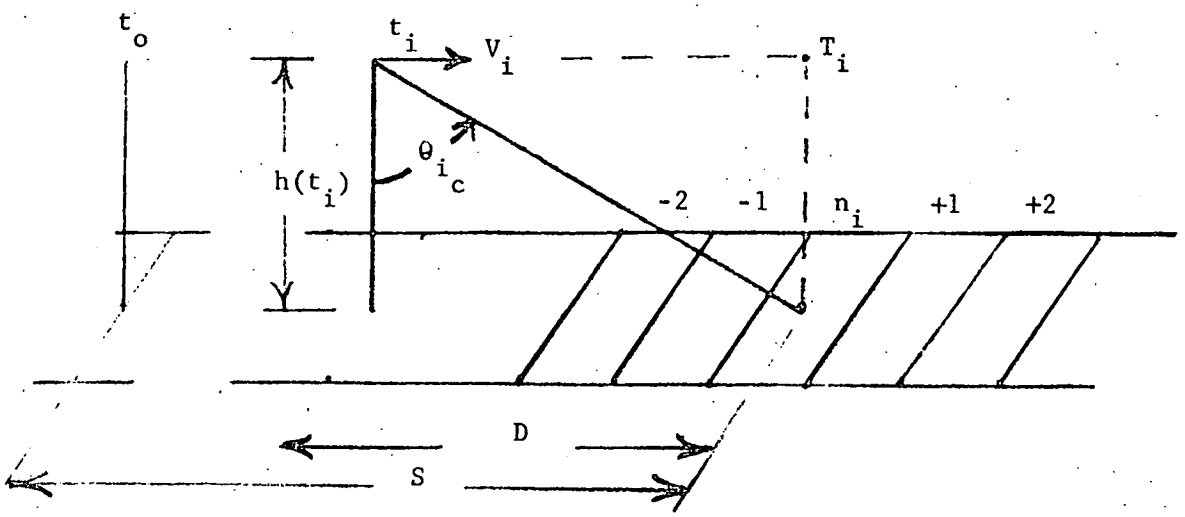

$$\tan \theta_{ic} = \frac{D}{h(t_i)} = \frac{\int_{t_i}^{T_i} V dt}{h(t_i)}$$

Illustrative Table of Unique Times t_i that must be computed for each incidence angle for all patches when altitude and ground speed variations are accounted for.

DESIRED INCIDENCE ANGLE	PATCH NUMBER						
	-3	-2	-1	n_i (at T_i)	+1	+2	+3
$\theta_{(0^o)}$	t_a	t_b	t_c	T_i	t_d	t_e	t_f
θ_1	t_g	t_h	t_i	t_j	t_k	t_l	t_m
θ_2	t_n	t_o	t_p	t_q	t_r	t_s	t_t
θ_3	t_u	t_v	t_w	t_x	t_y	t_z	t_{aa}

FIGURE 3.2 FIXED θ_i GEOMETRY

Note that all other frequencies at the t_i data span are not used since they represent other incidence angles which may not be centered on the other desired patches. Stated differently, t_i, may not be correct for any other θ_{ic} for the other desired patches.

The output of this computation is a tabulation for each incidence angle, θ_{ic}, of σ_o for successive equal patches and the variable parameter time. Since a value of distance is associated with each data point σ_o vs distance curves can be directly plotted.

Since this computation retains specific patch identification, the program could be written so as to fill the σ_o vs θ_i array and thus also obtain σ_o vs θ_i data. Both options are available using this programming. For this reason the additional computation is worthwhile. The σ_o vs distance information can also be analyzed in terms of the statistical quantities of mean and variance of reflectivity for the constant incidence angles.

3.5 DATA SAMPLING FOR VARIABLE θ_i (θ_{ie})

The problem is the same as with fixed θ_i if variable speed and altitude are taken into account. Since σ_o vs θ_i curves are the usual output of this computation, the θ_i angles for one patch are allowed to be different from the next patch. This allows the use of most of the amplitudes in the Fourier transform of the data span. The angle from the aircraft to the center of each patch is computed and the doppler data corresponding to that angle is used.

The data sampling procedure for this variable θ_i case is as follows:

A. From a benchmark in the data record designated as t_o compute the times when over the center of equally spaced patches by solving $n_i d = \int_{t_o}^{T_i} V dt$ for T_i where

n_i = patch number

d = distance between patches

V = recorded ground speed, a function of time

T_i = time when over the center of patch n_i.

B. Process data with Fourier transform of a span of data centered at each T_i.

C. Select amplitude data reduced from doppler cells that are centered at angles from the aircraft forward and rearward to each patch in the sequence of patches of distance d apart. The incidence angles to each patch depend on the altitude of the aircraft at time T_i.

D. From Figure 3.3 we define θ_{ie} as $\theta_{mn} = \arctan \frac{(m_j - n_i)d}{h_{(T_i)}}$

E. The formulas for doppler frequency, fd, and doppler cell width, Δ f, are the same as the fixed θ_i case. Measure amplitude compared to the calibrate tone.

This timing sample technique differs from the fixed θ_i case in that during a fixed time corresponding to being over the center of a patch reflectivity data is obtained on all other patches regardless of the incidence angles to the patches. The computation is simpler if the user is interested only in σ_o vs θ_i curves and not σ_o vs distance plots.

3.6 PERIODIC SAMPLING TECHNIQUE

The previous two cases of Fixed and Variable θ_i gave reflectivity data for equal length resolved patches. Variations allowed in altitude and ground speed required accurate computation of elapsed time. Another simpler sampling technique can be used where the identity of a patch, once sampled, is forgotten. This technique is particulary useful over homogeneous surface such as water where data samples need not be reduced continuously. The sampling interval could be either time or distance determined. Distance was chosen and is so shown in Figure 3.1 as unresolved surface or Su in the Distance Computer block. Selection of distance also allows more meaningful mean and variance of reflectivity calculations in the presence of varying ground speed. For high sea state measurements the Δ S could be as much as 10 nautical miles depending on user preference. Figure 3.4, shows the geometry for Periodic Sampling. The time, T_i, is the start of a data span sampling. If Δ S is small, the sampled patches for successive periods may over lap but will be unrelated or unresolved. This Periodic Sampling technique is really a combination of both θ_{ie} and θ_{ic} in so far as measurements at all incident angles are made at any T_i, similar to θ_{ie}, but the incident angles are forced to be exact, similar to the θ_{ic} case.

$$\tan \theta_{mn} = \frac{(m_j - n_i)d}{h(T_i)}$$

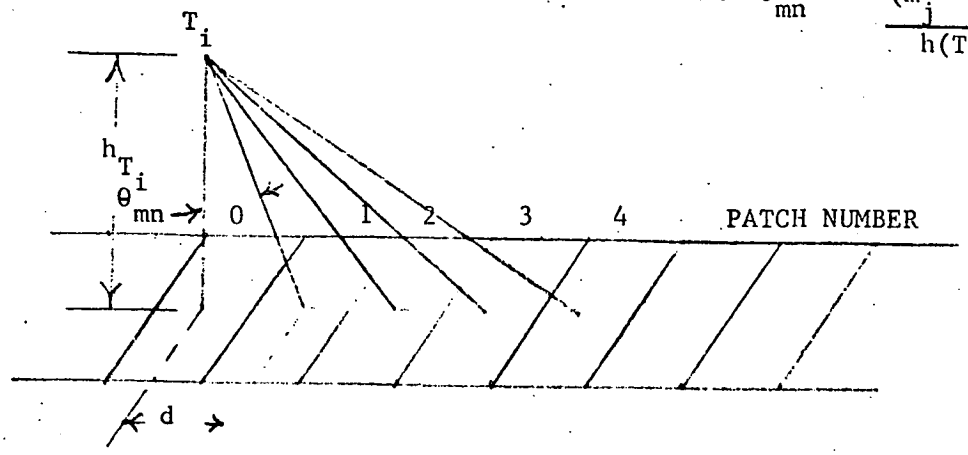

TABLE ILLUSTRATING UNIQUELY DEFINED DATA POINTS, $\sigma(\theta_{mn})$

NUMBER OF PATCH BENEATH AIRCRAFT, n	NUMBER OF OBSERVED PATCH, m				
	0	1	2	. . .	m
0	$\sigma(\theta_{00})$	$\sigma(\theta_{10})$	$\sigma(\theta_{20})$	. . .	$\sigma(\theta_{m0})$
1	$\sigma(\theta_{01})$	$\sigma(\theta_{11})$	$\sigma(\theta_{21})$	. . .	$\sigma(\theta_{m1})$
2	$\sigma(\theta_{02})$	$\sigma(\theta_{12})$	$\sigma(\theta_{22})$	. . .	$\sigma(\theta_{m2})$
.	.	.	.	. . .	.
.	.	.	.	. . .	.
.	.	.	.	. . .	.
n	$\sigma(\theta_{0n})$	$\sigma(\theta_{1n})$	$\sigma(\theta_{2n})$	. . .	$\sigma(\theta_{mn})$

Note that when n = m $\sigma(\theta_{mn}) = \sigma(0^\circ)$

FIGURE 3.3 VARIABLE θ_i GEOMETRY

The normal σ_o data would be plotted versus distance. However, for large homogeneous surfaces (25 nautical miles or more in length), each data sample could be used to provide a plot of σ_o vs θ data for that particular time and position.

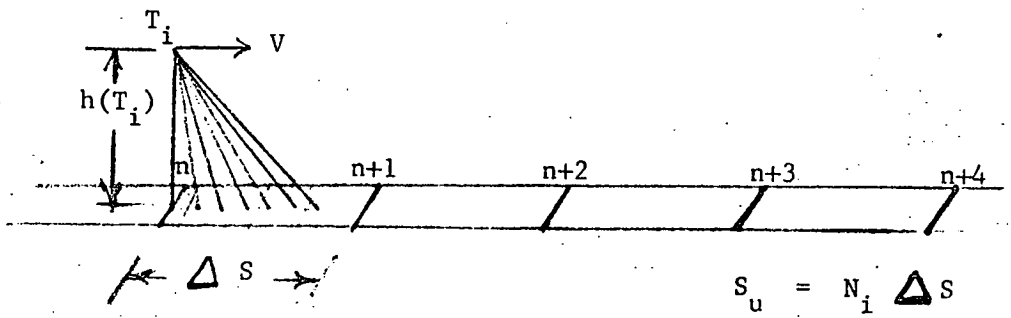

FIGURE 3.4 PERIODIC SAMPLING GEOMETRY

Document No. 2236

APPENDIX A

400 MHz TRANSMITTER

SPECTRAL ANALYSIS REPORT

HEWLETT hp PACKARD

1501 Page Mill Road, Palo Alto, California 94304 AREA CODE 415 326-7000

MEASUREMENT STANDARDS

CALIBRATION REPORT

Date October 13, 1967 Calibration No. H-1606

Item 400.85 MHz Transmitter, Model No. 2001020

Ident. Serial No. 101 Mfr. Teledyne

Submitted by Teledyne Telemetry

Ambient conditions: 24 ° C. - % R.H. Due -

This Transmitter was checked by means of the system shown on the attached sheets.

All instruments used in the test were checked recently against NBS traceable standards. The frequency measurements were made by comparison with the hp Frequency Standard which is traceable to NBS through VLF transmissions.

The D.C. voltage to the Transmitter was maintained at 27.9 ±.1 volts throughout the test.

The measurement results are shown on the three attached Single Sideband Signal to Phase Noise Plots. Except for the peak of minus 66 db at 120 Hz the noise plots are essentially the same as for the measurement system. Thus the noise output of the transmitter is less than the plots indicate except for the one peak at 120 Hz.

B. P. Hand, Manager

R23508(0)

0-703003

PROCEDURE FOR MEASURING PHASE NOISE

The set-up used to measure the phase noise of the Transmitter under test is shown in the attached block diagram.

The system utilizes a frequency synthesizer the output of which is phase locked in quadrature to the Transmitter signal through the phase lock loop. The resultant signal after passing through the low pass filter is the instantaneous voltage analog of the double side band phase noise contribution of both the Transmitter and the synthesizer. The spectrum of the resultant signal is measured in 1 Hz bandwidth increments by the wave analyzer and the output is integrated and plotted on the X-Y recorder.

The reference level is established by offsetting the frequency of the synthesizer by 1 KHz and setting the 0 db level on the wave analyzer at 1 KHz.

The system noise was checked by replacing the Transmitter with a second synthesizer. The system noise will be 3 db less than the resultant measurement if the noise spectra of the two synthesizers are identical.

Since it is desirable to express the resultant plot as RMS Phase Noise, and the wave analyzer is an average reading device, a correction of 1 db was added to the plot for the RMS correction. The resultant was also converted to single-side band phase noise by subtracting 6 db (for a total of minus 5 db for conversion to single-side band RMS phase noise).

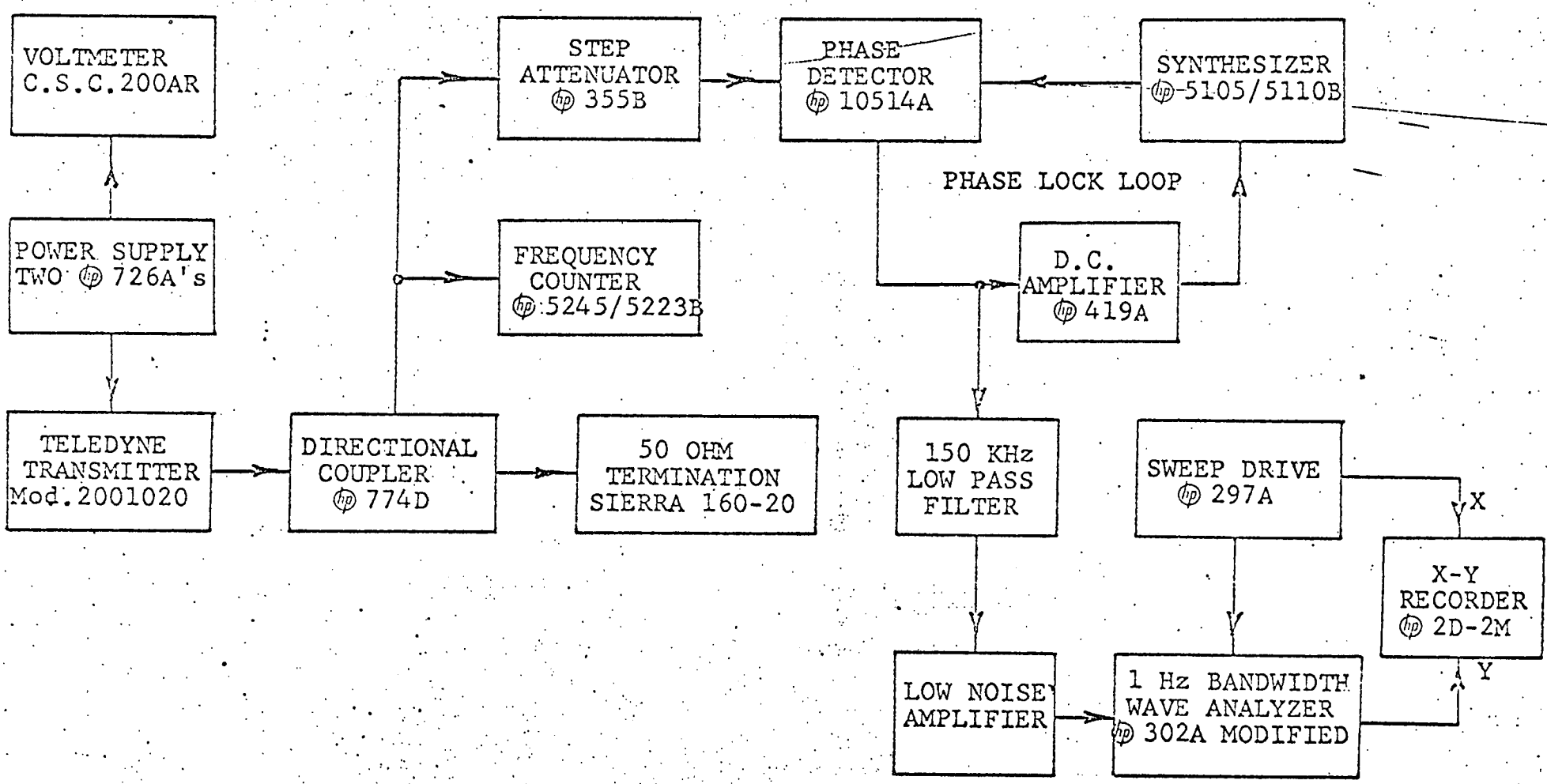

SETUP FOR CHECKING PHASE NOISE OF TELEDYNE TRANSMITTER

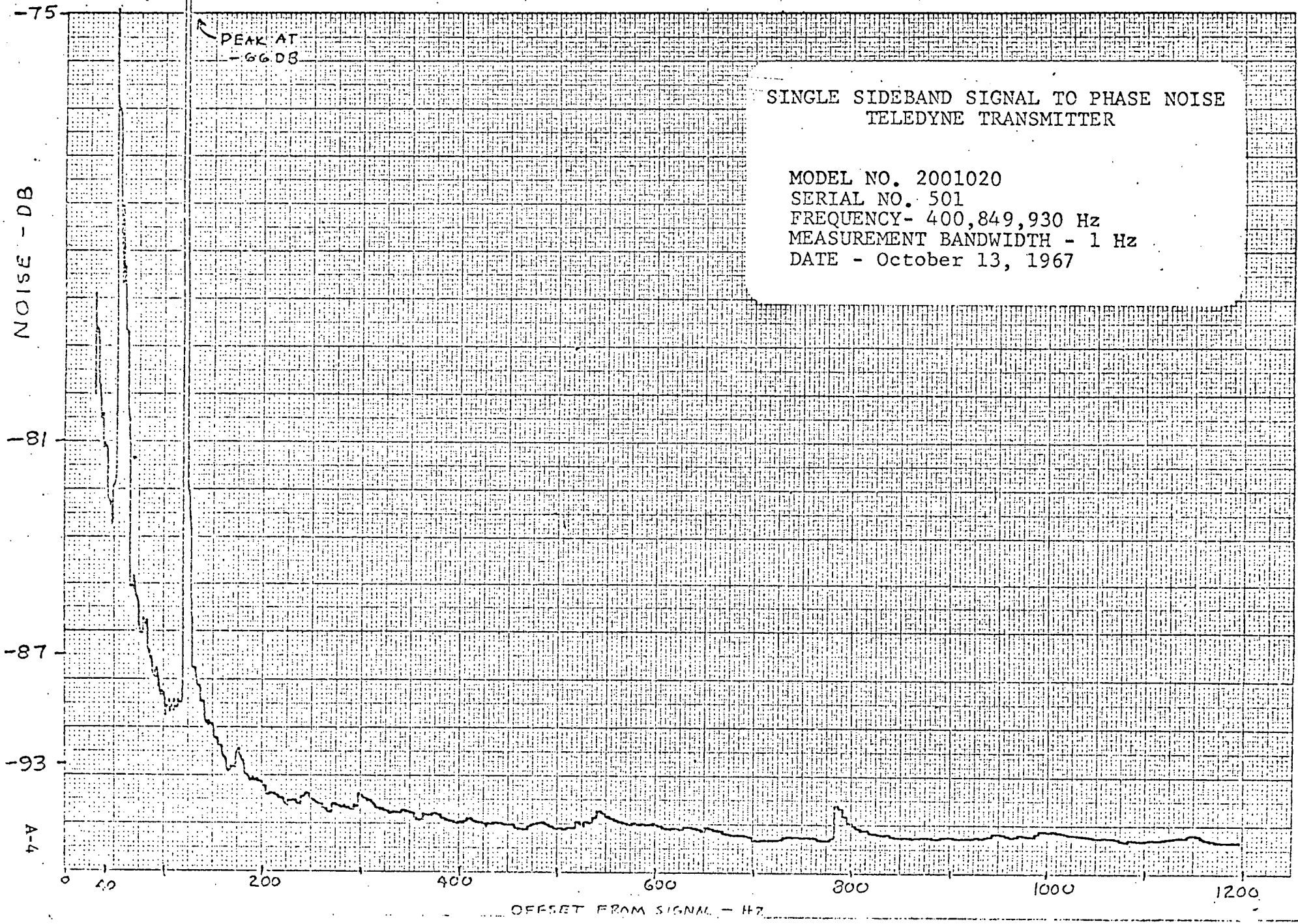

SINGLE SIDEBAND SIGNAL TO PHASE NOISE
TELEDYNE TRANSMITTER

MODEL NO. 2001020
SERIAL NO. 501
FREQUENCY- 400,849,930 Hz
MEASUREMENT BANDWIDTH - 1 Hz
DATE - October 13, 1967

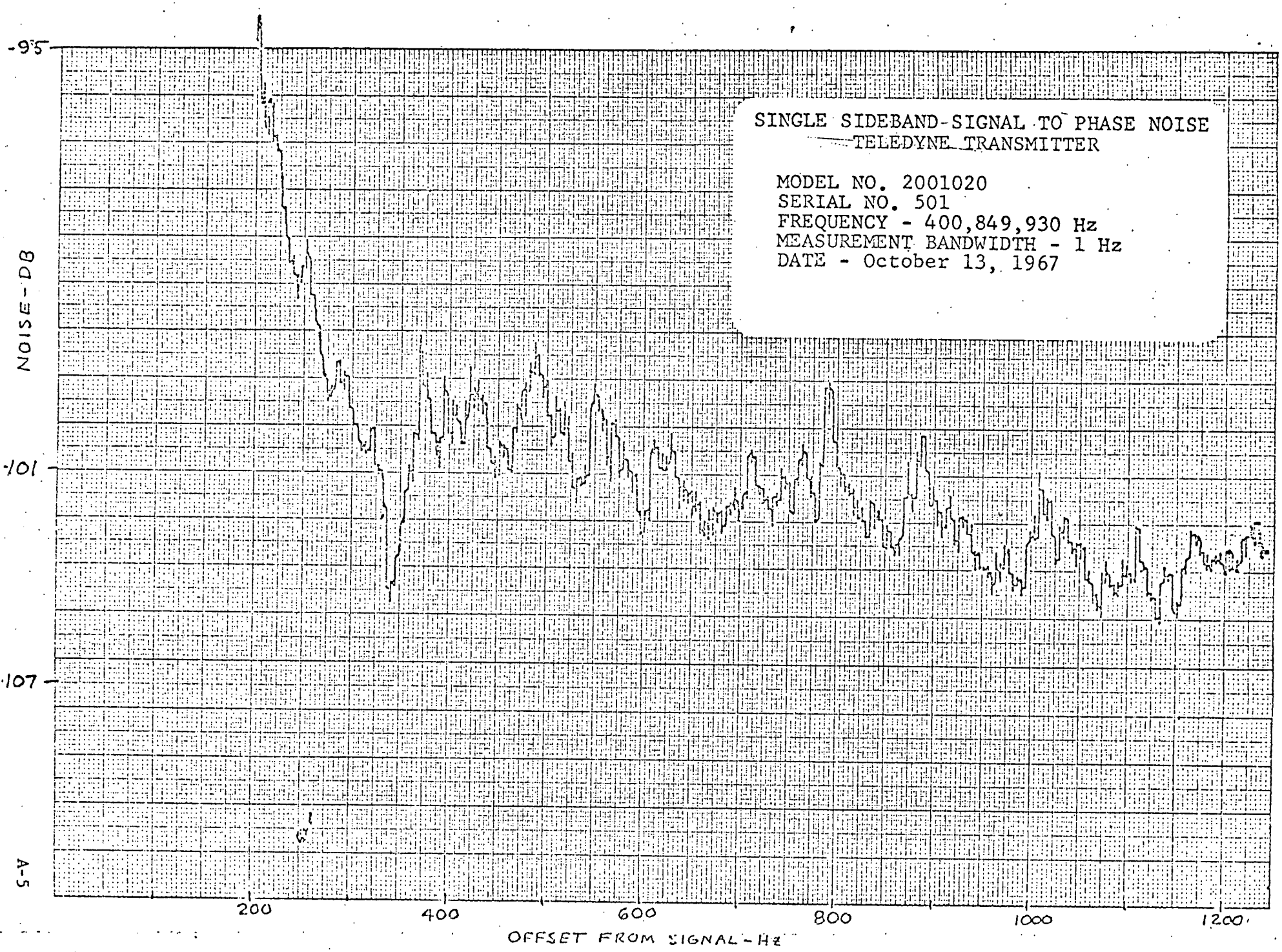

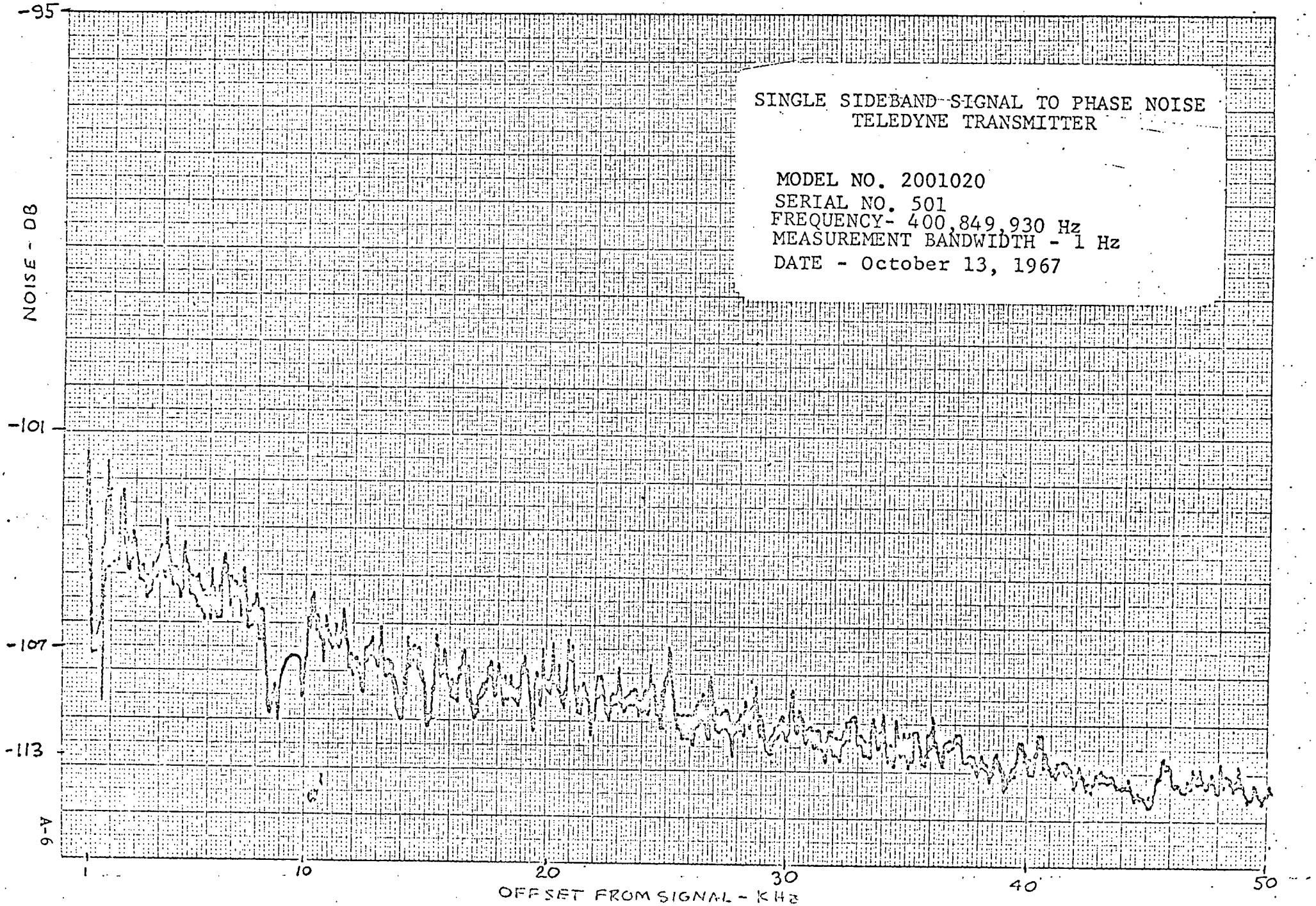

Document No. 2236

APPENDIX B

CALCULATION OF RETURN POWER

APPENDIX B

CALCULATION OF RETURN POWER

This appendix summarizes the method used to calculate the expected received power in the 400 MHz Scatterometer system.

A ground cell is illustrated in Figure B.1. The cross track width is determined by the effective two-way antenna pattern and the along track length is set by the desired resolution.

The received power from this ground cell can be expressed as:

$$P_R = \frac{P_T \lambda^2 G_T(\theta) G_R(\theta) A(\theta) \sigma_o(\theta)}{(4\pi)^3 R^4(\theta)} \qquad (1)$$

where

P_R = peak received power

P_T = effective peak transmitting power

$G_T(\theta)$ = transmitting antenna gain at angle (θ)

$G_R(\theta)$ = receiving antenna gain at angle (θ)

$A(\theta)$ = area of resolution cell

$\sigma_o(\theta)$ = radar cross section per unit area at angle (θ)

$R(\theta)$ = range to resolution cell

θ = angle of incidence

Determination of $A(\theta)$

The ground cell will be considered rectangular and have dimensions of d_1 and d_2. Referring to Figure B.2, the value of d_1 is given by the following:

$$d_1 = R(\theta) \psi(\theta) \qquad (2)$$

where $\psi(\theta)$ is the effective two-way beamwidth of the Scatterometer system at angle θ.

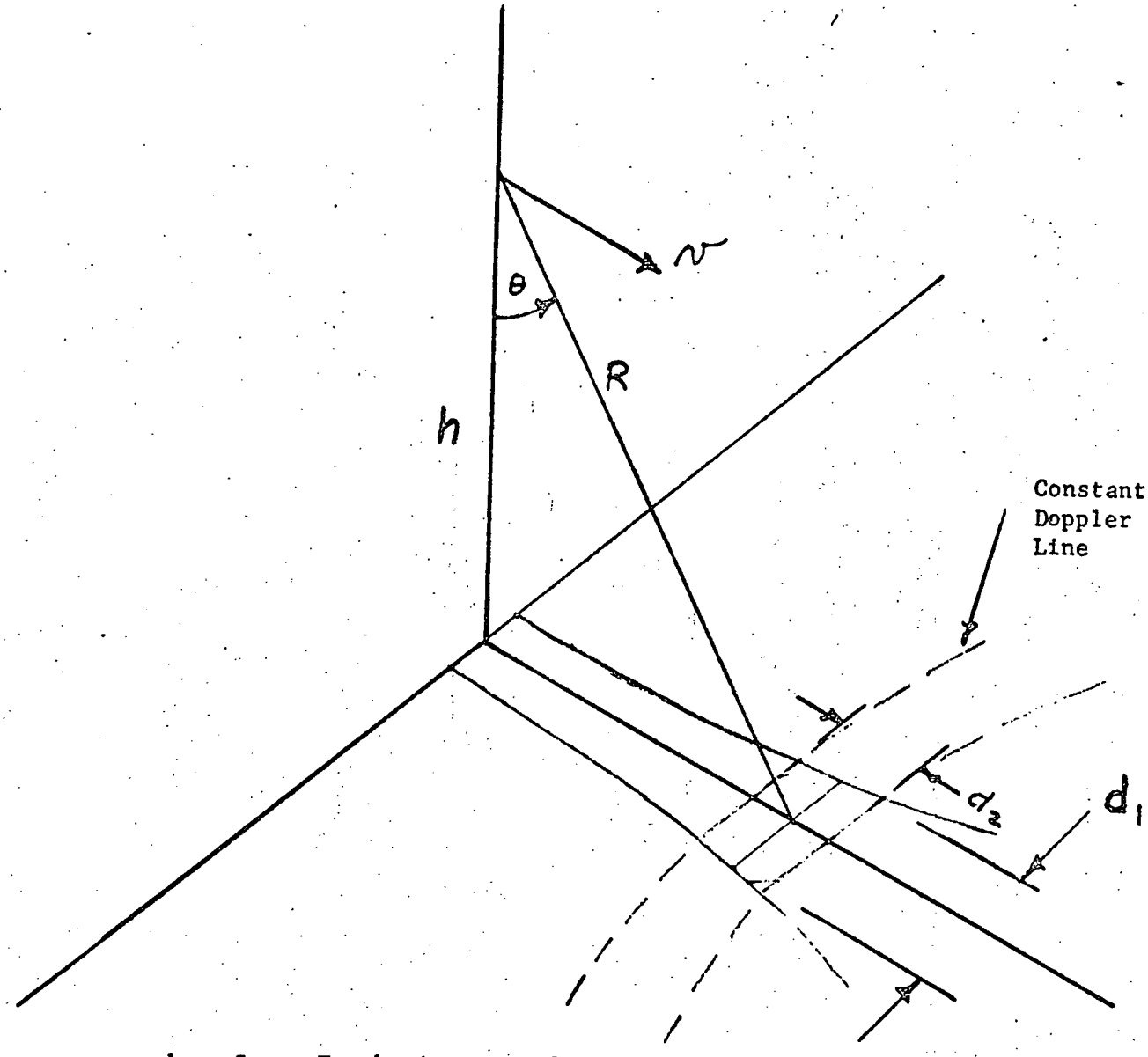

d_1 = Cross Track Distance of Resolution Cell

d_2 = Along Track Distance of Resolution Cell

θ = Angle Between the Range Line to Center of Resolution Cell and the Nadir

h = Altitude

$\sim$ = Aircraft velocity

FIGURE B.1 RESOLUTION CELL GEOMETRY

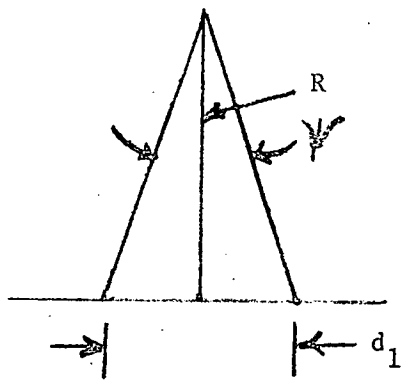

FIGURE B.2 CROSS TRACK GEOMETRY

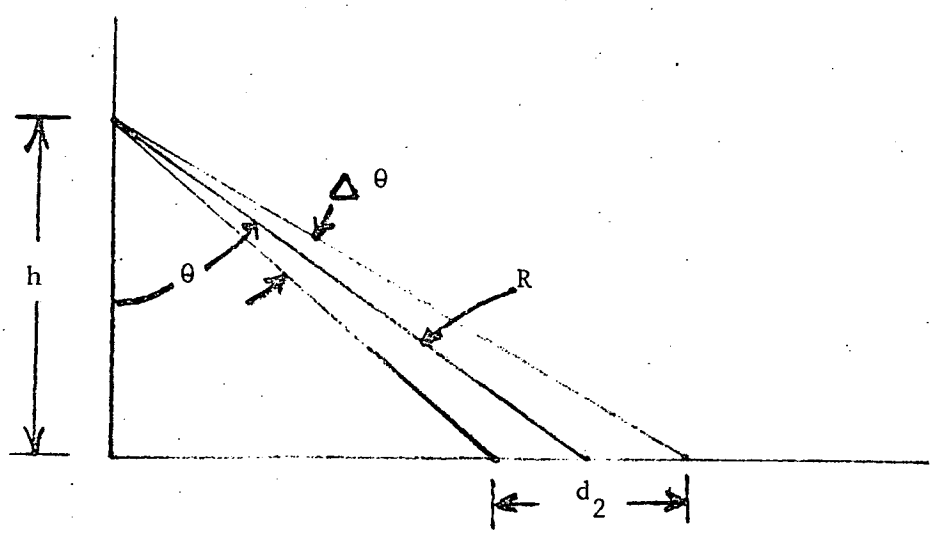

FIGURE B.3 ALONG TRACK GEOMETRY

The value of $\Psi(\theta)$ is defined by the following expression:

$$\Psi(\theta) = \frac{\int_{-\phi_1}^{\phi_2} G_T(\psi)_\theta \, G_R(\psi)_\theta \, d\psi}{G_T(\theta)_{max} \quad G_R(\theta)_{max}} \tag{3}$$

Referring to Figure B.3, the value of d_2 is given by the following:

$$d_2 = \frac{R \, \Delta\theta}{\cos \theta} \tag{4}$$

or in terms of altitude

$$d_2 = \frac{h \, \Delta\theta}{\cos^2 \theta} \tag{5}$$

Expression (1) can be written in terms of $\Psi(\theta)$ and $\Delta\theta$ to give the following:

$$P_R = \frac{P_T \lambda^2 G_{R_{max}} G_{T_{max}}}{(4\pi)^3 h^2} \sigma_o(\theta) \Psi \Delta\theta \cos\theta \tag{6}$$

Power calculations were made using Expression (6). The value of Ψ was taken to be constant and equal to 5° and $\Delta\theta$ was taken to be 3°.

Table B.1 is a tabulation of the values used for G^2 and σ_o as a function of the angle of incidence. Table B.2 is a tabulation of the return power.

A sample calculation is given below:

Output of power amplifier	+43 dbm
Antenna Switch Loss	-.7 db
Antenna VSWR (< 1.5)	-.2 db
Filter Loss	-1.0 db
Power into antenna feed line	+41.1 dbm

TABLE B.1

θ	G(θ)	G_θ^2	σ_o		cos θ
			WATER	WOODS	
1.5°	-4.3	-8.6	+18	- 1	0
4.5	-4.1	-8.2	+18	- 1.5	0
7.5	-3.7	-7.4	+16.5	- 2.0	0
10.5	-2.8	-5.6	+15	- 2.5	0
13.5	- .9	-1.8	+13	- 3.0	0
16.5	.9	1.8	+10	- 5.0	- .2
19.5	2.7	5.4	+ 7	- 7.0	- .25
22.5	4.3	8.6	+ 2.5	- 9.0	- .35
25.5	5.7	11.4	- 3	-11.5	- .45
28.5	7.0	14.0	- 9	-14.5	- .6
31.5	8.1	16.2	-15	-17.0	- .7
34.5	9.2	18.4	-21	-20	- .84
37.5	10.0	20.0	-27	-23.5	-1.0
40.5	10.7	21.4	-32.5	-26	-1.2
43.5	11.4	22.8	-39	-29	-1.4
46.5	12.0	24.0	-45	-32	-1.6
49.5	12.4	24.8	-50	-35.5	-1.9
52.5	12.7	25.4	-56	-38.5	-2.16
55.5	13.1	26.2	-60	-41	-2.5
58.5	13.1	26.2		-44	-2.8

TABLE B.2

POWER RETURN PER CELL

	WATER		WOODS	
θ	dbm	Milliwatts	dbm	Milliwatts
1.5	-57.9	1.62×10^{-6}	-76.9	2.0×10^{-8}
4.5	-57.5	1.77×10^{-6}	-77.0	2.0×10^{-8}
7.5	-58.2	1.5×10^{-6}	-76.7	2.07×10^{-8}
10.5	-57.9	1.61×10^{-6}	-73.4	4.5×10^{-8}
13.5	-56.1	2.45×10^{-6}	-72.1	6.1×10^{-8}
16.5	-55.7	2.7×10^{-6}	-70.7	8.5×10^{-8}
19.5	-55.2	3.0×10^{-6}	-69.2	12.0×10^{-8}
22.5	-56.6	2.2×10^{-6}	-68.1	15.5×10^{-8}
25.5	-59.4	1.15×10^{-6}	-67.9	16.2×10^{-8}
28.5	-62.9	$.51 \times 10^{-6}$	-68.4	14.5×10^{-8}
31.5	-66.8	$.21 \times 10^{-6}$	-68.8	13.0×10^{-8}
34.5	-70.7	$.085 \times 10^{-6}$	-69.7	10.8×10^{-8}
37.5	-75.3	$.029 \times 10^{-6}$	-71.8	6.5×10^{-8}
40.5	-79.6	$.011 \times 10^{-6}$	-73.1	4.8×10^{-8}
43.5	-84.9		-74.9	3.2×10^{-8}
46.5	-89.9		-76.9	2.0×10^{-8}
49.5	-94.4		-79.9	1.0×10^{-8}
52.5	-99.3		-82.6	$.55 \times 10^{-8}$
55.5	-103.3		-84.6	$.33 \times 10^{-8}$
58.5			-87.9	$.16 \times 10^{-8}$

λ^2	8 db	(2.5 feet)
$(1/4\pi)^3$	-33 db	
$1/h^2$	-60 db	(1,000 feet)
$\Delta\theta = 3^o$	-12.8 db	
$\psi = 5^o$	-10.6 db	

$$P_{R_\theta} = -67.3 \text{ dbm} + 10 \log G^2(\theta) \cos\theta$$

From Table B.1, obtain data for τ_o for water at $\theta = 22.5^o$, $G^2\theta$ at 22.5^o, and cos θ at 22.5^o.

$$P_{R_\theta} = -67.3 + 2.5 + 8.6 - .35 = -56.55 \text{ dbm}$$

Document No. 2236

APPENDIX C

SCATTEROMETER ANTENNA ELEMENT

PATTERN INVESTIGATION

TABLE OF CONTENTS

LIST OF FIGURES

LIST OF FIGURES - continued

SCATTEROMETER ANTENNA ELEMENT PATTERN INVESTIGATION

1.0 INTRODUCTION

Controlling the radiation pattern of a VHF antenna mounted on an airplane is more an art than a science. For airplane shapes do not conform to the simple, plane surfaces which are assumed in antenna pattern synthesis, and the surface currents generated on the airplane structure are not easily treated analytically. Therefore, experimental techniques are commonly used to obtain a desired radiation pattern, and the "art" lies in securing agreement of experimental results with a theoretical model. Some "art" has been used to obtain the element pattern shapes for the Scatterometer Antenna [1] as described in this report.

The Scatterometer Antenna consists of two linear arrays of dipoles mounted under the wing of a P3A airplane and extending the full distance between the two inboard engine nacelles as shown in Figure 1-1. These two arrays produce narrow pencil beam patterns in the cross-track plane, and they are both horizontally polarized. One polarization lies along the flight track axis, the other along the cross track axis; and they are referred to as E-plane track and H-plane track, respectively.

2.0 RADIATION PATTERN REQUIREMENT

The design goal for the track-plane radiation pattern shape is shown in Figure 1-2. The limits shown there were established to maintain acceptable round-trip signal variations due to changes in range and angle of incidence at the ground. The track-plane beam shape is controlled entirely by the individual array elements, and the necessary restriction on size, complexity, and location of these elements limits the degree to which the pattern shape can be approximated.

---

1 Proposal No. NB66-1069, "400 Mc Scatterometer Airborne System," Emerson Electric Co., prepared for NASA Manned Spacecraft Center, Houston, Texas, June, 1966.

3.0 ELEMENT DESIGN DETAILS

3.1 Initial Design

An examination of the available mounting surface, the environmental conditions in flight, and the pattern shape, led to the choice of a pair of dipoles as the best radiating element for the Scatterometer Antenna Array. The radiation intensity was reduced in the nadir direction and maximized at $\pm 60^{\circ}$ both by adjusting the height of the dipoles above the mounting surface and by feeding the two dipoles with 180° relative phase difference. A dipole spacing of 0.6λ caused the peak in the radiation pattern to appear at $\pm 60^{\circ}$. This spacing was subsequently reduced to 0.54λ. In order to avoid a pattern null at 0°, the two dipoles were to be fed with unequal amplitudes. Figure 3-1 shows the dipole arrangement and the expression for the track plane element radiation pattern, $E(\theta)$.

3.2 Effect of Dipole Height

Ordinarily, a dipole is mounted a quarter wave from a reflecting ground plane so that its maximum radiation is in the direction perpendicular to the ground plane. For the Scatterometer, however, minimum radiation is desired in this direction; therefore, the distance between dipole and ground plane, S, was increased to nearly 0.5λ. At this spacing, radiation of the dipole and its image (which has 180° phase reversal) cancel in the perpendicular direction and add at or near the directions parallel to the ground plane surface. The amount of attenuation, α, in the perpendicular direction relative to the direction 60° away from perpendicular, is shown in Figure 3-2 for both H- and E-planes of the dipole. The curves differ by more than 7 db, the difference in gain of a single dipole in the E- relative to the H-plane.

Several measurements were made on single dipoles mounted on a 1/5th scale mock-up of the wing section to note the attenuation obtained with varying dipole heights, S. The radiation patterns of Figure 3-3 show the H-plane pattern of a single dipole. The ripple in the pattern is due to reflections, and the relative attenuation of the nadir compared to 60° agrees with the curves of Figure 3-2.

An E-plane pattern is shown in Figure 3-4 where the dipole height is $S = .48\lambda$. The signal level at the nadir is close to that for the H-plane dipole as shown in Figure 3-3. As expected, there is lower gain at wide angles in the E-plane than there is in the H-plane. Bending the dipole arms down extends the pattern to slightly greater angles, although the angular positions of the peaks change only slightly. The effective height is reduced also, and the gain at the nadir is increased as shown in Figure 3-5 ($S = .48\lambda$). It is then necessary to increase the balun height from $.48\lambda$ to $.52\lambda$ to get the same effective dipole height as the straight dipole at $S = .48\lambda$.

3.3 Effects of Mounting Panel Height

The dipoles are attached to a mounting panel which in turn is attached to the wing. Early models of the panel were made with a 45° taper on the leading and trailing edges. When the dipoles were close to 0.5λ above the mounting panel, then ripples appeared in the element radiation pattern where a smooth response was desired. This was caused by the relatively abrupt edge of the mounting panel where, as the angle of view changes, the image of the dipole suddenly shifts from the mounting panel surface to the wing surface, and the dipole is correspondingly farther from its image. This effect is shown in Figures 3-6, 3-7, and 3-8 for the H-plane track polarization. The equivalent heights of the 27-inch wide mounting plates are 1.25",

2.0", and 3.5", respectively. By adding longer tapers to the edges of the mounting plate, this effect can be adequately reduced. A taper slope of 5 to 1 has proven sufficient for a 2-3/4" panel height. This length is not critical; a taper ratio of 4 might work nearly as well and, in general, the greater the taper length, the closer the approximation to a flat ground plane. What is quite critical, however, is the symmetry of the dipole positions on the mounting plate. The distance from the dipole to the edge of the mounting plate should be the same at both edges of the mounting plate, and preferably the tapers should be similar although this is not as essential as the symmetry.

Less significant than the panel height, but observable in the radiation pattern, is the effect of wing shape and the length of the mounting surface in the track plane. Generally, the forward lobe is slightly broader than the aft lobe, and this effect is increased if the dipoles are moved forward on the wing. The radiation patterns of Figures 3-9 and 3-10 show this broadening of the forward (right side of pattern) beam when the dipoles are moved forward an equivalent distance of 30 inches on the wing.

3.4 Amplitude Unbalance

In the original design concept, the signal level at the nadir was to be controlled by unbalanced excitation of the two dipoles. A practical difficulty was found with this method, however, because the position of the null was found to depend on the amplitude unbalance. The reason for this is that the forward and aft dipoles do not have identical radiation patterns; they have nearly mirror image symmetry, as illustrated in Figure 3-11. This results from the lack of symmetry in their locations on the mounting plate, one on each edge. The pattern control with unbalanced amplitudes was found to be too

imprecise, and it prompted investigation of a slightly different scheme.

3.5 Sum and Difference Excitation

The excitation of the dipoles with 180° phase difference produces a null at the nadir, the plane of symmetry, and maxima at angles of about ±60°. Changing the phase of one dipole by 180° places the maximum radiation back at the nadir with correspondingly lower wide angle radiation. By superimposing both sum and difference excitations with 90° relative phase between them, the radiation level at the nadir relative to ±60° can be varied without introducing interference nulls within the angular range in the pattern. The relative amplitude at the nadir is proportional only to the sum channel input level and, since this level is quite low, only a small fraction of the total power need be diverted to the sum input.

A circuit diagram for the simultaneous excitation of the dipoles in both the sum and difference modes is shown in Figure 3-12. A directional coupler diverts the required amount of signal into the sum terminal to adjust the signal level at the nadir. For proper operation, the line lengths between directional coupler and hybrid junction must be adjusted to maintain the 90° relative phase difference. Furthermore, the line lengths from the hybrid to the two dipoles must be equal also to maintain this phase relationship.

A set of sum channel H-plane track radiation patterns is shown in Figure 3-13. The lowest curve is for two dipoles only, and the minimum on-axis corresponds to the individual dipole minima resulting from their heights of 0.5λ above the mounting panel surface. This minimum can easily be filled-in, as shown by the remaining curves in Figure 3-13, by placing a parasitic dipole element midway between the two

active dipoles and at about half their height. The parasitic dipole lies in a plane of symmetry so that its net excitation is zero for the difference mode input and maximum for the sum mode. The radiation by this parasitic dipole can be varied a few db by changing its height; while this means of control is not practical, it indicates that the parasitic dipole height is not a critical parameter.

Besides improving efficiency, the parasitic dipole improves the side-lobe level of the cross-track array pattern. This results from its action of filling in the minimum at the nadir. Otherwise this null at the nadir would attenuate the main beam relative to the side lobes, causing a higher apparent side-lobe level. One other advantage of using the parasitic dipole is that it allows the active dipoles to be raised to a full half wavelength above the mounting panel surface which, in turn, spreads the beam peaks to greater angles and improves the linearity of the pattern shape in the region between 10 and 90 degrees from the nadir.

3.6 E-Plane Track Element

Obtaining gain at wide angles is difficult for the E-plane track polarization as discussed in Section 3.2. Two element types in addition to bent dipoles were tested in a search for higher gain at wide angles. One of these was a pair of circular loops of one wavelength circumference. The general result with loops was similar to that with bent dipoles, as shown in Figure 3-14. The angle at which maximum gain occurred was not increased, as had been expected because it turns out that the loop, unlike the dipole, has an in-phase image rather than the 180° phase shift such as occurs between the dipole and its parallel image. The loop offered little pattern advantage to offset its physical and electrical complexity,

and so it has not been pursued further.

The other type of element tried was a pair of vertical monopoles with 180° relative phases. This element did increase the wide angle radiation as shown in Figure 3-15, and as we expected from its geometry. The monopoles have a null at the nadir which was eliminated by bending the tips of the dipoles toward each other. The average shape of the monopole pattern is quite close to the desired track plane patterns shape. It is unsatisfactory, however, because of the large oscillations about the average value presumably caused by surface currents in the mounting structure. In an array, these ripples might be reduced, in which case this would be an excellent choice since it provides the greatest peak separation and provides more peak gain at wide angles than the dipoles.

The conclusion from the tests of different element configurations, typically illustrated above, is that bent dipoles give the best over-all performance and are, therefore, adopted as the E-plane track radiating elements.

4.0 EXPERIMENTAL ELEMENT PATTERNS

The mounting plate configuration has been in the process of evolution during this period, while the scale model element pattern behavior has been investigated. Consequently, there have been a number of configurations which were at one time considered as final. The track plane patterns for these configurations which follow show that the basic characteristic of the patterns are relatively constant. The finer details do change, and even these are representative only. They can be modified, and a final determination is planned to be made with full scale dipoles. The fore and aft spacing of 0.54λ between element dipoles was adopted for all of the tests to be described below.

4.1 Initial Patterns

The initial developments led to a mounting plate height, h, of only 1.25 to 1.5 inches; width, w = 26"; and fairing tapers of T > 5h. (See Figure 3-1.) The best E-plane track pattern is shown in Figure 4-1, and the best H-plane track pattern is shown in Figure 4-2. Cross-track patterns were measured at various angles through the H-plane track beam. A composite of these patterns is shown in Figure 4-3. The pattern through the nadir, $\theta = 0$, should probably follow the dashed curve to the level corresponding with that in Figure 4-2. It is believed that the 60° peak of the track pattern was pointing at the ground and receiving sufficient signal to fill in the null. The cross-track patterns were measured through the aft beam, which is on the left-hand side in all track plane patterns.

4.2 Design Configuration No. 1

The No. 1 design configuration of the mounting plate arose during initial discussions at NASA on the method of attaching the panels to the wing of the airplane. They were to be attached to 2-3/4" I-beams which were spaced 25" apart along the wing. The panel dimensions were w = 26", h = 2.75", T = 5h. Radiation pattern measurements indicated that the I-beams had little influence on the patterns. They were positioned as close to the H-plane track dipoles as possible, and it was observed that the smoothness of H-plane track patterns was increased by closing all gaps between the beam and the panel and wing surfaces with metal tape. The E- and H-plane track patterns are shown in Figures 4-4 and 4-5, and in general they have sharper nulls than expected.

4.3 Design Configuration No. 2

As a second design approach, the mounting plate width was increased from 26" to 35", and a single I-beam 3-1/2" deep was proposed. The leading and trailing edge tapers were again T = 5h, where h = 2.75".

The E- and H-plane track patterns shown in Figures 4-6 and 4-7 resemble closely previous patterns. They are relatively smooth, the peaks occur at approximately the same angular positions, and the null depth is set by the amount of signal diverted into the sum channel. The attenuation figures are comparable to the coupling factor of the directional coupler shown in Figure 3-1.

4.4 Design Configuration No. 3

A third mounting plate design proposal consisted of a 35-inch wide plate, 2-3/4" high, with 10 to 1 leading edge taper and 5 to 1 trailing edge taper. This panel would be held down by a single large beam on each wing. Most of the elements would not be affected by this beam. However, the beam was mocked-up for the nearest dipole, and radiation pattern tests indicated its presence had negligible effect for both E- and H-plane track polarizations.

The track plane radiation patterns for this mounting plate were satisfactory and generally similar to earlier patterns. The H-plane track pattern for 12-db attenuation of the sum channel is shown in Figure 4-8. The E-plane track pattern is shown in Figure 4-9, and it was obtained without the aid of a parasitic dipole. In this case, the sum channel was attenuated 9 db, and the two individual sum and difference patterns that were added together are shown in Figure 4-10. A parasitic element could be used and would be desirable for assisting in meeting the side-lobe levels in the cross-track

plane. The improvement produced by the parasitic dipole is shown in Figure 4-11, where no attenuation was used for any channel. The use of the parasitic dipole produces more gain and a much better pattern shape, as explained earlier (See Figure 3-13).

4.5 Design Configuration No. 4

The last design configuration which was tried consisted of a modification of Configuration No. 3—the 10 to 1 taper was reduced to 5 to 1 by extending the 35" width to 50" at the leading edge of the mounting plate. With this mounting plate, a smooth symmetrical pattern for H-plane track polarization, normally the easy one, could not be obtained. After some investigation, it was finally found that the fore and aft dipole patterns were quite different, as shown in Figure 4-12. The forward dipole has a very deep null, whereas the aft dipole has the null filled in. The dipoles were physically interchanged, then the entire mock-up was inverted, but the pattern of the forward dipole in all cases had the deep null—indicating that the effect was due to the mounting plate, not the dipoles.

The extension of the ground plane near the forward dipole produced a more complete image and, since the dipole was $\lambda/2$ above the plate surface, more complete cancellation occurred in the radiation pattern. The aft dipole pattern remained relatively unchanged from its pattern on other similar mounting plates. For example, Figures 4-13 and 4-14 show individual fore and aft dipole patterns for both E- and H-plane track on the mounting plate configuration, No. 2, 35-inch wide, 2-3/4 inches high, with 5 to 1 tapers on both edges. The mirror image symmetry mentioned earlier is apparent in these patterns.

5.0 CROSS-TRACK ARRAY PATTERN

In the cross-track plane, a narrow pencil beam pattern is generated by an array of twelve elements. The elements consist of pairs of dipoles as described above in Section 4.0. A Dolph-Tschebycheff amplitude distribution is used in feeding the twelve elements to obtain a narrow 6° beamwidth with design side-lobe levels of -24 db.

5.1 Feed Scheme

The cross-track array of twelve elements is fed from the center by a series of ten directional couplers. The feed circuit which will be used is shown in Figure 5-1. Notice that in contrast to the original proposal and to the element circuits, all the forward dipoles are now fed from one line source and all the aft dipoles are fed from a second, identical, line source. These two line sources each form a cross-track array beam, and all the random errors are summed up for each array separately. The two array outputs are then combined in a sum-and-difference circuit to generate the track plane pattern for one polarization. A second circuit, similar to that in Figure 5-1, is required for the other polarization.

Several notable features of the feed system are 1) the directional coupler has 10-db coupling and thus removes only 1/2 db of the power from the difference channel. Thus, the gain is lowered at the peak of the track-plane by, at most, 1/2 db. 2) A second feature is the series coaxial pad attenuator in the sum channel circuit. This attenuator can be changed to reduce the gain at the nadir if this should be required. Coaxial pad attenuators, having identical phase lengths, can be purchased in 1-db steps from several manufacturers. The preservation of path length, or phase length, is important because sum-and-difference patterns combine to produce a smooth symmetrical pattern only when they are in a 90° phase relationship. The 90° phase shift is produced by the directional coupler

so that it is only necessary to have equal path lengths from the directional coupler output terminals to the hybrid junction sum-and-difference terminals. 3) A third feature of this feed circuit is the phase shifter in series with one array input line. The path lengths between the array input terminals and the hybrid junction terminals should be equal so that the null is aligned perpendicular to the mounting panel surface. This normal direction may not be aligned with the nadir if the angle of attack of the wing varies in flight. It would be possible to shift the null direction a few degrees by means of the phase shifter so that minimum signal is transmitted perpendicular to the ground. The variations in pattern shape at wide angle resulting from small shifts in the null position could be determined and calibrated on the full-scale mock-up. Also, fixed line lengths may be more desirable than an adjustable phase shifter because there would be less possibility of a misadjustment of the phase shifter causing an incorrect calibration in the field.

5.2 Path Length Compensation for Dihedral

The phase lengths of lines ℓ_1 through ℓ_{11} in Figure 5-1 must be chosen such that a plane wave front is transmitted from the array. The lengths of these lines will be adjusted to compensate for the wing dihedral angle, and variations in height of the dipoles on the fuselage. These lengths can be calculated with sufficient accuracy if the actual dimensions of the aircraft are available. Only one set of cables is labeled in the sketch of 5-1 but, of course, the same requirements apply to the other three unlabeled sets of cables. Furthermore, it is essential that when the two dipoles No. 6 are 180° out of phase with each other, so also are all other pairs of like-numbered dipoles. This requirement can be checked by making bridge-type insertion phase measurements

between the array center power divider input terminal and each dipole terminal.

5.3 Theoretical Cross-Track Array Pattern

The Dolph-Tschebycheff distribution is designed to produce equal 24-db side lobes in the cross-track plane and a main beam having a 6° half-power beamwidth. The coupling coefficients shown in Figure 5-1 are calculated to divide the total input power among the twelve elements with the following relative current distribution:

$$I_1 = I_{12} = 1.71$$
$$I_2 = I_{11} = 1.74$$
$$I_3 = I_{10} = 2.38$$
$$I_4 = I_9 = 2.96$$
$$I_5 = I_8 = 3.41$$
$$I_6 = I_7 = 3.65$$

The current distribution, together with the element spacing of 0.83λ, will produce the following beamwidths:

Amplitude (db)	Beamwidth (Degrees)
-3 db	6.0
-10 db	10.1
-20 db	13.0
$-\infty$ db	15.0

An approximate cross-track radiation pattern is shown in Figure 5-2.

5.4 Errors

The choice of 24 db for the design side-lobe level was based on the experimental fact that the side lobes

are generally higher than calculated because of errors. Therefore, a lower side-lobe level is used in design than is expected in practice. In the present case, the one-way side-lobe level specified is 20 db. Therefore, a 4-db margin of error was allowed. The limitation on designing for even lower side lobes is that the beamwidth increases as the side-lobe levels decrease, and the specified beamwidth is 6.0°.

There are several sources of error which can affect the array performance, the largest being the array element pattern. The element pattern requires minimum radiation at the nadir in the track plane. To some degree, this effect carries over into the cross-track plane where it tends to reduce the main beam gain more than the side-lobe gains. The effect is an apparent increase in side-lobe level. The parasitic element aids in reducing this side-lobe "enhancement" as described earlier (Para. 3.6).

Another element pattern error is that caused by variations in the wing size and shape, the fuselage contour, and the engine nacelles. These factors cause small differences in the element patterns which can be treated as errors in amplitude or phase of the elements. These errors would be largest in the vertical transverse plane.

Vibration of the dipole elements is a possible source of error also. Displacement of the dipole laterally would be equivalent to a phase shift, and this would be random in nature. However, a large excursion would be necessary to produce a serious phase error since the free space wavelength is 29-1/2 inches. For example, a half-inch excursion would produce only six degrees phase error. This long wavelength also eases the problem of cutting feed line cables to the correct length. A tolerance of ±1/16" in cable length would be equivalent to only ±1.1 phase shift in the teflon dielectric.

The phase and amplitude errors produced in the feed system will probably be the smallest contributor to any increase of side-lobe level. The amplitude errors due to the directional couplers will be less than ±.3 db.

6.0 ESTIMATED ANTENNA PERFORMANCE

6.1 Gain

The gain of the array can be determined by adding the element gain to the array gain and subtracting the feed losses. Using the element described in Para. 4.4 which had a 35" wide, 2-3/4" high mounting plate, the measured element peak gains were 8.6 db for the H-plane track and 2.6 db for the E-plane track polarization. The estimated array gain is 12.5 for the 24-db design using .83λ element spacing. Therefore, the following table shows the estimated peak gains:

Gain Factor	Track Plane Polarization	
	E	H
Elements	2.6	8.6
Array	12.5	12.5
	15.1 db	21.1 db
Loss Factor		
Cables	0.8	0.8
Directional Coupler	0.5	0.5
Power Splitters	0.3	0.3
	1.6 db	1.6 db
Net Est. Gain:	13.5 db	19.5 db

The cable loss is the largest single factor reducing the power gain of the antenna. This loss is estimated using the value of 3.4 db/100 ft. as the attenuation of UT-250 semi-rigid coaxial cable. The array is center-fed, and it is estimated that there are 20 feet of cable in each half array. But since not all of the energy travels the full distance, an average length of 10 feet is used for estimating. Another 15 feet of cable is estimated for connecting the center power divider in the array via the sum-and-difference circuit to the transmit-receive switch.

6.2 Contour Plot

Because of the unusual shape of the track-plane element pattern, the space shape of the array beam looks like a saddle, or the valley between two adjacent hills. Equal amplitude contours appear as shown in Figure 6-1, as determined from the measured track-plane radiation patterns, Figures 4-2 and 4-3, and the estimated cross-track array pattern, Figure 5-2. The cross-track array pattern is quite narrow compared with the cross-track element pattern, Figure 4-3, hence the contour curves can be approximated by just the product of the two principal axis beams. The cross-track element patterns will tend to increase the side lobes of the array, but these are not plotted in Figure 6-1. For example, at the intersection of planes 26° aft and about 20° right or left of the nadir, there will be side-lobe peaks of approximately -37 db amplitude—that is, excluding error effects on the side-lobe level.

7.0 CONCLUSIONS

This study of element radiation patterns on the one-fifth scale mock-up of the wing section and dipoles has demonstrated that a smooth track-plane pattern shape can be obtained for two orthogonal polarizations which closely approximates the estimated gain versus angle of arrival requirements. The peak gain requirement of 17 db is exceeded for H-plane track polarization (19.5 db) but is not achieved for E-plane track polarization (13.5 db). This difference in gain results from the basic pattern characteristics of a half-wave dipole radiator. The pattern shapes for the two polarizations can be made nearly identical out to $\pm 40^{\circ}$ in the track plane.

The method of feeding the dipoles has evolved from the original concept to the use of individual linear arrays fed via a sum-and-difference circuit to control the gain and pattern shape in the region of the nadir. Also, parasitic dipoles have been employed to improve the radiation pattern characteristics and array efficiency, and to reduce random errors and side-lobe levels in the cross-track plane. Feeding the two line arrays separately from the sum-and-difference circuit allows a phase shifter to be inserted in the line which may be used to maintain minimum radiation at the nadir when the airplane trim or angle of attack is varied (this to be evaluated on full-scale mock-up).

And, lastly, the effects of mounting plate shape have been evaluated. The dipoles are mounted a half-wavelength above the mounting plate surface, and they are therefore critically sensitive to its shape. A wide flat plate is desired, but the dipoles must be mounted symmetrically on the plate. That is, the break in the surface where tapering begins should be the same distance from the nearest dipole on both fore and aft edges of the plate. The tapers of 5 to 1 are adequate, and identical tapers seem to be less essential than symmetrical mounting of the dipoles.

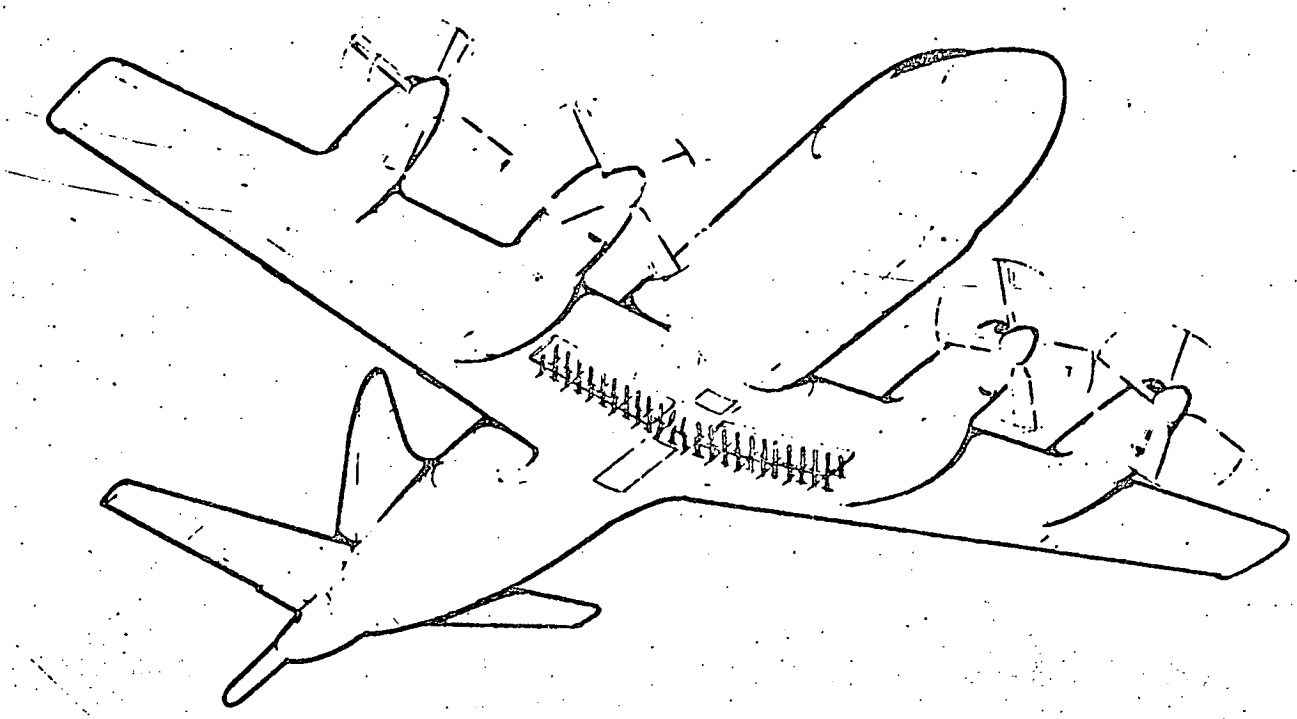

Figure 1-1. ANTENNA ARRAY INSTALLATION

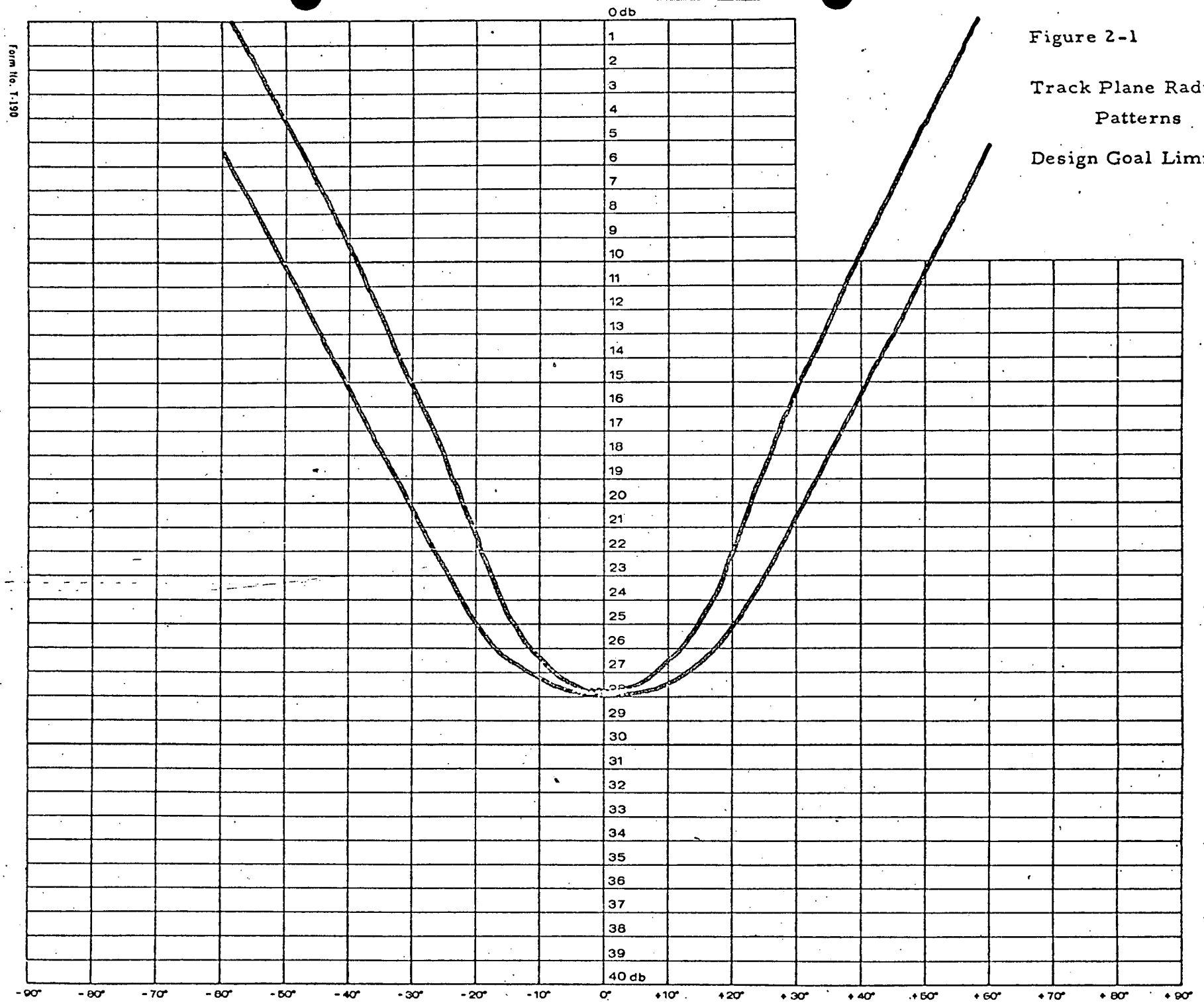

Figure 2-1

Track Plane Radiation Patterns

Design Goal Limits

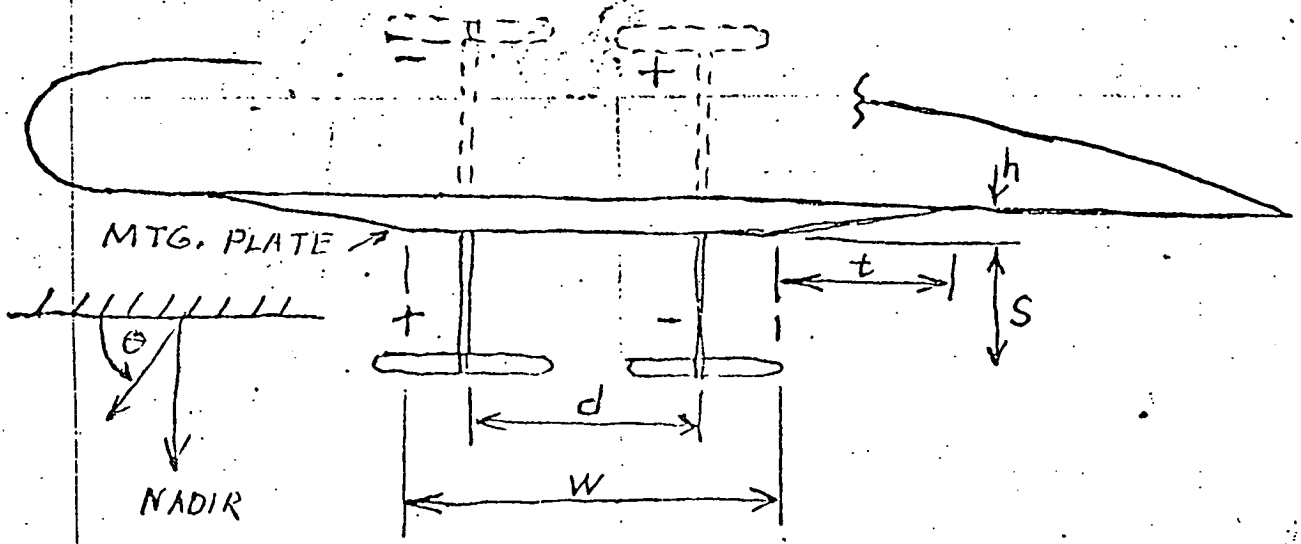

$$E_{\Delta}(\theta) = 4\left[\sin\left(\frac{2\pi s}{\lambda}\sin\theta\right)\right]\left[\sin\left(\frac{\pi d}{\lambda}\cos\theta\right)\right]\left\{\begin{array}{l} 1 \text{ - H-plane} \\ \\ \dfrac{\cos\left(\frac{\pi}{2}\cos\theta\right)}{\sin\theta} \text{ E-plane} \end{array}\right\}$$

$$E_{\Sigma}(\theta) = 4\left[\sin\left(\frac{2\pi s}{\lambda}\sin\theta\right)\right]\left[\cos\left(\frac{\pi d}{\lambda}\cos\theta\right)\right]\left\{\begin{array}{l} 1 \text{ - H plane} \\ \\ \dfrac{\cos\left(\frac{\pi}{2}\cos\theta\right)}{\sin\theta} \text{ E-plane} \end{array}\right\}$$

Figure 3-1

Array elements consist of a quadrupole - two driven elements plus their images. "d" and "s" are both approximately 0.5λ.

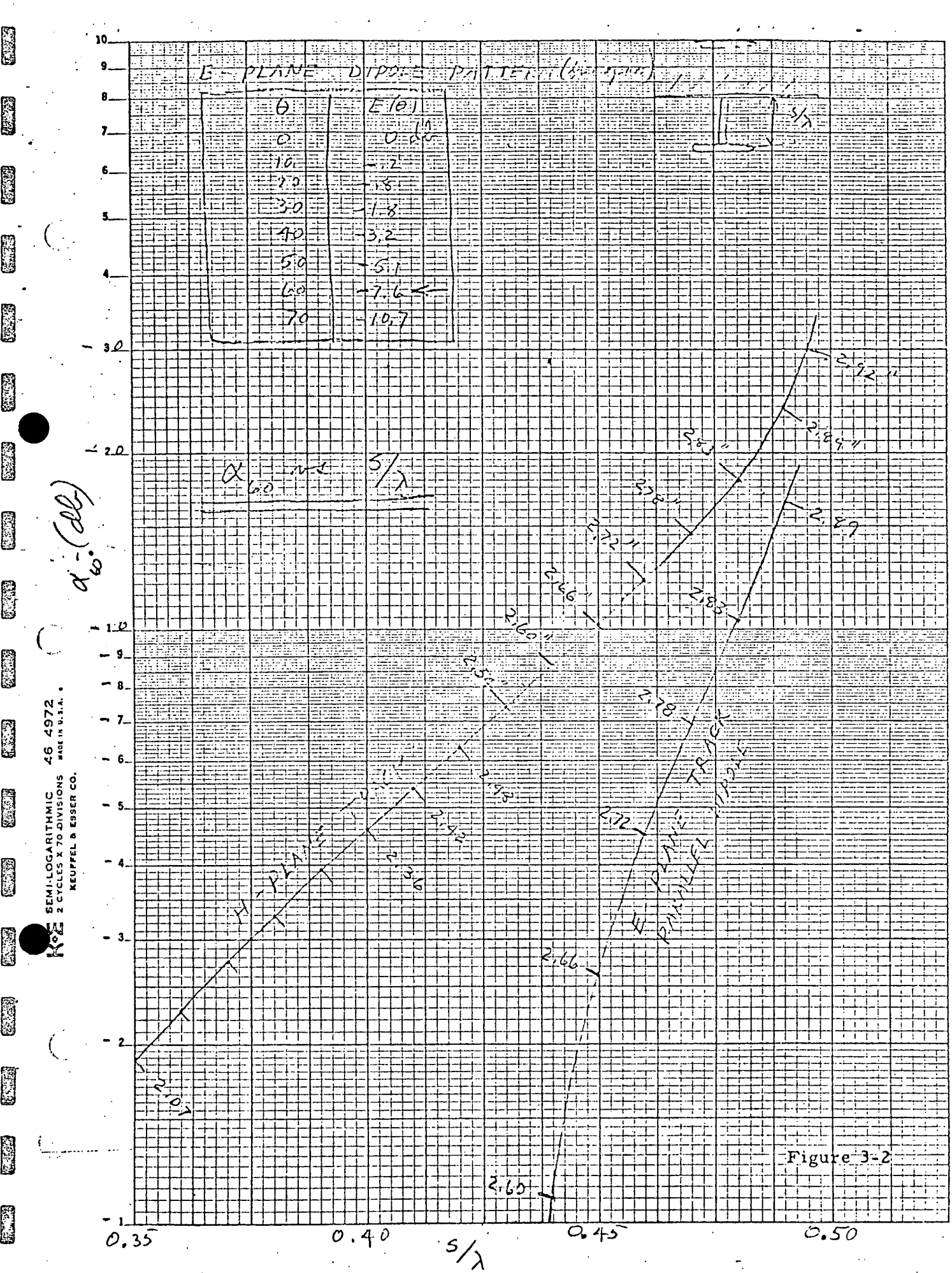
E - PLANE DIPOLE PATTERN (½ λ DIPOLE)
θ
E(θ)
0
0.00
10
-.2
20
-1.8
30
-1.8
40
-3.2
50
-5.1
60
-7.6
70
-10.7
S/λ
α60 = (dB)
E PLANE
PARALLEL TO AXIS
H PLANE
2.12
2.83
2.89
2.82
2.22
2.46
2.60
2.58
2.78
2.72
2.58
2.52
2.46
2.66
2.65
2.0
0.35
0.40
0.45
0.50
S/λ
SEMI-LOGARITHMIC
2 CYCLES X 70 DIVISIONS
KEUFFEL & ESSER CO.
46 4972
MADE IN U.S.A.

Figure 3-2

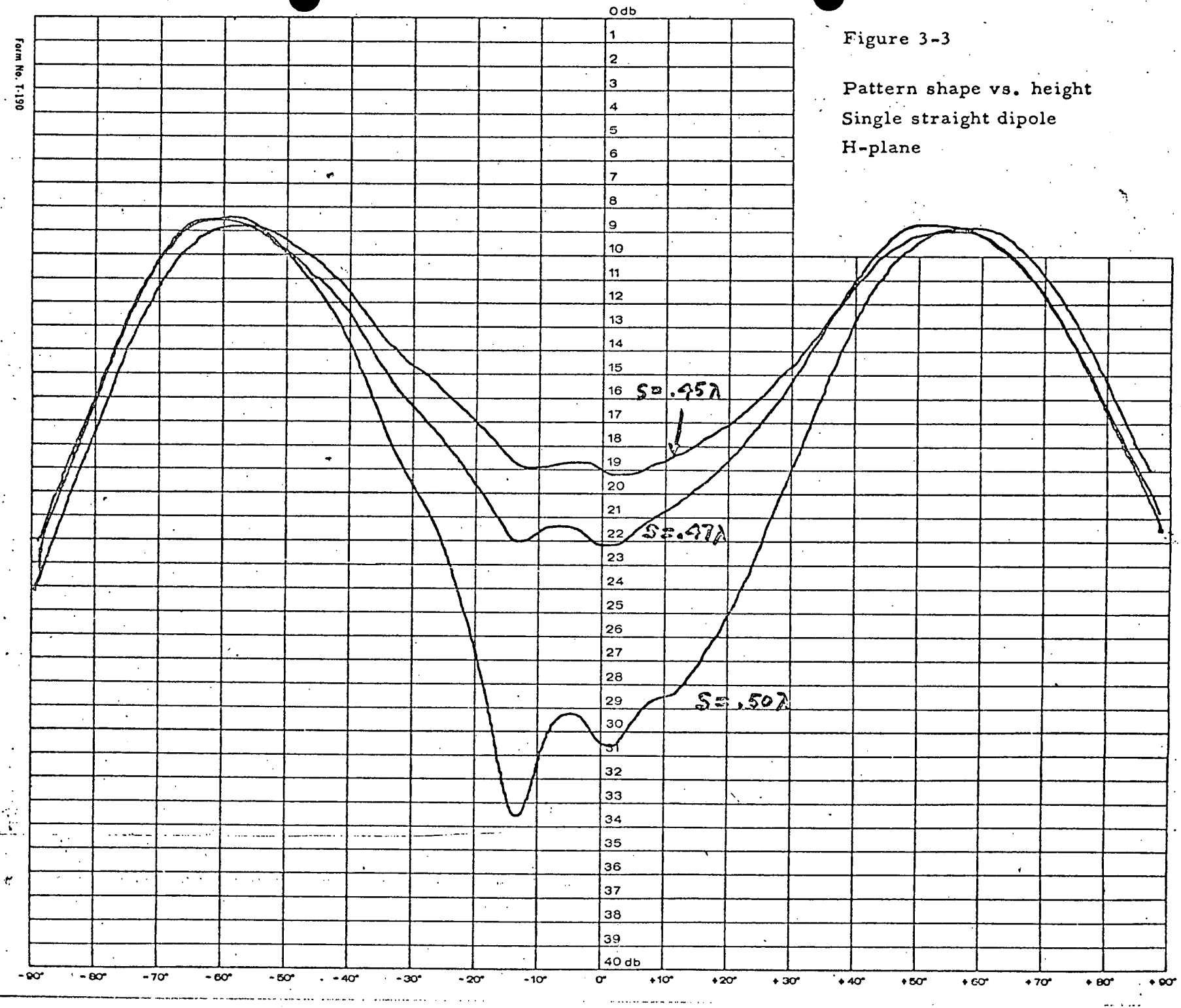

Figure 3-3

Pattern shape vs. height
Single straight dipole
H-plane

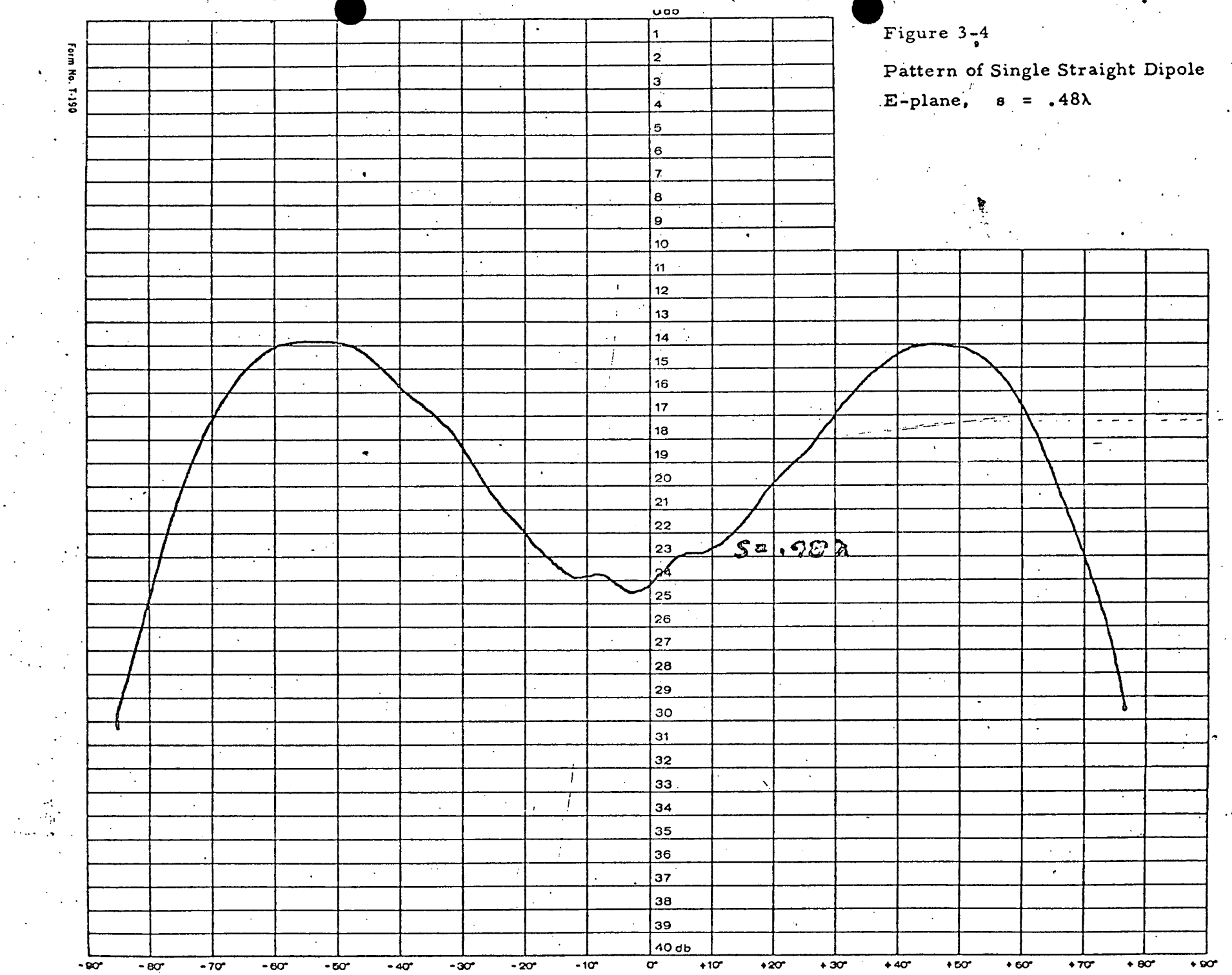

Figure 3-4

Pattern of Single Straight Dipole

E-plane, s = .48λ

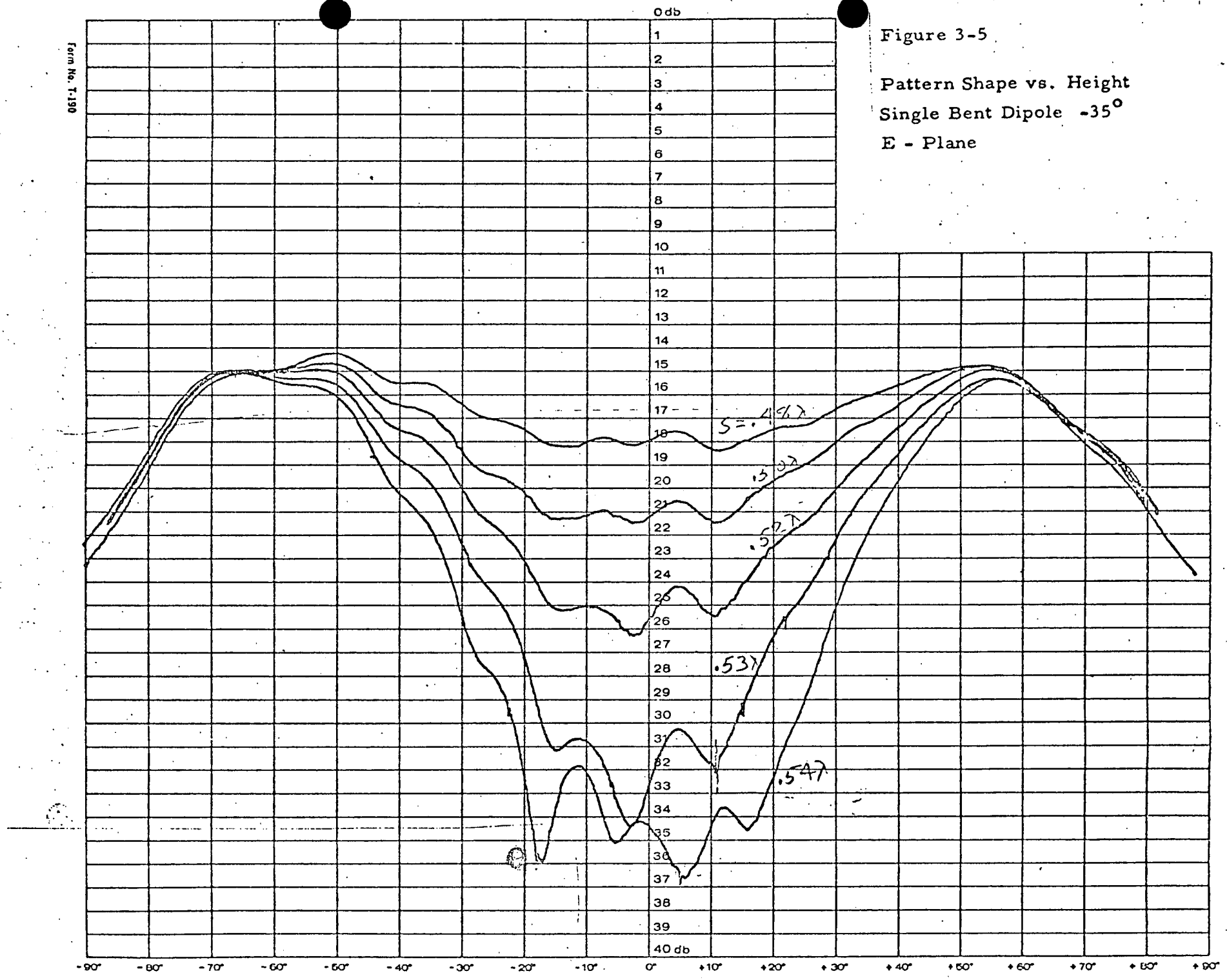

Figure 3-5

Pattern Shape vs. Height
Single Bent Dipole -35°
E - Plane

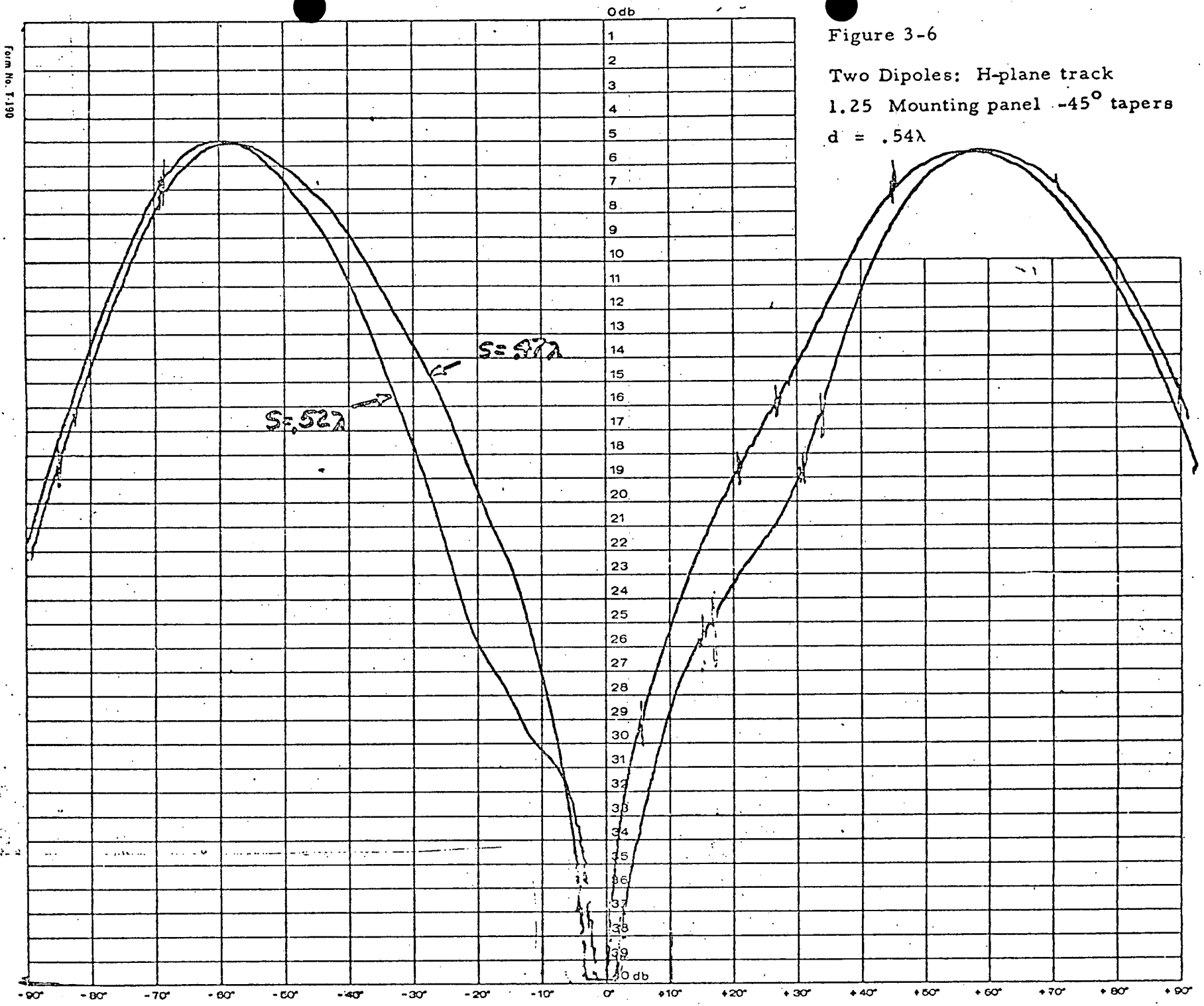

Figure 3-6

Two Dipoles: H-plane track

1.25 Mounting panel -45° tapers

d = .54λ

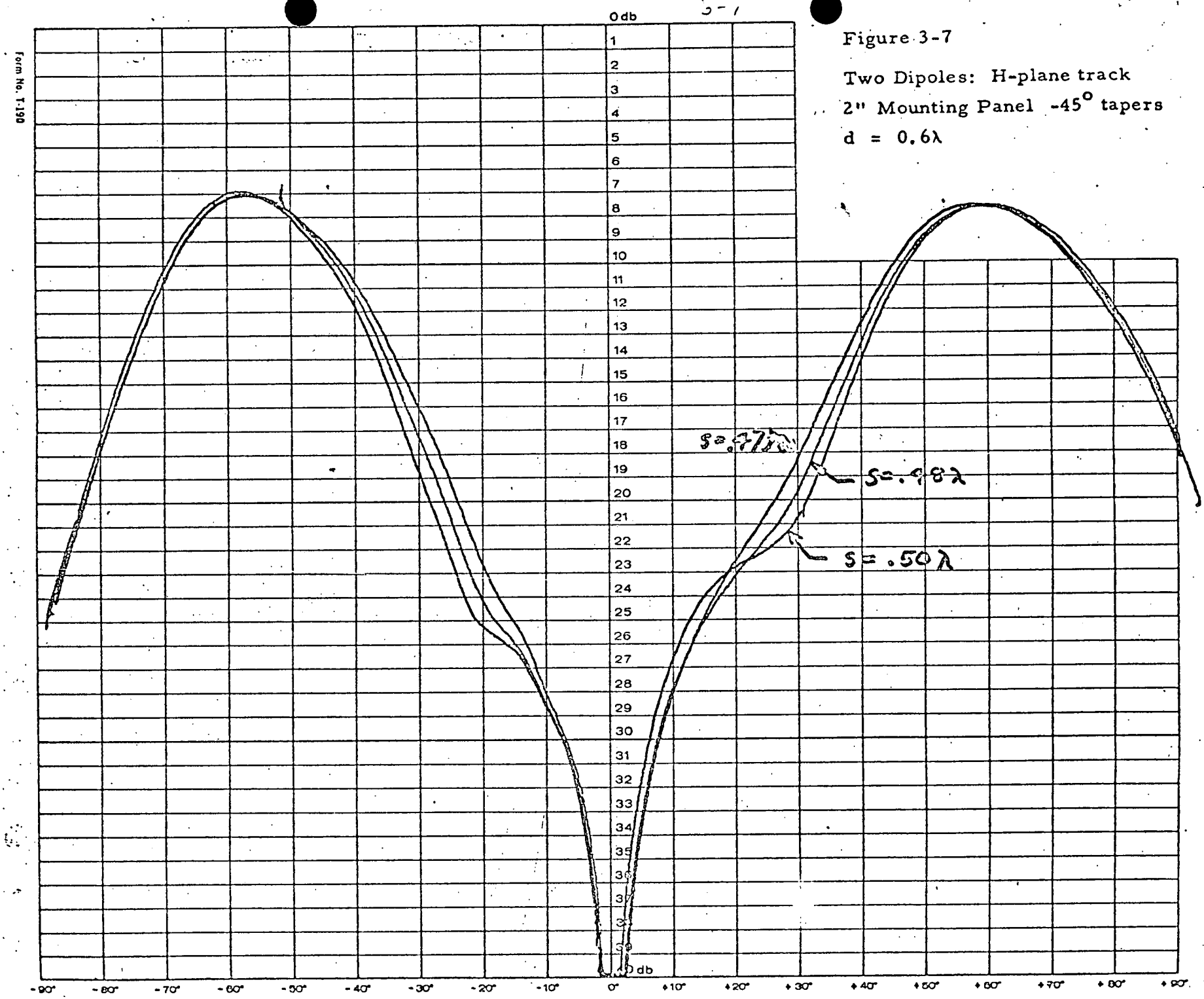

Figure 3-7

Two Dipoles: H-plane track

2" Mounting Panel -45° tapers

d = 0.6λ

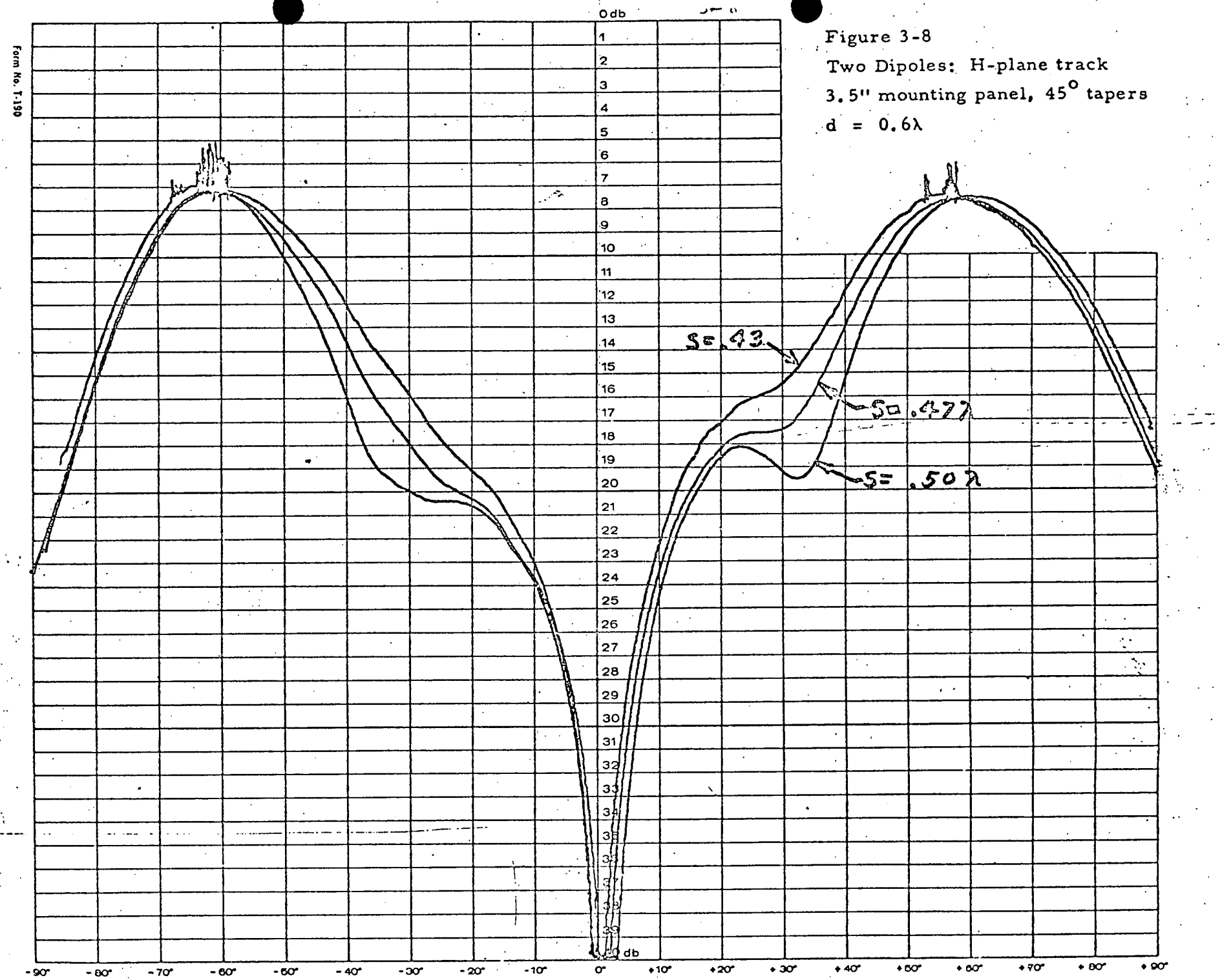

Figure 3-8

Two Dipoles: H-plane track

3.5" mounting panel, 45° tapers

$d = 0.6\lambda$

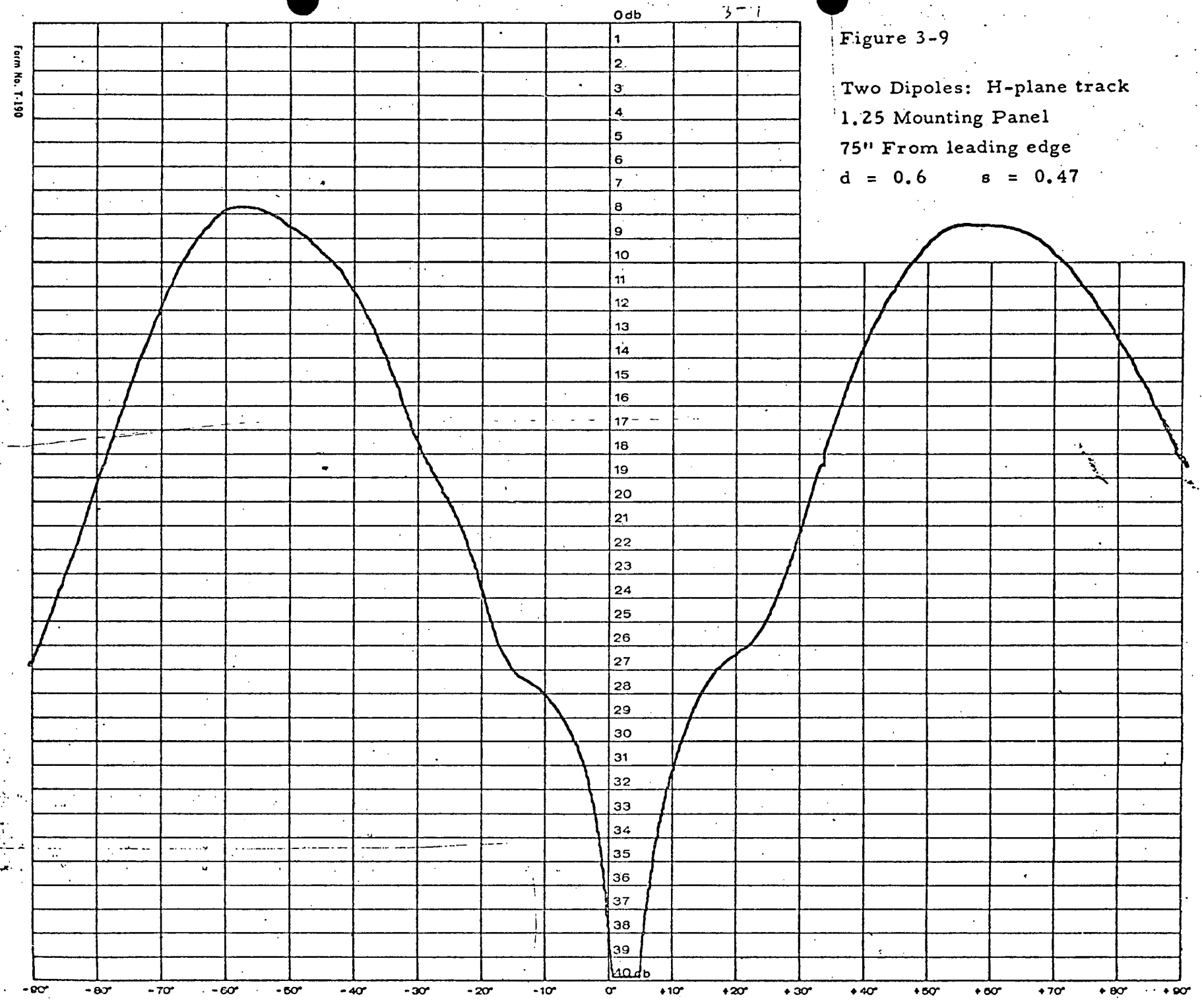

Figure 3-9

Two Dipoles: H-plane track

1.25 Mounting Panel

75" From leading edge

d = 0.6 s = 0.47

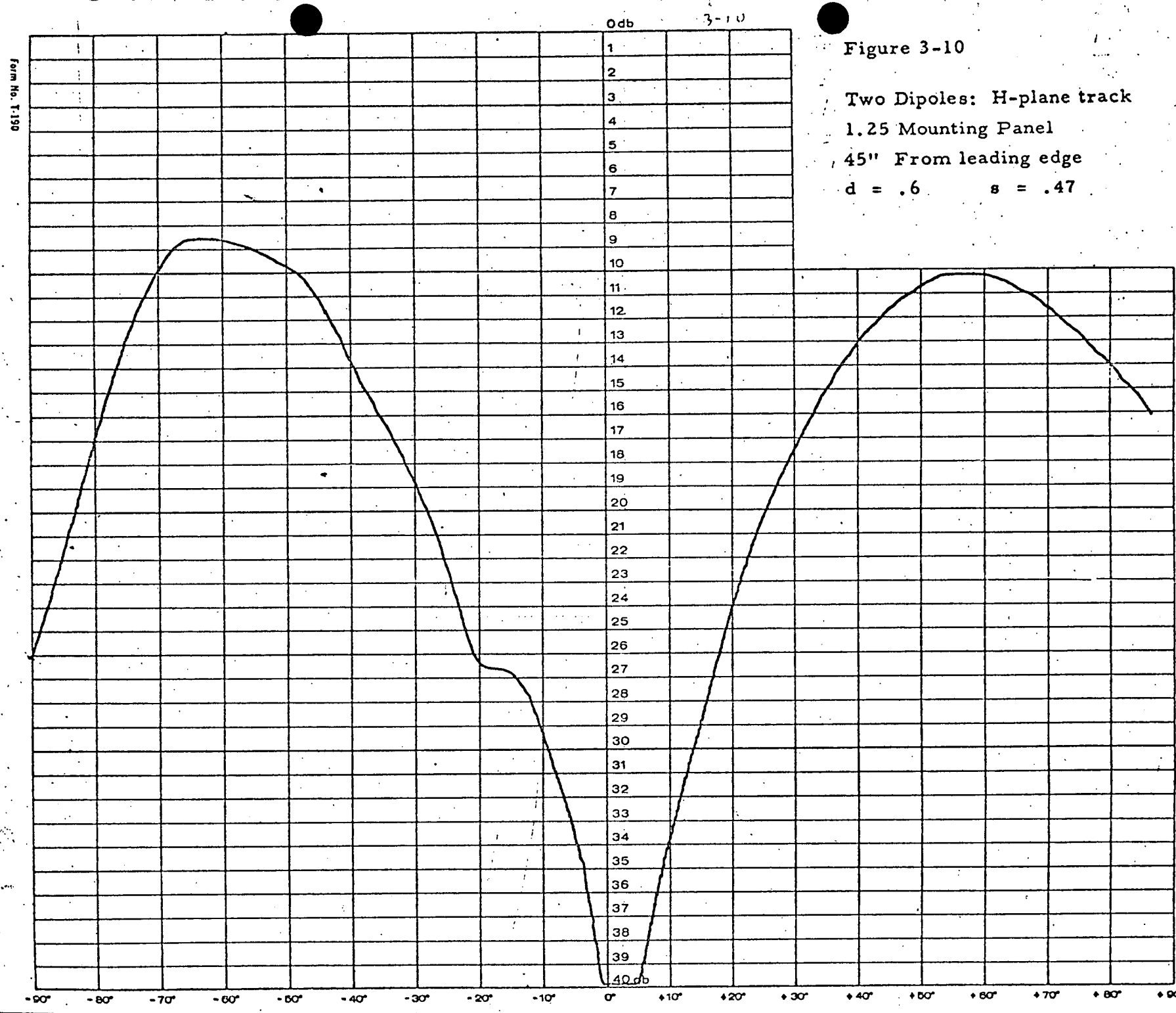

Figure 3-10

Two Dipoles: H-plane track
1.25 Mounting Panel
45" From leading edge
d = .6 s = .47

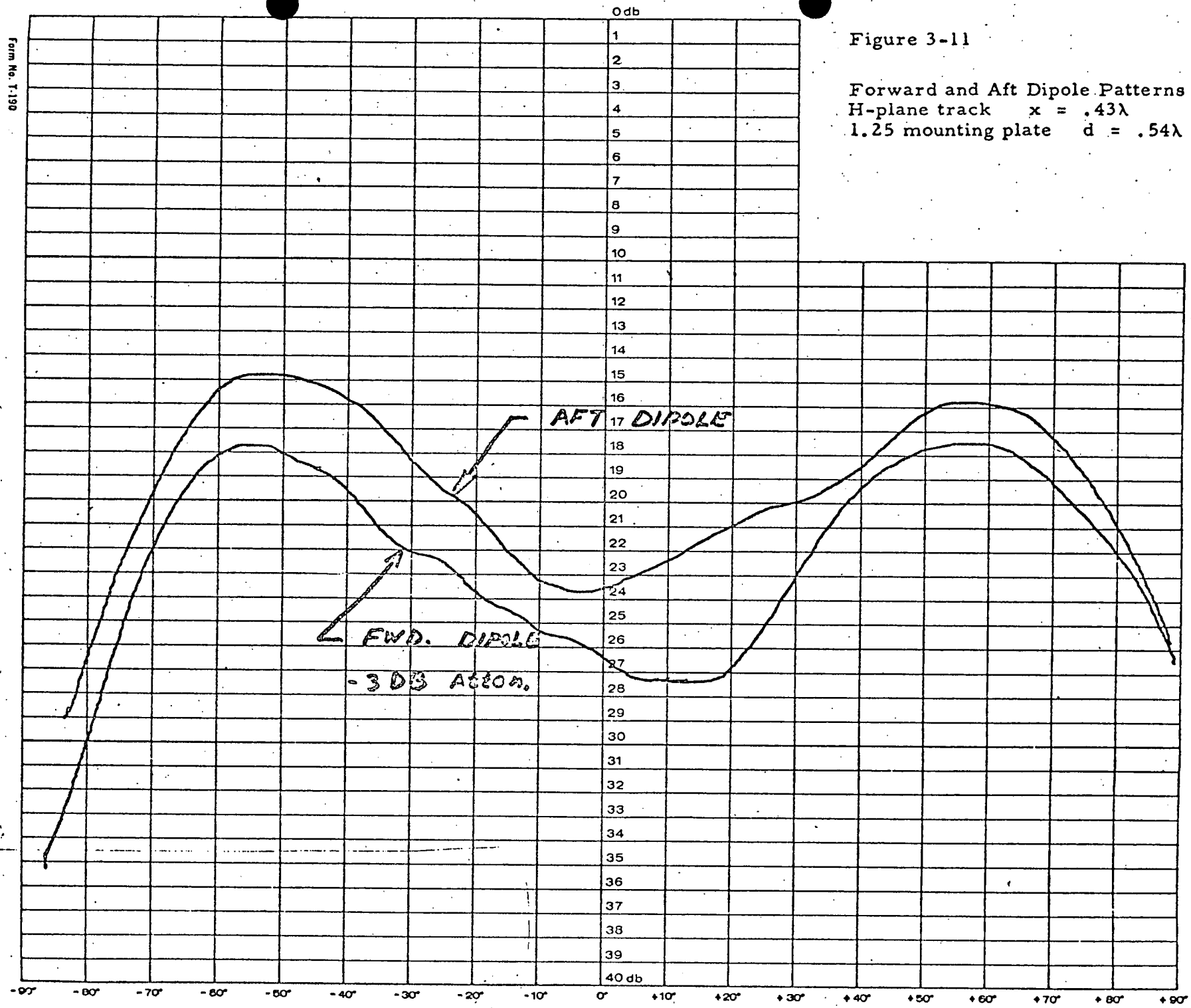

Figure 3-11

Forward and Aft Dipole Patterns
H-plane track x = .43λ
1.25 mounting plate d = .54λ

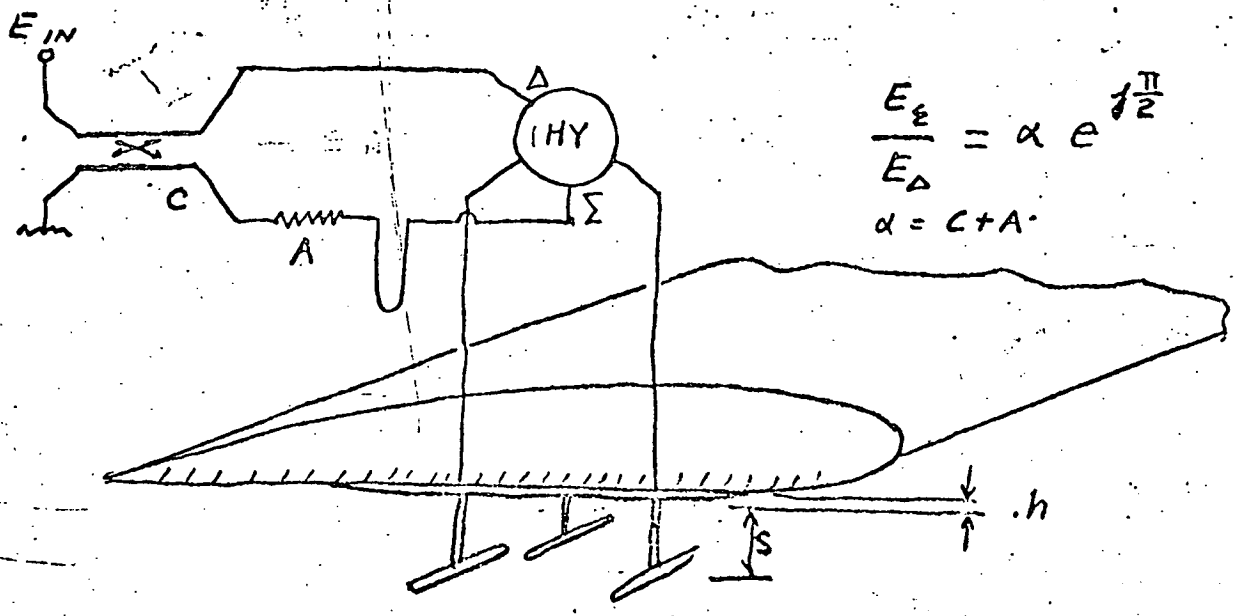

Figure 3-12 - Circuit Diagram

for feeding sum-and-difference modes simultaneously with relative amplitudes, α, db, and relative phase of 90°.

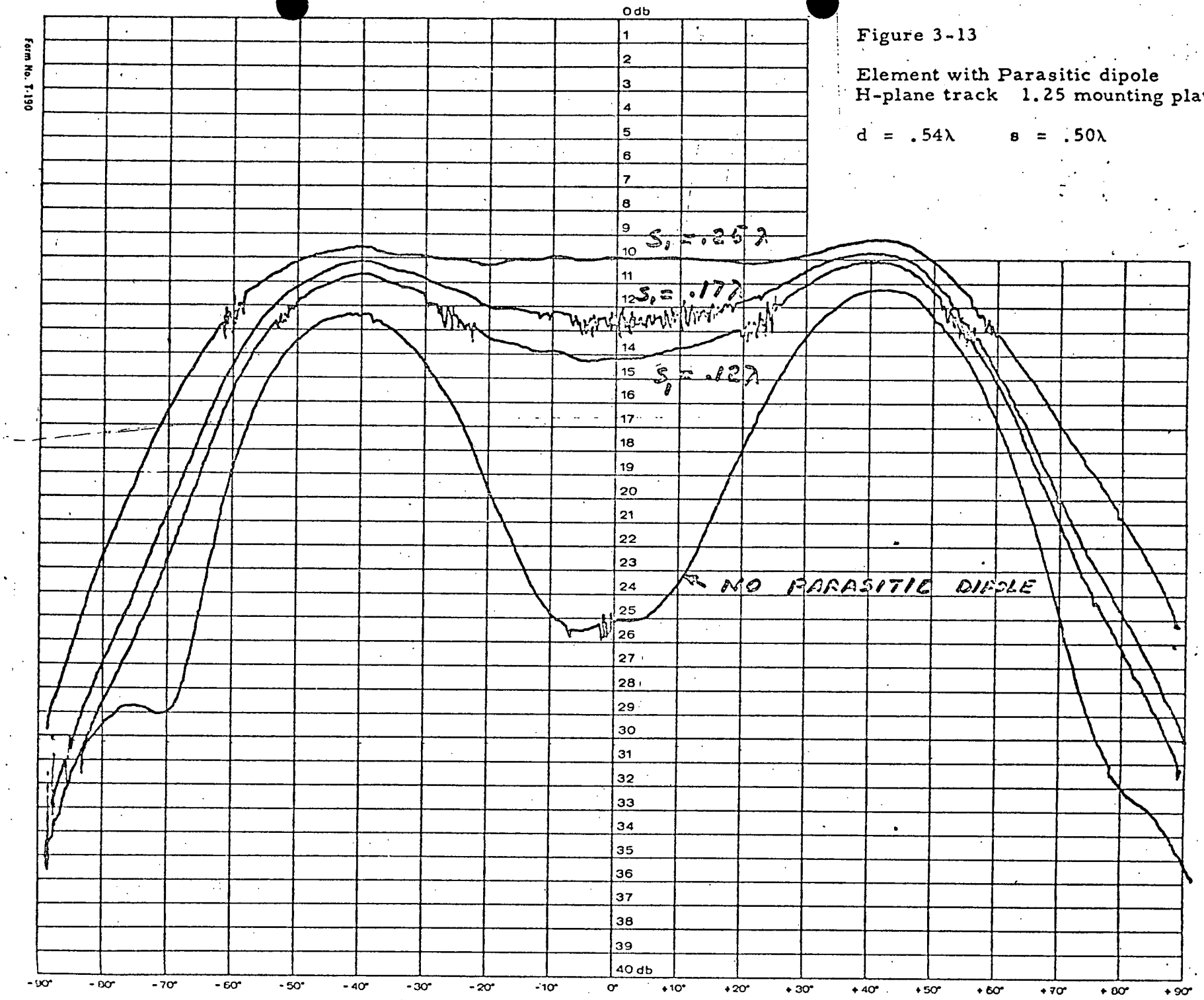

Figure 3-13

Element with Parasitic dipole
H-plane track 1.25 mounting plate

d = .54λ s = .50λ

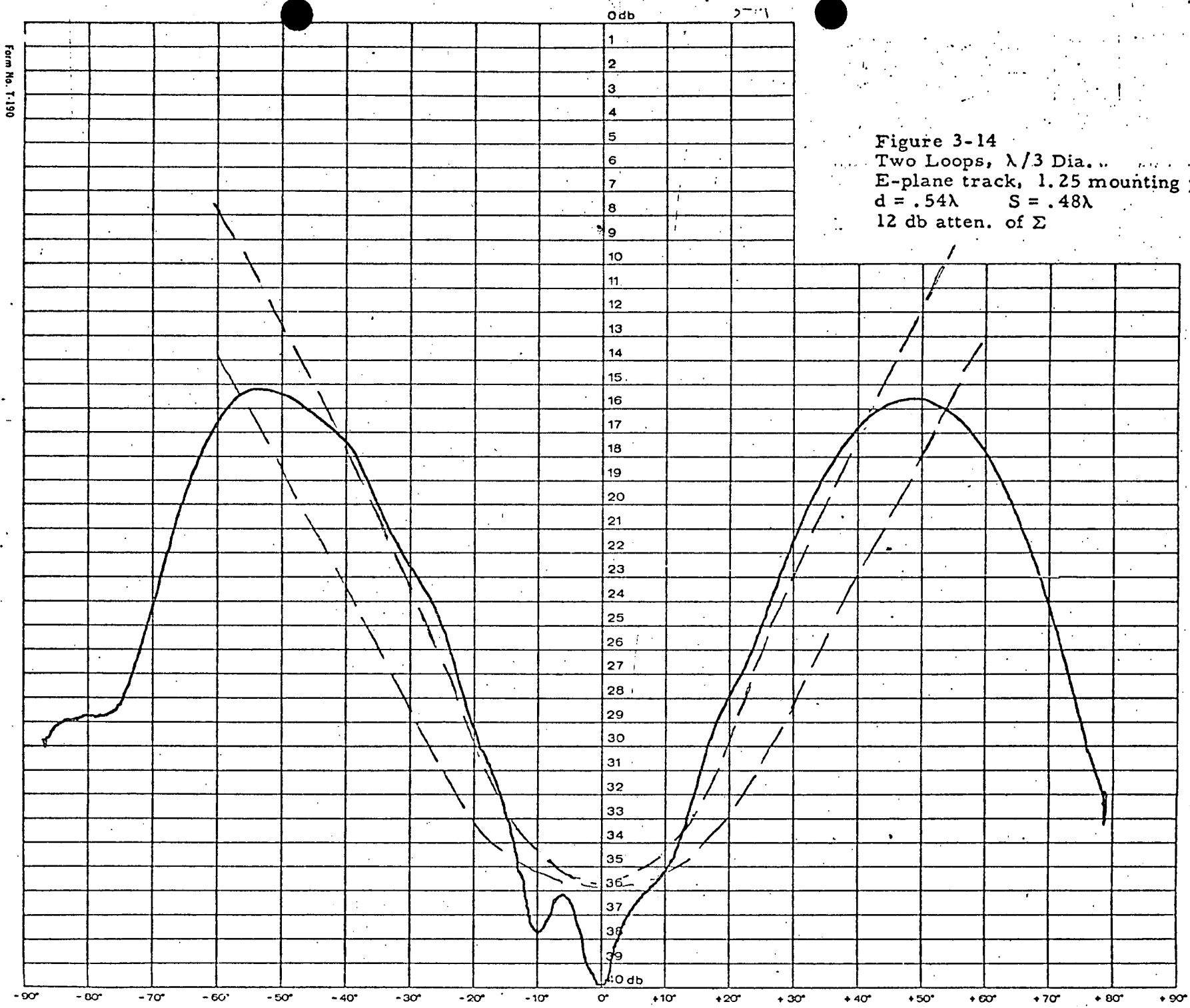

Figure 3-14
Two Loops, $\lambda/3$ Dia.
E-plane track, 1.25 mounting plate
$d = .54\lambda$ $S = .48\lambda$
12 db atten. of Σ

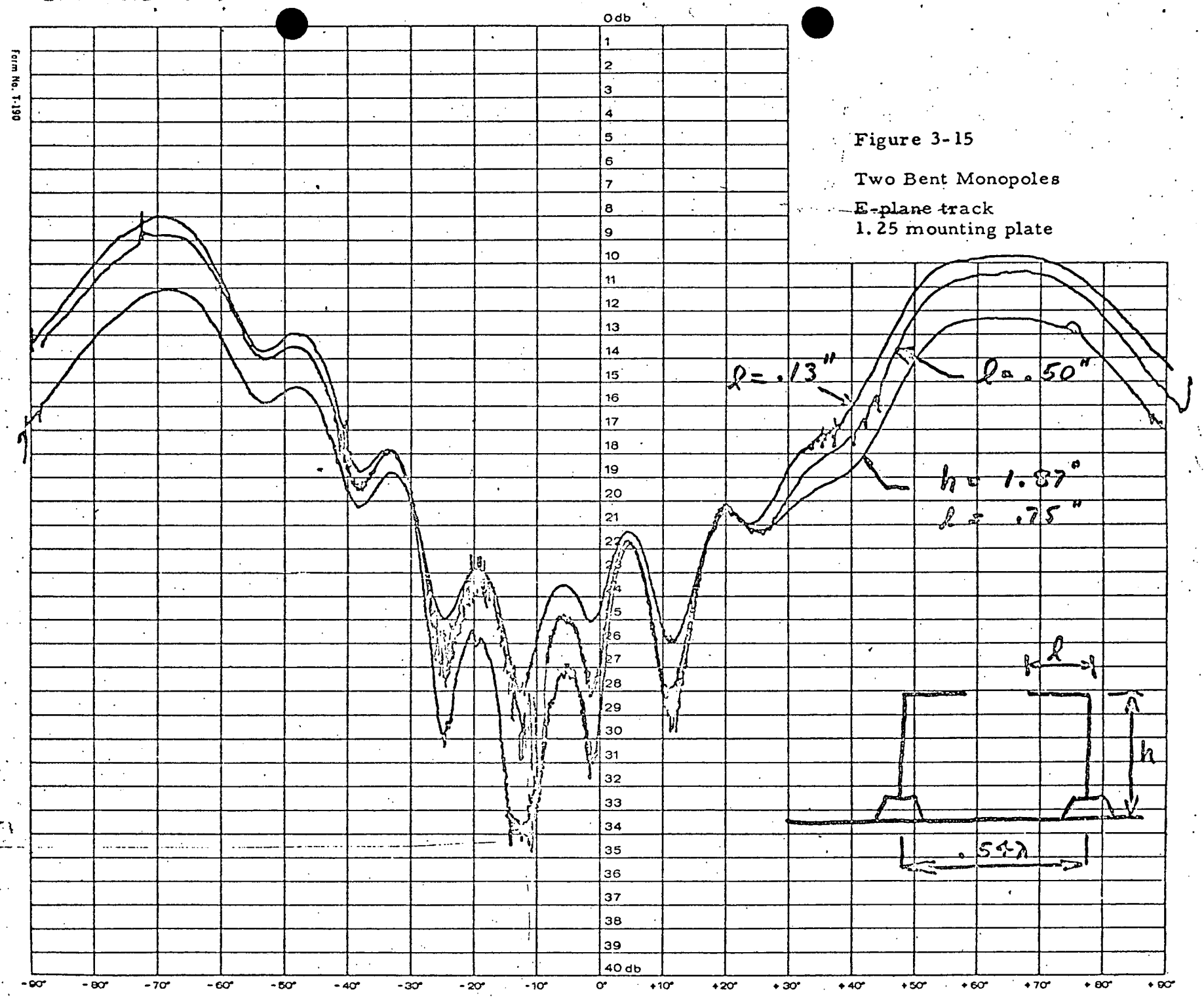

Figure 3-15

Two Bent Monopoles

E-plane track
1.25 mounting plate

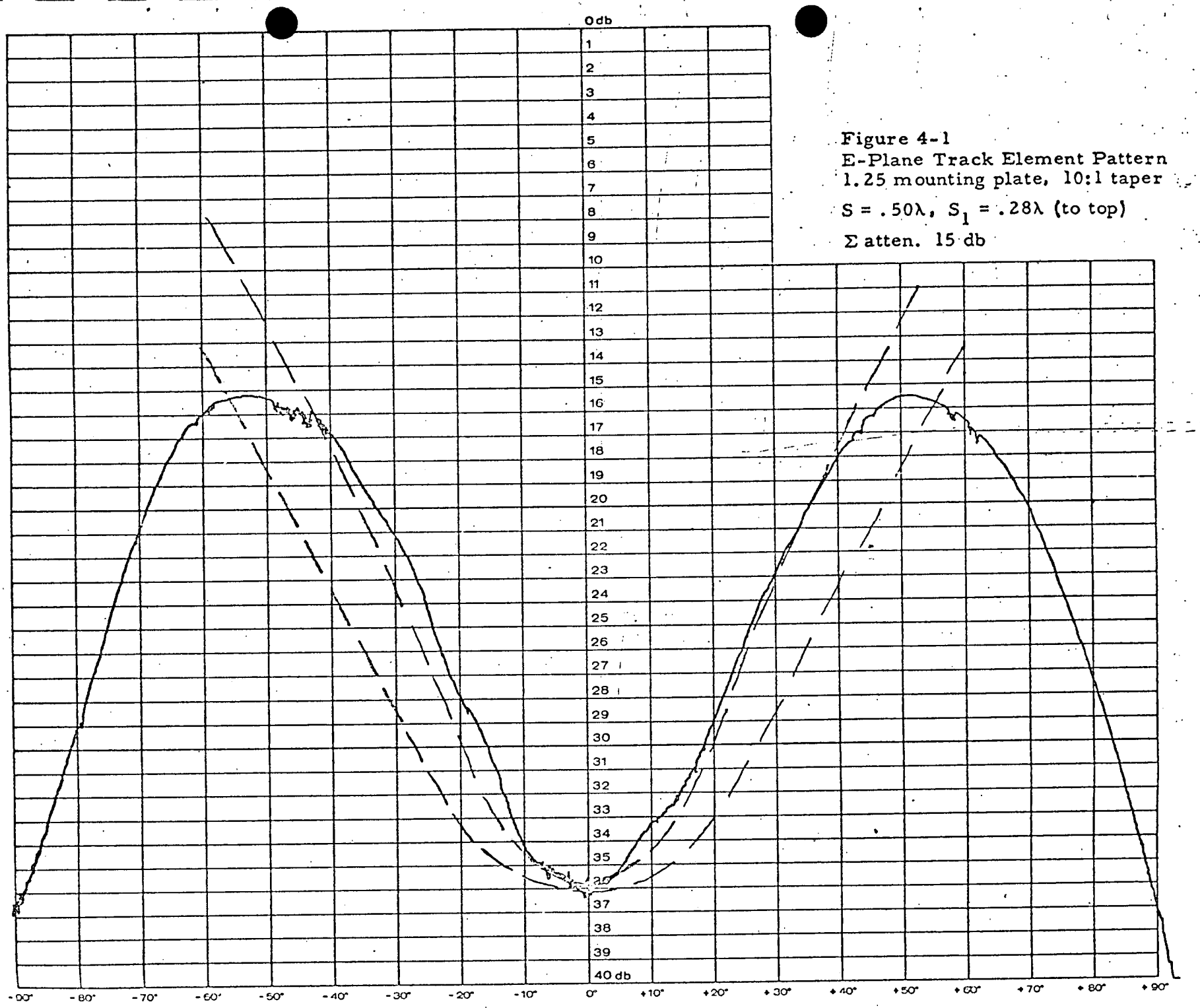

Figure 4-1
E-Plane Track Element Pattern
1.25 mounting plate, 10:1 taper
$S = .50\lambda$, $S_1 = .28\lambda$ (to top)
Σ atten. 15 db

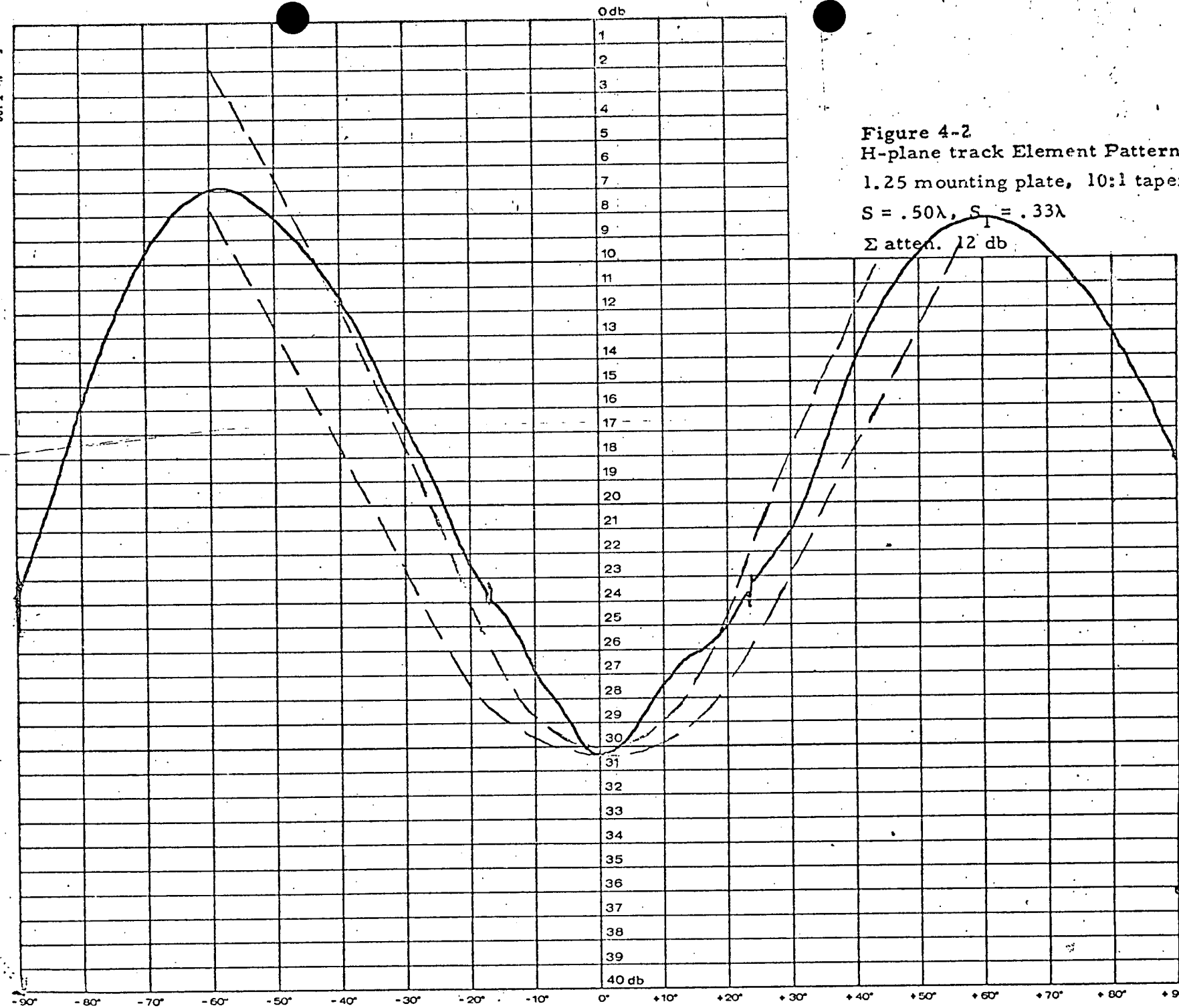

Figure 4-2
H-plane track Element Pattern
1.25 mounting plate, 10:1 tapers
$S = .50\lambda$, $S_1 = .33\lambda$
Σ atten. 12 db

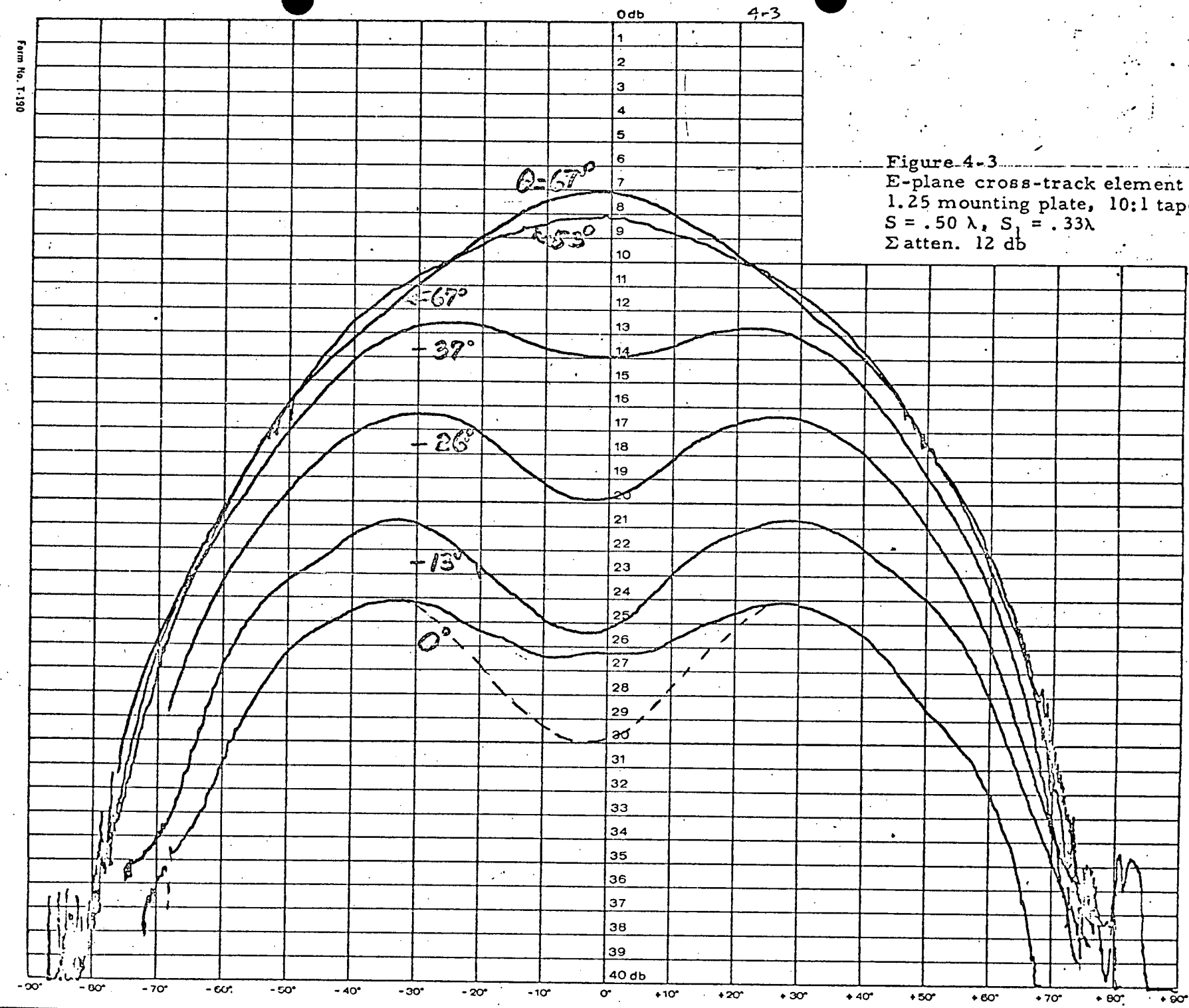

Figure 4-3
E-plane cross-track element pattern
1.25 mounting plate, 10:1 taper
$S = .50\ \lambda$, $S_1 = .33\lambda$
Σ atten. 12 db

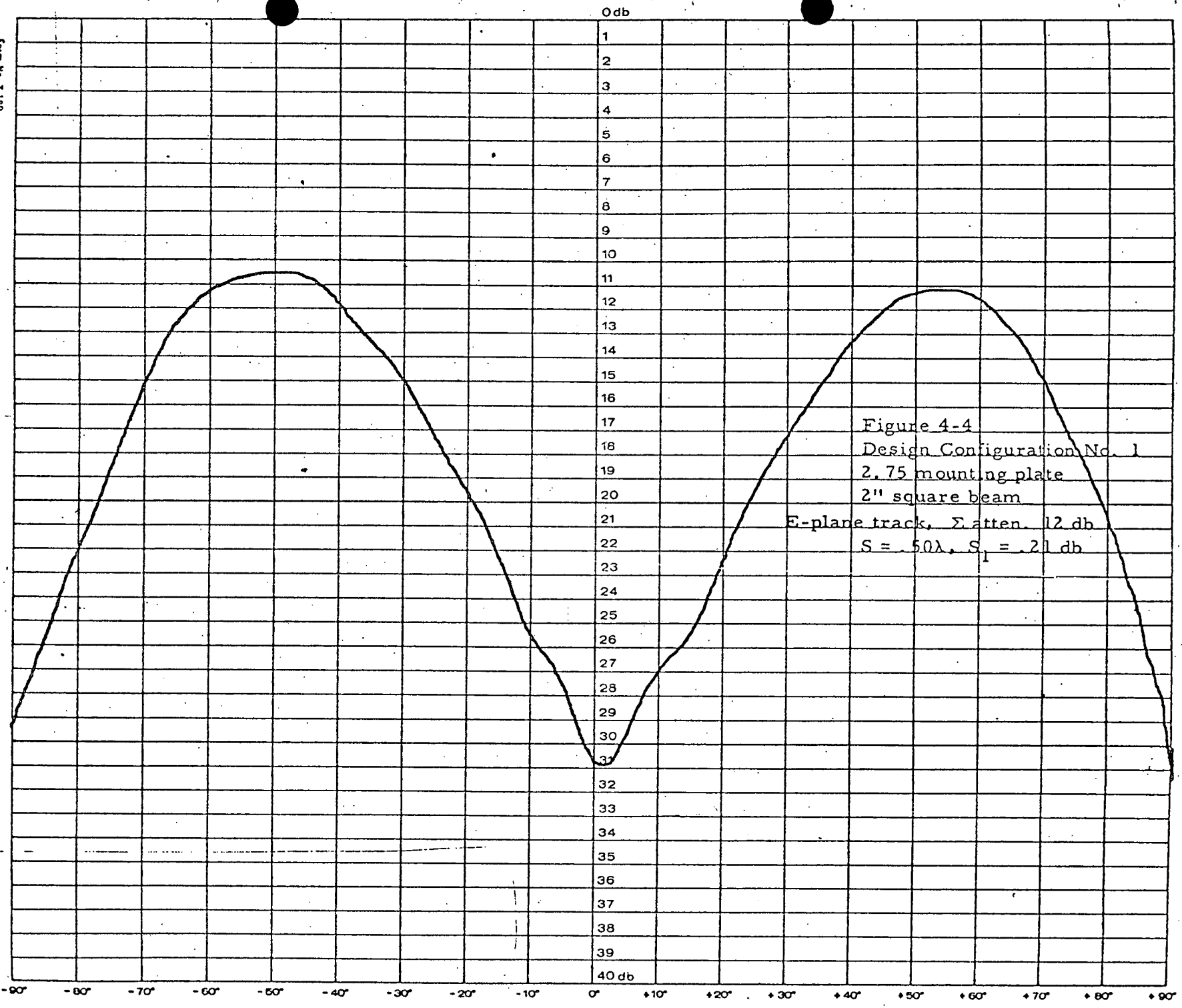

Figure 4-4
Design Configuration No. 1
2.75 mounting plate
2" square beam
E-plane track, Σ atten. 12 db
$S = .50\lambda$, $S_1 = .21$ db

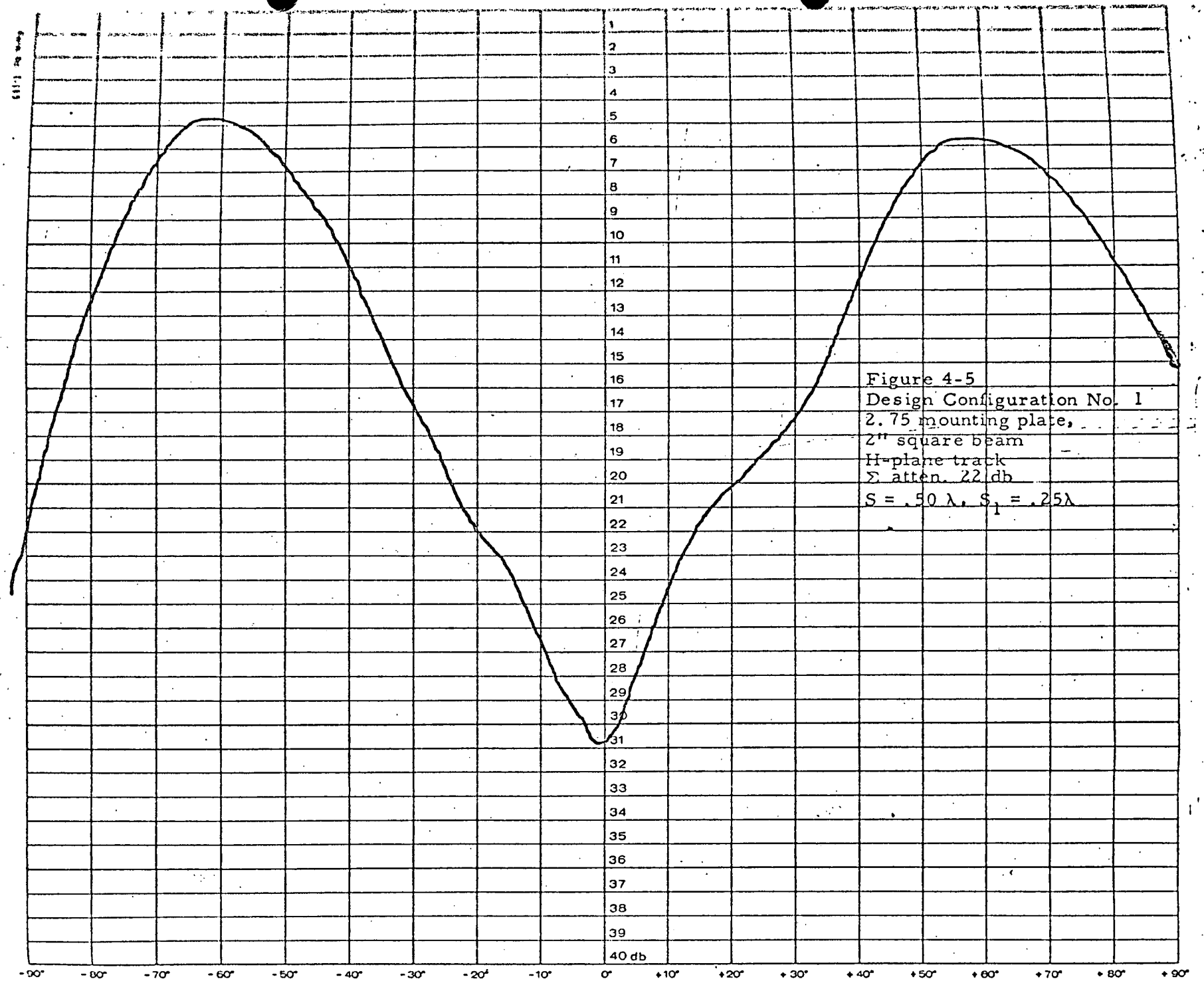

Figure 4-5
Design Configuration No. 1
2.75 mounting plate,
2" square beam
H-plane track
Σ atten. 22 db
$S = .50\lambda$, $S_1 = .25\lambda$

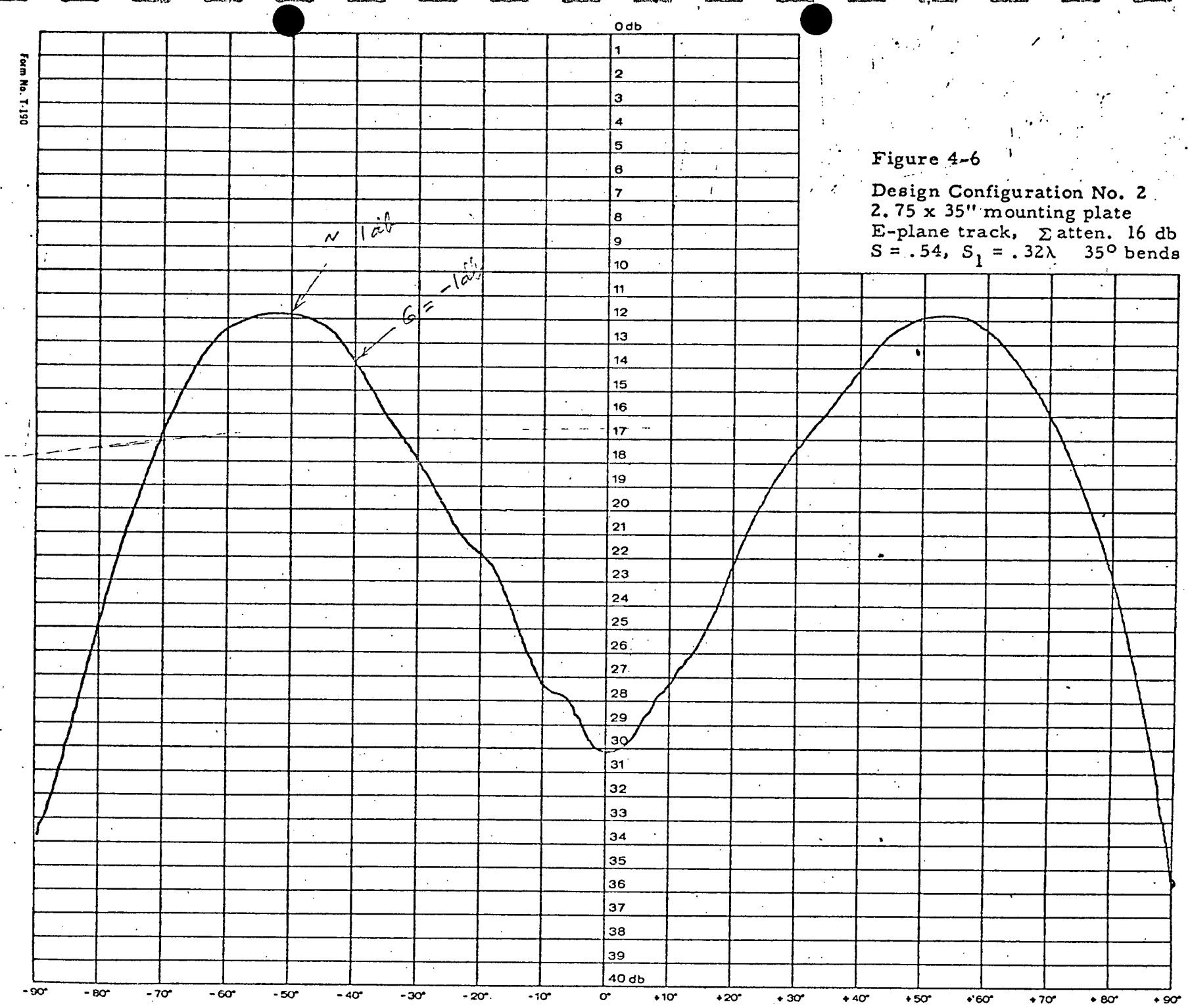

Figure 4-6

Design Configuration No. 2
2.75 x 35" mounting plate
E-plane track, Σ atten. 16 db
$S = .54$, $S_1 = .32\lambda$ 35° bends

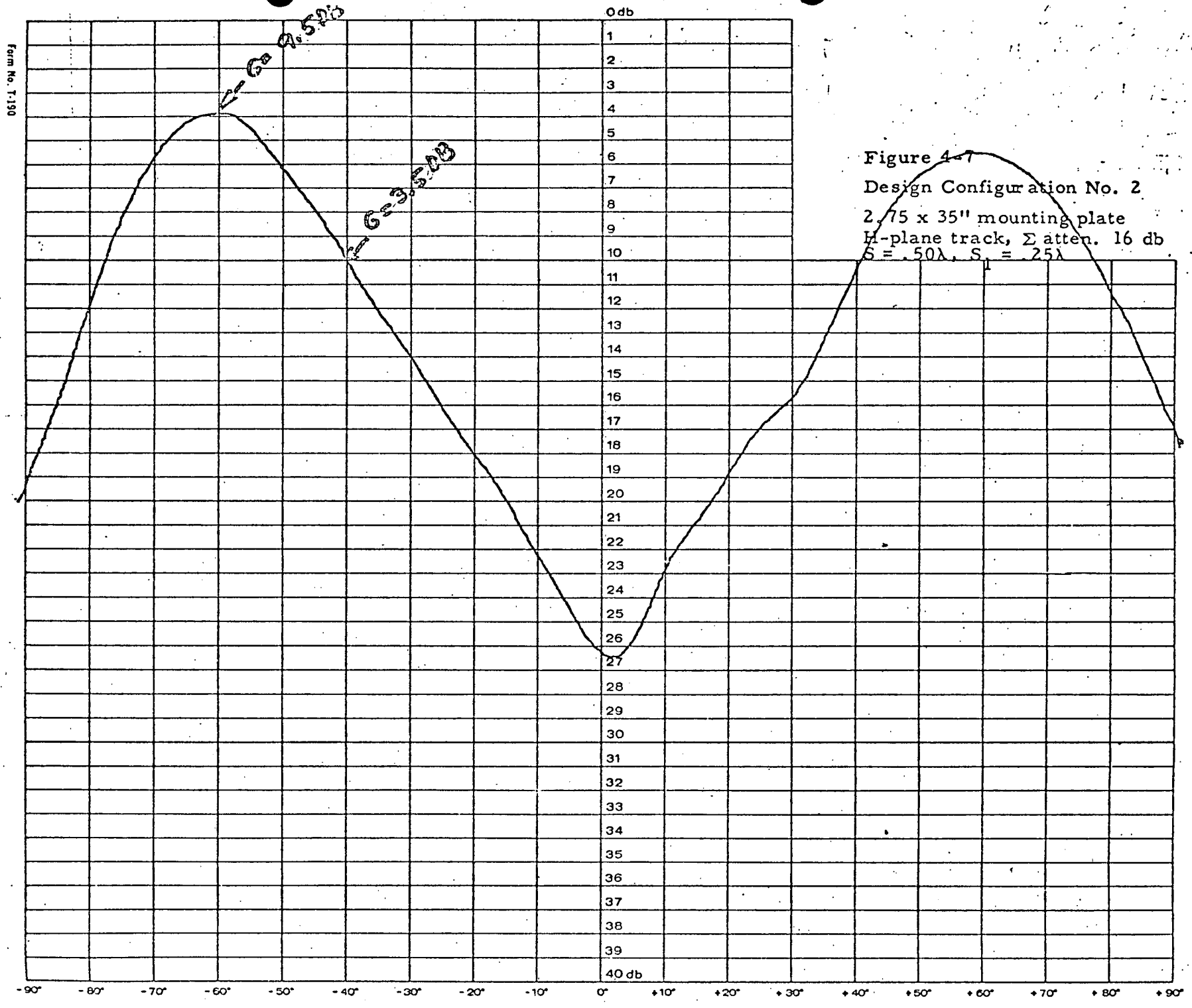

Figure 4-7

Design Configuration No. 2

2.75 x 35" mounting plate

H-plane track, Σ atten. 16 db

$S_0 = .50\lambda$, $S_1 = .25\lambda$

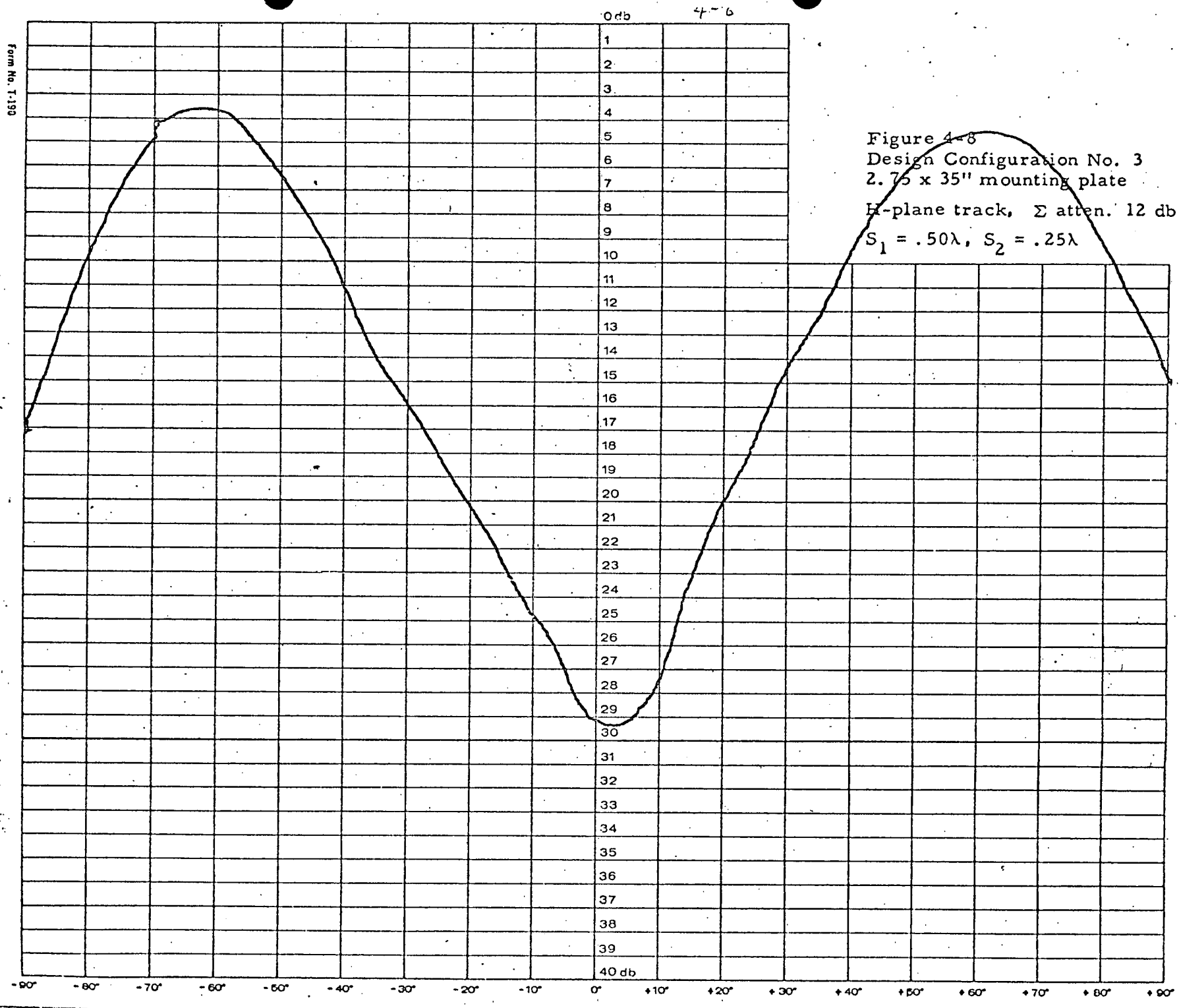

Figure 4-8
Design Configuration No. 3
2.75 x 35" mounting plate
H-plane track, Σ atten. 12 db
$S_1 = .50\lambda$, $S_2 = .25\lambda$

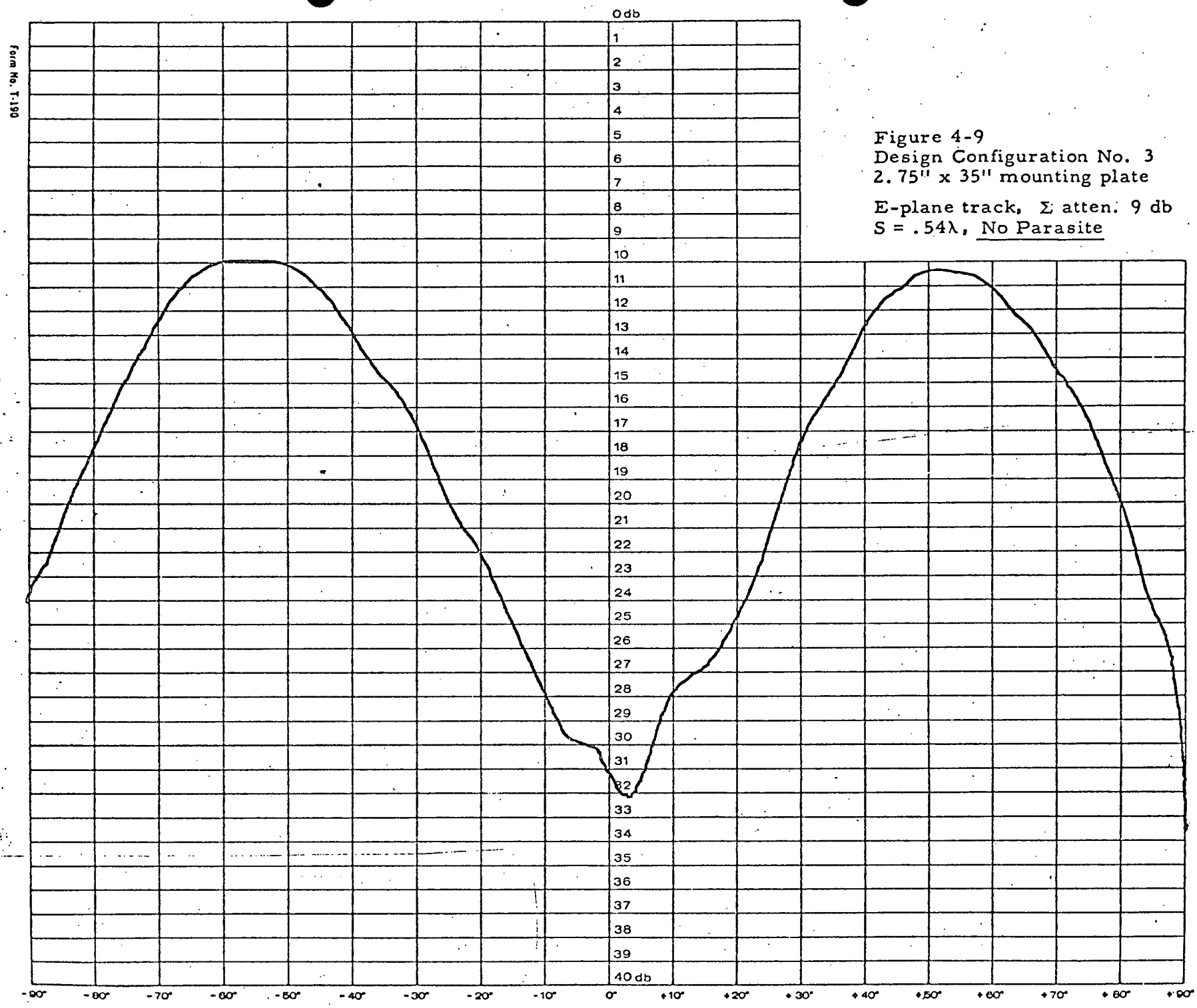

Figure 4-9
Design Configuration No. 3
2.75" x 35" mounting plate

E-plane track, Σ atten. 9 db
$S = .54\lambda$, No Parasite

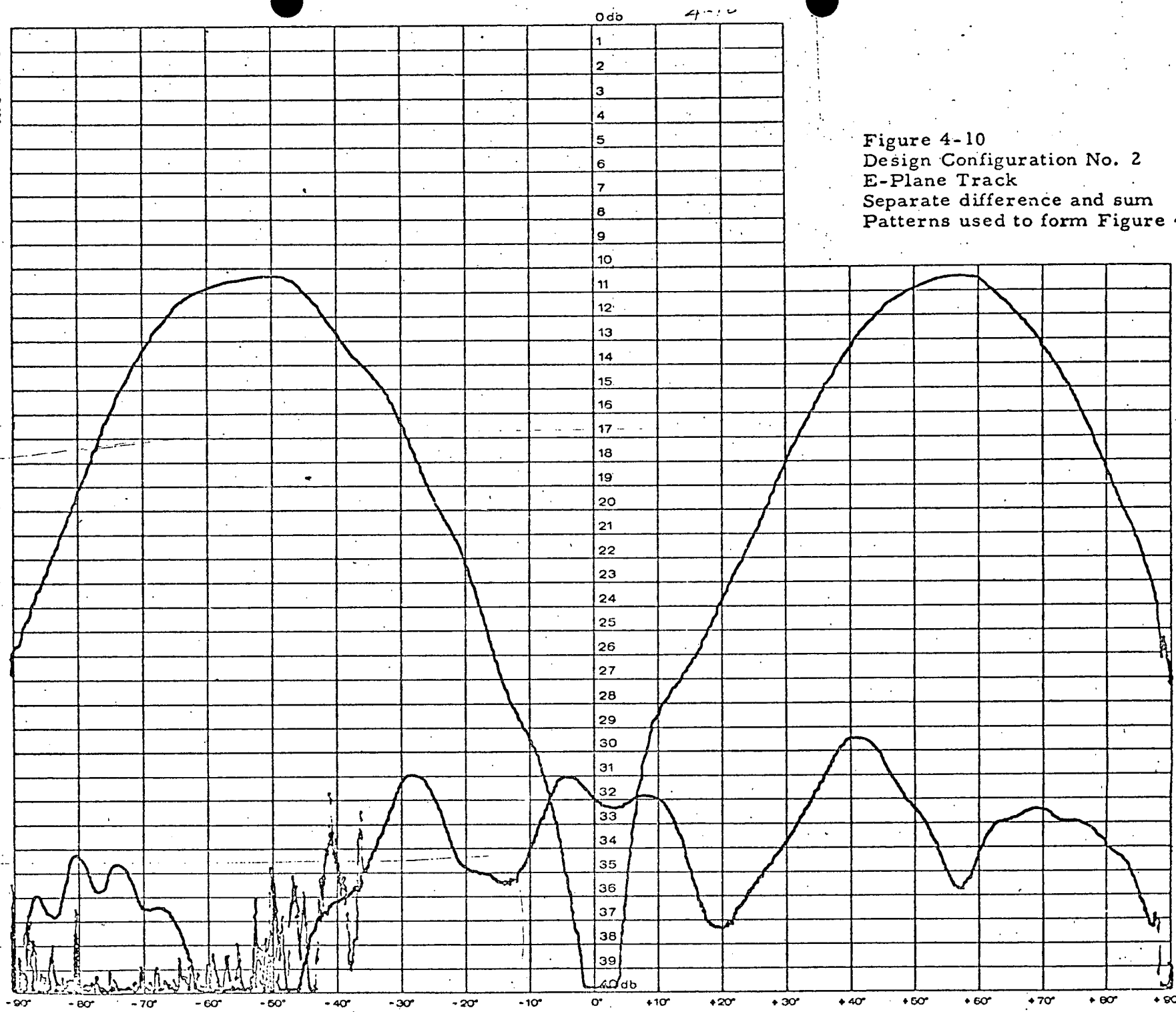

Figure 4-10
Design Configuration No. 2
E-Plane Track
Separate difference and sum
Patterns used to form Figure 4-9.

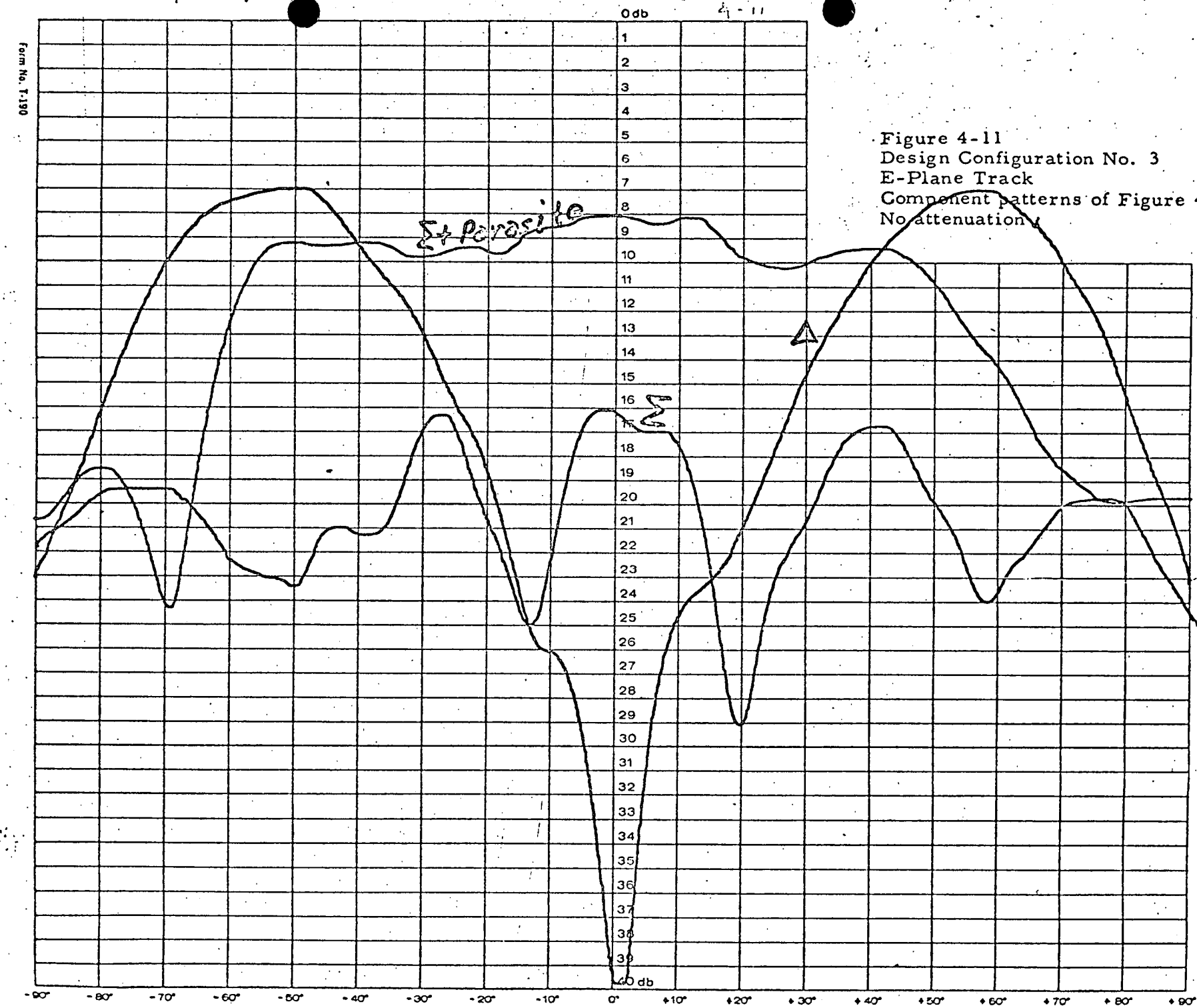

Figure 4-11
Design Configuration No. 3
E-Plane Track
Component patterns of Figure 4-9
No attenuation

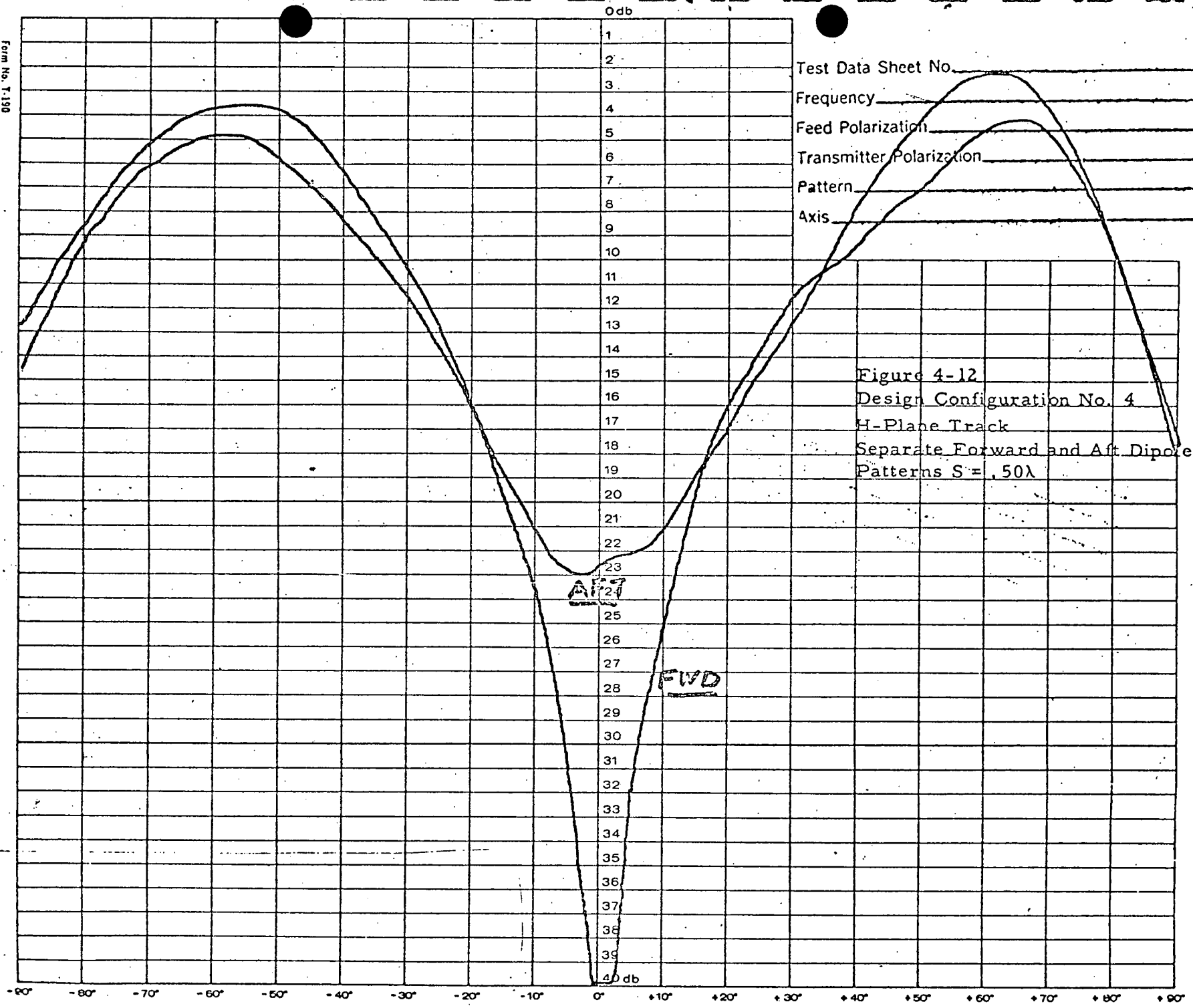

Figure 4-12
Design Configuration No. 4
H-Plane Track
Separate Forward and Aft Dipole
Patterns S = .50λ

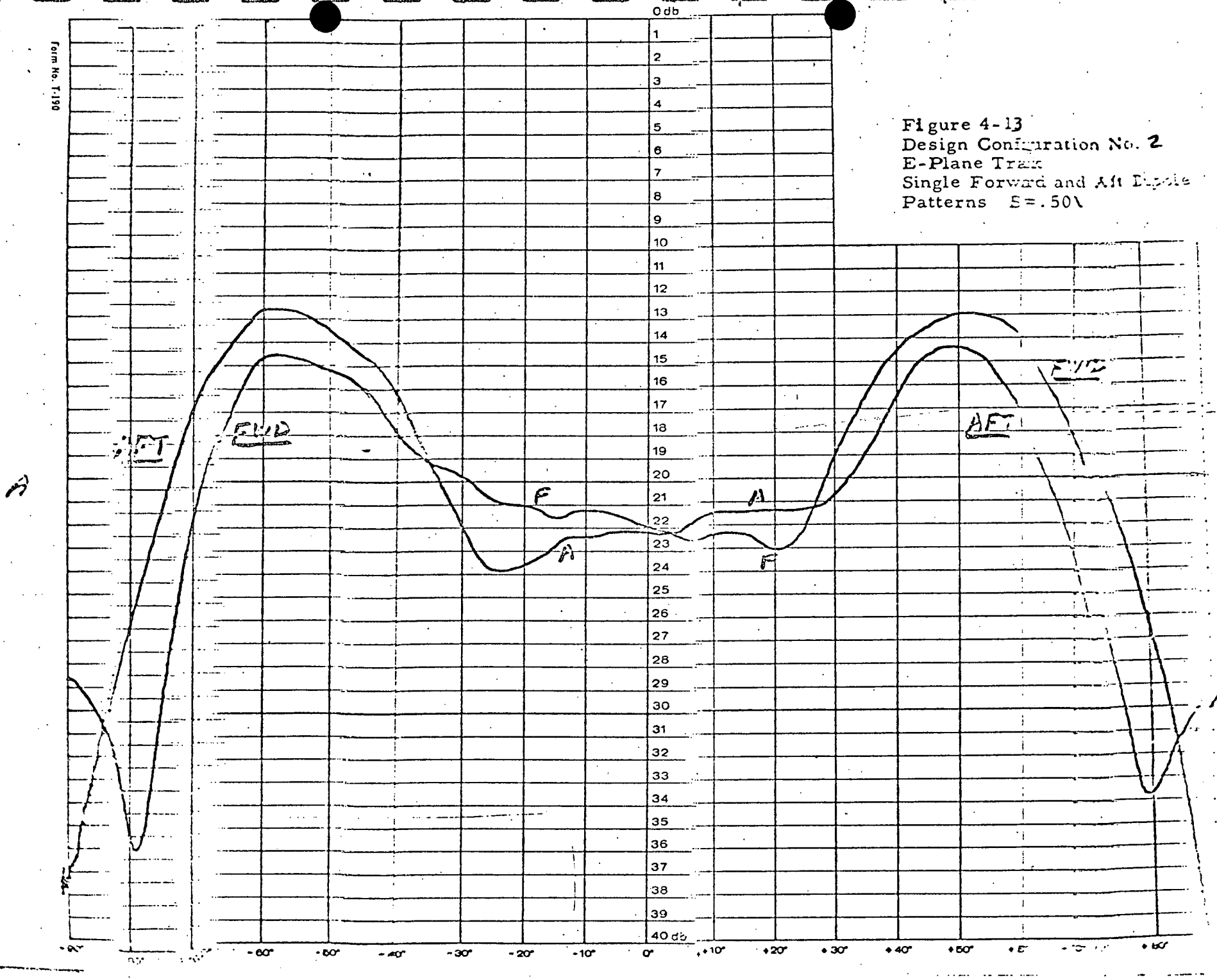

Figure 4-13
Design Configuration No. 2
E-Plane Trak
Single Forward and Aft Dipole
Patterns S = .50\

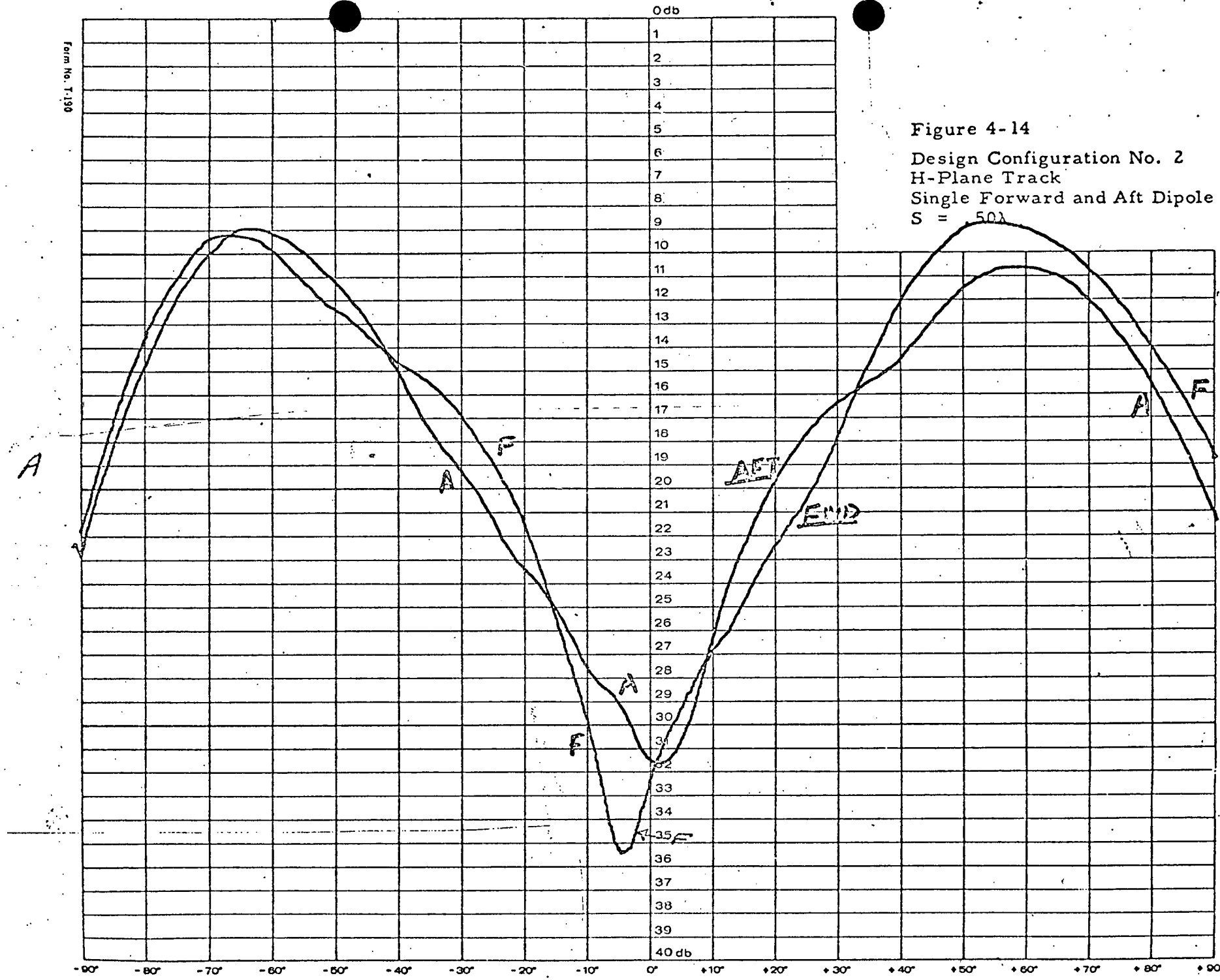

Figure 4-14

Design Configuration No. 2
H-Plane Track
Single Forward and Aft Dipole Patts.
S = .50λ

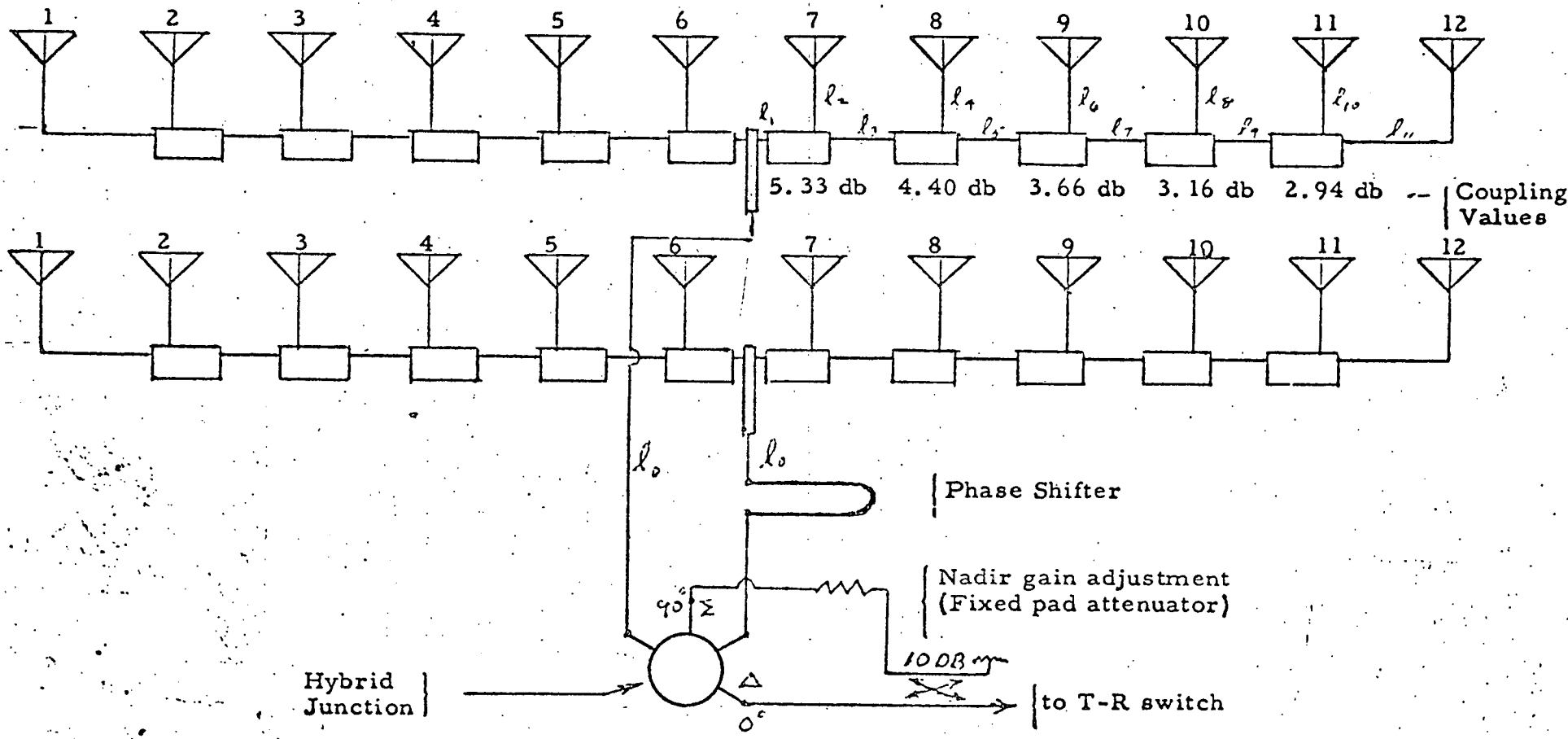

Figure 5-1. Array Feed System for one polarization

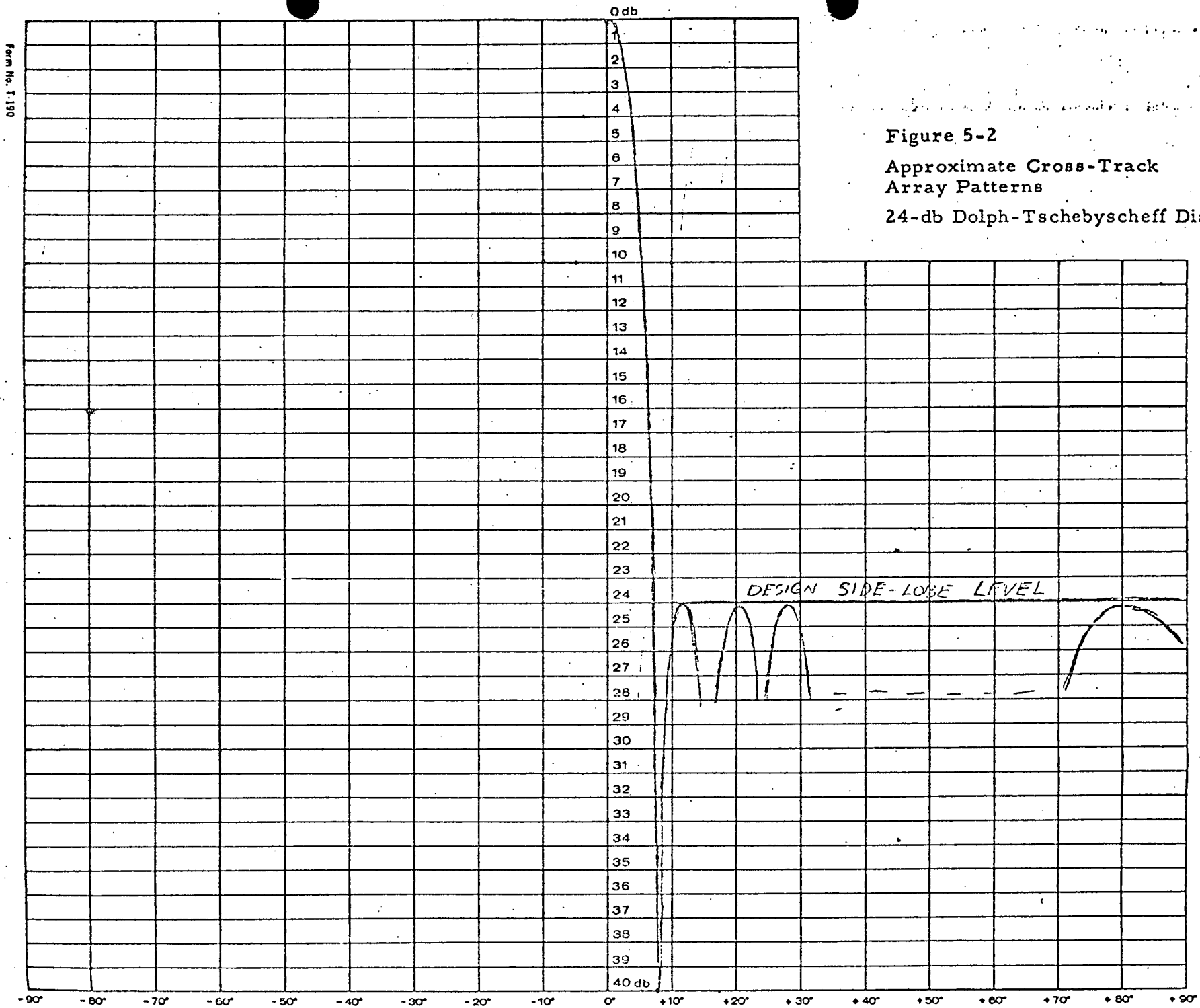

Figure 5-2

Approximate Cross-Track Array Patterns

24-db Dolph-Tschebyscheff Distr.

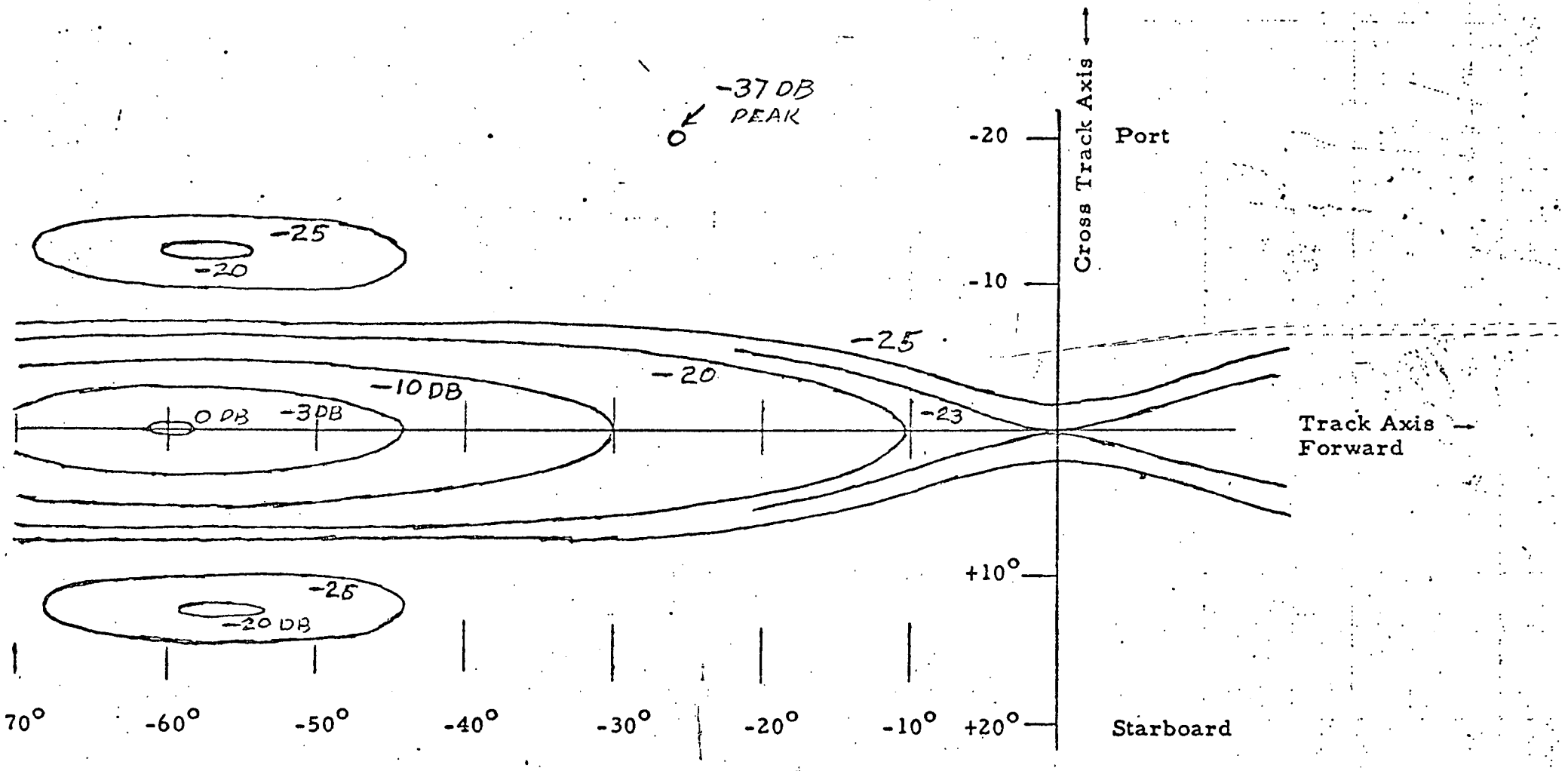

Figure 6-1. Typical Contour Plot of Aft Beam
Based on Pattern of Figures 4-2, 4-3, and 5-2.

Document No. 2236

APPENDIX D

SUMMARY DISCUSSION OF

VIBRATION TEST RESULTS

Since stress analyses indicated a sound design, failures were not anticipated prior to vibration tests. However, failures did occur during the early stages of the test. (1) These failures were at first attributed to poor welding, but additional tests revealed that, while welding was a factor, it was not the only cause of failure. It was determined after further testing of several design and process control ideas, that the cause of the failures was a combination of test severity, unreliable material, inadequate manufacturing process control, and marginal design.

Included in the tests conducted prior to January 19, 1968, was an effort to evaluate the effects of the simulated mount structure. To do this, the elements were mounted directly on the rigid magnesium slip table. It was found that, due to lack of compliance, the slip table imposed an even greater stress on the elements than the simulated structure. The testing of November 20, is remarked on here because of the immediate failures obtained, as recorded in the Wyle report. An outside source was used for the welding of these elements with the idea that such action would provide better quality perhaps not present in Rantec's shop. These units were welded by the TIG process, using Eutetic No. 680 rod and an engineered welding procedure. The welder was certified to MIL-T-5021, as required by MIL-W-8611. (The Rantec Welders are similarly certified). These elements then were all subjected to Magnaflux inspection and 100% Radiographic inspection. All elements were certified to be of sound welds and free of cracks, etc.

These were the elements tested November 20th. The failures were, after considerable study, judged to be due to overheating of the 1020 steel which destroyed its as-rolled strength. Consultation with metallurgical people established that the steel at .035 wall was too thin to accept this treatment.

On November 30, several reinforcement schemes were subjected to vibration testing, all of which subsequently failed:

(1) Ref. Wyle Deviation Notice, Page 74 of Appendix I.

1. Specimen A, an H Plane Element Part No. 70155040, of 1020 tubing assembly welded by Rantec, fitted with gussets fabricated from the 1020 tubing, and assembled as follows.

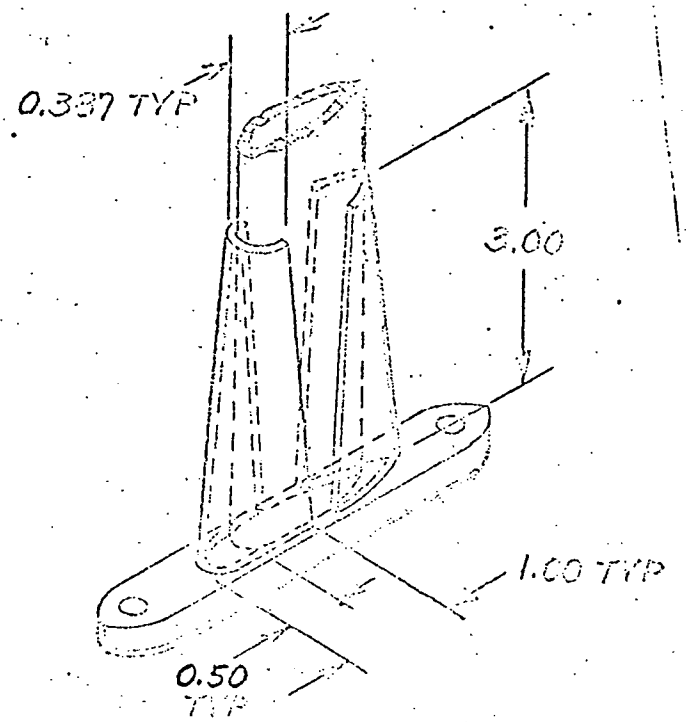

2. Specimen B, an E Plane Element (Part No. 70155069), of 1020 steel tubing was gusseted in a much different manner.

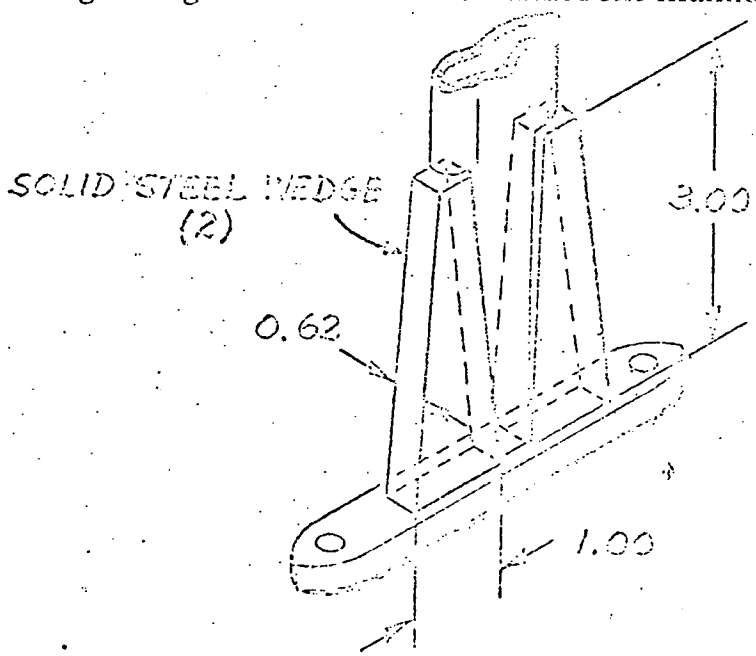

3. Specimen C, an E Plane Element which failed in the foot area on a previous test. This unit was machined to remove the damaged areas resulting in shortening the legs by approximately .50 inch. New feet were then silver brazed to the legs using a Class 12 brazing wire. One leg was brazed to obtain a sharp britt while the other was filled to get a fillet.

4. Specimen D, was a H Plane Mechanical Assembly, part no. 70155040, which was welded by Rantec and then sent outside to a Heat-Treating Company where it was normalized and then shot-peened. This unit was found to have small cracks in the foot welds after return from heat-treat. Unfortunately, no inspection was made on this before processing.

All of these elements failed, with all the failures being in the 1020 steel in weld adjacent areas. It was now definite that a change in material would be required.

The testing conducted on Dec. 9 was a last effort to utilize the 1020 tubing. This was once again a complete failure. The other three (3) elements tested were of 4130 steel in a 1¼ inch equiv. dia. streamline tubing. Failures were as recorded. This test, except for the 1020 failure, was inconclusive in that the units were not properly prepared as to flatness of mounting feet and welding assembly technique. This test was conducted on the rigid magnesium slip table. The simulated mount was not used.

On 16 December 1967, vibration tests at Wyle resumed with two units of a new design in aluminum plate, one previously tested E Plane in 1020 steel modified to have a semi-rigid leg support design, and one H Plane of the 4130 large tubing, with welded feet and with the arms torched brazed in place. The two aluminum units were initially tested directly on the slip table. Failures occurred in both

units as noted. The simulated mount was then put into place, and all four elements mounted on it. The two aluminum units were mounted to provide additional driving action and mass. Out of this testing, unit number 3 failed and unit number 4 partially failed. Unit number 4 survived approximately 45 minutes dwell in the Y Axis at 100 Hz and 15 G's.

The arms later failed in the Z axis.

On January 2, following the encouraging results obtained on the two aluminum units on December 16, four new aluminum units (strictly mechanical) were subjected to the vibration test on the simulated mount. The results of this test indicated that units of similar design should be entirely feasible although weight and aerodynamic drag would be increased over that of the steel tubing designs.

Shortly after the preceeding test, a supply of 4130 streamline tubing, in a smaller size than the .065 wall tubing, became available. This turned out to be one inch equivalent dia tubing of .049 wall X .57 (Minor axis), 4130 steel in 2.5:1 fineness ratio. With this material two new units were fabricated, one H parasitic No. 70155038, and one H mechanical assembly No. 70155040. These were tested on January 13 using the simulated mount. Due to a flatness problem with the mount, several mounting screws broke. This, plus Wyle down time, limited the testing time to that described in the Wyle report. However, since no failure occurred in the elements, it was decided to firm up the design and build a full set for test.

On Jan. 16 the simulated mount and a full set of aluminum elements:

1 - 70155081 H. Parasitic

1 - 70155082 E. Parasitic

2 - 70155078 H. Active

2 - 70155080 E. Active

was subjected to testing as back-up to the steel design. The test report indicates, that with some additional work, these designs should be satisfactory except for weight and drag. This test also revealed that the mount required additional work.

On January 19th, a full set of steel elements was mounted on the simulated mount and a full scale vibration test entered into at Wyle Labs. These units were the product of previous work, with all of the 1020 tubing replaced by 4130 tubing of .049 wall. The elements were redesigned as follows:

1. 70155038 H Parasitic - Changed to 4130 tubing for the legs and tapered 4130 rod for the reflector arms.
1. 70155037 E Parasitic - Changed to 4130 tubing for the legs.
2. 70155056 H Active - Changed to 4130 tubing for the legs and cross member. Added 4130 sheet gussets to the foot-leg attachment and changed the reflector arms from 4130 streamline tubing to tapered 4130 rod.
2. 70155068 E Active - Changed to 4130 tubing in the legs and mast. Added 4130 sheet gussets to both the foot-leg attachments and to the reflector arm-mast joints.

As noted in the Wyle report, a mounting screw broke on E1 after about 14 minutes of dwell in the Z axis. The screw was replaced and the dwell was completed. In the 2nd dwell test the same screw broke after about six minutes. It was replaced and test was continued. After about 22 minutes of dwell, a sharp pop was heard (like a screw letting go). The test was stopped and it was found that the screw had failed again. The dwell test was continued without replacing the failed screw and was completed without change in frequency or excursion. The screw was replaced before continuing with the next dwell test. No further failure was experienced in the Z axis.

The cycling and dwell test was completed in the X axis. Unit H2 was dwelled at about 385Hz, which was the resonance in the reflector arms, not in the body. After about 7 minutes, a screw in the top cap sheared off. It was replaced and the test continued. H1 was dwelled under the same condtion but a higher frequency. After about 12 minutes it also experienced a top cap screw failure. The problem was

resolved as being simply that the screws, of a non-locking type, were backing out due to the vibration and then quickly fatiguing to failure. Peridically re-tightening these cap screws eliminated any further breaking. The X axis was completed with no other failure noted.

The Y axis was completed without any apparent damage noted. All units were then removed and it was found that there were cracks in the H Parasitic unit and in one of the H Plane Active units. All units, plus the mount, were returned to Rantec and an electrical check conducted on the four active elements. All were good electrically.

A subsequent review of the failures revealed that the failed units had not undergone adequate inspection prior to test. The H Plane Active unit had its legs heated and sprung open to fit the mount due to the soft tooling used. The units which passed were inspected and found to be free of cracks. This is a reasonable indication that cracking was already present in the failure units. Subsequent discussion with ESD and NASA personnel concluded with their acceptance of the test as having been successful, except for the H Parasitic element.

On February 8th, the mount and two new H Parasitic units went into test, one to the same print revision as that which failed, and one with a reinforcement over the head areas where the cracks had occurred. This test was conducted using the aluminum mechanical units, mentioned before, as mass drivers. It was necessary to do this since the H Parasitic unit does not have a low frequency resonance in itself, but does resonate, as recorded, when driven.

As noted by Wyle, HP1 failed in the X axis at one of the foot welds. This was not expected.

HP2, which was in a Y axis, was then switched to the X axis position. HP1 was removed and the test was restarted. The X axis was completed and the Y axis begun. HP2 failed in the same way as did HP1. HP3, which was received from Rantec earlier, was then mounted in position and the whole test started again. HP3 completed all three axes without failure. Subsequent inspection of the two

failed units revealed that there was evidence of cracking before test. This was the opinion of several people considered to be knowledgeable in this field. In both units, there appeared to be rust in some areas and bright metal in others. Unfortunately, these two units had not been magnafluxed before testing. In reviewing the inspection records, it was found that HP3 had not been magnafluxed either. It was then sent out, and was magnafluxed and X-rayed. The report was acceptable; no cracks or defects were detected. The test was considered as successfully concluded.

On the basis of the foregoing experience, and knowledge gained, these designs were released to production. Fabrication and inspection requirements were specifically detailed and enforced.